TÉCNICO LISBOA

UNIVERSIDADE DE LISBOA
INSTITUTO SUPERIOR TÉCNICO

Mesenchymal Stromal Cell-based Strategies to Enhance Tissue Vascularization: Exploring Magnetic Field Stimulation and Design of Fluidic Models for Vascular Studies

Ana Carina Baeta Manjua

Supervisor: Doctor Carla Alexandra Moreira Portugal

Co-supervisor: Doctor Frederico Castelo Alves Ferreira

Thesis approved in public session to obtain the PhD degree in

Bioengineering

Jury final classification: Pass with distinction

2020

UNIVERSIDADE DE LISBOA
INSTITUTO SUPERIOR TÉCNICO

Mesenchymal Stromal Cell-based Strategies to Enhance Tissue Vascularization: Exploring Magnetic Field Stimulation and Design of Fluidic Models for Vascular Studies

Ana Carina Baeta Manjua

Supervisor: Doctor Carla Alexandra Moreira Portugal

Co-supervisor: Doctor Frederico Castelo Alves Ferreira

Thesis approved in public session to obtain the PhD degree in

Bioengineering

Jury final classification: Pass with distinction

Jury

Chairperson: Doctor Joaquim Manuel Sampaio Cabral, Instituto Superior Técnico, Universidade de Lisboa

Members of the Committee:
Doctor Dimitrios Stamatialis, Faculty of Science and Technology, University of Twente, The Netherlands
Doctor Johannes Gerardus Elisabeth Gardeniers, Faculty of Science and Technology, University of Twente, The Netherlands
Doctor Joaquim Manuel Sampaio Cabral, Instituto Superior Técnico, Universidade de Lisboa
Doctor Jorge Manuel Ferreira Morgado, Instituto Superior Técnico, Universidade de Lisboa
Doctor Ana Margarida Pires Fernandes Platzgummer, Instituto Superior Técnico, Universidade de Lisboa
Doctor Carla Alexandra Moreira Portugal, Faculdade de Ciências e Tecnologia, Universidade Nova de Lisboa

Funding Institution

FCT – Fundação para a Ciência e Tecnologia

2020

ABSTRACT

Cardiovascular diseases have emerged as the leading causes of morbidity worldwide. Despite its high incidence, the development of cardiac tissue engineering remains vastly unexplored demanding the fabrication of vascularized artificial tissue substitutes. Hoping to contribute with novel strategies, this project aims to enhance angiogenesis through the application of non-invasive short-term magnetic stimulation.

Firstly, a pioneering investigation on smart responsive magnetic hydrogels revealed the potential to regulate protein sorption upon cyclic variation of the magnetic field intensity by inducing mechanical changes on the hydrogel.

A platform for angiogenesis was then investigated using external static magnetic fields to stimulate mesenchymal stromal cells (MSCs). Interestingly, while culturing MSCs on magnetic scaffolds (PVA and gelatin) enhances the magnetic effect on MSCs organization and angiogenic induction, it was also demonstrated that MSCs are magnetic sensitive with ability to migrate and align according with the magnetic field direction even without the mechanotransduction mediation of the magnetic scaffold. Importantly, magnetic stimulation, with or without scaffold, increases the secretion of key angiogenic growth factors (e.g. VEGF-A).

The potential to magnetically manipulate angiogenic MSCs processes was revealed by the ability to drive human umbilical vein endothelial cells (HUVECs) towards angiogenesis both *in vitro* and *ex vivo*. The capacity to modulate the angiogenic behavior of the cells was further studied for different magnetic field intensity under static or frequency-pulsed magnetic stimulation, highlighting the possibility to either boost the angiogenic efficiency for cardiac repair or to inhibit vascularization to prevent tumor progression in cancer patients.

Lastly, the project focused on the fabrication of blood vessel *in vitro* models to explore the concept of magnetic stimulation using co-cultures (MSCs and HUVECs) for improvement of HUVECs sprouting. The project finalizes by combining key elements to identify the benefits of magnetic stimulation on reverting induced vascular ischemia, aiming to develop novel therapeutic options for these conditions.

Keywords: Magnetic Fields, MSCs, HUVECs, Angiogenesis, Scaffolds

RESUMO

As doenças cardiovasculares são das principais causas de morbidade mundiais. Apesar da elevada incidência, o desenvolvimento da engenharia de tecidos cardíacos permanece muito inexplorado, exigindo a fabricação de tecidos artificiais pré-vascularizados. Para contribuir com novas estratégias, este projeto visa explorar angiogénese por aplicação de estímulos magnéticos não invasivos de curta duração.

Uma investigação pioneira sobre hidrogéis magnéticos inteligentes revelou potencial para regular a sorpção de proteínas mediante variação cíclica da intensidade do campo magnético, induzindo alterações mecânicas no hidrogel.

Uma plataforma para angiogénese foi então investigada usando campos magnéticos estáticos externos para estimular células estromais mesenquimais (MSCs). Curiosamente, embora a cultura de MSCs em hidrogéis magnéticos (PVA e Gelatina) melhore o efeito magnético na organização e indução angiogénica de MSCs, também foi demonstrada a magneto-sensibilidade das MSCs pela capacidade de migrarem e alinharem de acordo com a direção do campo magnético, mesmo sem hidrogéis magnéticos a mediarem a mechanotransdução. É importante ressaltar que se observou que a estimulação magnética, na presença ou ausência dos hidrogéis, proporciona o aumento da secreção do factor de crescimento angiogénico VEGF-A. A possibilidade de manipular magneticamente processos angiogénicos de MSCs foi revelado pela capacidade de conduzir células endoteliais (HUVECs) à formação de estruturas vasculares, *in vitro* e *ex vivo*.

A modulação do comportamento angiogénico das células foi ainda estudada para diferentes intensidades de campo magnético sob estimulação magnética estática ou pulsada por frequência, destacando a potencial de aumentar a eficiência angiogénica das células para reparação cardíaca ou para inibição da vascularização na progressão tumoral.

Por fim, o projeto dedicou-se ao desenvolvimento de modelos *in vitro* de vasos sanguíneos para explorar o conceito de estimulação magnética usando co-culturas (MSCs e HUVECs) para induzir a formação de tecido vascular. O projeto finaliza combinando elementos-chave para demonstrar os benefícios da estimulação magnética na reversão da ischemia induzida, a fim de identificar novas opções terapêuticas para estas condições.

Palavras Chave: Campos Magnéticos, MSCs, HUVECs, Angiogénese, Hidrogéis

DEDICATION

To my mother, Ana Bela, the most important person of my life, for the unconditional support in the pursue of my dreams and for being my inspiration every day.

To my dear grandmother, Maria, for always being so proud of me and of my academic success.

To these two people I love the most, who are no longer here with me but to whom I owe everything I am, I want to express my love and gratitude by dedicating to them the achievement of this goal and the end of an era in my life.



"All of our dreams can come true if we have the courage to pursue them." – Walt Disney

ACKNOWLEDGMENTS

My PhD journey over these four years would not have been accomplished without the presence and valuable contribution of many people. Despite our professional proactivity and independence, acquired over the years of experience, at the end of the day we still require the cooperation and friendship of our colleagues. Therefore, I would like to acknowledge some of the people that contributed for this thesis.

To Professor Joaquim Cabral, I would like to express my gratitude for giving me the opportunity to be a part of the PhD Program in Bioengineering – Cell Therapies and Regenerative Medicine, for which I am glad to have been selected, and for allowing me to become a member of the Stem Cell Research Group (SCERG) from iBB-IST, where I developed the largest part of my research work. As coordinator of the PhD program and PI of SCERG, I would like to thank the professor for the availability and support over the development of my research work.

To Professor João Crespo, I would like to thank for the chance to be a member of the REQUIMTE research group. A special thanks for the opportunities provided over the years, for believing in me and for always having a positive and enthusiastic attitude about the work I was developing. Also, to all my REQUIMTE lab colleagues and friends, thanks for your companionship and cooperative spirit.

To my supervisors, Professor Frederico Ferreira and Doctor Carla Portugal, I would like to thank for the guidance and support throughout the hardships of the project, for keeping me motivated during the PhD while also giving me the independence to engage in my own creative ideas and execute them. Also thank you for complementing each other in the co-supervision of my work. For all your efforts, I am very grateful. To Professor Frederico, a special thanks for all the new ideas and solutions, for the suggestions of collaborations and interconnected projects that elevate the work to a higher level as well as my own personal experience. To Carla, with whom I've been working for almost a decade, I want to thank for all the opportunities, for allowing me to grow as a scientist, for the constant support and motivation. In particular, I want to express my gratitude for

the friendship, support and understanding during very difficult moments of my personal life.

To Professor Han Gardenier from the University of Twente, I would like to thank for receiving me at the Mesoscale Chemical Systems (MCS) group. I am very thankful for the great scientific and social environment you promoted in the group and for everything that I have learned in the microfluidics expertise during my internship.
In this regard, a special thanks to Burcu Gumuscu for supervising my work in Twente. I cannot explicit how thankful I am for making sure to check how I was doing, for looking hard for solutions to avoid delays in the work and for teaching me so many techniques and tips to improve my skills. I am very honored for the chance to meet and work with you.

To all the people from the University of Twente (UT), with whom I collaborated, and in particular to all the MCS members, I would like to thank for the help, for all the enjoyable social times and for providing me with so many good memories. A special thanks to Laura Vargas, whom I hold very dear and who was so important in my integration in the group; Arturo, for having such a positive vibe; Brigitte Boogaard, for the assistance with the bureaucratic documents; Stefan Schlautmann, for being extra nice and patient in teaching me the soft lithography procedures in the Clean Room; Erwin Berenschot, for the much appreciated help using SolidWorks; Ine Segers and Irene Konings, for the assistance with the confocal analysis; Jean-Baptiste Blonde, for the cell lines for my cell culture experiments; and Ayush Kharel, for assisting me with the mechanical measurements. Without you, I would not have been able to successfully finish all the tasks.
And I could not finish the UT acknowledgements without expressing my gratitude to the dear friendships that were built throughout the way. In special to Yasser, Miguel, Ignaas, Maria Fernandez, Daniel, Merhnaz, Sandriens, Akash and David: thank you so much for all the good moments, for the places we visited, the meaningful conversations, the brainstormings and the unique friendship. And I would also like to thank my friends from the Sagittarius archery group, where I could relax and practice the sport I love in the company of very special people. To all of you, I truly appreciated your kindness and friendship, which I hope will remain for a long time.

To my SCERG/iBB friends, thanks for everything, for the help, friendship and companionship over these four years.
To Ana Fernandes and Carlos Rodrigues, a special thank you for the guidance, support, brainstorming sessions and very dear friendship. Thank you also for, in cooperation with Jaqueline and Geni, finding a way to organize and solve the multiple situations with equipment, reagents or lab organization and for simplifying our work. Jaqueline, thank you for being so attentive with our complaints and requests. Your arrival was definitely an important one in the group. On a special note, I thank Marta Costa, Marta Carvalho and João Silva for kindly teaching me the first steps of cell culture, alongside with Fábio Garrudo, which was also a great help in sharing the knowledge. A special thanks to Teresa Silva and Ana Rita Gomes for the times you took my photos at confocal or accompanied me to analyses at IMM. This thesis would also never be complete without acknowledging my "miguito", Diogo Pinto, for teaching me to devise improved work strategies and for the brainstorming sessions at the very beginning of my introduction to cell culture, for integrating me in the group and improving my social abilities during a complicated moment in my life. Without your help to pull me through that, I might not have being able to successfully finish this important stage in my life.

To the friends and colleagues from lab 2, a huge thanks for the nice cooperation in assisting me with techniques you are more familiar with or occasionally sharing reagents for urgent experiments. In particular, to Diogo Nogueira, Teresa, Ana Rita, André Rodrigues, João Cotovio and Fábio Garrudo, thank you for the amazing moments in and out of the lab. The door in-between the labs is meaningless when the friendship is real. To all the other friends that have come and gone from Lab 2, but remain very dear friends (Leonor Resina, Kikas, Mariana Pina), a huge thank you for playing a big part in my journey, and for the amazing out-of-work dinners and parties.

To the colleagues and friends from "my" Lab 3, I have a lot to be thankful for, in particular the nice and cooperative environment, the friendship and the good vibe. To Cristiana Ulpiano and Sara Morini, a big thank you for all the amazing moments, the jokes and the friendship that turns a bad day into a bright one. To Marília Silva, André Branco, Sara Bucar and Miguel Fuzeta, those that listen to my frustrations and also the first to celebrate my victories, even adventuring into my small corner of the world (my hometown), those

that criticize me the most but also cheer me up and motivate me to do better, a huge thank you for the outstanding great memories and friendship during these years.

A huge thanks to my hometown “squad” friendships (Joana, Sara, Sarita, Isa, Tânia, Marta), for the unconditional support, for believing that I am able to do everything, no matter how challenging, for cheering me up, and most of all, for being there in the good and the bad moments.

A thank you to my cousins and brother for the support and for being proud of everything I have achieved. In particular, to my brother for the overcriticism, specially with the aesthetics of presentations, layouts or posters, but especially for motivating my creativity and making me thrive to improve and do better.

And to my mother, thank you for being my inspiration. You are the main reason I moved forward to finish this PhD.

Finally, I would like to acknowledge the financial support from Fundação para a Ciência e a Tecnologia (FCT-MEC) for the PhD grant (SFRH/BD/114043/2015). This work was also supported by LAQV-REQUIMTE and iBB under FCT/MEC (UID/QUI/50006/2013 and UID/BIO/04565/2020) and co-financed by the ERDF under the PT2020 Partnership Agreement (POVI-01-0145-FEDER-007265).

TABLE OF CONTENTS

ABSTRACT ..... **i**

RESUMO ..... **iii**

ACKNOWLEDGMENTS ..... **vii**

TABLE OF CONTENTS ..... **xi**

LIST OF FIGURES ..... **xvi**

LIST OF TABLES ..... **xxi**

ABBREVIATIONS ..... **xxiii**

CHAPTER I – Introduction ..... **- 3 -**

I.1. Motivation and Project Aim ..... **- 3 -**

I.2. Project Strategy and Research Decisions ..... **- 7 -**

I.3. Dissertation Overview ..... **- 13 -**

I. References ..... **- 15 -**

CHAPTER II – State of the art ..... **- 23 -**

State of the Art ..... **- 23 -**

II.1. Magnetic Field and Biological Applications ..... - 23 -

II.2. Smart Magnetic Hydrogels and Magnetic Stimulation ..... - 26 -

II.3. Angiogenesis Mechanisms and Strategies to Improve the Phenomena ..... - 29 -

II.4. Blood Vessels Models and Recent Advancements in the field ..... - 34 -

II. References ..... **- 40 -**

CHAPTER III – Magnetic-responsive PVA hydrogels for remote modulation of protein sorption ..... **- 53 -**

III.1. Introduction ..... **- 54 -**

III.2. Experimental Section ..... **- 57 -**

Materials. ..... - 57 -

Synthesis of the magnetic nanoparticles (MNPs). ..... - 57 -

Preparation of the magnetic-responsive hydrogel membranes. ..... - 57 -

Structural characterization of the MNPs and hydrogel membranes. ..... - 58 -

Young's modulus of the magnetic hydrogel. ..... - 58 -

Surface roughness of the hydrogel. ..... - 59 -

Surface contact angles of the hydrogel. ..... - 59 -

Protein sorption studies under static and dynamic magnetic field conditions. ..... - 59 -

Confocal microscopy measurements. ..... - 60 -

III.3. Results and Discussion ..... **- 60 -**

3.1. Magnetic-responsive behavior of the hydrogel membranes ..... - 60 -

3.2. Impact of the magnetic behavior of hydrogel membranes on protein sorption ..... - 65 -

3.3. Control of protein sorption in hydrogel membranes under cyclic magnetic field conditions - 67 -

III.3. Conclusions ..... **- 72 -**

III.5. References ..... **- 74 -**

Chapter III. Supplementary Information ..... **- 78 -**

CHAPTER IV – Magnetic stimulation combined with magnetic-responsive scaffolds to enhance the angiogenic potential of MSCs in vascular tissue engineering ..... **- 85 -**

IV.1. Introduction ..... **- 86 -**

IV.2. Experimental Section ..... **- 88 -**

Scaffold Fabrication. ..... - 88 -

MNPs and Magnetic Responsive Scaffold Characterization. ..... - 89 -

Cell culture. ..... - 89 -

Human Bone Marrow Mesenchymal Stromal Cells (BM MSC) metabolic activity and proliferation curves. ..... - 91 -

Cell viability and morphology assay ..... - 91 -

Metabolite analysis. ..... - 91 -

Immunophenotype characterization of magnetically stimulated MSCs. ..... - 92 -

Cytotoxicity Assay. ..... - 92 -

Quantitative reverse transcription-polymerase chain reaction analysis (RT-PCR). ..... - 92 -

Quantification of VEGF secretion by enzyme-linked immunosorbent assay (ELISA). ..... - 93 -
In vitro endothelial cell tube formation assay. ..... - 94 -
Wound healing and MSCs migration assay. ..... - 94 -
Chick Chorioallantoic Membrane (CAM) assay and neo-vessel quantification. ..... - 95 -
Statistical analysis. ..... - 95 -

IV.3. Results ..... - 96 -
3.1. Scaffolds magneto-responsiveness are modulated by MNPs load and magnetic exposure. .. - 96 -
3.2. Magnetic forces impact on 2D and 3D cultures of MSCs. ..... - 98 -
3.3. MSCs geometry and alignment in scaffolds are magnetic field-dependent. ..... - 101 -
3.4. Magnetic exposure enhances VEGF-A production in MSCs cultured on magnetic scaffolds. .... - 103 -
3.5. Improved HUVECs *in vitro* sprouting induced by MSCs exposure to magnetic stimulation. ..... - 106 -
3.6. Induced faster response on HUVECs wound healing and MSCs migration are related with magnetic field incidence. ..... - 108 -
3.7. MSCs magnetic effect prompts increased *ex vivo* vessel formation. ..... - 110 -

IV.4. Discussion ..... - 112 -

IV.5. Conclusions ..... - 117 -

IV.6. References ..... - 119 -

Chapter IV. Supplementary Information ..... - 125 -

CHAPTER V – Magnetic field configurations for improved control of the angiogenic potential of mesenchymal stromal cells ..... - 133 -

V.1. Introduction ..... - 134 -

V.2. Experimental Section ..... - 136 -
Scaffold Fabrication. ..... - 136 -
Magnetic profiles characterization and experimental setup. ..... - 137 -
Cell culture. ..... - 137 -
Human MSC proliferation values ..... - 138 -
Cell viability and morphology assay. ..... - 138 -
Quantitative reverse transcription-polymerase chain reaction analysis. ..... - 139 -
Quantification of VEGF expression by enzyme-linked immunosorbent assay (ELISA). ..... - 139 -
In vitro endothelial cell tube formation assay. ..... - 139 -
Statistical analysis. ..... - 140 -

V.3. Results ..... **- 140 -**
3.1. Effect of the magnetic field on MSCs proliferation and morphology ..... - 140 -
3.2. Impact of the magnetic field on the expression of VEGF-A gene ..... - 144 -
3.3. Control of VEGF-A protein secretion under magnetic exposure ..... - 145 -
3.4. Magnetic effect on the sprouting potential of HUVECs ..... - 146 -
V.4. Discussion ..... **- 150 -**
V.5. Conclusions ..... **- 154 -**
V.6. References ..... **- 155 -**
CHAPTER VI – Design of blood vessel devices for vascularization models using magnetic scaffolds ..... **- 163 -**
VI.1. Introduction ..... **- 164 -**
VI.2. Experimental Section ..... **- 166 -**
2D Chips Fabrication. ..... - 166 -
Magnetic Hydrogel Preparation. ..... - 167 -
Magnetic Hydrogel Patterning. ..... - 167 -
3D Constructs Fabrication. ..... - 168 -
Magnetic Gelatin Mechanical Characterization. ..... - 169 -
Cell Culture. ..... - 169 -
Co-culture of MSCs and HUVECs and Magnetic Stimulation. ..... - 170 -
Computational modeling of fluid flow and VEGF diffusion. ..... - 170 -
Flow velocity tracking measurement. ..... - 171 -
VEGF and Endothelin-1 measurement using ELISA. ..... - 171 -
Morphological analysis. ..... - 171 -
CD31 Immunostaining. ..... - 172 -
Statistical analysis. ..... - 172 -
VI.3. Results ..... **- 172 -**
3.1. Design and Hydrogel Patterning of 2D chips for cell culture. ..... - 172 -
3.2. Three-dimensional Single Channel Model fabrication and characterization. ..... - 176 -
3.3. Cell Culture strategies on 2D and 3D models. ..... - 176 -
3.4. VEGF diffusion and velocity profile simulations on 2D chips. ..... - 182 -
3.5. Co-culture and magnetic stimulation. ..... - 186 -
3.6. Endothelin-1 secretion by HUVECs on 2D and 3D models. ..... - 189 -
VI.4. Discussion ..... **- 191 -**
VI.5. Conclusions ..... **- 193 -**

VI.6. References ..... **- 195 -**

Chapter IV. Supplementary Information ..... **- 199 -**

CHAPTER VII – Cardiac ischemia disease modeling in magnetic *in vitro* models of vascular network ..... **- 203 -**

VII.1. Introduction ..... **- 204 -**

VI.2. Experimental Section ..... **- 206 -**

Fabrication of 2D chips. ..... - 206 -

Design and Fabrication of the Vascular Hierarchical 3D Model. ..... - 206 -

Magnetic Hydrogel Preparation. ..... - 207 -

Magnetic Hydrogel Patterning on 2D chips and vascular hierarchical model. ..... - 207 -

Cell culture. ..... - 208 -

Co-culture on the models. ..... - 208 -

Ischemia Disease Induction. ..... - 209 -

Reperfusion and Magnetic therapy to reverse Ischemia condition. ..... - 209 -

Endothelin-1 measurement using ELISA ..... - 209 -

Immunohystochemical analysis ..... - 210 -

Immunofluorescence confocal laser microscopy ..... - 210 -

Electron microscopy ..... - 210 -

VII.3. Results and Discussion ..... **- 211 -**

3.1. *In vitro* Ischemia Characterization. ..... - 211 -

3.2. Reversible Ischemia condition. ..... - 212 -

VI.4. Conclusions ..... **- 217 -**

VI.5. References ..... **- 218 -**

CHAPTER VIII – Conclusions and Future Perspectives ..... **- 223 -**

VIII. 1. CONCLUSIONS ..... **- 223 -**

VIII. 2. Limitations of the Work and Future Directions ..... **- 226 -**

VIII. 3. References ..... **- 232 -**

LIST OF PUBLICATIONS ..... **- 235 -**

LIST OF FIGURES

Figure I. 1. Representation of MSCs therapy for cardiovascular disease, showing the stages of cardiac repair…… - 4 –

Figure I. 2. Illustration of the sequential stages of the work developed during this PhD project…….. - 13 –

Figure II. 1. Illustration of the preparation and implantation of an engineered magnetic scaffold to prompt bone regeneration under external magnetic stimulation…….... - 28 –

Figure II. 2. Illustration of the mechanisms and signaling pathways involved in sprouting angiogenesis triggered by inflammatory cues from a hypoxic tissue……..- 30 –

Figure II. 3. Illustration of organ-on-chip platforms for modeling human physiology and pathophysiology……...- 39 –

Figure III. 1. Size distribution of the MNPs and macro/microscopic characterization of the PVA hydrogel membranes…….- 61 -

Figure III. 2. Profilometry images of PVA hydrogels and their respective surface roughness, Sq……...- 62 –

Figure III. 3. Characterization of the magneto-responsive responsive behavior of the PVA hydrogel…….. - 63 -

Figure III. 4. Environmental SEM (ESEM) images of surfaces and cross sections of nonmagnetic PVA hydrogel membrane and PVA hydrogel membrane with 0.25% and 1% MNPs before exposure to the magnetic field…….. - 64 -

Figure III. 5. Time-dependent trypsin sorption at magnetic hydrogel surfaces doped with 0.25% (w/v) of MNPs under different magnetic field intensities……- 66 –

Figure III. 6. Evolution of trypsin content along time in a PVA hydrogel membrane doped with 0.25% (w/v) of MNPs when exposed to magnetic field cycles varied between 0 and 1 T and glycerol contact angles obtained along OFF/ON magnetic field cycles at 0.08 T for a magnetic hydrogel matrix with 0.25% (v/w) of MNPs upon exposure to OFF/ON magnetic field cycle at 1 T……... - 68 -

Figure III. 7. Confocal microscopy orthogonal images obtained along the Z-axis of a magnetic hydrogel membrane with 0.25% (v/w) MNPs upon immersion in a solution of FITC-albumin in the absence of magnetic fied and exposed to an OFF/ON magnetic field cycle…….- 69 -

Figure III. 8. Evolution of trypsin sorption in a PVA hydrogel membrane doped with 0.25% (w/v) of MNPs when exposed to (A) OFF/ON and (B) ON/OFF magnetic field cycles varied between 0 and 0.45 T…….- 71 -

Figure III. S1. Optical microscopy images of the PVA hydrogel membranes doped with 0.25% (w/v) MNPs before and after exposure to ON/OFF magnetic field cycles.. - 79 -

Figure III. S2. Images of PVA hydrogel membrane doped with 0.25% MNPs acquired along the Z-axis of the membrane (membrane thickness) by fluorescence confocal microscopy analysis……- 80 -

Figure III. S3. Magnetization saturation curves obtained for PVA hydrogels doped with 0.25% of MNPs and 1% of MNPs……...- 81 -

Figure III. S4. Environmental SEM surface and cross-section images obtained for hydrogel membranes doped with 0.25% MNPs before exposure to the magnetic field and after exposure to an OFF/ON magnetic field cycle at 1T……- 81 -

Figure IV. 1. Magnetic gelatin and PVA morphologic characterization and roughness assessment using 3D confocal imaging…… - 97 -

Figure IV. 2. Characterization of ferromagnetic properties and magnetic behavior of the hydrogels in response to a low intensity external magnetic field. hydrophilicity of the hydrogels (Contact angle and VSM magnetization assessment)…..……- 98 -

Figure IV. 3. Phenotypic characterization and proliferation curves of 2D cultures od MSCs under magnetic field exposure and morphologic observation of the magnetic effect in 2D (cell alignment) and 3D cultures (no magnetic impact) of MSCs……- 100 -

Figure IV. 4. MSCs interaction with magnetic scaffolds revealed differences depending on the nature of the scaffold and the magnetic exposure (Proliferation, encapsulation, alignment and elongation on gelatin and formation of heterogenous 3D biostructures in PVA)……- 102 -

Figure IV. 5. Evaluation of gene expression and secretion of VEGF-A molecule reveals a positive enhancement using magnetic gelatin or 2D cultures of MSCs and a potential for angiogenesis inhibition using magnetic PVA or 3D cultures……- 105 -

Figure IV. 6. *In vitro* angiogenic sprouting of human endothelial cells (HUVECs) showed enhancement though indirect magnetic stimulation in 2D cultures of MSCs and further improved in MSCs cultured on magnetic gelatin while sprouting inhibition was observed under magnetic exposure for MSCs cultured on magnetic PVA……- 107 -

Figure IV. 7. Magnetic fields increased the velocity of wound healing by treating HUVECs with conditioned media from MSCs exposed to the magnet. Improvement of MSCs migration was observed through their capability to elongate and migrate according with the intensity of the magnetic field……... - 109 -

Figure IV. 8. Magnetic stimulation revealed to improve *ex vivo* angiogenesis through implementation of CAM (Chick Choriollantoic Membrane) assay…… - 111 -

Figure IV. 9. Schematic of the hypothetical process involved in blood vessel regeneration using a magnetic gelatin scaffold for future cell therapy clinical translation……..- 116 -

Figure IV. S1. Structural characterization of the magnetic hydrogels to complement the characterization included in the main report (UV spectroscopy analysis, swelling analysis)……... - 125 -

Figure IV. S2. The incorporation of MNPs on the materials did not compromise fibroblasts viability in cytotoxicity assay, revealing the potential biocompatibility of these hydrogels for cellular experiments…….. - 126 -

Figure IV. S3. Supplementary z-stack of confocal microscopy images of the MSCs encapsulated within the thickness of the magnetic gelatin matrix…….. - 127 -

Figure IV. S4. Supplementary images of the aggregates spontaneously formed by the low adherence of the MSCs to the PVA matrix after 24h in comparison with the aggregates produced by hanging drop and the adherence and alignment in the gelatin. Supplementary images of MSCs alignment and encapsulation on gelatin……..- 127 -

Figure IV. S5. Extended experiments of 5 days show a decrease in the angiogenic potential of the gelatin whereas PVA results are inconsistence between the donors…….. - 128 -

Figure IV. S6. Magnetic exposure does not induce overexpression of other complementary angiogenic genes (bFGF, hGF)…….…- 128 -

Figure IV. S7. Tube length is not significantly affected by magnetic influence in sprouting assessment……... - 129 -

Figure IV. S8. Supplementary images of the entire process of HUVECs monolayer repair improved by the conditioned media (CM) of MSCs magnetically stimulated in comparison with the control where magnetic was not applied……- 129 -

Figure IV. S9. Supplementary images of the entire process of MSCs monolayer repair directly induced by magnetic field exposure in comparison with the control condition where the MSCs were left to naturally repair the monolayer……..- 130 -

Figure V. 1. Setup for static and non-uniform magnetic field modes using neodymium magnets with different intensities. Timeline for the stages of the experiment, from the scaffold fabrication to the analysis after the magnetic exposure…….- 141 -

Figure V. 2. Magnetic profiles of neodymium magnets (circular magnet of 0.08T and square magnet of 0.45T) used in MSCs experiments under dynamic mode, with a steady velocity of 0.005 m/s for a total period of 24h…… - 142 -

Figure V. 3. Proliferation curves and morphologic observation of MSCs cultured on gelatin scaffolds and MSCs monolayer exposed to static and non-uniform magnetic fields with 0.08T and 0.45T……...- 143 -

Figure V. 4. VEGF-A expression values using RT-PCR technique to compare static and dynamic modes (low and high frequencies) and magnetic intensities (0.08T and 0.45T)……...- 144 -

Figure V. 5. VEGF-A protein quantification for magnetic gelatin and control condition (MSCs monolayer) for each condition (static, lower and higher frequency) and corresponding donor (A, B, C), according with the magnetic intensity (0.08T and 0.45T)……...- 146 -

Figure V. 6. Representative images of endothelial cells tube-like structures obtained from MSCs conditioned media cultured in each condition……..- 148 -

Figure VI. 1. Image of a representative assembled device during cellular experiments and assembled 2D chips in all three geometries. Schematic representation of the mechanisms of cell seeding in the initial stage of the experiment and the process of VEGF transport into the HUVECs compartment……- 173 -

Figure VI. 2. Overview of the photolithography and soft lithography procedures, representing type III…….- 175 -

Figure VI. 3. Molding fabrication procedures for the 3D single channel model of magnetic gelatin and representative stress-strain curves for the mechanical characterization by compression testing of the magnetic gelatin…… - 177 -

Figure VI. 4. Top view phase contrast images of HUVECs migration overtime on 2D chips. Fluorescent imaging of viable HUVECs to assess adherence and proliferation under perfusion mode for 2D and 3D models……. - 180 -

Figure VI. 5. Confocal imaging of endothelial tissue and sprout ramifications for 2D chips using VEGF supplementation strategy. Characterization of viable HUVECs proliferation and tissue formation under perfusion, VEGF supplementation and HUVECs multiple seeding conditions……. - 183 -

Figure VI. 6. Computational models of 2D chips for VEGF time-dependent diffusion from the media channels to the endothelial cell (HUVECs) culture compartment through the hydrogels. Computational fluid flow modeling to predict linear velocities distribution within the 2D media channels and subsequent validation……... - 186 -

Figure VI. 7. Confocal imaging of MSCs and HUVECs co-culture on the 2D and 3D models, with magnetic field application on day 6 for 24 h. Immunofluorescence images of the co-culture to distinguish the population of HUVECs and MSCs……. - 188 -

Figure VI. 8. Quantification of Endothelin-1 on 2D chips and 3D models comparing the effects of static and perfusion mode on the stimulation of endothelium tissue formation, and the impact of different fabrication techniques of 2D chips on the increase of Endothelin-1 concentration (no magnetic field applied). Influence of the application of magnetic stimulation on the 24h of the experiment on 2D and 3D Models using perfusion mode. (No multiple HUVECs seeding and VEGF supplementation strategies were followed)……..- 190 -

Figure VI. S1. Schematic representation of the sequential steps of the first days of experiment, including the patterning of the chips with hydrogels (gelatin and matrigel), the cell culture pre-conditioning and the cell seeding on the chips…….- 199 -
Figure VI. S2. Fluorescence Imaging for the optimization procedures described in Table 1, featuring the representative images for the effects reported with the different strategies on 3D models and 2D chips…….- 199 –

Figure VI. S3. Parameters and mathematical assumptions of the computational model for VEGF diffusion on 2D chips……... - 200 -

Figure VII. 1. Representation of the models used for HUVECs and MSCs co-culture in a ischemic disease modeling (multi-branched mesoscale model, linear shaped 2D chip, commercial insert Transwell)…… - 205 -

Figure VII. 2. Representation of the effect induced by hypoxic/ reperfusion condition on a co-culture of MSCs and HUVECs in 2D chips of PDMS…… - 213 -

Figure VII. 3. Representation of the effect induced by hypoxic/ reperfusion condition on a co-culture of MSCs and HUVECs in a mesoscale device featuring the hierarchical organization of the native blood vessels……..- 214 -

Figure VII. 4. Representation of the effect induced by hypoxic/ reperfusion condition on a co-culture of MSCs and HUVECs using a commercial Transwell with a magnetic scaffold of gelatin to culture MSCs separately of the HUVECs, cultured in a standard polystyrene culture plate……..- 215 -

LIST OF TABLES

Table I. 1. Paracrine factors secreted by MSCs[15]. .....- 6 -

Table III. S1. Mass balance to trypsin in the supernatant and in the membrane during the OFF/ON variation of the magnetic field between 0 T and 1 T.....- 78 -

Table III. S2. Mass balance to trypsin in the supernatant and in the membrane during the OFF/ON variation of the magnetic field between 0 T and 0.45 T.....- 78 -

Table III. S3. Mass balance to trypsin in the supernatant and in the membrane during the ON/OFF variation of the magnetic field between 0 T and 0.45 T.....- 78 -

Table IV. S1. Supplementary sequences of the primers used for qRT-PCR analysis. .....- 125 -

Table IV. S2. Validation of the results through the quantification of metabolites released from the MSCs throughout the experiments (day 1 to 5). This table allows to conclude that the results obtained regarding the angiogenic expression and protein release of VEGF-A were not related to the stressful condition of the cells for depletion of glucose and nutrients. The MSCs values of lactate even after 5 days were still above 1 mM and the levels of lactate were satisfactory. .....- 126 -

Table IV. S3. Supplementary details from the inoculation process of CAM assay. The table features information regarding the number of inoculated eggs, the number of eggs that survived the process, the total number of embryos used for analysis and the total number of pairs. .....- 130 -

Table VI. 1. Experimental strategies applied on 2D and 3D models to promote angiogenic behaviour on HUVECs. Each model was assessed on stahes of vasculogenesis based on the the capacity of the HUVECs to adhere to the walls of the channels (A), the ability to migrate to the lumen region (M) and ultimately the capacity to form endothelial tissue (ET).....- 178 -

ABBREVIATIONS

A

ABS – Acrylonitrile butadiene styrene

Anti-Anti – Antibiotic-Antimycotic

B

BM – Bone Marrow

BSA – Bovine Serum Albumin

BHA - beta-Hydroxybutyric acid

C

CA – Contact angle

CM – Conditioned Media

CAM – Chick Chorioallantoic Membrane

CD14 – Cluster of differentiation 14

CD73 – Ecto-5'-nucleotidase

CD90 – Cluster of differentiation 90

CD105 – Endoglin

CD31 – Platelet Endothelial Cell Adhesion Molecule

D

DAPI – 4,6-diamino-2-phenylindole

DMEM – Dulbecco's Modified Eagle Medium

DNA – Deoxyribonucleic acid

E

ECM – Extracellular Matrix

EthD – Ethidium Bromide

ELISA – Enzyme-linked Immunosorbent Assay

F

FBS – Fetal bovine serum

FACS – Fluorescence activated cell sorting

bFGF – basic Fibroblast Growth Factor

FDA – Food and Drug Administration

Fe_3O_4 – Iron oxide

FABP4 – Fatty acid-binding protein

G

GA - Glutaraldehyde

GAPDH – Glyceraldehyde 3-phosphate dehydrogenase

GFP – Green Fluorescent Probe

H

HGF – hepatocyte Growth Factor

HCL – Hydrochloric acid

HLA-DR – Human leukocyte antigen D related

HUVECs – Human Umbilical Vein Endothelial Cells

HF – High Frequency

HLA-DR – Human Leukocyte antigen, MHC class II cell surface receptor

L

LF – Low frequency

M

MSCs – Mesenchymal Stromal Cells

MNPs – Magnetic Nanoparticles

MTT – 3-(4,5-Dimethylthiazol-2-yl)-2,5-Diphenyltetrazolium Bromide

MMP– Matrix metalloproteinase

mRNA – messenger Ribonucleic acid

MDC – Macrophage-derived chemokyne

N

N_2 – Nitrogen

NH_4OH – Ammonium hydroxide

NAC - nascent popypeptide-associated complex

P

PVA – Polyvinylalcohol

PBS – Phosphate buffered saline

PDMS – Polydimethilsiloxane

PCL – Polycaprolactone

PFA – Paraformaldehyde

PLA – Polylactic acid

PCR – Polymerase chain reaction

R

RNA – Ribonucleic acid

RT-pPCR – Real-time quantitative polymerase chain reaction

RGC32 – Response gene to complement 32

S

SD – Standard Deviation

SEM – Scanning electron microscopy

SPP1 – Secreted phosphoprotein 1

T

TEM – Transmission electron microscopy

TCP – Tissue culture polystyrene

T

VEGF – Vascular Endothelial Growth Factor

VSM – Vibrating Sample Magnetometer

Chapter I



Introduction

CHAPTER I – Introduction

This chapter describes the project motivation, presents the goals and introduces the research decisions of the investigation. The chapter finalizes with a brief dissertation overview.

I.1. Motivation and Project Aim

The constant dedication of researchers to unravel novel treatments and to provide an answer for cardiovascular diseases lies at the heart of the progressive advances in stem cell therapies and tissue engineering. Cardiovascular diseases are a group of diseases characterized by damages to the heart and blood vessels. Those are one of the highest causes of mortality at a value of approximately 30% worldwide, alongside with cancer[1,2]. The incidence of cardiovascular diseases is still rising, and among such conditions ischemic heart disease is currently the leading cause of death and disability worldwide, requiring novel therapies to both improve life quality and extend survival in the patient population[3].

Despite current options to re-perfuse occluded arteries, involving percutaneous coronary intervention and surgical procedures, these strategies are not able to reverse necrotic or ischemic tissue, which have the potential to be regenerated through the use of stem cells[4,5]. Alternative therapies have been studied to address the problem using strategies involving gene, protein and stem cell therapies to avoid scar formation and adverse remodeling. Tissue regeneration approaches using bone marrow stem cells have been reported to prevent endothelial tissue damage and cardiomyocyte loss[1,6].

Bone marrow-derived stem cells, including mesenchymal and hematopoietic stem cells, have been exhaustively tested in tissue/organ regeneration in pre-clinical and clinical studies. Mesenchymal stromal cells (MSCs) are classified as multipotent adult stem-like cells with the potential to differentiate into a variety of cell types[7]. Initially identified in bone marrow, these cells can also be found in umbilical cord blood, adipose tissue, and the heart[8]. MSCs have been reported to be associated with tissue remodeling, addressing rehabilitation of cardiac infarct conditions through differentiation into

cardiomyocyte and endothelial phenotypes in rodent models of myocardial infarction, also being responsible for improving myocardial perfusion and functional capacity upon MSCs autologous infusion[8,9,10].

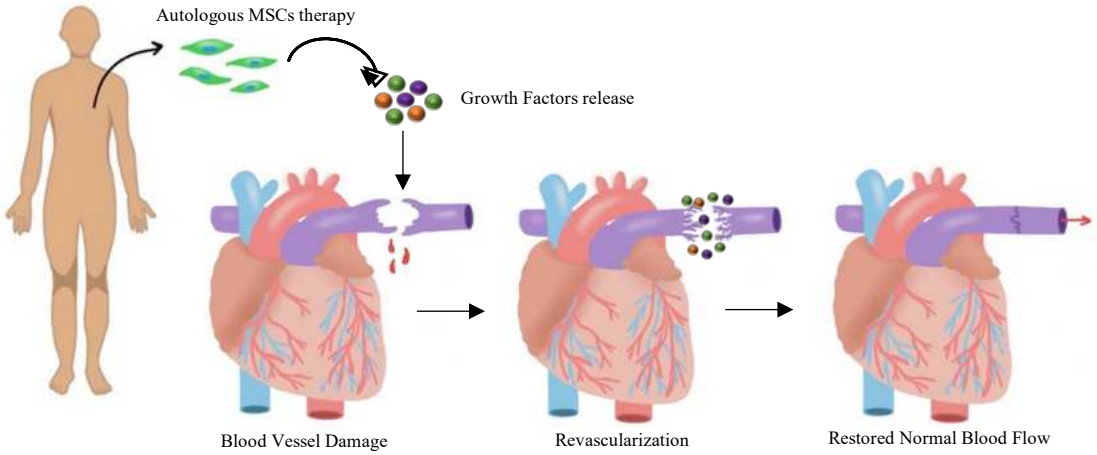


Figure I. 1. Representation of MSCs therapy for cardiovascular disease, showing the stages of cardiac repair.

In cardiac repair, many strategies for cardiovascular regeneration have been explored, particularly through stem cells infusion via direct and indirect mechanisms, including cardiac and vascular differentiation and paracrine effects (Figure I. 1)[11,12]. Among these mechanisms, the activation of endogenous precursors to promote neovascularization, the favorable modulation of extracellular matrix and the inhibition of apoptosis or hypertrophy have been the most reported. Particularly, the paracrine effect of MSCs secreted molecules has been proposed as the reason behind the therapeutic effect of transplanted MSCs and other stem cells on injured tissues[12,13]. This effect refers to the release of factors such as cytokines, chemokines, growth factors, exosomes or microparticles to the damaged tissue by the transplanted stem cells[13]. Those molecules are signaling factors responsible for initiating various processes of restoration of the tissue[13]. A list of the factors released from MSCs are presented on Table I. 1, highlighting the importance of these cells in therapeutic treatments for cardiovascular diseases.

However, despite intense progress over the last 15 years, the stem cell therapy for cardiovascular disease remains a young science, with mostly small clinical trials and inconclusive results.

In fact, one of the major issues surrounding the development of cell therapies, such as MSCs therapy, is that, despite evoking a positive response, long-term engraftment and

persistence of these cells is rare[14]. Although this thesis does not endeavor into clinical translation, a future perspective of this work would be related with the implantation of a vascularized engineered tissue, loaded with MSCs, able to maintain a continuous release of growth factors to the injury site for the amount of time needed to trigger the endothelial cells of the native nearby tissue towards angiogenesis in a strategy for tissue repair and remodeling. Our followed approach to develop a system able to non-invasively trigger angiogenesis in endothelial cells through MSCs stimulation by increasing the release of growth factors envisage a novel treatment option for these diseases as our motivation.

Throughout this project we aim to develop an original research strategy using non-invasive low intensity magnetic fields to trigger tissue repair, namely by promoting angiogenesis. This magnetic concept was initially inspired by reports stating the mechanic behavior of ferrogels and the possibility to induce hydrogel deformation, mostly described as magnetic responsiveness through contraction/retraction movements of the ferrogel[15,16,17,18]. Hence the magnetic field functioning as an actuator was a promising research tool to investigate the influence of these magnetic-induced mechanic effects on cellular adhesion and behavior. So far, magnetic control of cellular processes has been described through the use of biofunctional nanoparticles[19], involving magnetic field gradients to promote cancer cell death[20] or to remotely regulate adrenal hormones release[21], among other clinical applications for arthritis, chronic pain, hyperthermia treatments, drug release systems and magnetic resonance imaging[22,23].

Since the priority in tissue repair procedures depends on the release of growth factors, our strategy focus in directly stimulating MSCs into cellular stress, via magnetic exposure, to enhance the release of angiogenic molecules to the media. As an addition, the mechanical stimuli induced by ferrogels on the vascularization phenomena could also potentially be compared to the blood circulation, propelled by contraction/ retraction movements of the blood vessels, which might also result in the stimulation of endothelial cells for a further improved magnetic effect through co-cultures of MSCs and HUVECs[24]. Moreover, during vascularization processes, the behavior of endothelial cells is highly influenced not only by vascular permeability, nutrient transport and growth factor concentration gradients[25] but also by mechanical stimulation such as shear stress and circumferential strains[26]. This highlights the interest of using ferrogels, which can undergo mechanical changes upon magnetic exposure, in this project to explore novel therapies for cardiovascular diseases.

The magnetic field role on molecular and cellular interaction, directed towards angiogenesis prompting, was overall the research question during this investigation.

Table I. 1. Paracrine factors secreted by MSCs[15].

Secreted Factor	Function
Proangiogenesis	
• **FGF-2**	• Endothelial and smooth muscle proliferation;
• **FGF-7**	• Endothelial cell proliferation
• **MCP-1**	• Angiogenesis through recruitment of monocytes
• **PDGF**	• Smooth muscle proliferation
• **PIGF**	• Angiogenesis promotor
• **TGF- ß**	• Vessel maturation
• **VEGF**	• Endothelial cell proliferation, migration, tube formation
Remodeling of extracellular matrix	
• **MMP1**	• Loosens matrix, tubule formation
• **MMP2**	• Loosens matrix, tubule formation
• **MMP9**	• Loosens matrix
• **PA**	• Degrades matrix
• **TNF- α**	• Degrades matrix, modulates cell proliferation
Stem cell proliferation, recruitment, and survival	
• **bFGF**	• Proliferation of endothelial and smooth muscle cells
• **G-CSF**	• Proliferation and differentiation of neutrophils
• **IGF-1**	• Cell proliferation, inhibition of apoptosis
• **M-CSF**	• Proliferation and differentiation of monocytes
• **Tß4**	• Cell migration
• **SDF**	• Progenitor cell homing
• **SFRP1**	• Cell development
• **SFRP2**	• Inhibition of apoptosis, cell development
Immunomodulatory	
• **HO1**	• Inhibition of T-cell proliferation
• **HGH**	• Inhibition of $CD4^+$ T-cell proliferation
• **IDO**	• Inhibition of innate/adaptive immune cell proliferation
• **iNOS**	• Inhibition of inflammation
• **IL-6**	• Regulation of inflammation, VEGF induction
• **PGE_2**	• Inhibition of inflammation

I.2. Project Strategy and Research Decisions

To accomplish the goal of promoting angiogenesis to repair damaged tissue, we devised a strategy to remotely control, in a non-invasively mode, the sprouting phenomena in endothelial cells. Human Umbilical Vein Endothelial Cells (HUVECs) were used as models for endothelial cells. As a tool for remote control, magnetic fields, at low intensity, were applied to initiate a magnetic response from the hydrogel embedded with iron oxide nanoparticles (Fe_3O_4). To actively influence cell culture, the magnetic field should be combined with a magnetic scaffold to provide cell adhesion and support while being able to stimulate the cells through reversible structural modifications (e.g. topographic changes/ roughness, wettability, swelling) and changes in mechanical properties ascribed to the magnetic forces. To achieve this effect, polymeric hydrogels were selected due to their elasticity and potential for a faster magnetic responsiveness[28].

This thesis research questions and strategies are organized as:

Part I.

Proteins play an important role on cell regulation processes. According to many reports, protein interactions are responsible to mediate focal cell adhesions and thus alter cell response and behavior[29,30,31]. Therefore, the first research question was to assess remote control of biomolecules (e.g. protein) interactions when adsorbed at the surface of a synthetic hydrogel (PVA). The proteins used as models in the experimental trials were trypsin and albumin. Trypsin (23 kDa[32], pI: 10.1-10.5[33]) is an enzyme responsible for the process of cell tissue detachment, but also involved in catalytic and bioseparation processes. Bovine serum albumin (BSA) (66 kDa[34], pI: 4.7-4.9[34]) is a globular protein commonly present on serum, with physiological role of transport of hormones and regulation of pH and osmotic pressure[35]. BSA and Trypsin were used to study the ability to magnetically control protein adsorption to the scaffold. Fluorescently labeled BSA with Alexa Fluor 488 (green) was used to identify the capacity of the protein to migrate within the hydrogel. This first part of the work intended to provide a better knowledge on the magnetic responsiveness of the PVA embedded with magnetic nanoparticles and evaluate the capacity to use magnetic fields to regulate protein sorption/desorption by cyclic variation of the magnetic field.

Part II.

The second part of this project explores the biological impact of magnetic remote forces and magnetic polymers (acting as scaffolds for cell culture) on cell behavior. The study envisages the regulation of vascularization mechanisms hoping to identify a potential application for the regeneration of damaged tissues in cardiovascular diseases.

These studies aimed at understanding the mechanisms involved in the stimulation of the angiogenic behavior on the cells directly or through mechanotransduction phenomena (conversion of external mechanical stimuli into intracellular electrical or chemical signals[36]), induced by the combination of magnetic forces and magnetic scaffolds.

To study the effect of magnetic stimulation on angiogenesis, two strategies were followed, investigating the magnetic impact on: (1) endothelial cells and (2) MSCs. Concerning studies on endothelial progenitor cells, HUVECs were used as model cells to directly induce angiogenesis. However, and although HUVECs are known to be sensitive to shear stress stimulation[37,38], they did not show a magnetic response in preliminary experiments. The angiogenic potential of MSCs was also studied when the cells were exposed to magnetic stimulation. In the literature, MSCs role in vascular repair and regeneration through the secretion of growth factors (Table I.1) such as vascular endothelial growth factor (VEGF) has been previously studied[13] whereas the secretion of VEGF-A, among other factors, has been reported to enhance *de novo* formation of stable vasculature by endothelial cells in several vasculogenesis models *in vitro* and *in vivo*[39,40].

MSCs obtained from bone marrow were selected as model cells for this study. However, other MSCs sources, such as adipose tissue and umbilical cord blood, could have been explored. In fact, experimental trials were performed with umbilical cord blood and adipose tissue MSCs but the results were not as promising as those obtained from the bone-marrow source, in particular regarding cell adhesion to the scaffolds and magnetic response. Many other studies have also described bone-marrow MSCs as the most prone to provide external stimulation responses[41,42,43,44], thus supporting our choice.

Regarding the magnetic field possible impact on MSCs, three mechanisms are the most probable to potentiate an effect. First, the application of an external force on the integrin-ligand bond (focal adhesion points on the cell surface between integrins and the cytoskeleton of the ECM) creates an external pull, which is transferred across the cell membrane and results in cytoskeleton deformation[45]. The second mechanism could be associated with the deformation of the plasma membrane mediating ion flux into/ out of

the cell through stretch-activated ion channels or g-protein coupled receptors[42]. Finally, the primary cilium, an immotile microtubule-based organelle has been recently implicated as a mechanosensory structure in several cell types including MSCs[46]. Based on these reported possible impacts, our study observed MSCs behavior after culture on magnetic scaffolds and exposure to magnetic fields in terms of proliferation curves, viability, cell alignment and distribution, multipotency and overall secretion of angiogenic molecules.

Whether magnetic fields alone would be able to drive MSCs into releasing sufficient amount of growth factors to trigger angiogenesis *in vitro,* with ability to be translated to an *in vivo* environment in the future, was the main research question of the work. Hence, the effect of direct static magnetic fields or of magnetically activated ferrogel scaffolds as agents to stimulate MSCs was investigated regarding the secretion of angiogenic-regulator molecules, such as VEGF-A. The conditioned media of MSCs, enriched in growth factors, was then used to promote the formation of microvessel-like structures from human umbilical vein endothelial cells (HUVECs), offering insight for a potential co-culture of MSCs and HUVECs for vascularization applications.

The hypothesis of achieving a co-culture of HUVECs and MSCs for cardiac regeneration has also been recommended on previous works based on how bone marrow MSCs yielded a decrease in myocardial scarring by 3 months, thus highlighting the beneficial tissue remodeling of MSCs[47] and its importance in soft tissue repair[41]. Nevertheless, this hypothesis was not pursued in this stage of the project, where HUVECs were indirectly stimulated by the magnetic field through the conditioned media of MSCs.

Research strategies concerning magnetic scaffolds as a support for MSCs adhesion and growth, and also to be used as a mechanotransduction tool to mediate the magnetic forces, involved the use of two materials. Magnetic PVA synthetic hydrogel, previously used on the protein sorption studies (**I**), was here developed for cell studies. However, MSCs showed to have poor adhesion to PVA, a synthetic polymer, even after using coatings of fibronectin, collagen or laminin. Consequently, a natural polymer (gelatin from porcine skin), derived from denaturated collagen, was used for cell culture experiments. The two scaffolds with different bio-affinity were used to compare the effect of the magnetic fields on MSCs, consequently promoting different types of cell organization. The gelatin presented ideal properties as a scaffold and has been largely used in tissue engineering due to its regenerative and therapeutic characteristics ascribed from the similarities with the extracellular matrix. Important reported properties for its

use in scaffold production are its biocompatibility, biodegradability, low antigenicity, and accessible functional groups that allow for chemical interactions with other biomolecules, as well as material cost-effectiveness[48]. As gelatin material is also classified as a hydrogel, we expected to obtain similar magnetic responsiveness to the PVA when used with ferromagnetic nanoparticles.

Another research decision was related with the experimental time. Preliminary trials were performed with cell cultures exposed to magnetic fields over times ranging from 30 min to 7 days, to conclude that major effects were obtained after 24 h of exposure. Still, some experiments were also performed after 5 days for a better understanding of the importance of the exposure time on cell behavior. Those assays also offer insights on the reversibility of the effects induced on the cells, and eventual magnetic cytotoxicity. Cytotoxic effects after prolonged magnetic exposure have been reported using static magnetic fields[49,50,51] or magnetic field gradients[20,52]. Those reports indicated beneficial effects up to 24 h with genotoxicity and cell death being observed after longer periods. In resume, the scope of the project is to enhance angiogenesis by magnetic stimulation, aiming to provide novel cellular therapies for cardiovascular diseases. The study is focused on investigating possible improvement of VEGF-A secretion from MSCs under magnetic stimulus directly or through scaffold mechanotransduction. First, the effect of the magnetic field on MSCs behavior was evaluated based on its capacity to express different angiogenic factors presented on Table I.1, such as VEGF-A, basic Fibroblast Growth Factor (bFGF) and hepatocyte growth factor (hGF). Nonetheless, the dominance of the magnetic impact on VEGF secretion from MSCs over the other studied angiogenic factors allowed for further work focusing solely on this factor. Moreover, such studies were then performed assessing the impact of MSCs secretome on the formation of new microvessels by HUVECs through both *in vitro* and *ex vivo* experiments.

Part III.

The project then evolved into exploring the possibility to modulate cellular angiogenic behavior by manipulating magnetic field parameters. The biological impact of the magnetic field intensity on the cells was studied using neodymium magnets able to produce an intensity of 0.08 T and 0.45 T. Moreover, the effect of different frequency regimes, directly or through activation of a magnetic scaffold of gelatin, on cellular behavior was also analyzed.

These studies were motivated by magnetic pulsed therapy which is known to be used for the clinical treatment of chronic and acute muscular pain[53,54], and has also been a topic of discussion for researchers due to its impact in cell life, such as involvement in cellular membrane magneto-mechanical stress, thus reflecting on intracellular mechanisms with the modulation of membrane ion channels[55]. Pulsed magnetic fields were also reported to be responsible for the suppression of cell growth due to magnetic pressure, for magnetically inducing cell division and reprogramming, and also impacting on cellular machinery with the migration of membrane receptor proteins[55,56]. Considering that previous studies reported both beneficial and negative impacts of pulsed magnetic fields in biological applications, the research question here addressed is whether magnetic field intensity and static or pulsed magnetic stimulation have different effects on the angiogenic behavior of MSCs.

This study investigates the performance of static magnetic regimes on cell cultures continuously exposed to a specific magnetic field intensity (0.08 T or 0.45 T), against dynamic regimes obtained by cyclic variation of the magnetic field between OFF (no magnetic application) and ON stages (magnetic exposure with an intensity of 0.08 T or 0.45 T). Two different dynamic regimes were considered, one with lower frequency (LF) and another with higher frequency (HF), leading to different periods of exposure of the cells to the magnetic field. The investigation followed similar experimental design as described previously (**I**), mainly concerning the evaluation of MSCs angiogenic behavior with magnetic exposure of 24h. Ultimately, the study investigates the possibility to manipulate angiogenesis positively or negatively using different magnetic field regimes. The results showed the potential to modulate the tissue according with the target disease (e.g. enhancing vascularization to treat cardiovascular diseases or inhibiting angiogenesis to reduce tumor growth).

Part IV.

The part IV of this thesis concerns integration of the magnetic gelatin scaffolds in a new design of perfusion vascular system on the design of perfusion vascular systems. The development of this system aims to replicate the hierarchical complexity and dimensions of the native blood vessels and simulate the fluidic conditions of the blood stream. This part of the work was developed in the MCS (Mesoscale Chemical Systems) group in the University of Twente (The Netherlands) headed by Prof. Han Gardenier, specialized in microfluidic design and fabrication.

Different systems were designed, developed and assessed. Microfluidics technology was applied to the macroscale in 2D models of blood vessels fabricated in PDMS (polydimethylsiloxane). With these 2D models, the impact of the channel geometry and configuration in the cellular biological behavior was explored using three different designs and methodologies, including the fabrication of individualized cell compartments through incorporation of capillary barriers in the PDMS construct. The second fabrication approach was used to obtain 3D single-channel blood vessels made of magnetic gelatin following molding procedures to mimic the inner and outer diameters of the largest arteries and veins (aorta and vena cava).

During this study, our knowledge of magnetic stimulation effect on cells (**I, II, III**) was applied by patterning the 2D chips, and fabricating the 3D models, with magnetic gelatin for MSCs adhesion and support. In this work, several optimization strategies were initially followed using HUVECs to select the best conditions to promote cell adhesion and the formation of endothelial tissue on the chips. MSCs were later used with HUVECs in co-culture experiments for a vascularization proof of concept using magnetic stimulation. Conclusively, this part of the study provided *in vitro* models for vascularization and defined platforms for disease modeling of cardiovascular conditions such as cardiac ischemia.

The final part of this study concerns the development of an *in vitro* hypoxic/ re-oxygenation model of vascular ischemia. The efficiency to induce vascular ischemia condition on a novel mesoscale design was compared with: 2D blood vessel models and commercial inserts for disease modeling. The mesoscale chip was developed with rounded channels to feature the interconnected hierarchical ramifications of average-sized arteries/ veins and arterioles/venules in a complex vascular network model. The fabrication of the mesoscale model involved the layer-by-layer concept by combining and bonding two mirrored parts of the model and filling the lower half of the construct with magnetic gelatin. This final part of the project explored the possibility to revert the damage induced on blood vessels tissue by ischemia using magnetic stimulation, already known for enhancing angiogenic behavior, and thus restore normal circulation.

As a final remark, the work developed over these stages hoped to elucidate avenues of regenerative and cardiovascular disease control by modulating cell fate and behavior through magnetic stimulation (Figure I. 2).

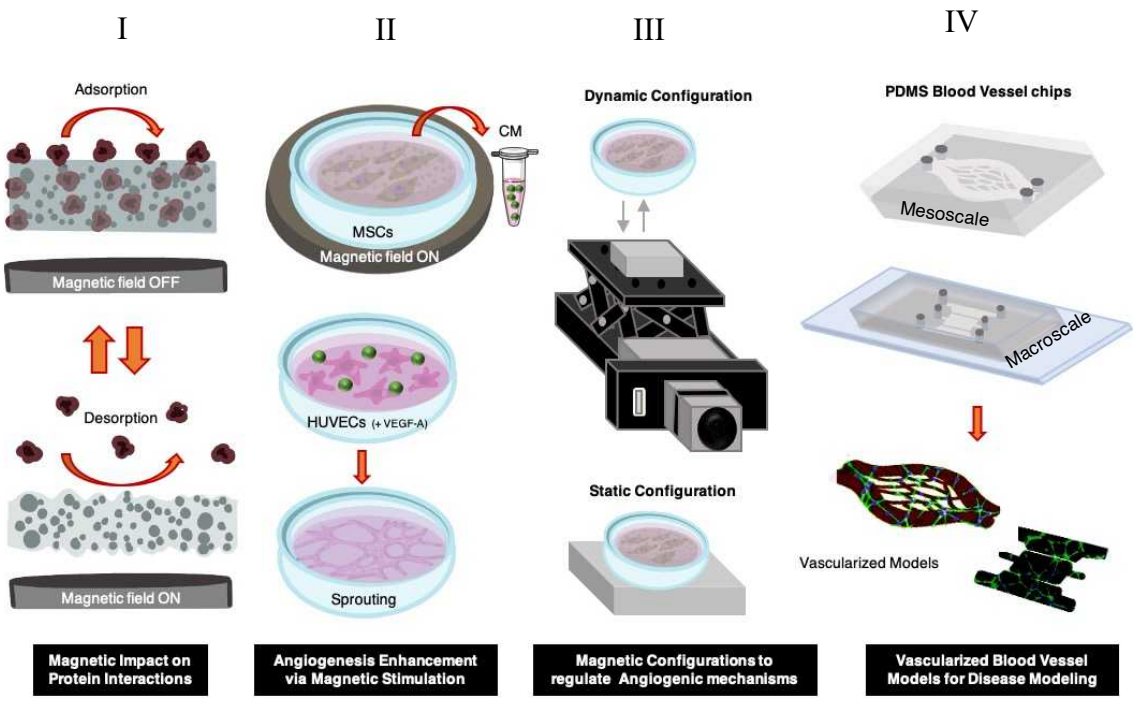


Figure I. 2. Illustration of the sequential stages of the work developed during this PhD project. Adapted from [57].

I.3. Dissertation Overview

This thesis is organized in eight chapters. **Chapter 1** describes the motivation of this work alongside with the project aim and major research decisions are provided in the contextual information of this chapter, finalizing with a brief thesis overview.

Following this chapter, **Chapter 2** presents a state of the art describing the most recent advances of the use of magnetic fields in tissue engineering and regenerative medicine, along with literature reported advances of the main concepts explored in the thesis.

Chapter 3 presents and discusses the results on the capacity to magnetically modulate biomolecules sorption at the surface of a magnetic hydrogel of PVA. The work suggests the potential capability of magnetic hydrogels to control tissue engineering processes/ mechanisms based on an efficient regulation of protein adhesion/sorption to tissue scaffolds.

Chapter 4 explores the use of an external magnetic field to stimulate MSCs, cultured on top of magnetic scaffolds, into increasing the secretion of growth factors (e.g. VEGF-A, bFGF, hGF) to trigger the angiogenic behavior on HUVECs both *in vitro* and

in vivo. The study compares the efficiency of magnetic hydrogels made of PVA and gelatin, when used as scaffolds for MSCs, and shows the potential to manipulate cellular processes through short-term, static magnetic stimulation.

Chapter 5 gain additional insight on the effect of different magnetic field regimes on MSCs as a stimulation for VEGF-A production. Within this chapter, the optimization of this effect and the possibility to modulate cell angiogenic behavior through manipulation of the magnetic field intensity, or by using dynamic frequency variation regimes, was explored. The different regimes aimed to compare the impact on the regulation of vascularization mechanisms under static mode, ensuring continuous exposure of the cell culture to a constant magnetic field, or under pulsed magnetic stimulation, achieved by cyclic variation of the magnetic field at different variation frequencies.

In **Chapter 6** the knowledge obtained from previous chapters is applied for the development of blood vessel *in vitro* models in a proof of concept of the magnetic stimulation to enhance angiogenesis on HUVECs. During this chapter, the effect of the geometry of the blood vessel models, perfusion mode and angiogenic strategies in co-cultures (MSCs and HUVECs) exposed to magnetic stimulation, was studied. In this chapter, 2D models, following microfluidic technology, and 3D models, made of magnetic gelatin, were developed to recapitulate artery and vein dimensions, aiming to induce the formation of endothelial tissue.

Chapter 7 investigates the efficiency of a vascular ischemic disease model, comparing the performance of a commercial construct suited for disease modeling with the new 2D chips designs (Chapter 6), but updated to introduce a device with a multi-branched vascular network geometry. The study investigates the effect of the application of the magnetic field on an ischemia disease model to revert the tissue damage created by disease induction. This chapter exploits the results obtained on the previous studies to prove the efficiency of the magnetic field, when combined with magnetic scaffolds, as a promising therapeutic alternative to treat vascular ischemia.

Finally, major conclusions, project limitations and future directions for further research are discussed in **Chapter 8**.

I. References

1. Sun, R. *et al.* Advances in stem cell therapy for cardiovascular disease (Review). *Int. J. Mol. Med.* **38**, 23–29 (2016).
2. Taylor, D. A. & Robertson, M. J. The basics of cell therapy to treat cardiovascular disease: One cell does not fit all. *Rev. Esp. Cardiol.* **62**, 1032–1044 (2009).
3. Terashvili, M. & Bosnjak, Z. J. Stem Cell Therapies in Cardiovascular Disease. *J. Cardiothorac. Vasc. Anesth.* **33**, 209–222 (2019).
4. Briffa, T. *et al.* Long term survival after evidence based treatment of acute myocardial infarction and revascularisation: follow-up of population based Perth MONICA cohort, 1984-2005. *BMJ* **338**, b36–b36 (2009).
5. Faiella, W. & Atoui, R. Therapeutic use of stem cells for cardiovascular disease. *Clin. Transl. Med.* **5**, 34 (2016).
6. Zannad, F., Agrinier, N. & Alla, F. Heart failure burden and therapy. *EP Eur.* **11**, v1–v9 (2009).
7. Pontikoglou, C., Deschaseaux, F., Sensebé, L. & Papadaki, H. A. Bone Marrow Mesenchymal Stem Cells: Biological Properties and Their Role in Hematopoiesis and Hematopoietic Stem Cell Transplantation. *Stem Cell Rev. Reports* **7**, 569–589 (2011).
8. Chen, S. *et al.* Effect on left ventricular function of intracoronary transplantation of autologous bone marrow mesenchymal stem cell in patients with acute myocardial infarction. *Am. J. Cardiol.* **94**, 92–95 (2004).
9. Hare, J. M. *et al.* Comparison of allogeneic vs autologous bone marrow–derived mesenchymal stem cells delivered by transendocardial injection in patients with ischemic cardiomyopathy: the POSEIDON randomized trial. *JAMA* **308**, 2369–2379 (2012).
10. Siamak, D. *et al.* Mesenchymal Progenitor Cells Differentiate into an Endothelial Phenotype, Enhance Vascular Density, and Improve Heart Function in a Rat Cellular Cardiomyoplasty Model. *Circulation* **108**, II-253-II–258 (2003).
11. Humar, R., de Miguel, L. S., Kiefer, F. N. & Battegay, E. J. Formation of new blood vessels in the heart can be studied in cell cultures. *ALTEX Altern. zu Tierexperimenten* **24 Spec No**, 35–38 (2007).
12. Leri, A., Kajstura, J. & Anversa, P. Cardiac Stem Cells and Mechanisms of Myocardial Regeneration. *Physiol. Rev.* **85**, 1373–1416 (2005).

13. T., K. *et al.* Marrow-Derived Stromal Cells Express Genes Encoding a Broad Spectrum of Arteriogenic Cytokines and Promote In Vitro and In Vivo Arteriogenesis Through Paracrine Mechanisms. *Circ. Res.* **94**, 678–685 (2004).
14. Copland, I. B. Mesenchymal stromal cells for cardiovascular disease. *J. Cardiovasc. Dis. Res.* **2**, 3–13 (2011).
15. Filipcsei, G., Csetneki, I., Szilágyi, A. & Zrínyi, M. Magnetic field-responsive smart polymer composites. *Adv. Polym. Sci.* **206**, 137–189 (2007).
16. Szabó, D., Szeghy, G. & Zrínyi, M. Shape transition of magnetic field sensitive polymer gels. *Macromolecules* **31**, 6541–6548 (1998).
17. Zrínyi, M. Intelligent polymer gels controlled by magnetic fields. *Colloid Polym. Sci.* **278**, 98–103 (2000).
18. Zhou, G. Y. & Jiang, Z. Y. Deformation in magnetorheological elastomer and elastomer-ferromagnet composite driven by a magnetic field. *Smart Mater. Struct.* **13**, 309–316 (2004).
19. Monzel, C., Vicario, C., Piehler, J., Coppey, M. & Dahan, M. Magnetic control of cellular processes using biofunctional nanoparticles. *Chem. Sci.* **8**, 7330–7338 (2017).
20. Subramanian, M., Miaskowski, A., Jenkins, S. I., Lim, J. & Dobson, J. Remote manipulation of magnetic nanoparticles using magnetic field gradient to promote cancer cell death. *Appl. Phys. A* **125**, 226 (2019).
21. Rosenfeld, D. *et al.* Transgene-free remote magnetothermal regulation of adrenal hormones. *Sci. Adv.* **6**, eaaz3734 (2020).
22. Colbert, A. P. *et al.* Static magnetic field therapy: a critical review of treatment parameters. *Evid. Based. Complement. Alternat. Med.* **6**, 133–139 (2009).
23. Quittan, M., Schuhfried, O., Wiesinger, G. F. & Fialka-Moser, V. [Clinical effectiveness of magnetic field therapy--a review of the literature]. *Acta Med. Austriaca* **27**, 61–68 (2000).
24. Lee, J., Packard, R. R. S. & Hsiai, T. K. Blood flow modulation of vascular dynamics. *Curr. Opin. Lipidol.* **26**, 376–383 (2015).
25. Senger, D. R. *et al.* Stimulation of endothelial cell migration by vascular permeability factor/vascular endothelial growth factor through cooperative mechanisms involving the alphavbeta3 integrin, osteopontin, and thrombin. *Am. J. Pathol.* **149**, 293–305 (1996).
26. Dartsch, P. C. & Betz, E. Response of cultured endothelial cells to mechanical

stimulation. *Basic Res. Cardiol.* **84**, 268–281 (1989).

27. A., T. B. *et al.* Preclinical Studies of Stem Cell Therapy for Heart Disease. *Circ. Res.* **122**, 1006–1020 (2018).
28. Okay, O. Hydrogel Sensors and Actuators. *Hydrogel Sensors and Actuators* **6**, 1–15 (2010).
29. Kim, B. & Emmons, S. W. Multiple conserved cell adhesion protein interactions mediate neural wiring of a sensory circuit in C. elegans. *Elife* **6**, e29257 (2017).
30. Gallegos, L. L. *et al.* A protein interaction map for cell-cell adhesion regulators identifies DUSP23 as a novel phosphatase for β-catenin. *Sci. Rep.* **6**, 27114 (2016).
31. Yang, X., Hou, D., Jiang, W. & Zhang, C. Intercellular protein–protein interactions at synapses. *Protein Cell* **5**, 420–444 (2014).
32. CUNNINGHAM, L. W. J. Molecular-kinetic properties of crystalline diisopropyl phosphoryl trypsin. *J. Biol. Chem.* **211**, 13–19 (1954).
33. Walsh, K. A. B. T.-M. in E. [4] Trypsinogens and trypsins of various species. in *Proteolytic Enzymes* **19**, 41–63 (Academic Press, 1970).
34. Ota, A. *et al.* Using SRM-MS to quantify nuclear protein abundance differences between adipose tissue depots of insulin-resistant mice. *J. Lipid Res.* **56**, 1068–1078 (2015).
35. Medda, L., Monduzzi, M. & Salis, A. The molecular motion of bovine serum albumin under physiological conditions is ion specific. *Chem. Commun.* **51**, 6663–6666 (2015).
36. Martinac, B. Mechanosensitive ion channels: molecules of mechanotransduction. *J. Cell Sci.* **117**, 2449 LP – 2460 (2004).
37. Sheng, X., Liu, Y., Wang, J., Li, X. & Shu, B. HUVECs respond to low shear stress stimulation by activating Wnt/β-catenin signaling pathway. *Xi Bao Yu Fen Zi Mian Yi Xue Za Zhi* **33**, 1657–1661 (2017).
38. dela Paz, N. G., Walshe, T. E., Leach, L. L., Saint-Geniez, M. & D'Amore, P. A. Role of shear-stress-induced VEGF expression in endothelial cell survival. *J. Cell Sci.* **125**, 831–843 (2012).
39. Watt, S. M. *et al.* The angiogenic properties of mesenchymal stem/stromal cells and their therapeutic potential. *Br. Med. Bull.* **108**, 25–53 (2013).
40. Pankajakshan, D. & Agrawal, D. K. Mesenchymal Stem Cell Paracrine Factors in Vascular Repair and Regeneration. *J. Biomed. Technol. Res.* **1**, 1–21 (2014).
41. Murphy, M. B., Moncivais, K. & Caplan, A. I. Mesenchymal stem cells:

environmentally responsive therapeutics for regenerative medicine. *Exp. Mol. Med.* **45**, e54–e54 (2013).

42. Delaine-Smith, R. M. & Reilly, G. C. Mesenchymal stem cell responses to mechanical stimuli. *Muscles. Ligaments Tendons J.* **2**, 169–180 (2012).
43. Pittenger, M. F. *et al.* Mesenchymal stem cell perspective: cell biology to clinical progress. *npj Regen. Med.* **4**, 22 (2019).
44. Leppik, L., Oliveira, K. M. C., Bhavsar, M. B. & Barker, J. H. Electrical stimulation in bone tissue engineering treatments. *Eur. J. Trauma Emerg. Surg.* **46**, 231–244 (2020).
45. Liedert, A., Claes, L. & Ignatius, A. Signal Transduction Pathways Involved in Mechanotransduction in Osteoblastic and Mesenchymal Stem Cells. in *Mechanosensitive Ion Channels* **1**, 253–265 (2008).
46. Malone, A. M. D. *et al.* Primary cilia mediate mechanosensing in bone cells by a calcium-independent mechanism. *Proc. Natl. Acad. Sci. U. S. A.* **104**, 13325–13330 (2007).
47. R., W. A. *et al.* Intramyocardial Stem Cell Injection in Patients With Ischemic Cardiomyopathy. *Circ. Res.* **108**, 792–796 (2011).
48. Afewerki, S., Sheikhi, A., Kannan, S., Ahadian, S. & Khademhosseini, A. Gelatin-polysaccharide composite scaffolds for 3D cell culture and tissue engineering: Towards natural therapeutics. *Bioeng. Transl. Med.* **4**, 96–115 (2018).
49. Dornelles, E. B. *et al.* Cytotoxic effects of moderate static magnetic field exposure on human periphery blood mononuclear cells are influenced by Val16Ala-MnSOD gene polymorphism. *Environ. Sci. Pollut. Res. Int.* **24**, 5078–5088 (2017).
50. Lin, C.-T. *et al.* Long-term continuous exposure to static magnetic field reduces popolysaccharide-induced cytotoxicity of fibroblasts. *Int. J. Radiat. Biol.* **84**, 219–226 (2008).
51. Ghodbane, S., Lahbib, A., Sakly, M. & Abdelmelek, H. Bioeffects of Static Magnetic Fields: Oxidative Stress, Genotoxic Effects, and Cancer Studies. *Biomed Res. Int.* **2013**, 602987 (2013).
52. Akimoto, T. *et al.* Alternating magnetic field enhances cytotoxicity of Compound C. *Cancer Sci.* **109**, 3483–3493 (2018).
53. Fernandez, M. I., Watson, P. J. & Rowbotham, D. J. Effect of pulsed magnetic field therapy on pain reported by human volunteers in a laboratory model of acute pain†. *BJA Br. J. Anaesth.* **99**, 266–269 (2007).

54. Abdulla, F. A. *et al.* Effects of pulsed low-frequency magnetic field therapy on pain intensity in patients with musculoskeletal chronic low back pain: study protocol for a randomised double-blind placebo-controlled trial. *BMJ Open* **9**, e024650 (2019).
55. Zablotskii, V., Polyakova, T., Lunov, O. & Dejneka, A. How a High-Gradient Magnetic Field Could Affect Cell Life. *Sci. Rep.* **6**, 37407 (2016).
56. Zablotskii, V. *et al.* Effects of high-gradient magnetic fields on living cell machinery. *J. Phys. D, Appl. Phys.* **49**, 23
57. Manjua, A. C., Alves, V. D., Crespo, J. G. & Portugal, C. A. M. Magnetic Responsive PVA Hydrogels for Remote Modulation of Protein Sorption. *ACS Appl. Mater. Interfaces* acsami.9b03146 (2019). doi:10.1021/acsami.9b03146

Chapter II



State Of The Art

CHAPTER II – State of the art

The present chapter presents a literature review on the main topics of the project, from magnetic fields applications and combination with smart hydrogels to the newest strategies to successfully trigger angiogenesis and finalizes with the recent advances on the biofabrication of blood vessel models.

State of the Art

II.1. Magnetic Field and Biological Applications

Magnetic forces play a crucial role in the daily life of living organisms through the synchronization with the earth's geomagnetic field (20-70 μT), which has been suggested to have contributed for human evolution and seasonal behavior (e.g. migration) of certain species[1,2].

In recent decades, extensive progress in industry and science has led to the development of equipment and devices able to generate static and electromagnetic fields. Hence, the vulnerability of biological tissues and cells, with diamagnetic properties, were directly exposed, raising questions as to whether magnetic forces would impact on human's health[3,4].

Even though poorly discussed, the action of magnetic field at the molecular level, in particular on cell communication, behavior and secretory activity, has been an investigation field showing rapid advances.

Despite the low diamagnetic susceptibilities of the cells, which translate in relatively small biological effects, some investigators believe that a sufficient magnetic gradient with the application of non-uniform magnetic field could potentially induce stronger effects in cell function, shape and spatial organization[5]. Ultimately understanding the mechanism behind magnetic physics would revolutionize the magneto therapy efficacy[6].

Notwithstanding the concerns on a potential negative impact of magnetic forces on biological tissues and cells, an increasing number of approved medical devices (e.g. neodymium magnets, magnetic nanoparticles and magnetic biomaterials) has allowed for

the application of magnetic field at the clinical level for acute and chronic pain treatment, repair of wounds and bone fractures, as well as destruction of cancer cells[7].

Over the years, the interest toward clinical application of magnetic and electromagnetic stimulation has increased worldwide. Magnetic and electromagnetic field are increasingly been utilized to treat musculoskeletal injuries in post-surgical, post traumatic and chronic wounds and reduction of edema. This represents a major therapeutic factor in the acceleration of pain and stress relief, and thus contribute to healing processes. However, their utilization will be facilitated by searching for biophysical mechanisms of action as well as by determining the exact dosimetry for the application[8].

The evaluation of whether static magnetic field therapy is efficient in humans depends on understanding and identifying the adequate dosages of static magnetic fields and treatment regimens and on analyzing the effect of the application of permanent magnets in humans[9].

Cardiovascular magnetic resonance imaging (MRI) evolved over the past decades from an effective research tool into a clinically proven, safe and comprehensive imaging modality. This technique provides anatomic and functional information in acquired and congenital heart disease and it is the most precise technique for quantification of ventricular volumes, function and mass[10].

Other clinical applications involving magnetic fluids, are increasingly used for clinical applications such as drug delivery, magnetic resonance imaging and magnetic fluid hyperthermia[11]. Hyperthermia has been developed as a cancer treatment for several decades and comprises the direct injection of superparamagnetic biocompatible nanoparticles into tumor tissue and their subsequent heating due to Brownian and Néel relaxation processes in an alternating magnetic field[11]. Depending on the applied temperature and the duration of heating, this treatment either results in direct killing of tumor cells or makes the cells more susceptible to concomitant radio or chemotherapy[11]. Magnetically induced interstitial hyperthermia is particularly relevant for deep-seated and poorly accessible tumors.

A novel preparation of microspheres incorporating a dextran magnetite complex has been reported for applications in arterial embolization and inductive hyperthermia of liver tumors in rats[12]. Another study achieved positive temperature differences between tumor and normal liver and subsequent therapeutic responses in experimental rabbit liver tumors after arterially infused ferromagnetic microspheres[13].

Numerous other biomedical and bioengineering applications for superparamagnetic iron oxide nanoparticles have been explored for tissue repair, immunoassays, as drug carriers for therapeutic delivery[14], detoxification of biological fluids, cell separation[15] and also as labeling agents for magnetic resonance imaging (MRI) in cell tracking studies[16].

The combination of MSCs and iron oxide nanoparticles in biological applications have been described to provide promising effects by enhancing MSCs homing effect[17], in promoting cardiac differentiation of embryonic stem cells[18] and in tumor growth inhibition in mice[19].

In our body, cells are constantly exposed to many internal and external stimuli, such as magnetic fields, which are associated with cellular stress. The cell stimulation by these stress sources (stressors) can trigger a variety of responses, which depends on the severity and duration of stress encountered. During the stimulation process, the cells can either re-establish cellular homeostasis and return to the former state or adopt changes according with the new environment[20]. Usually, stressors trigger a cascade of processes, including potential cell repair mechanisms, temporary adaptation, cell autophagy or trigger cell death[21]. Most of the responses intend to restore the normal physiology and functioning of the cells.

One of the first magnetic biological impacts on the cells is related with magnetically induced movement of ions in solution (e.g. electrolytes), thus inducing the formation of electrical fields and currents[22]. This effect might be especially important when the cell receptors are affected by changes in the magnetic field configuration, which translate into changes in the electrical currents on the cells, thus influencing cell fate[22]. The second biological effect corresponds to a magneto-mechanical effect of reorientation on certain molecules associated with induced torques by uniform static magnetic fields on molecules with anisotropic magnetic properties. This results in cellular reorientation and spatial ordering ascribed to an effect in cell structures that are magnetically and mechanically inhomogeneous. This effect translates in the redistribution of stresses within cells (e.g. deformation of intracellular structures, change of membrane permeability) upon application of an uniform magnetic field[22]. Another reported effect is related with spatially non-uniform magnetic field exerting ponderomotive forces on magnetically non-uniform cell structures. This magnetic forces are proportional to the gradient of the square of magnetic field and the difference of magnetic susceptibilities of the component of the cell and its environment[22]. Additionally, magnetic fields are known to be able to exert

translational forces on ferromagnetic structures, such as magnetite and ferritins presented in the cells[22].

Static magnetic fields can also modify energy levels and spin orientation of electrons as well as the spin states of free radicals, which, in turn, changes the relative probabilities of molecule recombination, possibly resulting in biological consequences[22].

Other non-linear mechanisms of magnetic effects on cells have been recently explored to explain the reasons behind the possibility to extract a weak magnetic signal from noise on the cells (e.g. stochastic non-linear resonance, self-tuned Hopf bifurcations)[22].

In a more practical vision, past studies have indicated that a static magnetic field alone do not have a lethal effect on the basic properties of cell growth and survival under normal culture conditions, regardless of the magnetic density[23]. Other controversial observations have also suggested that no effect on changes in cell growth rate and in cell cycle distribution were produced by extremely strong static magnetic fields (up to a maximum of 10 T)[23]. It has also been reported that treatments with trace amounts of ferrous ions in the cell culture medium and exposure to a static magnetic field increases DNA damage[23].

In conclusion, the mechanisms of interaction of magnetic fields with cell structures remain poorly understood and systemized thus requiring a more intensive investigation.

II.2. Smart Magnetic Hydrogels and Magnetic Stimulation

One of the main challenges nowadays has been the fabrication of new multifunctional smart materials with intelligence at the material level, including sensing changes in environmental conditions, processing the sensed information and actuating by responding to the stimulus[24,25]. The development of stimuli-responsive gels is however often impaired by delayed responses to the stimulation associated with structural damage and rapid changes in swelling rate[26]. Additionally, kinetic restrictions are also usually found in response to the friction between the polymer network and the swelling agent[26].

Magnetic polymer gels are unique intelligent materials able to respond to different stimuli. These soft materials with elastic properties and adaptive magnetic sensibility (ferrogels) have been vastly studied, mostly due to their capability to mediate the magnetic susceptibility of magnetic nanoparticles [26].

Magnetic nanoparticles (MNPs) with particle size below 30 nm are known to possess superparamagnetic effect, with each particle creating a single magnetic domain[27,28]. This nanoscale magnetic field created in the scaffolds by MNPs contributes

to produce micro magnetic driving force at the interface between cells and scaffolds. Among various MNPs, Fe_3O_4 possess unique magnetic properties and excellent biocompatibility and nontoxicity, with particular interest in tissue engineering, magnetic hyperthermia and magnetic targeting[29,30,31]. These MNPs are also the only metal oxide nanoparticles approved by US Food and Drug Administration for clinical use[32].

The advantages of these Fe_3O_4 MNPs in the medical field have triggered the interest to incorporate Fe_3O_4 nanoparticles into biomaterials for tissue engineering[33,34]. Moreover, Fe_3O_4 MNPs can largely improve the mechanical properties of scaffolds, in particular their stiffness, strength and, due to topologic effect, its surface area[35].

When a magnetic-sensitive gel is exposed to an external magnetic field, two types of interactions can be identified: field-particle and particle-particle interactions[36,37]. The field-particle interaction is dominant when the external magnetic field is non-uniform due to the particle attraction to regions of stronger magnetic intensities. Changes in the molecular conformation (e.g. macroscopic changes in shape and/ or motion) of the gel can also occur as a consequence of the dielectrophoretic/ magnetophoretic mechanisms associated with the magnetic exposure. This effect can be further enhanced by the crosslinking of the hydrogel. However, if the magnetic field is uniform there are no attractive/ repulsive field-particles interactions due to the lack of a field gradient. In this case, particle-particle interactions are prevalent, leading to a significant change in the structure of the particle aggregates, and the magnetic field induces electric or magnetic dipoles.

The ability of these magnetic-field-sensitive gels to undergo a quick controllable change of shape, associated with the peculiar magnetoelastic properties, can be used to mimic muscular contraction[38]. This highlights the possibility of these magnetic-field-sensitive gels to be used as an artificial muscle for medical approaches.

Magnetic elastomers[39] as well as magnetic gels (ferrogels)[40] have been developed recently with applications as soft actuators, micromanipulators, artificial muscles, tunable or adjustable mounts, and as suspension devices[41].

For instance, the fabrication of Fe_3O_4/poly-l-lactide composites using extruding process has been described to enhance the osteogenic differentiation capability[42]. In Figure II. 1, a porous scaffold, doped with MNPs and loaded with drugs and cells, was implanted to promote bone regeneration using magnetic stimulation[43]. Another study reported the high compatibility of magnetic scaffolds containing chitosan and Fe_3O_4 MNPs for C2C12 cells[44]. Dextran grafter maghemite nanoarchitectures integrated

with chitosan-based scaffolds have also been reported to stimulate the proliferation of both MG63 (human osteosarcoma cells from malignant bone tumors) and human mesenchymal stem cells[45]. Likewise, poly(ϵ-caprolactone)/iron-doped hydroxyapatite scaffolds were characterized with favorable cell viability, adhesion and proliferation and excellent effect in promoting osteogenesis *in vitro*[46].

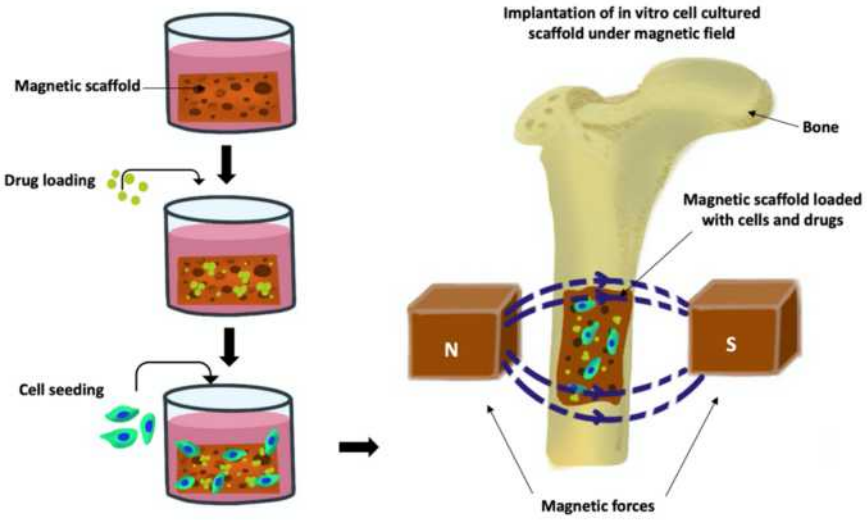


Figure II. 1. Illustration of the preparation and implantation of an engineered magnetic scaffold to prompt bone regeneration under external magnetic stimulation. Adapted from [43].

In most cellular studies, magnetic scaffolds are used as a support for cellular adhesion and growth in replacement of the extracellular matrix (ECM). However, the interactions between cells and matrix are controlled by several signal factors and by a complex flow and force-controlled system in feedback mechanisms. Mechanotransduction phenomena can occur at the ECM level due to negatively charged components of the ECM, glucosaminoglycans (e.g. articular cartilage), providing the tissue with electromechanical properties[47]. The negative charge of glucosaminoglycans contrast with the fixed charge of free electrolytes present in the medium, thus creating physicochemical responses and charge-dependent osmotic swelling pressure. Upon external mechanical loading or magnetic-induced mechanical changes, these electric potentials are developed in a signal transduction mechanism dependent on the external mechanical stimulation[48,49]. Cells, such as the chondrocytes, also tend to respond to the mechanical stimuli by activating multiple regulatory pathways, affecting ECM production and function[50,51].

The biological effects observed in a magnetic actuator such as a magnetic scaffold can be related to the mechanical properties of the cytoskeleton upon mechanical loading.

Magnetic tweezers have also been reported to activate mechanosensitive ion channels to study and control the production of specific proteins[52,53].

Osteoblasts and fibroblasts seeded onto magnetic polymer nanofibers were observed to align to the applied magnetic field while increasing cell proliferation rates[54].

Soft mechanical stimulation of magnetic hydrogel scaffolds by external magnetic field was demonstrated to be able to induce mesenchymal stem chondrogenesis without the addition of growth factors[55]. Another work reported the effect of the magnetic actuation of ferrogel scaffolds in the reduction of fibrosis and inflammation, as well as enhancing muscle regeneration in severe muscle injuries[56].

Overall, it has been reported how magnetic field stimulation can activate numerous sensitive receptors on cell surface and accelerate bone healing by increasing calcium content and new bone density[57,58,59,60].

II.3. Angiogenesis Mechanisms and Strategies to Improve the Phenomena

A number of diseases are associated with reduced vascular perfusion and could be improved using provascularization strategies. Some examples that could benefit from proangiogenic therapies are the peripheral vascular disease, ischemic heart disease, wound healing, and cell and tissue transplantation[61]. Usually aging patients suffer from slower healing responses, especially after surgery and during fracture repair so it is likely that proangiogenic therapy would improve the healing response of elderly patients in many situations[62].

Angiogenesis, which consists on the formation of new blood vessels from existing ones, is relatively rare in adults. The presence of angiogenesis in adults is limited to regeneration areas derived from an injury or tumor growth[63,64].

Despite the increasingly development of tissue engineered constructs, the lack of mature and functional vasculature limits the size and impairs the complexity and efficiency of vascular scaffold models[65]. Recent advances have focused on better regulation of growth factor delivery and attempts to better mimic natural processes by delivering combinations of multiple growth factors, cells and bioactive materials in the right spatial and temporal setting. However, thus far both angiogenic growth factors and cell-based therapies have failed to promote a robust healing response in a variety of ischemic diseases during clinical trials [65]. For the progress of vascular tissue engineering,

a more thorough understanding of the mechanisms that regulate healthy and pathogenic angiogenesis are required[66].

Briefly, the complex mechanism of angiogenesis is initiated when the increase in concentration of pro-angiogenic factors produced by inflammatory or tumor cells activate quiescent endothelial cells from an existing vessel in response to injury and/or hypoxia[67,68,69]. The activated cells differentiate into tip cells, creating elongated sprouts/ new vessels toward the stimulus through active migration (Figure II. 2)[67,68,70].

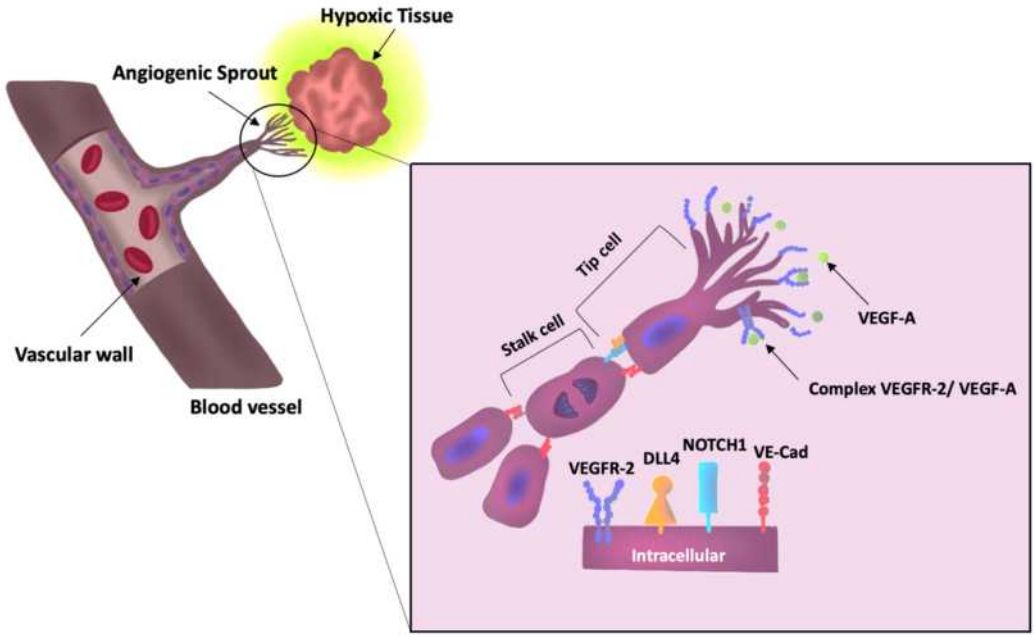


Figure II. 2. Illustration of the mechanisms and signaling pathways involved in sprouting angiogenesis triggered by inflammatory cues from a hypoxic tissue. Adapted from [69].

After capillary formation, endothelial cells secrete chemotactic signaling molecules to recruit perivascular cells (pericytes in the capillaries and smooth muscle cells in larger vessels). These cells later migrate along the newly formed vessels to unsheathe the endothelium, while providing stability, cell differentiation, and vessel permeability[70].

Among the key features of the angiogenic mechanism are temporal regulation, spatial organization, cellular crosstalk, active remodeling and interaction with the ECM. When these features are dysregulated, the development of new vasculature is abnormal (e.g. tumor angiogenesis)[64]. Tumorigenic vessels are characterized by having an excessive tortuosity, larger lumens, hyperpermeability and uncontrolled sprouting. These characteristics result of the disruption of the tightly regulated sequence of stimuli

necessary to deliver healthy angiogenesis, including excessive or sustained release of proangiogenic factors[64]. Relatedly, angiogenesis obtained on tissue engineered scaffolds is also stimulated by the addition of single growth factors, resulting in poorly organized and immature blood vessels, reminiscent of tumoral angiogenesis.

In vivo angiogenesis is tightly regulated via spatial cues that direct vessel sprouting and maturation. Ischemia or inflammation act as stimuli able to provoke a localized release of growth factors, cytokines and chemokines, which effectively creates a gradient within the extracellular space[68]. The internal signaling response, and consequent cell proliferation and migration, as well as chemical sensing, is a dynamic process which follows an organized timed schedule[71].

Consequently, temporal delivery of bioactive molecules in a tissue engineered scaffold is crucial in the development of vascularized blood vessels. This is usually achieved through the incorporation of growth factors and other molecules into the scaffolds by non-covalent adsorption in the scaffold material. In these cases, growth factor release is based on the affinity of the molecules with the scaffold matrix or dependent on molecule diffusion through the scaffold matrix[72,73]. The use of natural polymer-based scaffolds is usually preferred for their biocompatibility and biodegradation following implantation[74,75]. Scaffolds acting as delivery systems allow for control over the diffusion of several compounds with different chemical affinities and diffusion coefficients[76]. It is possible to regulate drug release by altering the properties and composition of the material or by changing the method of retaining the drug[72].

Due to its potent effect on angiogenesis, VEGF-A is the most commonly used growth factor for drug delivery or patterning of the scaffolds. For instance, the combination of Vascular endothelial growth factor (VEGF-A) and Angiopoietin-2 (Ang-2,) followed by sequential addition of Platelet-derived growth factor (PDGF) and/or Angiopoietin-1 (Ang-1), has shown to promote vascular maturation *in vitro*[77]. Another study used polyelectrolyte layers to encapsulate recombinant human bone morphogenetic protein-2 (rhBMP-2) and recombinant human vascular endothelial growth factor (rhVEGF), showing controlled release of the encapsulated factors over time both *in vitro* and *in vivo*[78]. The functionalization of a nanocomposite fibrous scaffold with VEGF, fibroblast growth factor (FGF) and Bone morphogenetic protein-2 (BMP2) has also led to the release of these factors at different times, resulting in increased tissue vascularization and bone regeneration[79].

In addition, it is also possible to trigger the release of growth factors from the scaffolds through mechanic stimulation[80]. In these circumstances, the external mechanical stimulation forces the cells to apply traction forces capable to deform the scaffold at the microscopic level, resulting in the release of the entrapped molecules[80]. This concept was achieved through the incorporation of a drug into an alginate gel and allowing the cells to apply pressure on the matrix, thus stimulating molecule release[80]. Recently, another method used cell-specific traction forces as a biophysical trigger to induce growth factors release from the biomaterial[81].

Nonetheless, the controlled delivery of biomolecules is often impaired by a too short half-life and a fast degradation of the molecules *in vivo*. This may lead to uncontrollable pharmacokinetics and the risk of delivering supraphysiological doses, thus highlighting the need for the development of more sophisticated stimulation technologies that allow for continuous release of growth factors[77].

Another important parameter to prompt angiogenesis is related with the interactions between cells and extracellular matrix, which are mediated by transmembrane proteins (e.g. integrins), which are able to initiate intracellular signaling cascade, including cell attachment, migration and differentiation[82,83]. To improve the adhesion of the cells to the biomaterial, scaffolds are usually coated with proteins such as collagen, laminin and fibronectin[83] (among others), containing specific amino acid sequences which act as cell binding epitopes. Scaffolds surface topography and physical/chemical properties, such as wettability and electric charges, can also affect cell adhesion on a biomaterial surface[84]. Cell adhesion followed by migration in the pores and subsequent proliferation is a necessary feature for the fabrication of a 3D structure.

It has been shown that the mechanical properties of the scaffolds, such as stiffness, porosity, hydrophobicity and internal architecture (e.g. alignment) are able to highly impact on the cellular behavior *in vitro*. Endothelial cells, in particular HUVECs, have been reported to increase the expression of matrix metalloproteinases (MMP2, MMP3, MMP4, MMP14) and of VEGF-A when cultured on stiffer scaffolds such as polydimethylsiloxane (PDMS). The metalloproteinases were downregulated by the decreased stiffness of the substrate[85]. The increased stiffness (1-10 kPa) of polyacrylamide scaffolds has been reported to promote endothelial cell response to VEGF-A by increasing VEGFR-2 internalization. Also, increasing the stiffness of collagen-coated polyacrylamide (3-3000 Pa) has resulted in increased expression of

functional proteins and growth factors in HUVECs, also triggering angiogenic behavior[86,87].

Regardless of the scaffolds, the physiology of vascular cells is affected by the mechanical forces of the pulsatile flow. Physiologic shear stress upregulates vasodilators, antioxidant enzymes and tissue plasminogen activator to confer atheroprotective responses[88].

The endothelial layer of blood vessels is constantly exposed to the blood stream and hemodynamic forces (shear stress and tangential forces), to which the cells respond by changing their morphology and gene expression[89,90]. These mechano-transduction processes and responses of primary human endothelial cells and smooth muscle cells have reported cell-type specific differences responsible for vascular tissue integrity. The endothelial cells tend to function as a mechanical sensor when exposed to mechanical loading and are able to orient along the vascular axis *in vivo* when exposed to cyclic tensile strain, hydrostatic pressure or fluid shear stress[91].

Endothelial cells subjected to shear stress are able to convert mechanical stimuli into intracellular signals that affect cellular functions. Long-term shear stress on endothelial cells seeded on polypropylene hollow fibers has been reported to promote endothelial cell adhesion and a reorganization of the actin cytoskeleton, as well as extracellular matrix production[92]. HUVECs seeded on the lumen of living tissues with application of increased shear stress showed a complete confluent monolayer of elongated HUVECs and oriented in parallel with the flow direction[93]. In another study, rat aortic endothelial cells were seeded on the lumen of polyurethane grafts and exposed *in vitro* to shear stress for 6 days followed by implantation into syngeneic rats. The results showed that usual graft thrombosis had been inhibited and confluent endothelium was observed after 3 months from the implantation[94,95]. However, shear stress is also responsible for inhibiting the proliferation of endothelial cells while limiting sprouting in low flow regions, such as tumor microenvironment and ischemia[96,89].

Oxygen concentration is also an important regulator of angiogenesis, helping to drive the sprouting of endothelial cells toward injured tissues by increasing VEGF-A transcription in the presence of hypoxia conditions [63, 64,97,98, 99]. Attempts to recreate a hypoxic environment has revealed promising therapeutic results in bone tissue engineering *in vitro* and *in vivo*[100,101].

Nonetheless, although this review focused mostly on endothelial cells as the primary cell type to trigger angiogenesis, it is important to highlight that other supportive cells (e.g. pericytes and macrophages) are involved in the complex signaling pathways of *in*

vivo angiogenesis[70,102]. Consequently, the use of endothelial cells alone is usually inefficient to replicate physiological angiogenesis in tissue engineering approaches. To mimic the angiogenic natural mechanism, combinations of proangiogenic cells that reside within the vascular niche have been used, in particular perivascular cells such as pericytes, vascular smooth muscle cells, mesenchymal stromal cells (MSCs) and fibroblasts[103].

Recently, a co-culture system using endothelial cells and bone marrow MSCs encapsulated in Methacrylated Gelatin (Gel-MA) microspheres was used to study the ability of MSCs to mimic the function of pericytes and increase angiogenesis. Interestingly, the results indicated that MSCs differentiated toward a pericyte phenotype and both enhanced vascularization and integrated the system with the host tissue during *in vivo* experiments[104].

The knowledge of the conditions and factors able to influence positively or negatively on angiogenesis process could be further exploit as a therapeutic strategy of enormous benefit to a wide range of medical and tissue engineering applications.

II.4. Blood Vessels Models and Recent Advancements in the field

The extracellular matrix, aside from serving as a physical support for cells, plays an integral role in regulating the distribution of nutrients, gases (oxygen and nitric oxide), and soluble effectors (morphogens, growth factors, hormones, and cytokines). The gradients of these molecules are crucial to regulate biological processes such as cell differentiation during tissue development[105,106], angiogenesis during tissue repair in the adult[107,68], and tumor cell invasion responsible for metastatic stage[108].

One of the main reasons for inadequate therapeutic research approaches in high-morbidity vascular diseases resides in the therapeutic programs relying on animal models to poorly predict the human pathophysiology and tissue responses to drugs.

The process of mimicking a patient's native tissue architecture also remains a challenge, hindering readouts of the patient outcome and development of novel treatment strategies. The availability of physiologically relevant *in vitro* models of tissues and organs to better understand the complex signaling mechanisms and drug effects at a patient-specific and cellular level is fundamental for the development of this field[109].

The spatial presentation of diffusible molecules in tissues is complex and dependent on the distribution and morphology of vascular structures, including the porosity and structure of the surrounding extracellular matrix as well as the density of the

cells and their metabolic activity[110]. Studying these processes *in vitro* has been significantly improved by microfluidic approaches, able to provide a high degree of control over the timing and spatial distribution of biological factors[111,112].

Several states of tissues (e.g. developmental, regeneration, pathological) rely on angiogenesis. This highlights the need to fabricate *in vitro* vascular models able to replicate the native conditions, including the hydrodynamic forces through controlled flow velocity and the dimensions and geometries of the blood vessel models to accommodate different cell types involved in this signaling process[113].

The blood vessels possess complex geometries made of interconnections, bifurcations and loops, with significant variation within diameters (ranging from 4 mm to 5 μm), thus hampering the biomimetic process[113]. The fabrication of blood vessels models requires further investigation regarding the characteristics of native blood vessels, including structural and mechanical properties and overall dimensions (e.g. thickness, diameters). In particular, changes in the thickness of the blood vessel walls result in a decrease in the mechanical properties of the vessels and have been associated with various diseases, including coronary heart disease and atherosclerosis. For instance, the mimicry of carotid intimal-medial thickness can be used to predict coronary heart disease and atherosclerotic disease as it has been observed a higher thickness in patients with cardiovascular disease associated with increased stiffness of carotid arteries[114].

The three distinct layers of blood vessels includes the intima, a single layer of endothelial cells, the media, layers of elastic tissue and smooth muscle cells (SMCs), and the adventitia, composed by elastic fibers and fibroblasts. Imprinting, injection-molding and polymer casting are replication methods developed to fabricate devices using platforms with desired sizes and geometries[114].

The hemodynamics of blood (non-Newtonian fluid) flow are associated with two different regimes of shear rates[115]. When blood flows in large vessels, at low shear rate, viscosity decrease due to mechanisms of disassembly of large cell aggregates while the flow into smaller vessels, at a high shear rate, induces deformability of the cells and determines shear thinning[115]. This interrelation between the viscosity of the blood and the vessel diameter is the Fåhræus–Lindqvist effect and one of the keys to understand blood flow dynamics. This is an essential knowledge for the fabrication of vascular networks models, which may be used as a diagnostic device for pathologies, to study the effect of cell deformability on the behavior of a blood circulation network as well as to simulate vascular anomalies[115].

Additionally, vascular systems *in vivo* include several cell types in continuous remodeling by stimuli from endothelial, nervous, immune, and endocrine cells to play a key role in graft perfusion and integration of implants into the host vascular system[116,117]. Despite significant improvements of current technologies to create 3D blood vessels, the fabrication of a single functional engineered vascular system with multiscale vessel networks from large vessels to capillaries has remained challenging[118].

Strategies to overcome these hurdles include the induction of vascularization within tissue constructs by incorporation of growth factors to yield vasculogenesis[119], seeding endothelial cells directly in the *in vitro* model to stimulate angiogenesis[120] or the design of biocompatible materials with engineered microfluidic channels using microfabrication techniques since it has been reported that natural or synthetic scaffolds mixed with proangiogenic factors are able to induce *de novo* formation of capillaries[121,122,123]. So far the induction of vascularization in tissue constructs prior to implantation has revealed improved implant integration with the host tissue, leading to the formation of capillary-like structures in the host vasculature and restoring the damage on the native tissue[118].

Another promising method requires the use of magnetic iron oxide particles, either attached to the cells or incorporated in the cells by endocytosis, to drive magnetic forces into triggering stem cell differentiation towards desired vascular cell phenotypes[124,125]. The magnetically labeled cells or cell sheets have the advantage to be driven by magnetic forces to the desirable locations[124,125,126]. One approach reported a confluent endothelium on the luminal surface of a vascular scaffold formed by cells labeled with magnetic microbeads. In this study, the process of cell seeding and endothelium assembly was driven by external magnets[127]. Endothelial cells loaded with superparamagnetic iron oxide nanoparticles has been also used for *in vitro* endothelialization[127]. Overall, magnetic forces are known to dramatically accelerated cell seeding, cell adhesion and monolayer assembly. This was described in morphologic studies where a high level of cell retention was obtained after magnetic-force-driven cell seeding[127].

Electrospinning techniques have also been explored to produce nanofiber-based vascular networks. For instance, improved pre-vascularization has been reported by seeding HUVECs on layer-by-layer aligned polycaprolactone (PCL)/ cellulose nanofiber matrices. This resulted in aligned fiber matrices after implantation and proper integration with the host vasculature[128].

Recent reports also demonstrated *in vitro* perfusable vessels with endothelialization of the hydrogel channels to mimic endothelial cell migration, vascular barrier function and inflammatory response[129]. Unfortunately, these models lacked the natural endothelial morphogenesis[130].

Advances in microfabrication, microfluidic technology, and tissue engineering has led to a large number of studies exploring chip-vascular devices, typically based on microchannel-like structures enclosed in bulk elastomers (most commonly PDMS). These microfluidic devices allow flow to be controlled to match the physiological conditions while providing spatiotemporal variations over chemical cues[131]. However, common microfluidic techniques, usually combined with soft lithography technologies, function as individual platforms and produce channels with a uniform height and a rectangular cross section that do not capture the size hierarchy observed *in vivo*[132]. Hence, most of these models exhibit fabrication limitations, in particular concerning the development of layer-by-layer devices[130].

A recent study avoided chip-based bulk vascular constructs by developing a simple elastomeric and biomimetic blood vessel construct closely mimicking the physio-anatomical properties of those *in vivo* with the purpose of integrating multiple organs on chips, revealing the biofunctionality of the developed endothelium upon treatment with pharmaceutical compounds[130].

Fiber microfluidics, consisting on the incorporation of nanofiber membranes in the microfluidic systems, emerged as a promising approach able to create uniform and complex microchannels over arbitrary lengths using thermal fiber drawing technique, a process in which a macrostructured preform is heated and drawn into extended lengths of microstructured fiber[133,134]. The process enables the fabrication of meters-long microfluidic fibers with non-rectangular cross-sectional shapes in a dimensionally reduced version of a scale-up microchannel, resulting in a flexible methodology[133].

However, the use of these membrane-based microfluidic chips have failed not only due to liquid leakage and lack of robustness and consistency but also because *in situ* fabrication of membranes may bring issues when requiring interfacial polymerization[135].

Over the past years, 3D printing, or additive manufacturing, has become an emerging technique in tissue engineering to fabricate complex and systematic architecture of vascular network, thus overcoming the flexibility limitations of other technologies[136]. 3D printing allows for the construction of vascular networks within tissues and organs, offering several selections for fabrication materials, such as polylactic

acid (PLA), nylon, acrylonitrile butadiene styrene (ABS), among others such as resins and thermoplastic elastomer (TPE), and printing techniques (stereolithography, digital light processing, fused deposition modeling, selective laser sintering, selective laser melting, electronic beam melting or laminated object manufacturing)[136].

In particular, laser-based fabrication has the advantage of allowing for the fabrication of both 2D and 3D in a layer-by-layer fashion in the presence of a photo mask, donor substrate, photo sensitive polymer, or photo initiator[137]. These type of indirect biofabrication is convenient when scaffolding biopolymers exhibited poor printability and manipulation complexity, highlighting the importance of sacrificial biopolymers for vascular network fabrication[137].

In this regard, one of the most appealing vascular networks using the printing technology concerned a 3D filament of carbohydrate glasses embedded with a hydrogel. The filament was then sacrificed to obtain a controlled geometry vessel in a cylindrical form and then seeded with endothelial cells[138].

Most recently, 3D Bioprinting has revolutionized the tissue engineering field due to its excellent potential to accurately positioning cell-laden constructs[139]. This sophisticated technology efficiently combines in situ cell seeding, biomaterials and growth factors in complex geometric structures with micro-channels and pore size capable to drive angiogenesis.

Bioprinting processes can be classified into extrusion (biomaterials/cells are drive from a syringe at a controllable volume flow rate by compressed air), droplet/ inkjet (non-contact technique which generates constructs in a layer-by-layer approach by deposition of tiny ink droplets) and laser-based bioprinting (based on the principles of laser-induced photopolymerization)[131].

Pressure assisted bioprinting (extrusion) is, alongside with inkjet, one of the most commonly used strategies for highly organized cell-loaded perfusable structures to promote angiogenesis and vasculature formation. Extrusion however used a pressure-based system instead of a thermal or piezoelectric actuator used in the inkjet system[140,141,142].

Benefitting from more precision in *in vivo* vasculature formation mechanism, 3D biomimetic organ-on-chips (Figure II. 3) have evolved to mimic native vascular network, achieving vessel microenvironments and cellular and tissue level crosstalk to allow replication of complex physiologies, vascular disease modeling platforms and drug screening[143,144,113].

Organ printing technology represents the most promising avenue to generate organo-specific branched vasculature, fundamental for the viability of tissue-engineered human organs. On magnetic vascular tissue engineering, it has been explored the possibility of robotic fabrication of intra-organ vessels with magnetic vascular tissue spheroids (containing embedded magnetic nanoparticles), able to fuse into tissues, as a key to generate vasculature[145,146,147]. However, highly complex printed organs are still in the early stages of development[124].

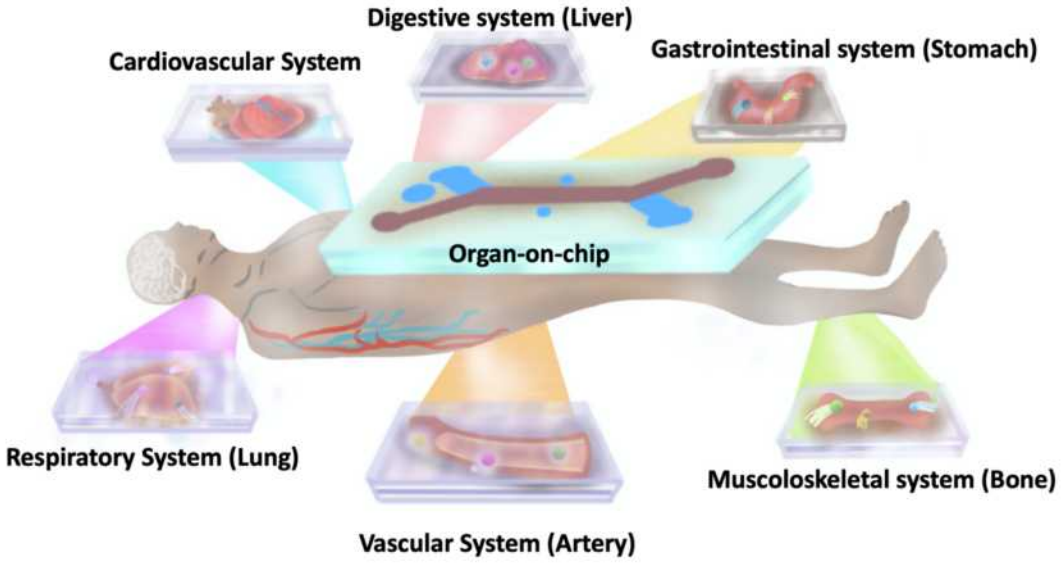


Figure II. 3. Illustration of organ-on-chip platforms for modeling human physiology and pathophysiology. Adapted from [148].

II. References

1. Kula, B. & Dró/.zd/.z, M. A study of magnetic field effects on fibroblast cultures Part 1. The evaluation of the effects of static and extremely low frequency (ELF) magnetic fields on vital functions of fibroblasts. *Bioelectrochemistry Bioenerg.* **39**, 21–26 (1996).
2. Saunders, R. Static magnetic fields: animal studies. *Prog. Biophys. Mol. Biol.* **87**, 225–239 (2005).
3. Ghodbane, S., Lahbib, A., Sakly, M. & Abdelmelek, H. Bioeffects of static magnetic fields: Oxidative stress, genotoxic effects, and cancer studies. *Biomed Res. Int.* **2013**, (2013).
4. Schenck, J. F. The role of magnetic susceptibility in magnetic resonance imaging: MRI magnetic compatibility of the first and second kinds. *Med. Phys.* **23**, 815–850 (1996).
5. Zablotskii, V., Polyakova, T., Lunov, O. & Dejneka, A. How a High-Gradient Magnetic Field Could Affect Cell Life. *Sci. Rep.* **6**, 37407 (2016).
6. Rumbaut, R. E. & Mirkovic, D. Magnetic therapy for edema in inflammation: a physiological assessment. *Am. J. Physiol. Circ. Physiol.* **294**, H19–H20 (2008).
7. Marycz, K. *et al.* Endurance Exercise Mobilizes Developmentally Early Stem Cells into Peripheral Blood and Increases Their Number in Bone Marrow: Implications for Tissue Regeneration. *Stem Cells Int.* **2016**, 5756901 (2016).
8. Markov, M. S. Therapeutic application of static magnetic fields. *Environmentalist* **27**, 457–463 (2007).
9. Colbert, A. P. *et al.* Static magnetic field therapy: a critical review of treatment parameters. *Evid. Based. Complement. Alternat. Med.* **6**, 133–139 (2009).
10. Marcu, C. B., Beek, A. M. & van Rossum, A. C. Clinical applications of cardiovascular magnetic resonance imaging. *Can. Med. Assoc. J.* **175**, 911 LP – 917 (2006).
11. Thiesen, B. & Jordan, A. Clinical applications of magnetic nanoparticles for hyperthermia. *Int. J. Hyperth.* **24**, 467–474 (2008).
12. Minamimura, T. *et al.* Tumor regression by inductive hyperthermia combined with hepatic embolization using dextran magnetite-incorporated microspheres in rats. *Int. J. Oncol.* **16**, 1153–1158 (2000).
13. Jones, S. K., Winter, J. G. & Gray, B. N. Treatment of experimental rabbit liver

tumours by selectively targeted hyperthermia. *Int. J. Hyperth. Off. J. Eur. Soc. Hyperthermic Oncol. North Am. Hyperth. Gr.* **18**, 117–128 (2002).

14. El-Boubbou, K. Magnetic iron oxide nanoparticles as drug carriers: preparation, conjugation and delivery. *Nanomedicine* **13**, 929–952 (2018).
15. Gupta, A. K. & Gupta, M. Synthesis and surface engineering of iron oxide nanoparticles for biomedical applications. *Biomaterials* **26**, 3995–4021 (2005).
16. Wang, P. C. & Shan, L. Essential Elements to Consider for MRI Cell Tracking Studies with Iron Oxide-based Labeling Agents. *J. Basic Clin. Med.* **1**, 1–6 (2012).
17. Yun, W. S. *et al.* Enhanced Homing Technique of Mesenchymal Stem Cells Using Iron Oxide Nanoparticles by Magnetic Attraction in Olfactory-Injured Mouse Models. *Int. J. Mol. Sci.* **19**, 1376 (2018).
18. Au, K.-W. *et al.* Effects of iron oxide nanoparticles on cardiac differentiation of embryonic stem cells. *Biochem. Biophys. Res. Commun.* **379**, 898–903 (2009).
19. Huang, Y., Mao, K., Zhang, B. & Zhao, Y. Superparamagnetic iron oxide nanoparticles conjugated with folic acid for dual target-specific drug delivery and MRI in cancer theranostics. *Mater. Sci. Eng. C* **70**, 763–771 (2017).
20. Poljšak, B. & Milisav, I. Clinical implications of cellular stress responses. *Bosn. J. basic Med. Sci.* **12**, 122–126 (2012).
21. Lakhotia, S. C. & Tripathi, A. K. Cellular stress responses: Preface. *J. Biosci.* **23**, 285 (1998).
22. Kondrachuk, A. The mechanisms of the effects of magnetic fields on cells. (2002).
23. Miyakoshi, J. Effects of static magnetic fields at the cellular level. *Prog. Biophys. Mol. Biol.* **87**, 213–223 (2005).
24. Osada, Y. Smart materials and structures. By M. V. Gandhi and B. S. Thompson, Chapman and Hall, London 1992, 310 pp., hardback, ISBN 0-412-37010-7. *Adv. Mater.* **5**, 313–314 (1993).
25. Schué, F. Biorelated polymers and gels Edited by Terno Okanno Academic Press, San Diego, 1998 pp 257, price US$64.95 ISBN 0-12-525090-8. *Polym. Int.* **49**, 236 (2000).
26. Filipcsei, G., Csetneki, I., Szilágyi, A. & Zrínyi, M. Magnetic Field-Responsive Smart Polymer Composites BT - Oligomers - Polymer Composites - Molecular Imprinting. in (eds. Gong, B., Sanford, A. R. & Ferguson, J. S.) 137–189 (Springer Berlin Heidelberg, 2007). doi:10.1007/12_2006_104
27. Shi, D., Sadat, M. E., Dunn, A. W. & Mast, D. B. Photo-fluorescent and magnetic

properties of iron oxide nanoparticles for biomedical applications. *Nanoscale* **7**, 8209–8232 (2015).

28. Dong, Q. *et al.* A molecular approach to magnetic metallic nanostructures from metallopolymer precursors. *Chem. Soc. Rev.* **47**, 4934–4953 (2018).
29. Cunha, C. *et al.* Hybrid composites made of multiwalled carbon nanotubes functionalized with Fe3O4nanoparticles for tissue engineering applications. *Nanotechnology* **23**, 465102 (2012).
30. Li, S. *et al.* Targeted imaging of brain gliomas using multifunctional Fe3O4/MnO nanoparticles. *RSC Adv.* **5**, 33639–33645 (2015).
31. Wang, F. *et al.* Injectable and thermally contractible hydroxypropyl methyl cellulose/Fe3O4 for magnetic hyperthermia ablation of tumors. *Biomaterials* **128**, 84–93 (2017).
32. Jia, Y. *et al.* Co-encapsulation of magnetic Fe3O4 nanoparticles and doxorubicin into biodegradable PLGA nanocarriers for intratumoral drug delivery. *Int. J. Nanomedicine* **7**, 1697–1708 (2012).
33. Chen, W., Long, T., Guo, Y.-J., Zhu, Z.-A. & Guo, Y.-P. Magnetic hydroxyapatite coatings with oriented nanorod arrays: hydrothermal synthesis, structure and biocompatibility. *J. Mater. Chem. B* **2**, 1653–1660 (2014).
34. Long, T., Guo, Y.-P., Tang, S., Guo, Y.-J. & Zhu, Z.-A. Emulsion fabrication of magnetic mesoporous carbonated hydroxyapatite microspheres for treatment of bone infection. *RSC Adv.* **4**, 11816–11825 (2014).
35. Hou, C., Song, S., Zhou, X., Wei, J. & Li, T. Electromagnetic and mechanical properties of Fe3O4-coated amorphous carbon nanotube/polyvinyl chloride composites. *Compos. Interfaces* **23**, 901–907 (2016).
36. Levon, K. Polymer gels: Fundamentals and biomedical applications by D. Derossi, K. Kajiwara, Y. Osada and A. Yamauchi, Plenum Press, New York and London (1991), 345 pp., price $85.00. *Polym. Adv. Technol.* **3**, 48 (1992).
37. Verdaguer, M. Molecular Electronics Emerges from Molecular Magnetism. *Science (80-.).* **272**, 698 LP – 699 (1996).
38. Zrínyi, M. Intelligent polymer gels controlled by magnetic fields. *Colloid Polym. Sci.* **278**, 98–103 (2000).
39. Carlson, J. D. & Jolly, M. MR fluid, foam and elastomer devices. *Mechatronics* **10**, 555–569 (2000).
40. Zrinyi, M., Barsi, L. & Büki, A. Deformation of ferrogels induced by nonuniform

magnetic fields. *J. Chem. Phys.* **104**, 8750–8756 (1996).

41. Raikher, Y. & Stolbov, O. Deformation of an ellipsoidal ferrogel sample in a uniform magnetic field. *J. Appl. Mech. Tech. Phys.* **46**, 434–443 (2005).
42. Pan, Y.-H. *et al.* Fabrication of Fe3O4/PLLA composites for use in bone tissue engineering. *Polym. Compos.* **38**, 2881–2888 (2017).
43. Sukumaran, A. *et al.* Drug Delivery Systems in Bone Regeneration and Implant Dentistry. *Curr. Concepts Dent. Implantol.* 239–265 (2015). doi:10.5772/60003
44. Ge, J., Zhai, M., Zhang, Y., Bian, J. & Wu, J. Biocompatible Fe3O4/chitosan scaffolds with high magnetism. *Int. J. Biol. Macromol.* **128**, 406–413 (2019).
45. Scialla, S. *et al.* Bioactive chitosan-based scaffolds with improved properties induced by dextran-grafted nano-maghemite and l-arginine amino acid. *J. Biomed. Mater. Res. Part A* **107**, 1244–1252 (2019).
46. D'Amora, U. *et al.* 3D additive-manufactured nanocomposite magnetic scaffolds: Effect of the application mode of a time-dependent magnetic field on hMSCs behavior. *Bioact. Mater.* **2**, 138–145 (2017).
47. Vikingsson, L. *et al.* Local deformation in a hydrogel induced by an external magnetic field. *J. Mater. Sci.* **51**, 9979–9990 (2016).
48. Mow, V. C., Ratcliffe, A. & Poole, A. R. Cartilage and diarthrodial joints as paradigms for hierarchical materials and structures. *Biomaterials* **13**, 67–97 (1992).
49. Abreu, E. Mow VC, Huiskes R:Basic Orthopaedic Biomechanics and Mechano-Biology. 3rd edition. *Biomed. Eng. Online - BIOMED ENG ONLINE* **4**, 1 (2005).
50. Valhmu, W. B. *et al.* Load-controlled compression of articular cartilage induces a transient stimulation of aggrecan gene expression. *Arch. Biochem. Biophys.* **353**, 29–36 (1998).
51. Brady, M. A., Waldman, S. D. & Ethier, C. R. The application of multiple biophysical cues to engineer functional neocartilage for treatment of osteoarthritis. Part I: cellular response. *Tissue Eng. Part B. Rev.* **21**, 1–19 (2015).
52. Pommerenke, H. *et al.* Stimulation of integrin receptors using a magnetic drag force device induces an intracellular free calcium response. *Eur. J. Cell Biol.* **70**, 157–164 (1996).
53. Bausch, A. R., Hellerer, U., Essler, M., Aepfelbacher, M. & Sackmann, E. Rapid stiffening of integrin receptor-actin linkages in endothelial cells stimulated with thrombin: a magnetic bead microrheology study. *Biophys. J.* **80**, 2649–2657 (2001).

54. Li, L., Yang, G., Li, J., Ding, S. & Zhou, S. Cell behaviors on magnetic electrospun poly-d, l-lactide nanofibers. *Mater. Sci. Eng. C* **34**, 252–261 (2014).
55. Fuhrer, R. *et al.* Pressureless Mechanical Induction of Stem Cell Differentiation Is Dose and Frequency Dependent. *PLoS One* **8**, e81362 (2013).
56. Cezar, C. A. *et al.* Biologic-free mechanically induced muscle regeneration. *Proc. Natl. Acad. Sci. U. S. A.* **113**, 1534–1539 (2016).
57. Huang, H.-M., Lee, S.-Y., Yao, W.-C., Lin, C.-T. & Yeh, C.-Y. Static magnetic fields up-regulate osteoblast maturity by affecting local differentiation factors. *Clin. Orthop. Relat. Res.* **447**, 201–208 (2006).
58. Zhu, Y. *et al.* Protein Corona of Magnetic Hydroxyapatite Scaffold Improves Cell Proliferation via Activation of Mitogen-Activated Protein Kinase Signaling Pathway. *ACS Nano* **11**, 3690–3704 (2017).
59. Wójcik-Piotrowicz, K., Kaszuba-Zwoińska, J., Rokita, E. & Thor, P. Cell viability modulation through changes of Ca2+-dependent signalling pathways. *Prog. Biophys. Mol. Biol.* **121**, 45–53 (2016).
60. Wang, J. *et al.* The effects of pulsed electromagnetic field on the functions of osteoblasts on implant surfaces with different topographies. *Acta Biomater.* **10**, 975–985 (2014).
61. Phelps, E. A. & Garcia, A. J. Update on therapeutic vascularization strategies. *Regen. Med.* **4**, 65–80 (2009).
62. Lu, C. *et al.* Effect of age on vascularization during fracture repair. *J. Orthop. Res. Off. Publ. Orthop. Res. Soc.* **26**, 1384–1389 (2008).
63. Viallard, C. & Larrivée, B. Tumor angiogenesis and vascular normalization: alternative therapeutic targets. *Angiogenesis* **20**, 409–426 (2017).
64. Ziyad, S. & Iruela-Arispe, M. L. Molecular mechanisms of tumor angiogenesis. *Genes Cancer* **2**, 1085–1096 (2011).
65. Fernandez de Grado, G. *et al.* Bone substitutes: a review of their characteristics, clinical use, and perspectives for large bone defects management. *J. Tissue Eng.* **9**, 2041731418776819 (2018).
66. Mastrullo, V., Cathery, W., Velliou, E., Madeddu, P. & Campagnolo, P. Angiogenesis in Tissue Engineering: As Nature Intended? . *Frontiers in Bioengineering and Biotechnology* **8**, 188 (2020).
67. Gerhardt, H. *et al.* VEGF guides angiogenic sprouting utilizing endothelial tip cell filopodia . *J. Cell Biol.* **161**, 1163–1177 (2003).

68. Carmeliet, P. & Jain, R. K. Molecular mechanisms and clinical applications of angiogenesis. *Nature* **473**, 298 (2011).
69. Pauty, J. *et al.* A Vascular Endothelial Growth Factor-Dependent Sprouting Angiogenesis Assay Based on an In Vitro Human Blood Vessel Model for the Study of Anti-Angiogenic Drugs. *EBioMedicine* **27**, 225–236 (2018).
70. Cathery, W., Faulkner, A., Maselli, D. & Madeddu, P. Concise Review: The Regenerative Journey of Pericytes Toward Clinical Translation. *Stem Cells* **36**, 1295–1310 (2018).
71. Bentley, K. & Chakravartula, S. The temporal basis of angiogenesis. *Philos. Trans. R. Soc. B Biol. Sci.* **372**, 20150522 (2017).
72. King, W. J. & Krebsbach, P. H. Growth factor delivery: How surface interactions modulate release in vitro and in vivo. *Adv. Drug Deliv. Rev.* **64**, 1239–1256 (2012).
73. Whitaker, M. J., Quirk, R. A., Howdle, S. M. & Shakesheff, K. M. Growth factor release from tissue engineering scaffolds. *J. Pharm. Pharmacol.* **53**, 1427–1437 (2001).
74. Rundhaug, J. E. Matrix metalloproteinases and angiogenesis. *J. Cell. Mol. Med.* **9**, 267–285 (2005).
75. Asghari, F., Samiei, M., Adibkia, K., Akbarzadeh, A. & Davaran, S. Biodegradable and biocompatible polymers for tissue engineering application: a review. *Artif. Cells, Nanomedicine, Biotechnol.* **45**, 185–192 (2017).
76. Nguyen, D.-H. T. *et al.* Biomimetic model to reconstitute angiogenic sprouting morphogenesis in vitro. *Proc. Natl. Acad. Sci.* **110**, 6712 LP – 6717 (2013).
77. Brudno, Y., Ennett-Shepard, A. B., Chen, R. R., Aizenberg, M. & Mooney, D. J. Enhancing microvascular formation and vessel maturation through temporal control over multiple pro-angiogenic and pro-maturation factors. *Biomaterials* **34**, 9201–9209 (2013).
78. Shah, N. J. *et al.* Tunable dual growth factor delivery from polyelectrolyte multilayer films. *Biomaterials* **32**, 6183–6193 (2011).
79. Kuttappan, S. *et al.* Dual release of growth factor from nanocomposite fibrous scaffold promotes vascularisation and bone regeneration in rat critical sized calvarial defect. *Acta Biomater.* **78**, 36–47 (2018).
80. Lee, K. Y., Peters, M. C. & Mooney, D. J. Controlled Drug Delivery from Polymers by Mechanical Signals. *Adv. Mater.* **13**, 837–839 (2001).
81. Stejskalová, A., Oliva, N., England, F. J. & Almquist, B. D. Biologically Inspired,

Cell-Selective Release of Aptamer-Trapped Growth Factors by Traction Forces. *Adv. Mater.* **31**, 1806380 (2019).

82. Ivaska, J. & Heino*, J. Adhesion receptors and cell invasion: mechanisms of integrin-guided degradation of extracellular matrix. *Cell. Mol. Life Sci. C.* **57**, 16–24 (2000).
83. Post, A., Wang, E. & Cosgriff-Hernandez, E. A Review of Integrin-Mediated Endothelial Cell Phenotype in the Design of Cardiovascular Devices. *Ann. Biomed. Eng.* **47**, 366–380 (2019).
84. Guo, S. *et al.* Parallel Control over Surface Charge and Wettability Using Polyelectrolyte Architecture: Effect on Protein Adsorption and Cell Adhesion. *ACS Appl. Mater. Interfaces* **8**, 30552–30563 (2016).
85. Zhao, D. *et al.* Substrate stiffness regulated migration and angiogenesis potential of A549 cells and HUVECs. *J. Cell. Physiol.* **233**, 3407–3417 (2018).
86. LaValley, D. J. *et al.* Matrix stiffness enhances VEGFR-2 internalization, signaling, and proliferation in endothelial cells. *Converg. Sci. Phys. Oncol.* **3**, 44001 (2017).
87. Santos, L. *et al.* Extracellular Stiffness Modulates the Expression of Functional Proteins and Growth Factors in Endothelial Cells. *Adv. Healthc. Mater.* **4**, 2056–2063 (2015).
88. Lee, J., Packard, R. R. S. & Hsiai, T. K. Blood flow modulation of vascular dynamics. *Curr. Opin. Lipidol.* **26**, 376–383 (2015).
89. Song, J. W. & Munn, L. L. Fluid forces control endothelial sprouting. *Proc. Natl. Acad. Sci.* **108**, 15342 LP – 15347 (2011).
90. Wragg, J. W. *et al.* Shear Stress Regulated Gene Expression and Angiogenesis in Vascular Endothelium. *Microcirculation* **21**, 290–300 (2014).
91. Greiner, A. M., Biela, S. A., Chen, H., Spatz, J. P. & Kemkemer, R. Temporal responses of human endothelial and smooth muscle cells exposed to uniaxial cyclic tensile strain. *Exp. Biol. Med. (Maywood).* **240**, 1298–1309 (2015).
92. Ott, M. J., Olson, J. L. & Ballermann, B. J. Chronic In Vitro Flow Promotes Ultrastructural Differentiation of Endothelial Cells. *Endothelium* **3**, 21–30 (1995).
93. Zhang, Z.-X. *et al.* Design of a novel bioreactor and application in vascular tissue engineering. *Appl. Surf. Sci.* **255**, 541–544 (2008).
94. Dardik, A., Liu, A. & Ballermann, B. J. Chronic in vitro shear stress stimulates endothelial cell retention on prosthetic vascular grafts and reduces subsequent in vivo neointimal thickness. *J. Vasc. Surg.* **29**, 157–167 (1999).

95. Gong, X. *et al.* Physiological pulsatile flow culture conditions to generate functional endothelium on a sulfated silk fibroin nanofibrous scaffold. *Biomaterials* **35**, 4782–4791 (2014).
96. Tun, W. M., Yap, C. H., Saw, S. N., James, J. L. & Clark, A. R. Differences in placental capillary shear stress in fetal growth restriction may affect endothelial cell function and vascular network formation. *Sci. Rep.* **9**, 9876 (2019).
97. Liao, D. & Johnson, R. S. Hypoxia: A key regulator of angiogenesis in cancer. *Cancer Metastasis Rev.* **26**, 281–290 (2007).
98. Pugh, C. W. & Ratcliffe, P. J. Regulation of angiogenesis by hypoxia: role of the HIF system. *Nat. Med.* **9**, 677–684 (2003).
99. Oladipupo, S. *et al.* VEGF is essential for hypoxia-inducible factor-mediated neovascularization but dispensable for endothelial sprouting. *Proc. Natl. Acad. Sci.* **108**, 13264 LP – 13269 (2011).
100. Deng, Z. *et al.* Hypoxia-Mimicking Cobalt-Doped Borosilicate Bioactive Glass Scaffolds with Enhanced Angiogenic and Osteogenic Capacity for Bone Regeneration. *Int. J. Biol. Sci.* **15**, 1113–1124 (2019).
101. Wu, C. *et al.* Hypoxia-mimicking mesoporous bioactive glass scaffolds with controllable cobalt ion release for bone tissue engineering. *Biomaterials* **33**, 2076–2085 (2012).
102. Ribatti, D. & Crivellato, E. Immune cells and angiogenesis. *J. Cell. Mol. Med.* **13**, 2822–2833 (2009).
103. Costa-Almeida, R., Granja, P. L., Soares, R. & Guerreiro, S. G. Cellular strategies to promote vascularisation in tissue engineering applications. *Eur. Cells Mater.* **28**, 51–67 (2014).
104. Liu, J., Chuah, Y. J., Fu, J., Zhu, W. & Wang, D.-A. Co-culture of human umbilical vein endothelial cells and human bone marrow stromal cells into a micro-cavitary gelatin-methacrylate hydrogel system to enhance angiogenesis. *Mater. Sci. Eng. C* **102**, 906–916 (2019).
105. Gurdon, J. B. & Bourillot, P. Y. Morphogen gradient interpretation. *Nature* **413**, 797–803 (2001).
106. Ashe, H. L. & Briscoe, J. The interpretation of morphogen gradients. *Development* **133**, 385–394 (2006).
107. Adams, R. H. & Alitalo, K. Molecular regulation of angiogenesis and lymphangiogenesis. *Nat. Rev. Mol. Cell Biol.* **8**, 464–478 (2007).

108. Kay, R. R., Langridge, P., Traynor, D. & Hoeller, O. Changing directions in the study of chemotaxis. *Nat. Rev. Mol. Cell Biol.* **9**, 455–463 (2008).
109. Sarker, M. D., Naghieh, S., Sharma, N. K. & Chen, X. 3D biofabrication of vascular networks for tissue regeneration: A report on recent advances. *J. Pharm. Anal.* **8**, 277–296 (2018).
110. Griffith, L. G. & Swartz, M. A. Capturing complex 3D tissue physiology in vitro. *Nat. Rev. Mol. Cell Biol.* **7**, 211–224 (2006).
111. Kim, S., Kim, H. J. & Jeon, N. L. Biological applications of microfluidic gradient devices. *Integr. Biol. (Camb).* **2**, 584–603 (2010).
112. Kim, B. J. & Wu, M. Microfluidics for mammalian cell chemotaxis. *Ann. Biomed. Eng.* **40**, 1316–1327 (2012).
113. Smith, Q. & Gerecht, S. Microfluidic Platforms in Vascular Tissue Engineering. *Curr Opin Chem Eng* 42–50 (2015). doi:10.1016/j.coche.2013.11.001.Going
114. Ebrahimi, A. P. Mechanical properties of normal and diseased cerebrovascular system. *J. Vasc. Interv. Neurol.* **2**, 155–162 (2009).
115. Fenech, M. & Meance, S. Lab on a Chip backside lithography †. 2096–2106 (2019). doi:10.1039/c9lc00254e
116. Guillemette, M. D. *et al.* Tissue-Engineered Vascular Adventitia with Vasa Vasorum Improves Graft Integration and Vascularization Through Inosculation. *Tissue Eng. Part A* **16**, 2617–2626 (2010).
117. Richards, D., Jia, J., Yost, M., Markwald, R. & Mei, Y. 3D Bioprinting for Vascularized Tissue Fabrication. *Ann. Biomed. Eng.* **45**, 132–147 (2017).
118. Miri, A. K. *et al.* Multiscale bioprinting of vascularized models. *Biomaterials* **198**, 204–216 (2018).
119. Martin, E. *et al.* Cell-Demanded Liberation of VEGF121 From Fibrin Implants Induces Local and Controlled Blood Vessel Growth. *Circ. Res.* **94**, 1124–1132 (2004).
120. Martineau, L. & Doillon, C. J. Angiogenic response of endothelial cells seeded dispersed versus on beads in fibrin gels. *Angiogenesis* **10**, 269–277 (2007).
121. Borenstein, J. T. *et al.* Microfabrication Technology for Vascularized Tissue Engineering. *Biomed. Microdevices* **4**, 167–175 (2002).
122. Klar, A. S. *et al.* Tissue-engineered dermo-epidermal skin grafts prevascularized with adipose-derived cells. *Biomaterials* **35**, 5065–5078 (2014).
123. Zhu, W. *et al.* Direct 3D bioprinting of prevascularized tissue constructs with

complex microarchitecture. *Biomaterials* **124**, 106–115 (2017).

124. Mironov, V., Kasyanov, V. & Markwald, R. R. Nanotechnology in vascular tissue engineering: from nanoscaffolding towards rapid vessel biofabrication. *Trends Biotechnol.* **26**, 338–344 (2008).
125. Sensenig, R., Sapir, Y., MacDonald, C., Cohen, S. & Polyak, B. Magnetic nanoparticle-based approaches to locally target therapy and enhance tissue regeneration in vivo. *Nanomedicine (Lond).* **7**, 1425–1442 (2012).
126. Estelrich, J., Escribano, E., Queralt, J. & Busquets, M. A. Iron oxide nanoparticles for magnetically-guided and magnetically-responsive drug delivery. *Int. J. Mol. Sci.* **16**, 8070–8101 (2015).
127. Perea, H., Aigner, J., Heverhagen, J., Hopfner, U. & Wintermantel, E. Vascular tissue engineering with magnetic nanoparticles: Seeing deeper. *J. Tissue Eng. Regen. Med.* **1**, 318–321 (2007).
128. Cui, L. *et al.* Vascularization of LBL structured nanofibrous matrices with endothelial cells for tissue regeneration. *RSC Adv.* **7**, 11462–11477 (2017).
129. Kim, S., Lee, H., Chung, M. & Jeon, N. L. Engineering of functional, perfusable 3D microvascular networks on a chip. *Lab Chip* **13**, 1489–1500 (2013).
130. Zhang, W. *et al.* Elastomeric free-form blood vessels for interconnecting organs on chip systems. *Lab Chip* **16**, 1579–1586 (2016).
131. Sasmal, P., Datta, P., Wu, Y. & Ozbolat, I. T. 3D bioprinting for modelling vasculature. *Microphysiological Syst.* **2**, 9 (2018).
132. Fenech, M. *et al.* Microfluidic blood vasculature replicas using backside lithography. *Lab Chip* **19**, 2096–2106 (2019).
133. Lee, J. *et al.* Microfluidics in structured multimaterial fibers. *Proc. Natl. Acad. Sci.* **115**, E10830–E10838 (2018).
134. Orf, N. D. *et al.* Fiber draw synthesis. *Proc. Natl. Acad. Sci.* **108**, 4743 LP – 4747 (2011).
135. Gumuscu, B. *et al.* Desalination by Electrodialysis Using a Stack of Patterned Ion-Selective Hydrogels on a Microfluidic Device. *Adv. Funct. Mater.* **26**, 8685–8693 (2016).
136. Hann, S. Y. *et al.* Recent advances in 3D printing: vascular network for tissue and organ regeneration. *Transl. Res.* **211**, 46–63 (2019).
137. Sarker, M. D., Naghieh, S., Sharma, N. K. & Chen, X. 3D biofabrication of vascular networks for tissue regeneration: A report on recent advances. *J. Pharm.*

Anal. **8**, 277–296 (2018).

138. Miller, J. S. *et al.* Rapid casting of patterned vascular networks for perfusable engineered three-dimensional tissues. *Nat. Mater.* **11**, 768–774 (2012).
139. Jafarkhani, M., Salehi, Z., Aidun, A. & Shokrgozar, M. A. Bioprinting in Vascularization Strategies. *Iran. Biomed. J.* **23**, 9–20 (2019).
140. Zhang, Y., Yu, Y. & Ozbolat, I. T. Direct Bioprinting of Vessel-Like Tubular Microfluidic Channels. *J. Nanotechnol. Eng. Med.* **4**, (2013).
141. Miri, A. K. *et al.* Multiscale bioprinting of vascularized models. *Biomaterials* **198**, 204–216 (2019).
142. Jia, W. *et al.* Direct 3D bioprinting of perfusable vascular constructs using a blend bioink. *Biomaterials* **106**, 58–68 (2016).
143. Abhishek, S. As featured in : Lab on a Chip. (2019). doi:10.1039/c9lc00469f
144. Pauty, J. *et al.* A Vascular Endothelial Growth Factor-Dependent Sprouting Angiogenesis Assay Based on an In Vitro Human Blood Vessel Model for the Study of Anti-Angiogenic Drugs. *EBioMedicine* **27**, 225–236 (2017).
145. Jakab, K. *et al.* Tissue engineering by self-assembly of cells printed into topologically defined structures. *Tissue Eng. Part A* **14**, 413–421 (2008).
146. Mironov, V., Kasyanov, V., Drake, C. & Markwald, R. R. Organ printing: promises and challenges. *Regen. Med.* **3**, 93–103 (2008).
147. Hashi, C. K. *et al.* Antithrombogenic property of bone marrow mesenchymal stem cells in nanofibrous vascular grafts. *Proc. Natl. Acad. Sci. U. S. A.* **104**, 11915–11920 (2007).
148. Zhang, Y. S., Zhang, Y.-N. & Zhang, W. Cancer-on-a-chip systems at the frontier of nanomedicine. *Drug Discov. Today* **22**, 1392–1399 (2017).

Chapter III



Magnetic-Responsive PVA Hydrogels For Remote Modulation Of Protein Sorption

Published as: Manjua, A. C., Alves, V. D., Crespo, J. G. & Portugal, C. A. M. Magnetic Responsive PVA Hydrogels for Remote Modulation of Protein Sorption. ACS Appl. Mater. Interfaces acsami.9b03146 (2019). doi:10.1021/acsami.9b03146

CHAPTER III – Magnetic-responsive PVA hydrogels for remote modulation of protein sorption

The present chapter investigates the impact of magnetic forces on the structural and mechanical properties of a hydrogel, doped with iron oxide nanoparticles, while studying the potential for reversibility of the combined biological effect of magnetic hydrogel and magnetic field on protein interactions with the hydrogel.

Outline

This work shows the ability to reversibly modulate protein sorption (protein adsorption and absorption) at polyvinyl alcohol (PVA) hydrogel membranes doped with magnetic iron oxide nanoparticles (MNPs) by adjustment of an external magnetic field. The ability to regulate protein sorption to the PVA hydrogel membranes is demonstrated by the subsequent protein sorption-released stages attained by cyclic variation of an external magnetic field. It is shown that protein sorption may be reverted in a non-invasive way by switching ON the magnetic field. The ability to magnetically regulate protein sorption and release is discussed and ascribed to the well-known ability of ferrogels to undergo volume contraction-distention when exposed to magnetic field forces. Hydrogel volume changes leads to reversible switches of the hydrogel porosity and/or surface contact angles (due to changes in surface roughness), influencing the protein diffusion and adsorption capacity to the hydrogel. Therefore, these magnetic hydrogels are regarded as promising candidates towards the development of functional devices for tissue engineering, drug release applications or biosensor systems, where the control of protein mobility, attachment or structural conformation at interfaces are essential steps to improve the efficiency of these processes.

Keywords: ferrogel, magnetic field, protein sorption, tissue engineering, biosensor, bioseparation, biocompatibility

III.1. Introduction

Protein-surface interactions exert a paramount role in the control of bioprocess performance. Non-specific adsorption of proteins promotes the uncontrolled accumulation of these molecules at surfaces leading to undesirable biofouling events[1-3], rendering processes with low efficiencies due to hindered molecular transport through the processing media. Besides the prejudicial effect of biofouling, the structural behavior of proteins at surfaces has important influence in molecular recognition mechanisms, as those inherent to affinity based separations processes[4], biosensors[5,6] and regenerative medicine systems[7, 8]. Protein-surface interactions are generally followed by changes of protein conformation whose amplitude depends on the surface and protein properties. Protein structural deformation at surfaces affects not only protein binding stability, but also it may generate higher or lower exposure of important epitopes (binding sites or molecular recognition peptide segments), thus ruling the accessibility of target solutes (e.g. enzymatic substrates, cells) to specific protein binding sites.

The ability to control protein behavior at surfaces is thus an essential aspect in bioprocessing[9] and different regenerative medicine issues, e.g. tissue engineering, organ implants, wound healing and (bio)artificial organs. The accessibility of transmembrane cell receptors (e.g. integrins) to specific peptide binding sequences (e.g. RGDS) contained in adhesion proteins at the tissue scaffold is determinant for the development of cell tissue. The intensity of cell adhesion defines the cell stability and density at scaffolds as well as the force balance established between the cytoskeleton and the scaffold which are primary activators of cell signaling mechanisms driving cell differentiation into tissues with desirable phenotypes[10]. In contrast, the development of surfaces exhibiting minimal protein adsorption remains as a major challenge in the design of implants and (bio)artificial organs with improved biocompatibility[11]. The adsorption of blood proteins (immunoglobulins) and their structural unfolding at surfaces are promotors of immune responses (e.g. complement activation), which may result in uncontrolled inflammation processes ending up in the rejection of the foreign body (e.g. implants) by the host (e.g. patients)[12]. Additionally, protein adsorption at surfaces prompts the formation of aggregates, which may cause the disruption of blood circulation increasing the risk of thrombosis.

Functional surfaces with tailored topographies and chemistries have been designed aiming to reduce protein adsorption while controlling their conformation at surfaces[13] in order to obtain a better control over molecular interfacial events. Both, protein adsorption capacity and structural behavior at surfaces are intimately related with surface hydrophilic/hydrophobic degree[14-16]. Hence, most surface functionalization strategies have involved the design of surfaces with tailored static[17, 18] or dynamic wettability (stimuli-responsive surfaces)[14, 19, 20] envisaging the development of anti-fouling surfaces or materials with improved biocompatibility, by the reduction of protein adsorption. In accordance to Wentzel[21], Cassie and Baxter[22] models, the surface wettability is influenced by the surface topography, i.e. surface roughness. Surface roughness is described to play a key role in modulating cell behavior for implant biomaterials (e.g. titanium, ceramics, stainless steel, and polymers)[23] .Roughness enhances the hydrophilic degree of surfaces with high free energy as well as the hydrophobic degree of surfaces with low free energy[14,19,24,25]. The relation between roughness and the surface hydrophilic/hydrophobic character has been exploited towards the design of responsive surfaces able to exchange between extreme hydrophilic (superhydrophilic) and hydrophobic (superhydrophobic) characters. This responsive behavior has been mostly achieved by incorporation of stimuli-sensitive molecules into surfaces with accentuated roughness[19].

Hence, hydrophilic-hydrophobic switches are due to the reversible changes of the free energy of the stimuli-responsive agents when exposed to variable stimuli conditions, e.g. pH, temperature or light, which are then amplified by the surface roughness. Such unique functionality has been explored towards the development of anti-fouling membranes and responsive tissue scaffolds envisaging an efficient modulation of cell behavior[26, 27], *i.e.* a better organization of cell co-cultures and on-demand cell detachment at/from the tissue scaffolds[28, 29] based on a suitable control of protein adsorption.

Aiming to explore the beneficial effects of stimuli-responsive surfaces, the combination of the photo-thermal properties of nanocomposite hydrogels with magnetic ability has been demonstrated to function as a heating source with controlled position and location of healing through a magnet for potential applications such as drug delivery, controlled catalysis and microdevices[30]. External high frequency alternating current electric fields can also be used to promote direct assembly of hard colloidal particles into linear chains and clusters within a soft thermo-responsive pNIPAAM hydrogel membrane to perform catalytic roles or function as tissue adhesives, artificial cartilage and sensors[31].

Thermo-responsive properties of pNIPAAM have also been explored towards the design of membranes which based on the swelling-unswelling mechanisms of pNIpAAM around the low critical solution temperature (LSCT) are capable of a reversible adjustment of pore sizes allowing for a better control of the permeate fluxes and solute permeation[32] and protein binding[33]. Furthermore, pH-responsive polymeric membranes have been reported with ability to reversibly enhance mass transport, by increasing the flux more than two orders of magnitude when switching the pH from 2 to 8[34].

However, the use of these responsive systems modulated by addition of mass agents, e.g. pH, are undesirable in most applications, since they involve the consecutive accumulation of the agents responsible for inducing the surface response. Likewise, the use of temperature-responsive surfaces is limited to thermal insensitive processes whereas photo-responsive behaviors are mostly ruled by slow reversible photo-isomerization reactions, leading to delayed responses or losses of responsive capacity.
Magnetic responsive soft polymers, *e.g.* hydrogels, integrating magnetic nanoparticles (MNPs), *e.g.* iron oxide nanoparticles, have shown to be able to respond to an adequate magnetic field in a fast mode, with reversible changes of their shape and volume[35,36]. For instance, the direct incorporation of covalently attached metal nanoparticles/ nanomagnets into the backbone of a hydrogel allows for the design of significantly stronger magnetic actuators with higher mechanical stability, muscle-like flexibility and shape memory effect with potential for their use in tissue engineering as soft actuators or artificial muscles[37,38].

Contraction-distension of these hydrogels is driven by the movements of the embedded MNPs induced by magnetic attractive-repulsive forces imposed by a non-uniform magnetic field[35]. Profiting from their magnetically driven shrinking/unshrinking ability, these hybrid assemblies have been applied as mechanical actuators, used for the design of membranes with adjustable pore sizes[39], as activators of molecular motors to mimic nature systems[40] and to modulate cell responses at magnetic responsive hydrogel scaffolds[41,42]. Magnetic hydrogels were shown to provide means to remotely induce mechanical forces with controlled direction and intensity, similar to that required for cell mechanotransduction (~1pN)[41]. This magneto-mechanical stimulation was showed to elevate the metabolic activity of aortic endothelial and cardiac cells in the presence of an alternate (AC) magnetic field ascribed to an accurate magnetic control of cellular organization[41]. In a different work from Tognato et al.[42] magnetic-responsive hydrogels

with anisotropic alignment of MNPs showed to be able to induce the differentiation of C2C12 myoblasts into myotubes in the absence of differentiation media.

This work reports the ability to regulate the sorption and release of proteins at PVA hydrogel with embedded magnetic nanoparticles taking advantage of the magnetic responsive ability of these materials. These studies were performed in order to understand the impact of the magnetic response of these hydrogels on protein sorption and release aiming to elucidate about their potential contribution for development of tissue engineering, drug release or biosensing systems with improved efficiency.

III.2. Experimental Section

Materials. $FeCl_3.6H_2O$, $FeCl_2.4H_2O$, potassium oleate, hitenol-BC and ammonium persulfate were purchased to Sigma-Aldrich whereas 25% aqueous ammonium solution were acquired from Fluka. Poly (vinyl)alcohol (PVA), glycerol, glutaraldehyde (GA), chloride acid (HCl) solution (37%) and BSA-FITC were supplied by Sigma-Aldrich.

Synthesis of the magnetic nanoparticles (MNPs). The magnetic nanoparticles (MNPs) were synthesized by chemical co-precipitation of two different iron salts $FeCl_3$ and $FeCl_2$ in alkaline media according to the protocol previously published by Olle et al. 2006[43]. Briefly, an aqueous solution with 25% of ammonium hydroxide (NH_4OH) was added to a mixture of $FeCl_3$ and $FeCl_2$ at 80^oC, under permanent stirring at 1250 rpm by purging N_2. Potassium oleate and ammonium persulfate were then added to the reaction mixture for production of Fe_3O_4 coated particles aiming to minimize particle aggregation. Hitenol-BC was used as a surfactant. The nanoparticles solution was then centrifuged and evaporated using ethanol solution.

Preparation of the magnetic-responsive hydrogel membranes. MNPs were dispersed by sonication in an 8% PVA aqueous solution, containing 1% glycerol. 3% of GA (crosslinking agent) and 3% of HCl (37%) were added to the solution and the final solution before casting onto glass plates. Magnetic responsive PVA hydrogel membranes containing different concentrations, up to 1% (w/v), of randomly dispersed MNPs were prepared. The magnetic loaded polymer solution was casted into a casting plate with a

volume (mL)/casting plate area (cm^2) ratio of 0.42 mL/cm^2, which allowed for the preparation of matrices with a thickness of ca. 250 μm.

Prior to use, the magnetic PVA hydrogel membranes were washed by immersion in a demineralized water bath. The removal of non-bound material upon swelling of PVA membrane in water was followed by UV-Vis spectrometry of the washing solution along time. The wash out of magnetic particles was inspected through determination of the iron content in the washing solution by inductively coupled plasma (ICP-AES), after sample digestion. No significative amount of MNP removal or additional clustering were observed along the washing procedures, revealing that the degree of polymer reticulation achieved with 3% of GA was enough to produce hydrogel membranes with good chemically and structurally stability in aqueous media.

Structural characterization of the MNPs and hydrogel membranes. The MNPs size distribution was accessed by transmission electron microscopy (TEM), using a TEM Hitachi H8100 with a LAB6 filament, and an acceleration tension of 200 kVolts. The MNP sizes were determined using the image j software, whereas average particle size was elicited by statistical analysis of a total of 320 counts and using a confidence level of 95%. The dispersion quality of the MNPs was inspected by optical microscopy using a microscope Olympus BH-2, equipped with a photo camera Casio Exilim Pro (EX-F1), and by scanning electron microscopy using a FEG-SEM equipment (JEOL, model JSM7001F) coupled to a light energy EDS detector (Oxford, model INCA 250).

Surface and cross-section of hydrogel membranes with MNPs contents ranging from 0% (without MNPs) to 1% MNPs were characterized in swollen state by environmental SEM (ESEM) upon frozen at -20 ºC, in order to minimize structural changes along the measurements due to dehydration. In contrast to conventional SEM analysis, ESEM does not require the pre-coating of the sample allowing analysis of the structure of swollen membrane hydrogel. Identical ESEM analyses were conducted for hydrogel membranes doped with 0.25% MNPs, before and after exposure to the magnetic field. ESEM analyses were carried out using a Tabletop Microscope (Hitachi, TM3030Plus).

Young's modulus of the magnetic hydrogel. The Young's modulus, E (kPa) of the hybrid hydrogel membranes was calculated based on the slopes of the stress-strain curves in the elastic region under puncture tests. The puncture tests were performed using a texturometer (TA-XT2 Stable Micro System, UK) equipped with a 2 mm diameter

cylindrical probe, which punctured PVA hydrogels with different concentrations of MNPs (2x2 cm^2), at a cross head speed of 0.5 mm/s. The values of the Young's modulus corresponded to the average values of at least three replicates.

Surface roughness of the hydrogel. The determination of surface roughness was initially attempted by atomic force microscopy (AFM) analysis. However, the dimension of the roughness details presented at the membrane surfaces with higher magnetic load exceeded the analytical range of this technique. For this reason, surface roughness measurements were performed by profilometry using an Ambios XP-200 profilometer equipped with a 2.5 μm tip by sequentially measuring profile lines with a 10 μm spacing and using TrueMap software for 3D images compilation. Profilometry measurements were performed using PVA membranes in their maximum swollen state, attained upon immersion of the PVA membranes in water for 30 min.

Surface contact angles of the hydrogel. Surface contact angles (CA) of hydrogels were determined using glycerol as the liquid phase, in the absence and presence of a non-uniform magnetic field up to 0.08T. Magnetic field was imposed by a neodymium magnet placed underneath the hydrogel membranes and the magnetic field intensity was varied adjusting the distance of the neodymium magnet to the hydrogel. The dynamic glycerol contact angles were determined in a sessile drop mode using a drop shape analyzer system coupled to a video camera connected to a PC for data acquisition and the determination of the CA along time using the CAM100 software. The final CA values were taken as the average of the values obtained for at least 3 replicates.

Protein sorption studies under static and dynamic magnetic field conditions. Protein sorption experiments were conducted by immersion of PVA hydrogel membranes with different MNP loads, in 1g/L trypsin and FITC-Albumin (only in dynamic field conditions) in a pH 8 Trizma buffer solution, in the absence and presence of magnetic field with different intensities up to 1 T. The supernatant was periodically sampled and analyzed by UV spectrophotometry at 280 nm in order to quantify the trypsin in the supernatant along time. The mass of trypsin sorbed (adsorbed and absorbed) in the hydrogel membrane in each moment was obtained by subtraction of the amount of trypsin in the initial solution by that present in the supernatant in the different sampling times.

Experiments at static magnetic field conditions were developed by keeping the magnetic field constant along the experiment time whereas dynamic magnetic field conditions were achieved by successively OFF/ON or ON/OFF magnetic field switching, where the magnetic field intensity was varied between 0 and 0.45T or 1T. Protein sorption studies at low magnetic field intensities < 0.5 T, were performed using a neodymium magnet, whereas a 3472 dipole H-frame electromagnet, from GMW Associates (USA) was used to produce magnetic field intensities higher than 0.5 T. The H-frame electromagnet was coupled to a refrigeration bath for controlling the temperature of the magnetic poles. Both experimental set-ups were mounted in a way to assure that the magnetic vector was perpendicularly oriented to the hydrogel surface.

Confocal microscopy measurements. Fluorescence emission confocal scans were acquired for hydrogel membranes used in FTIC-Albumin sorption tests in the absence of magnetic field and exposed to OFF/ON magnetic field cycle, using a Confocal Laser Scanning Microscope (LSM 700/ Carl Zeiss), with a 10 mW 488 nm laser. Afterwards, the image analysis was performed using ZEN 2.1 software (Carl Zeiss).

III.3. Results and Discussion

3.1. Magnetic-responsive behavior of the hydrogel membranes

Magnetic sensitive hydrogel membranes with isotropic magnetic morphology were obtained by random dispersion of iron oxide nanoparticles (MNPs), with sizes ranging from 2 nm to 20 nm and an average diameter of approximately 9 nm (Figure III. 1A), in polyvinyl alcohol (PVA) solution. PVA membranes with physically entrapped iron oxide nanoparticles (MNPs) were formed upon crosslinking of the PVA chains using glutaraldehyde (GA). The GA fraction added was such to confer a good structural stability and robustness to the membrane matrix, avoiding particle displacement and coalescence, with minimum detriment of the surface elasticity. These hybrid hydrogel membranes exhibited magnetic architectures, formed by randomly well-dispersed micro-MNP clusters (Figure III. S1 and Figure III. S2 in Supplementary Information) of heterogeneous sizes. As shown in Figures 1B and 1C, the hydrogels doped with 0.25% of MNPs exhibit MNP clusters, with sizes varying from 3 μm to 28 μm and an average

size of 16.7 µm ± 7.0 µm, whereas hydrogels doped with 1% MNPs showed lower sized clusters with dimensions varying between 2 µm to 12 µm and an average size of 5.6 µm ± 2.8 µm. These hydrogels were characterized regarding their magnetic properties by determination of their saturation magnetization curves (Figure III. S3 in Supplementary Information). A comparative analysis of the magnetization saturation curves showed an increase of the magnetic saturation from 0.031 emu/g to 0.192 emu/g due to the increase in the concentration of MNPs from 0.25% to 1%. The absence of hysteresis loops confirmed that both PVA hydrogels with 0.25% and 1% MNPs have a typical superparamagnetic behavior, without remnant magnetization upon removal of the magnetic field[44].

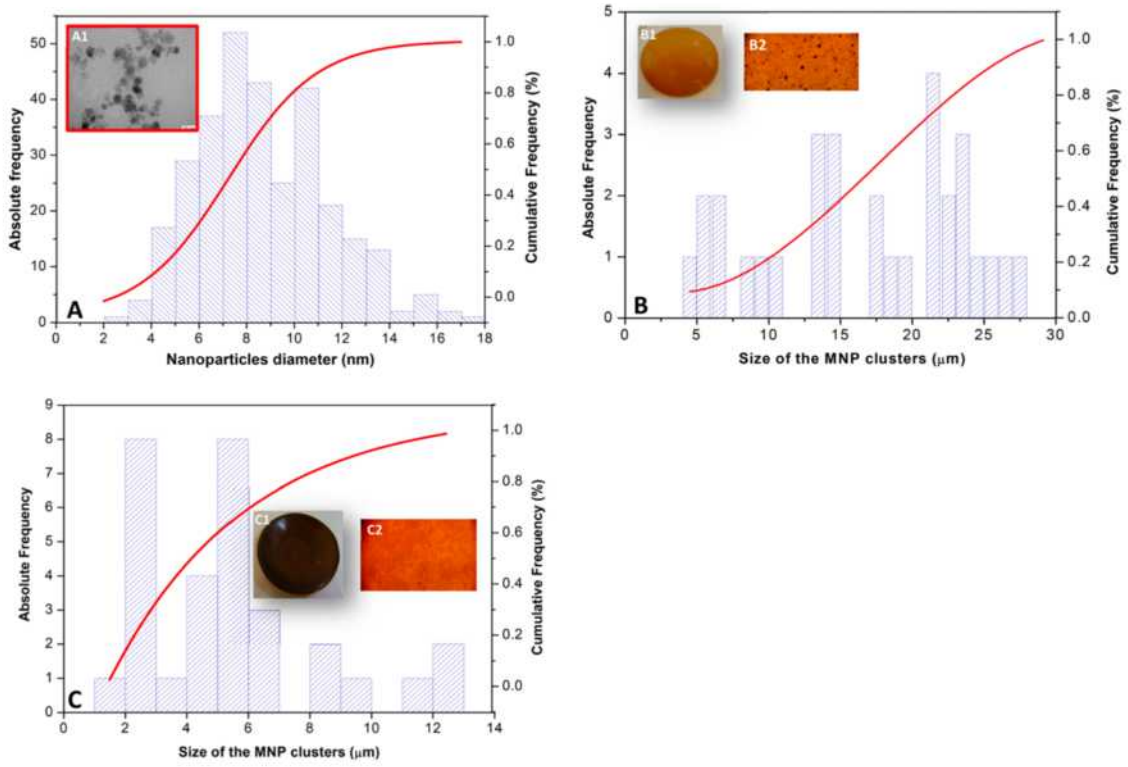


Figure III. 1. Size distribution of the **A**) magnetic nanoparticles (MNPs) obtained by ImageJ treatment of TEM analysis, **B**) MNP clusters in PVA hydrogels doped with 0.25% of MNPs, and **C**) MNP clusters in PVA hydrogels doped with 1% of MNPs, obtained by ImageJ treatment of the optical microscopy images. Relative and cumulative frequencies are represented by the bars and the red line, respectively. Insets: (A1) TEM image of the MNPs. Photos (B1 and C1) and optical microscopy images (B2 and C2) of PVA hydrogel membranes doped with 0.25% and 1% MNPs, respectively.

The impact of the MNP clusters on the surface roughness of the hydrogels was also studied by profilometry analysis. The profilometry images in Figure 2 showed an increase of the surface roughness from 219 nm to 852 nm, as the MNP content increased from 0% to 1%. However, considering the magnetic susceptibility of the MNPs and

assuming that entrapped MNPs can still move due to the elasticity of the hydrogel, one may hypothesize a potential influence of the magnetic field on the surface texture of PVA hydrogels (e.g. roughness). Taking into account the relationship between the surface roughness and the hydrophilic/hydrophobic character as expressed by Wentzel and Cassie-Baxter theories[19,20], the magnetic dependence of the surface properties was inspected by determining the impact of the magnetic field on the surface contact angle. Analyses of the surface contact angle (CA) were performed using glycerol as the solvent, in the absence and presence of a non-uniform magnetic field. The magnetic field was applied by placing a neodymium bar underneath the membrane whereas the magnetic field intensity was varied from 0 T to 0.08 T, by adjusting the distance between the neodymium magnet and the membrane.

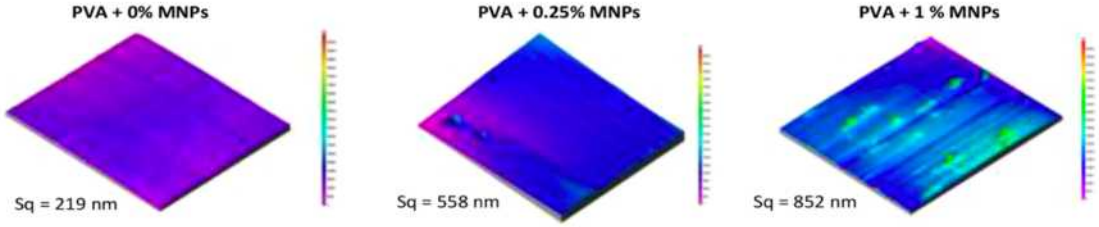


Figure III. 2. Profilometry images of PVA hydrogels and their respective surface roughness, Sq.

As shown in Figure III. 3A, the values of the contact angles obtained for the magnetic hydrogel membranes with MNP loads up to 1%, showed to decrease proportionally to the magnetic field intensity. As so, the contact angle of hydrogel membranes with 0.25% MNPs, which showed an initial value of 53° at 0T, decayed to 46°, at 0.05 T and to 28°, at 0.08T. Also, the effect of the magnetic field on the contact angles was found to depend on the MNPs load in the hydrogel. The highest contact angle decay was observed for hydrogels with lower MNP amounts. Hydrogels doped with 0.25% MNPs showed a contact angle decay of ca. 25° at 0.08T, whereas a decrease of only 14° was achieved for hydrogels with 1% MNPs at the same magnetic field intensity. Based on these results, a higher effect would be expected if higher magnetic field intensities were applied; however, the determination of surface contact angles at stronger magnetic fields was impaired by the impossibility to couple the drop shape analysis system used for the determination of the contact angles to powerful magnetic field sources, e.g. electromagnet system.

To clarify the role of MNPs in the hydrogels magnetic-response, the impact of magnetic field on hydrogels without MNPs was also inspected. As shown in Figure 3A, the contact angles of hydrogel membranes without MNPs remained invariable, not depending on the magnetic field conditions (noticeable by the overlapping of the data points obtained for hydrogels with 0% MNPs exposed to different magnetic field intensities – Figure III. 3A). This result confirms that the magnetic responsive behavior of these hydrogels was exclusively due to the magnetic susceptibility of the MNPs.

Since no chemical modifications were expectable due to the magnetic field, changes of the surface contact angles should be interpreted as a consequence of structural alterations taking place in hydrogel matrix when exposed to the magnetic field. These structural changes are thought to result from a synergistic effect of the magnetic susceptibility of the embedded MNPs and the elasticity of these hybrid membranes.

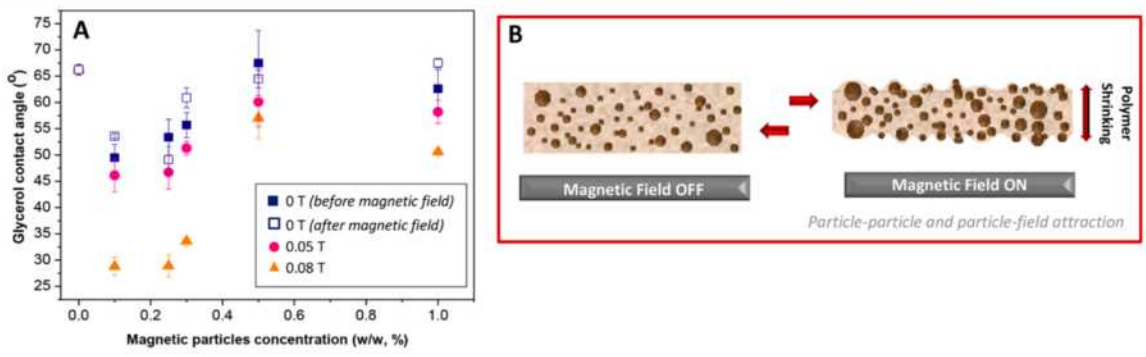


Figure III. 3. A) Impact of the magnetic field on the glycerol contact angle at the surface of nonmagnetic and magnetic hydrogels doped with different concentration of MNPs. **B**) Schematic representation of the magnetic induced reversible roughness of the hydrogel surface.

Despite their physical entrapment within the hydrogel membranes, MNPs may still be able to move in response to particle-particle and particle-field forces imposed by the applied magnetic field. The MNP mobility induced by the magnetic field is allowed by the elasticity of the hydrogel matrix, leading to the structural deformation of the hydrogel.

A schematic illustration of the possible deformation of PVA hydrogels when exposed the magnetic field perpendicularly oriented towards the hydrogel surface is shown in Figure III. 3B. According to this scheme, when the magnetic field is applied the MNPs are attracted to each and according to the magnetic field leading to the hydrogel shrinking. This hypothetical interpretation is in total agreement with the studies developed by Szábo et al[35] and Snyder et al[36], which showed the ability of ferrogels to

undergo volume and shape changes, leading to hydrogel volume shrinking in the presence of magnetic field. In this case, it plausible to think that membrane shrinking might bring a higher amount of MNPs closer to the membrane surface, leading to an increase of the surface roughness followed by an increase of the surface wettability. It is important to highlight that since Fe_3O_4 particles (MNPs) exhibit size-dependent saturation magnetization[45], the presence of some MNP clustering observed in the hydrogels, is expected to exert a beneficial effect on the magnetic responsive capacity of these hybrid hydrogels. Despite plausible, this explanation should be considered as a hypothetical interpretation given the impossibility to have a direct measurement of the hydrogel surface roughness in the presence of magnetic field.

Differences in the intrinsic porous structure (in the absence of magnetic field) of hydrogels doped with different amounts of MNPs may however, explain the lower surface contact angles observed for hydrogels with lower MNP contents, i.e. < 0.25% (Figure III. 3A).

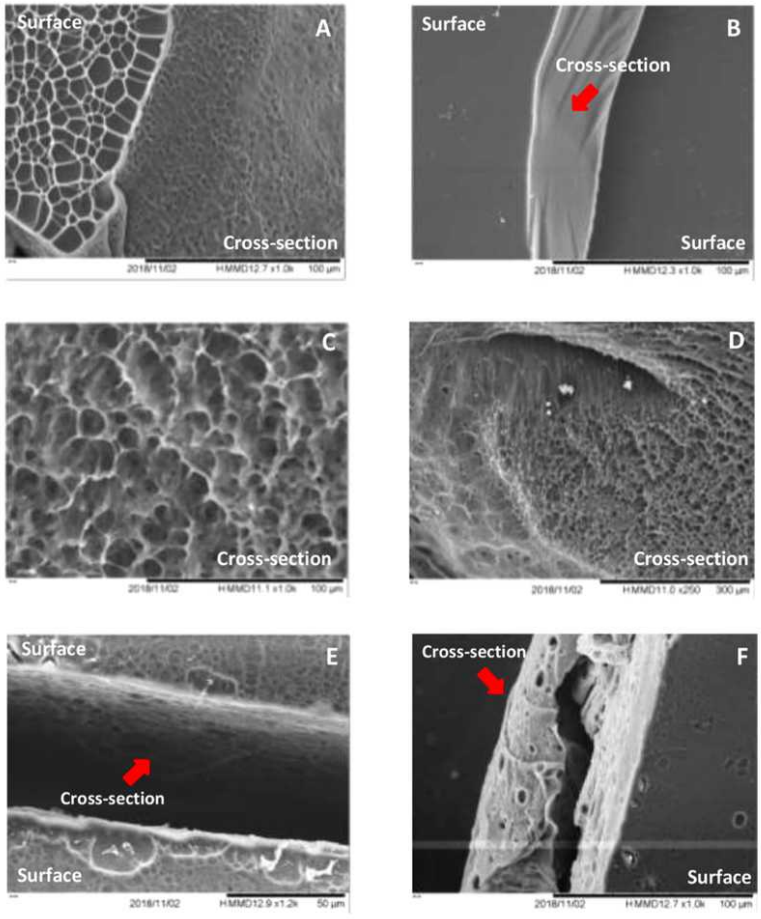


Figure III. 4. Environmental SEM (ESEM) images of surfaces and cross sections of nonmagnetic PVA hydrogel membrane (**A**, H_2O saturated; **B**, dry) and PVA hydrogel membrane with (**C**, **D**) 0.25% MNPs and **(E**, **F**) 1% MNPs before exposure to the magnetic field.

This effect was supported by analysis of swollen hydrogels with different MNP loads by environmental scanning electron microscopy (ESEM), which showed that the porosity of PVA hydrogels doped with 0.25% of MNPs (Figures III. 4C and 4D) was higher than that exhibited by PVA hydrogels without MNPs (Figure III. 4A) or with higher MNP contents, e.g. 1% (Figures III. 4E and 4F).

Independently of the reason underlying the magnetic behavior of the surface contact angles, it was important to note that the initial surface contact angles were promptly recovered upon removal of the magnetic field (compare filled and empty square symbols in Figure III. 3A), showing that these hybrid hydrogel membranes allowed for fast and reversible response to the magnetic field.

3.2. Impact of the magnetic behavior of hydrogel membranes on protein sorption

Surface properties, like roughness and wettability, define the nature of protein-surface interactions[46] which is a critical aspect in the performance of tissue engineering processes, bioseparations or biosensors, whose efficiency is highly dependent on protein attachment ability/stability, mobility and structural dynamics at interfaces. In this sense, studies were carried out aiming to evaluate the potential use of magnetic-responsive hydrogel membranes for the modulation of protein sorption (adsorption and absorption) in order to contribute to improving the performance of bioprocesses.

At this point, the readers should bear in mind that protein sorption considers both: i) protein adsorption, which results from the attachment of the proteins at the external and internal hydrogel surfaces, and ii) protein absorption, which was due to the diffusion of the protein molecules in solution into the hydrogel matrix. Protein adsorption and absorption processes were difficult to distinguish in the experimental conditions used in the present work. Thus, the individual effect of magnetic field on protein adsorption and absorption is not shown but discussed in terms of protein sorption.

Protein sorption studies were developed in the absence and presence of magnetic field oriented perpendicularly to the hydrogel surfaces doped with 0.25% and 1% MNPs, using trypsin as a model protein. Trypsin sorption profiles obtained at different magnetic field intensities (up to 1T) are shown in Figure III. 5A. The analysis of these profiles showed that the amount of trypsin in the membrane decreases proportionally to the magnetic field intensity, evidencing that the magnetic field reduces protein sorption

ability. In fact, the amount of trypsin sorbed, after 250 min, when exposed to a constant magnetic field intensity of 1T is insignificant when compared to the $9x10^{-3}$ g/cm^3 sorbed, during the same time in the absence of magnetic field.

The impact of the magnetic field on trypsin sorption in hydrogels without MNPs was also evaluated. As shown in the Inset of Figure III. 5A, the trypsin sorption profiles obtained at 0T and 1T were similar confirming that the magnetic induced variation of protein sorbed in the magnetic hydrogel membranes was actually ascribed to the magnetic-responsive behavior of the hydrogels and not to a potential intrinsic magnetic sensitivity of trypsin.

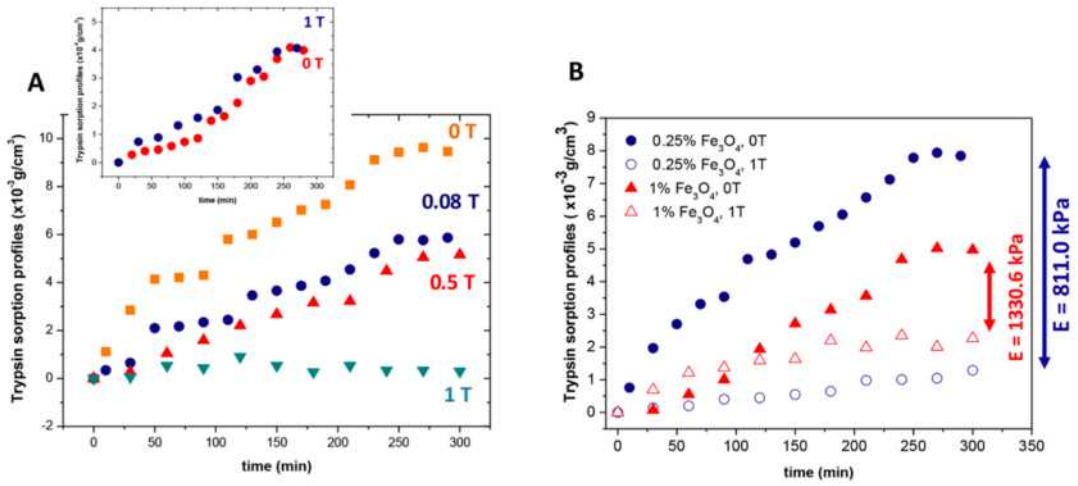


Figure III. 5. A) Time-dependent trypsin sorption at magnetic hydrogel surfaces doped with 0.25% (w/v) of MNPs under different magnetic field intensities. Inset: influence of magnetic field on the tryspin sorption at surfaces of nonmagnetic hydrogels at 0 and 1 T. **B**) Trypsin sorption observed at hydrogel surfaces with 0.25% (w/v) and 1% (w/v) of MNPs at 0 and 1 T, respectively, and Young's modulus, E (kPa).

As mentioned previously, the decrease of protein sorption in the presence of magnetic field should thus be de-convoluted in the two sorption components, i.e. the decrease of protein adsorption and absorption. Therefore, and assuming that both processes are present the decrease of protein absorption may correspond to a hindered diffusion of trypsin into the porous membrane structure caused by the shrinkage of the hydrogel volume when the magnetic field is applied. Instead, the decrease of protein adsorption at hydrogel membranes in the presence of magnetic field might be explained by the lower protein adsorption stability at hydrophilic surfaces.

The effect of the MNP content in the magnetic responsiveness of the hydrogel membranes was also investigated by a comparative analysis of the trypsin sorption

profiles obtained for hydrogels with 0.25% and 1% MNPs, at 0T and 1T. As depicted in Figure III. 5B the difference between the protein sorbed in the absence and presence of the magnetic field was higher in hydrogel membranes with 0.25% MNPs. These results are in agreement with the effect of the magnetic field on the contact angles discussed above and confirm the higher magnetic-responsiveness of hydrogel membranes with lower MNP content as well as their higher ability to magnetically modulate protein sorption. The higher magnetic responsiveness of hydrogels with lower MNP content may be related with the lower resistance to deformation of these hydrogels, which was confirmed by puncture tests. The higher resistance to deformation of hydrogels with higher MNP load was expressed by the increase of the Young modulus, E, from 811.0 ± 253.4 kPa to 1330 ± 59.6 kPa, when the concentration of MNPs increased from 0.25% to 1%. Based on these results, it is reasonable to think that hydrogels with high elasticity allow for higher levels of hydrogel volume contraction due to an easier mobility of the embedded MNPs and thus explaining their higher magnetic responsiveness. This result further suggests that the optimization of the magnetic responsiveness of these hydrogels relies on a good balance between the MNP load (high enough to assure the magnetic responsiveness of the hydrogel) and the resultant increase of the hydrogel resistance to deformation (low enough to allow the magnetic mobility of the MNPs entrapped in the hydrogel matrix).

3.3. Control of protein sorption in hydrogel membranes under cyclic magnetic field conditions

Studies about the impact of the magnetic field on the trypsin sorption profiles in the hydrogel membrane were also performed under cyclic variation of the magnetic field intensity between 0 T (magnetic field OFF) and 1 T (magnetic field ON) to evaluate the process reversibility. As shown in Figure III. 6A, the amount of trypsin in the membrane increased along the first stage, when the magnetic field was OFF. When the trypsin sorption plateau was reached, the magnetic field was switched ON at 1T, and a fast displacement of trypsin back to the supernatant solution was observed corresponding to the release of 61.8 % (Table III. S1, in Supplementary Information) of the total amount of the protein in the membrane.

The trypsin sorption into the hydrogel membrane was immediately restored when the magnetic field was switched OFF (2nd cycle). However, not only the protein sorption

plateau reached in the 2nd magnetic field cycle was higher but also the efficiency of the protein release decayed to 7.1%, suggesting a loss of the magnetic-responsive capacity of the membrane and the accumulation of protein in the hydrogel matrix.

The amount of trypsin sorbed and released at each magnetic field stage was calculated by a mass balance shown in Table S1 in S.I. It is important to highlight that no protein desorption due to thermal effects was expected since the temperature at the surface of the hydrogels was kept constant along the process.

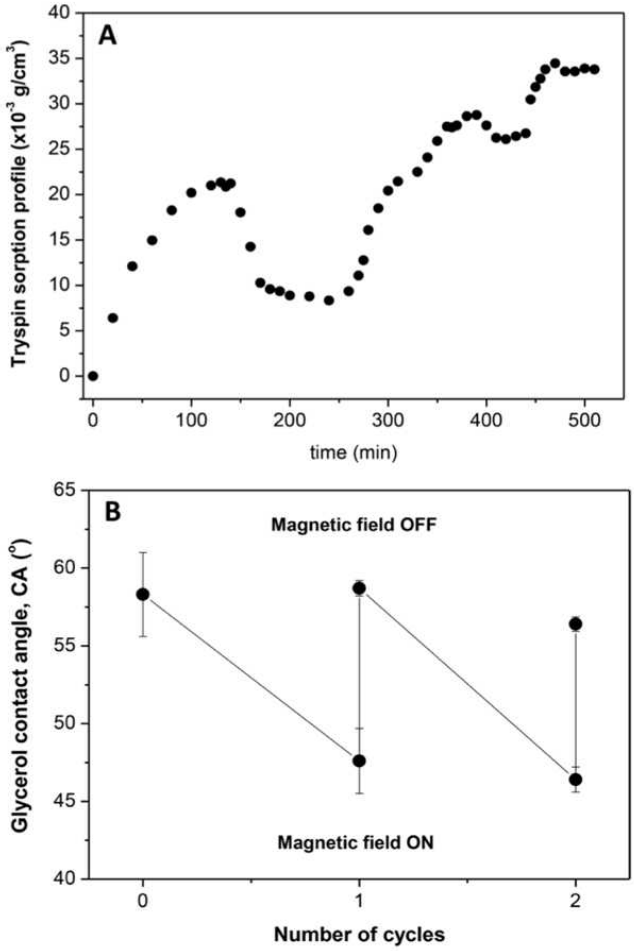


Figure III. 6. A) Evolution of trypsin content along time in a PVA hydrogel membrane doped with 0.25% (w/v) of MNPs when exposed to magnetic field cycles varied between 0 and 1 T. **B**) Glycerol contact angles, CA (deg), obtained along OFF/ON magnetic field cycles at 0.08 T for a magnetic hydrogel matrix with 0.25% (v/w) of MNPs upon exposure to OFF/ON magnetic field cycle at 1 T.

Additional studies were developed aiming at understanding the reasons underlying the higher protein retention (expressed by the increase of the protein sorption

plateau) and the decrease of protein release capacity of the hydrogels with the number of magnetic field cycles.

Analysis of the variation of the hydrogel surface contact angles were carried out under identical magnetic field cycle frequency (but with a lower magnetic field intensity of 0.08 T) showed that the contact angle switching amplitude was essentially preserved along the process (Figure III. 6B) suggesting that the magnetically induced mechanic activity of the hydrogel membrane was maintained. Therefore, losses of protein release ability seemed not to be related with losses in the magnetic responsive capacity of the hydrogel.

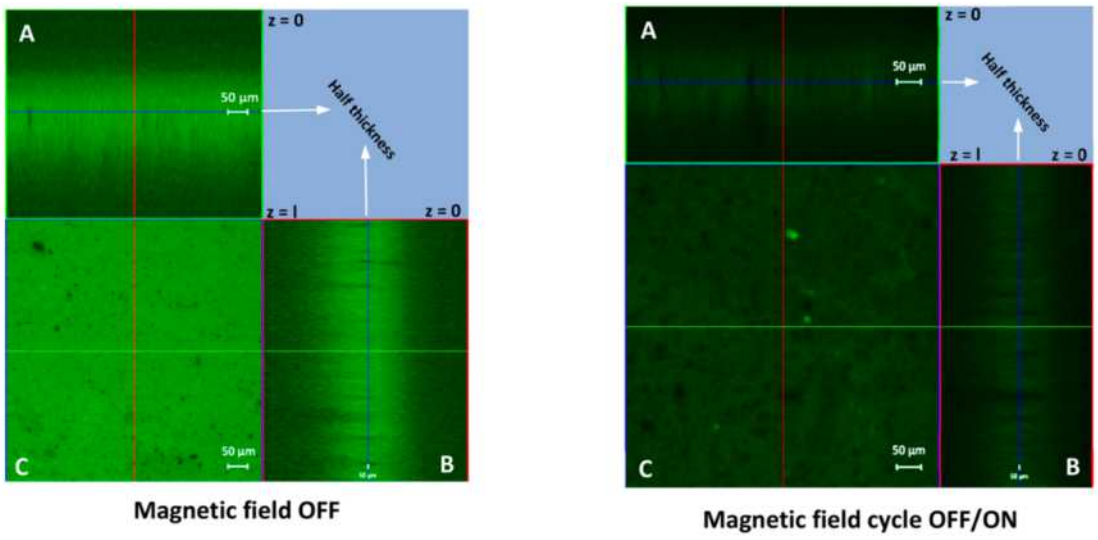


Figure III. 7. Confocal microscopy orthogonal images obtained along the Z-axis (thickness, from Z = 0 to Z = l) of a magnetic hydrogel membrane with 0.25% (v/w) MNPs upon immersion in a solution of FITC-albumin in the absence of magnetic fied and exposed to an OFF/ON magnetic field cycle. (**A**) Fluorescence emission signal obtained along the whole membrane thickness (Z = l), (**B**) fluorescence emission signal obtained along the whole membrane thickness orthogonal to the side represented in (**A**), and (**C**) microscopy image obtained at the half-thickness of the membrane.

In order to confirm the protein accumulation in the hydrogel along the magnetic field cycles the sorption studies were repeated using fluorescein isothiocyanate (FITC) labelled albumin (FITC-Albumin) instead of trypsin. Confocal microscopy images were acquired for hydrogel membranes doped with 0.25% MNPs after immersion in the protein solution in the absence (magnetic field OFF) and the presence of OFF/ON magnetic field cycles. It is important to highlight that to assure the analysis of the hydrogel membrane was carried out upon maximum protein desorption, the membrane was removed from the protein solution at the end of the ON magnetic field stage, while the magnetic field was still turned ON.

The confocal images depicted in Figure III. 7 confirmed the presence of protein inside the two hydrogel membranes, i.e. the membranes exposed and non-exposed to magnetic field cycles. The progressive increase of fluorescence emission from the membrane periphery to the membrane center, i.e. from Z=0 to the membrane half-thickness, unveiled the preferential accumulation of FITC-Albumin in the membrane core. However, a comparative analysis of the confocal images obtained for the two membranes showed a lower fluorescence signal in the membrane exposed to magnetic field cycle, suggesting a partial removal of protein during the ON magnetic field stage.

Also, it shows that a protein fraction remains entrapped in the hydrogel matrix, which is compatible with the progressive increase of the trypsin sorption plateau observed along the magnetic field cycles, as shown in Figure III. 6A.

The subsequent increase of the protein sorption maxima (i.e. protein sorption plateaus) suggests a continuous accumulation of protein in the membrane, which might be ascribed with the increase of the free volume inside the hydrogel matrix, potentially associated to the disruption of the hydrogel porous network caused by the magnetically induced mobility of the MNPs. Despite the efforts developed to confirm the presence of structural changes after exposure to the magnetic field cycles no changes in MNP dispersion quality (Figures III. S1 and S2 in Supplementary Information) or hydrogel porous structure (Figure III. S4 in Supplementary Information) were noticed by optical microscopy and ESEM analysis (Figure III. S2 and S4, in Supplementary Information).

In order to further clarify the reasons for the loss of protein sorption-desorption reversibility along the magnetic field cycles, protein sorption-release experiments were repeated at a lower magnetic field intensity of 0.45 T. The reduction of the magnetic field intensity aimed to induce a smoother movement of the MNPs in these conditions and thus preventing the hypothetical disruption of the hydrogel network. In this case, trypsin sorption was carried out by exposing hydrogel membranes doped with 0.25% MNPs to magnetic field cycles with opposite ON/OFF sequences, i.e. OFF/ON (Figure 8 A) and ON/OFF (Figure III. 8B) magnetic field sequences. The trypsin sorption profiles obtained during OFF/ON magnetic field cycles (Figure III. 8A) and the respective mass balances, listed in Table S2 in S.I., show that the membrane was able to release the total amount of trypsin sorbed during the first OFF/ON cycle. Although the small loss of the magnetic responsiveness observed through the subsequent magnetic field cycles (with membrane sorption and release capacity decaying to 19.4 % and 76.1 % after the 2nd cycle), the

magnetically induced protein sorption and release capacity of the PVA hydrogel was significant along the whole process time.

Experiments carried out under ON/OFF magnetic field conditions, depicted in Figure III. 8B (and the respective trypsin mass balance listed in Table III. S.3 in Supplementary Information), showed that trypsin sorption in the membrane (i.e. protein adsorption and absorption into the membrane matrix) was minimal while the magnetic field was kept ON.

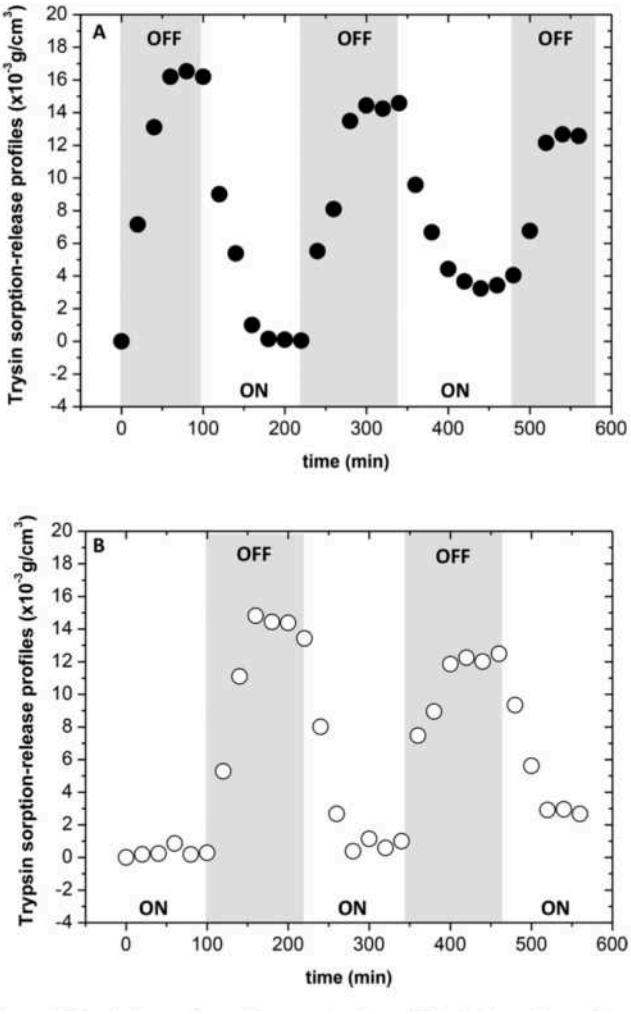


Figure III. 8. Evolution of trypsin sorption in a PVA hydrogel membrane doped with 0.25% (w/v) of MNPs when exposed to (**A**) OFF/ON and (**B**) ON/OFF magnetic field cycles varied between 0 and 0.45 T.

Then, when the magnetic field was switched OFF, an immediate increase of trypsin sorption was observed. A removal of 96.3 % of the total amount of trypsin in the membrane was observed after the 1st magnetic field cycle whereas it decayed to 78.6 % after the 2nd cycle.

The more efficient protein release observed for experiments carried out at lower magnetic field intensity (Figure III. 8) suggested that the accumulation of protein within the hydrogel matrix, observed when the magnetic field was increased up to 1 T, might actually be due to the presence of structural changes in the hydrogel. The mobility of the MNPs is certainly more abrupt at 1T, causing a more significant disruption of the hydrogel porous structure and the increased protein retention capacity observed in this case (Figure III. 7). Instead, the protein sorption and release behavior observed at 0.45 T suggests that the membrane structure is more likely preserved at lower magnetic field intensities allowing for a more efficient and reproducible magnetic responsive behavior.

Magnetically induced changes of the hydrogel structure may explain both, the decrease of protein adsorption and absorption, if the two processes were assumed to co-exist. Protein adsorption is known to depend on surface hydrophilicity decreasing as the surface hydrophilicity increases. Hence, the lower protein partitioning to the hydrogel in the presence of magnetic field, might be explained by variation of the surface hydrophilic degree imposed by the ON/OFF magnetic field cycles, with protein adsorption increasing at magnetic field OFF (decrease of the surface hydrophilicity) and decreasing at magnetic field ON (increase of surface hydrophilicity). Also, the decrease of protein sorption at the ON magnetic field stage might be ascribed with the hampered diffusion of proteins (and the protein solution), which might be related to the reduction in the hydrogel free volume caused by the magnetic hydrogel shrinking effect. Hydrogel shrinking-unshrinking is thought to emulate the peristaltic pumping effect, resulting in a higher amount of proteins inside the unshrunk hydrogels followed by protein released induced by hydrogel contraction.

III.3. Conclusions

This work describes the impact of magnetic field on the wettability of PVA hydrogels doped with iron oxide nanoparticles (MNPs) and the ability to modulate, in remote mode, protein sorption to these magnetic hydrogel membranes, by adjustment of the external magnetic field intensity. Magnetic field was shown to induce a decrease of the surface contact angles of PVA hydrogels, thus suggesting an increase of surface wettability. Surface wettability responds reversibly to ON/OFF magnetic field cycles with a total recovery of the initial surface contact angles upon removal of the magnetic field.

The magnetic behavior of these hydrogels was also shown to influence protein sorption.

Magnetic field was shown to reduce protein sorption ability while stimulating protein release from the hydrogel. Therefore, these hydrogels offered the capacity to magnetically control the protein content by cyclic variation of the magnetic field intensity. Still, this process seems not to be totally reversible due to the partial accumulation of protein into the hydrogel matrix, particularly evident when a magnetic field of 1T was used. The degree of reversibly of protein sorption-desorption processes was found to be improved by decreasing the magnetic field intensity to 0.45T.

The unique properties of these magnetic-responsive hydrogels suggest their promising use as smart devices which may offer a better control over the partitioning and mobility of proteins to/in porous media. Hence, they may contribute to the development of bioseparation systems with improved performances, e.g. less prone to biofouling, and to the design of magnetically-controlled drug delivery systems, biosensors and tissue engineering devices with better efficiencies.

III.5. References

1. Y. N. Wang, C. Y. Tang. Protein fouling of nanofiltration, reverse osmosis, and ultrafiltration membranes—The role of hydrodynamic conditions, solution chemistry, and membrane properties *J. Membr. Sci.* **2011**, *376*, 275–282.
2. I. H. Huisman, P. Prádanos, A. Hernández. The effect of protein–protein and protein–membrane interactions on membrane fouling in ultrafiltration *J. Membr. Sci*. **2000**, *179*, 79–90.
3. Q. Yang, H. Himstedt, M. Ulbricht, X. Qian, S.R. Wickramasinghe. Designing magnetic field responsive nanofiltration membranes. *J. Membr. Sci.* **2013**, *430*, 70–78.
4. U. Gottschalk. Bioseparation in Antibody Manufacturing: The Good, The Bad and The Ugly *Biotechnol. Prog*. **2008**, *24*, 496-503.
5. N. Chopra, V. G. Gavalas, L. G. Bachas, B. J. Hinds, L.G. Bachas. Functional One-Dimensional Nanomaterials: Applications in Nanoscale Biosensors. *Analytical Letters* **2007**, *40*, 2067–2096.
6. I. Tokarev, I. Tokareva, V. Gopishetty, E. Katz, S. Minko. Specific Biochemical-to-Optical Signal Transduction by Responsive Thin Hydrogel Films Loaded with Noble Metal Nanoparticles. *Adv. Mater.* **2010**, *22*, 1412–1416.
7. C. J. Wilson, R. E. Clegg, D. I. Leavesley, M. J. Pearcy. Mediation of Biomaterial–Cell Interactions by Adsorbed Proteins: A Review. *Tissue Engineering* **2005**, *11*, (1/2).
8. M. M. Stevens, J. H. George. Exploring and Engineering the Cell Surface Interface. *Science* **2005**, *310*, 1135-1138.
9. A. Y. Gebreyohannes, L. Giorno, I. F.J. Vankelecom, T. Verbiest, P. Aimar. Effect of operational parameters on the performance of a magnetic responsive biocatalytic membrane reactor. *Chemical Engineering Journal* **2017**, *308*, 853–862.
10. C. S. Chen. Mechanotransduction – a field pulling together? *Journal of Cell Science* **2008**, *121*, 3285-3292.
11. Y.-Xiong Wang, J. L. Robertson, W. B. Spillman, Jr., R. O. Claus. Effects of the Chemical Structure and the Surface Properties of Polymeric Biomaterials on Their Biocompatibility. *Pharmaceutical Research* **2004**, *21*
12. M. Irfan, A. Idris. Overview of PES biocompatible/hemodialysis membranes: PES–blood interactions and modification techniques. Materials Science and Engineering C **2015** *56*, 574–592.

13. S. Guedidi, C. A.M. Portugal, C. Innocent, J.-M. Janot, A. Deratani, J. G. Crespo. Fluorescence monitoring of trypsin adsorption in layer-by-layer membrane systems. *Enzyme and Microbial Technology* **2012**, *51*, 325-333.
14. A. Nayak, H. Liu, G. Belfort. An Optically Reversible Switching Membrane Surface. *Angew. Chem. Int. Ed.* **2006**, *45*, 4094 –4098.
15. P. Roach, D. Farrar, C. C. Perry. Surface Tailoring for Controlled Protein Adsorption: Effect of Topography at the Nanometer Scale and Chemistry. *J. Am. Chem. Soc.* **2006**, *128*, 3939-3945.
16. J. Grimaldi, M. Radhakrishna, S. K. Kumar, G. Belfort. Stability of Proteins on Hydrophilic Surfaces. *Langmuir* **2015**, *31*, 1005−1010.
17. S.-S. Li, Y. Xie , T. Xiang, L. Ma, C. He, S.-D. Sun, C.-S. Zhao. Heparin-mimicking polyethersulfone membranes – hemocompatibility, cytocompatibility, antifouling and antibacterial properties. *J. Membr. Sci.* **2016**, *498*, 135–146.
18. J. Lei, M. Ulbricht. Macroinitiator-mediated photoreactive coating of membrane surfaces with antifouling hydrogel layers. *J. Membr. Sci.* **2014**, *455*, 207–218.
19. H. S. Lim, J. T. Han, D. K. M. Jin, K. Cho. Photoreversibly switchable superhydrophobic surface with erasable and rewritable pattern. *J. Am. Chem. Soc.* **2006**, *128*, 14458-14459.
20. H. Qi, J. Cao, Y. Xin, X. Mao, D. Xie, J. Luo, B. Chu. Dual responsive in hydrogel membrane with selective protein adsorption and sustained release property. *Materials Science and Engineering C* **2017**, *70*, 347–356.
21. R. N. Wenzel. Resistance of solid surfaces to wetting by water. *Ind. Eng. Chem.* **1936**, *28*, 988-994.
22. A. B. D. Cassie, S. Baxter. Wettability of porous surfaces. *Trans. Faraday Soc.* **1944**, *40*, 546-561.
23. A. M. Ross, Z. Jiang, M. Bastmeyer, J. Lahann. Review: Physical Aspects of Cell Culture Substrates: Topography, Roughness, and Elasticity. Cell Culture Substrates. *Small*. 2012, 8, No. 3, 336-355.
24. T. Sun, L. Feng, X. Gao, L. Jiang. Bioinspired Surfaces with Special Wettability. *Acc. Chem. Res.* **2005**, *38*, 644-652.
25. X. Zhang, F. Shi, J. Niu, Y. Jiang, W. Zhiqiang. Superhydrophobic surfaces: from structural control to functional application. *J. Mater. Chem.* **2008**, *18*, 621-633.
26. D. Seliktar. Designing Cell-Compatible Hydrogels for Biomedical Applications. *Science* **2012**, *336*, 1124-1128.

27. A. W. Feinberg, A. Feigel, S.S. Shevkoplyas, S. Sheehy,G. M. Whitesides, K.K. Parker. Muscular Thin Films for Building Actuators and Powering Devices. *Science* **2007**, *317*, 1366-1370.
28. Y.-H. Chen, Y.-C. Chung, I-J. Wang, T.-H. Young. Control of cell attachment on pH-responsive chitosan surface by precise adjustment of medium pH. *Biomaterials* **2012**, *33*, 1336-1342.
29. H. K. Patra, Y. Sharma, M. M. Islam, M. J. Jafari, N. A. Murugan H. Kobayashi, A. P. F. Turner, A. Tiwari. **Inflammation-sensitive** in situ **smart scaffolding for regenerative medicine.** *Nanoscale* **2016**, *8*, 17213–17222.
30. C. Zhu, Y. Lu, J. Chen, S. Yu. Photothermal Poly(*N*-isopropylacrylamide)/Fe_3O_4 Nanocomposite Hydrogel as a Movable Position Heating Source under Remote Control. Magnetic Hydrogels. *Small* **2014**, No. 14, 2796-2800.
31. D. Morales, B. Bhari, M. D. Dickey, O. D. Velev. Bending of Responsive Hydrogel Sheets Guided by Field-Assembled Microparticle Endoskeleton Structures. Soft Actuators. *Small* **2016**, 12, No. 17, 2283-2290.
32. H. H. Himstedt, X. Qian, J. R. Weaver, S. R. Wickramasinghe. Responsive membranes for hydrophobic interaction chromatography. J. Membr. Sci. **2013**, *447*, 335–344.
33. L. Xiao, A. Isner, K. Waldrop, A. Saad, D. Takigawa, D. Bhattacharyya. Development of bench and full-scale temperature and pH responsive functionalized PVDF membranes with tunable properties. *J. Membr. Sci.* **2014**, *457*, 39–49.
34. S. P. Nunes, A. R. Behzad, B. Hooghan, R. Sougrat, M. Karunakaran, N. Pradeep, U. Vainio, K. Peinemann. Switchable pH-Responsive Polymeric Membranes Prepared via Block Copolymer Micelle Assembly. *ACS nano* **2011**, 3516-3522.
35. D. Szabó, G. Szeghy, M. Zrínyi. Shape Transition of Magnetic Field Sensitive Polymer Gels. *Macromolecules* **1998**, *31*, 6541-6548.
36. R. L. Snyder, V. Q. Nguyen, R. V. Ramanujan. Design parameters for magneto-elastic soft Actuators. *Smart Mater. Struct.* **2010**, *19*, 055017, 8pp
37. R. Fuhrer, E. K. Athanassiou, N. A. Luechinger, W. J. Stark. Crosslinking Metal Nanoparticles into the Polymer Backbone of Hydrogels Enables Preparation of Soft, Magnetic Field-Driven Actuators with Muscle-Like Flexibility. *Small* **2009**, No. 3, 383-388.
38. Y. Li, G.Huang, X. Zhang, B. Li, Y. Chen, T.Lu, T. J. Lu , F. Xu. Magnetic Hydrogels and Their Potential Biomedical Applications. *Adv. Funct. Mater.* **2013**, *23*, 660–672

39. X. Lin, B. N. Quoc, M. Ulbricht. Magnetoresponsive Poly(ether sulfone)-Based Iron Oxide cum Hydrogel Mixed Matrix Composite Membranes for Switchable Molecular Sieving. *ACS Appl. Mater. Interfaces* **2016**, *42*, 29001-29014.
40. I. Willner, B. Basnar, B. Willner. From Molecular Machines to Microscale Motility of Objects: Application as "Smart Materials", Sensors, and Nanodevices. *Adv. Funct. Mater*. **2007**, *17*, 702-717.
41. Y. Sapir-Lekhovitser, M. Y. Rotenberg, J. Jopp, G. Friedman, B. Polyak, S. Cohen. Magnetically actuated tissue engineered scaffold: insights into mechanism of physical stimulation. *Nanoscale* **2016**, *8*, 3386-3399.
42. R. Tognato, A. R. Armiento, V. Bonfrate, R. Levato, J. Malda, M. Alini, D. Eglin, G. Giancane, T. Serra. Stimuli-Responsive Nanocomposite for 3D Anisotropic Cell-Guidance and Magnetic Soft Robotics. *Adv. Funct. Mater.* **2018**, 1804647.
43. B. Olle, S. Bucak, T. C. Holmes, L. Bromberg, T. A. Hatton, D. I. C. Wang. Enhancement of Oxygen Mass Transfer Using Functionalized Magnetic Nanoparticles. *Ind. Eng. Chem. Res.* **2006**, *45*, 4355-4363.
44. G. Filipcsei, I. Csetneki, A. Szilágyi, M. Zrínyi. Magnetic responsive-field smart polymer composites. *Adv Polym Sci* **2007**, *206*, 137–189.
45. J. Ge, Y. Hu, M. Biasini, W. P. Beyermann, Y. Yin. Superparamagnetic magnetite colloidal nanocrystal clusters. *Angew. Chem. Int. Ed.* **2007**, *46*, 4342–4345.
46. C. A. M. Portugal. Functional membranes for the control of protein-surface interactions and transport properties. *Current Organic Chemistry* **2017**, *21*, 1725-1739.

Chapter III. Supplementary Information

Table III. S1. Mass balance to trypsin in the supernatant and in the membrane during the OFF/ON variation of the magnetic field between 0 T and 1 T.

Magnetic field	Trypsin in the supernatant (g)	Variation of Trypsin amount[1] (g)	Trypsin in the membrane (g)	Trypsin sorption[2] (%)	Trypsin release[3] (%)
OFF (initial)	5.55×10^{-3}	-	-	-	-
OFF 1	4.40×10^{-3}	1.10×10^{-3}	1.10×10^{-3}	20.0	-
ON 1	5.08×10^{-3}	-6.80×10^{-3}	4.20×10^{-4}	-	61.8
OFF 2	4.07×10^{-3}	1.01×10^{-3}	1.43×10^{-3}	19.8	-
ON 2	4.10×10^{-3}	-2.70×10^{-3}	1.40×10^{-3}	-	1.9
OFF 3	3.81×10^{-3}	2.90×10^{-3}	1.69×10^{-3}	7.1	-

Table III. S2. Mass balance to trypsin in the supernatant and in the membrane during the OFF/ON variation of the magnetic field between 0 T and 0.45 T.

Magnetic field	Trypsin in the supernatant (g)	Variation of Trypsin amount[1] (g)	Trypsin in the membrane (g)	Trypsin sorption[2] (%)	Trypsin release[3] (%)
OFF (initial)	3.77×10^{-3}	-	-	-	-
OFF 1	2.55×10^{-3}	1.22×10^{-3}	1.22×10^{-3}	32.4	-
ON 1	3.77×10^{-3}	-1.22×10^{-3}	0	-	100
OFF 2	2.68×10^{-3}	1.09×10^{-3}	1.09×10^{-3}	28.9	-
ON 2	3.51×10^{-3}	-8.30×10^{-4}	2.60×10^{-4}	-	76.1
OFF 3	2.83×10^{-3}	6.80×10^{-4}	9.40×10^{-4}	19.4	-

Table III. S3. Mass balance to trypsin in the supernatant and in the membrane during the ON/OFF variation of the magnetic field between 0 T and 0.45 T.

Magnetic field	Trypsin in the supernatant (g)	Variation of Trypsin amount[1] (g)	Trypsin in the membrane (g)	Trypsin sorption[2] (%)	Trypsin release[3] (%)
ON (initial)	3.70×10^{-3}	-	-	-	-
ON 1	3.69×10^{-3}	1.35×10^{-5}	1.35×10^{-5}	0.04	-
OFF 1	2.61×10^{-3}	1.08×10^{-3}	1.09×10^{-3}	29.2	-
ON 2	3.66×10^{-3}	-1.05×10^{-3}	4.00×10^{-5}	-	96.3
OFF 2	2.77×10^{-3}	8.95×10^{-4}	9.35×10^{-4}	24.5	-
ON 3	3.50×10^{-3}	-7.35×10^{-4}	2.00×10^{-4}	-	78.6

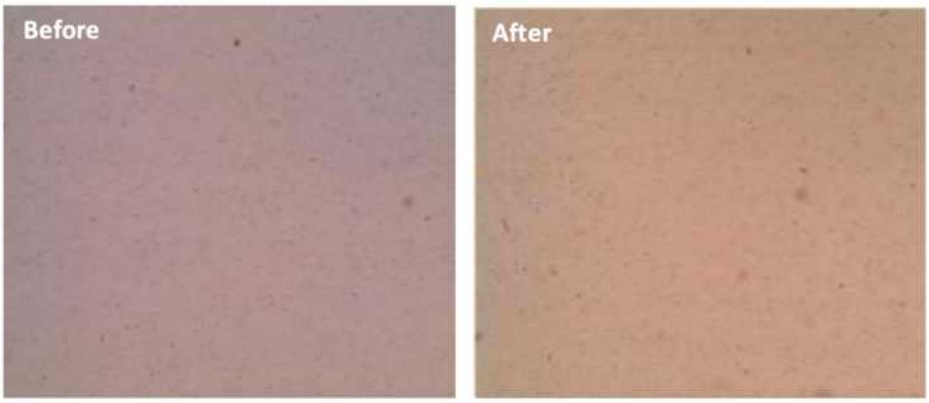
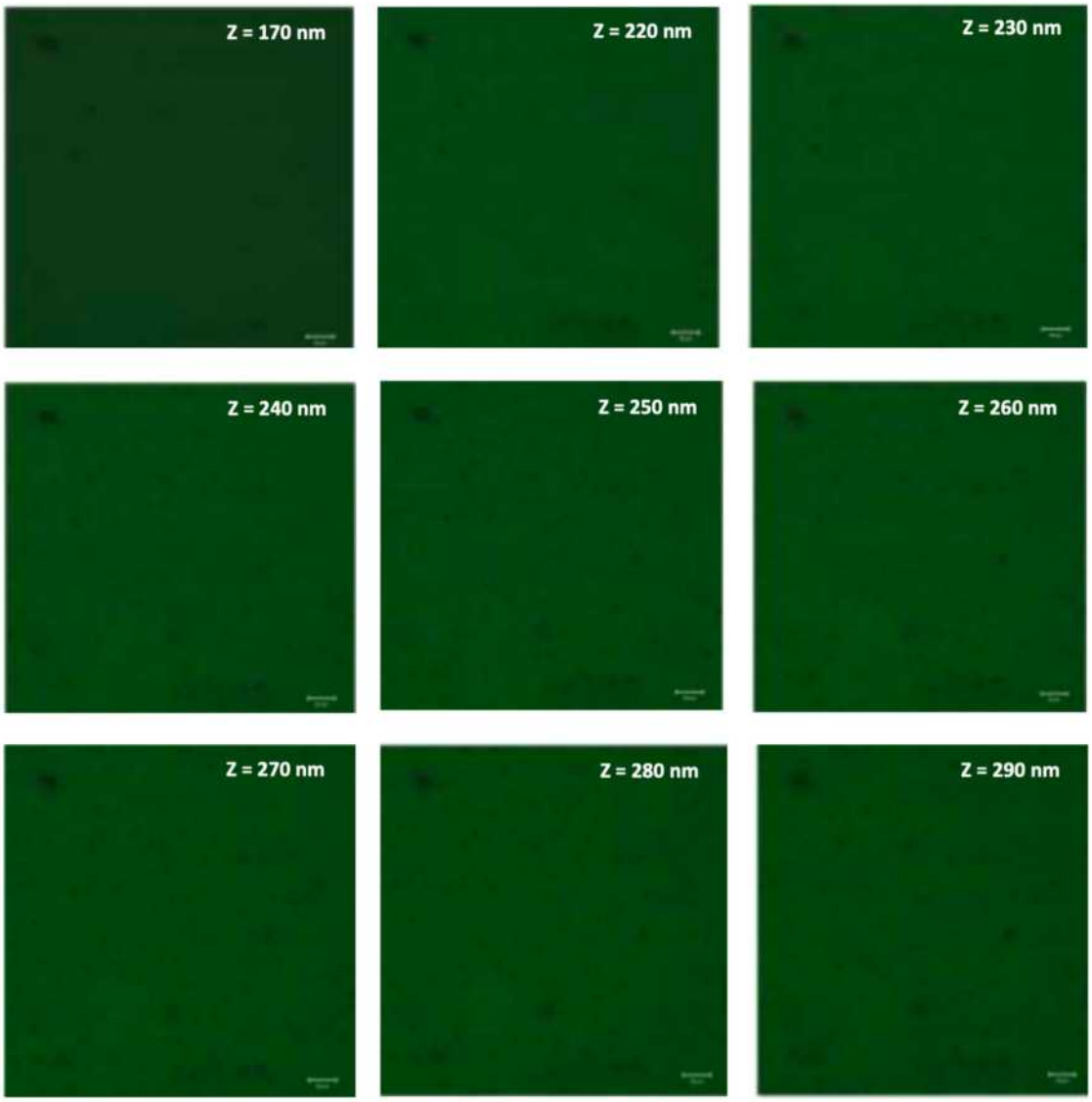


Figure III. S1. Optical microscopy images of the PVA hydrogel membranes doped with 0.25% (w/v) MNPs before and after exposure to ON/OFF magnetic field cycles. The images were obtained with an amplification of 100x.



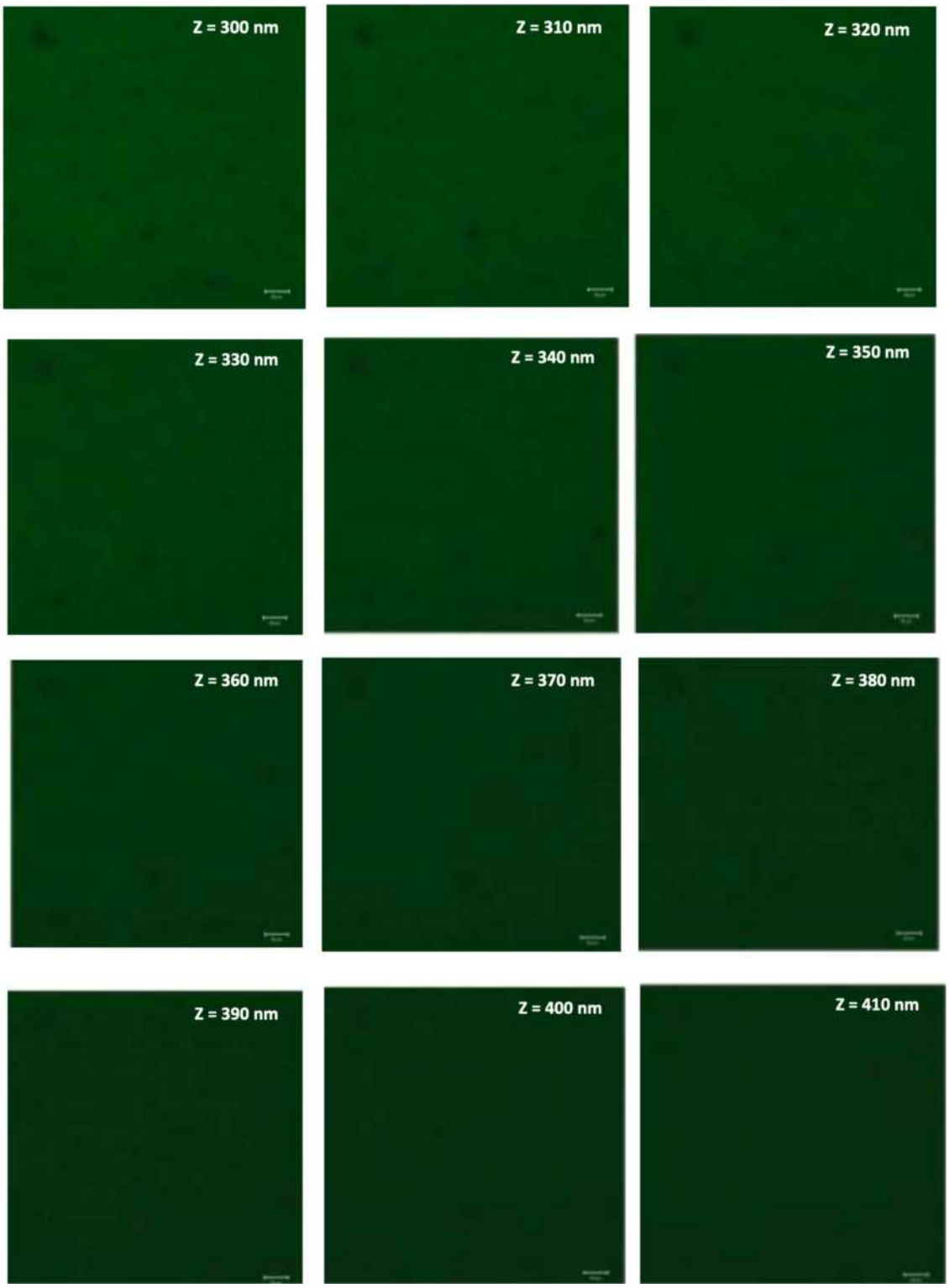


Figure III. S2. Images of PVA hydrogel membrane doped with 0.25% MNPs acquired along the Z-axis of the membrane (membrane thickness) by fluorescence confocal microscopy analysis. The green color corresponds to the presence of FITC-albumin and the black spots are compatible with the presence of MNP clusters.

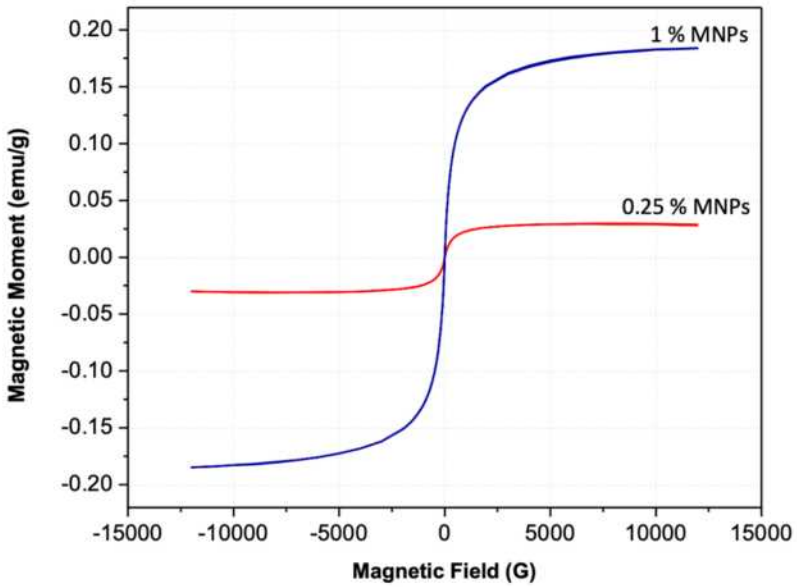


Figure III. S3. Magnetization saturation curves obtained for PVA hydrogels doped with 0.25% of MNPs and 1% of MNPs.

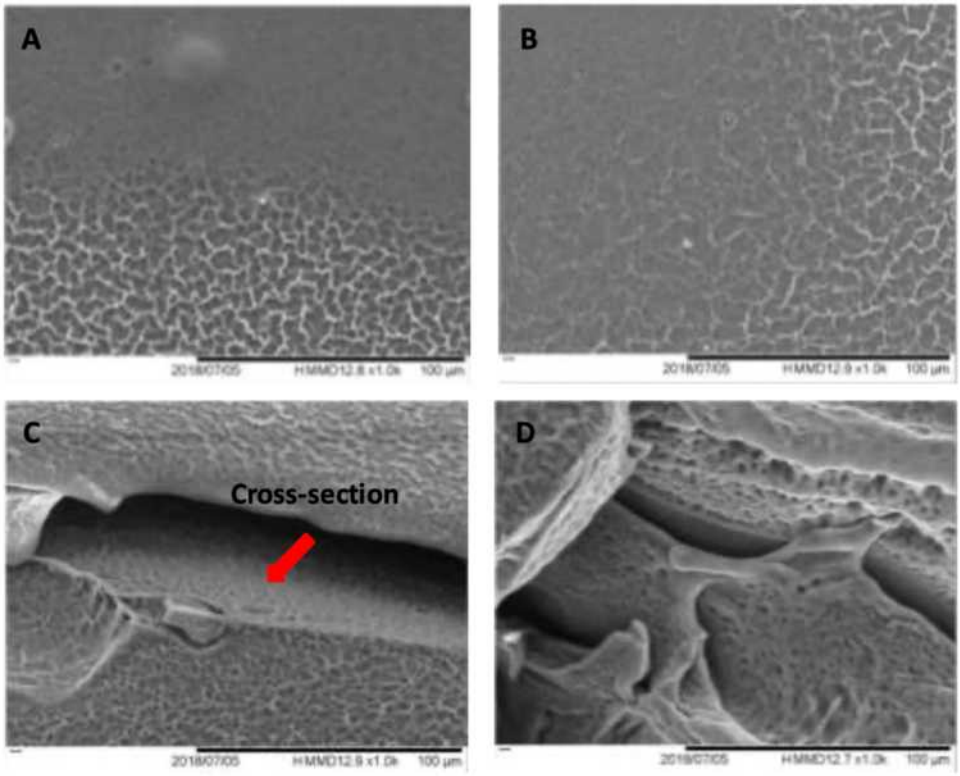


Figure III. S4. Environmental SEM surface (A, B) and cross-section images (C, D) obtained for hydrogel membranes doped with 0.25% MNPs before exposure to the magnetic field (A, C) and after exposure to an OFF/ON magnetic field cycle at 1T (B, D). The observed cracks were not caused by the magnetic field but they resulted from the cut of the membrane.

Chapter IV



Magnetic Stimulation Combined With Magnetic-Responsive Scaffolds To Enhance The Angiogenic Potential Of MSCs In Vascular Tissue Engineering

CHAPTER IV – Magnetic stimulation combined with magnetic-responsive scaffolds to enhance the angiogenic potential of MSCs in vascular tissue engineering

This chapter uncovers the biological impact of low intensity static magnetic fields (0.08 T) in the stimulation of MSCs and analyzes the magnetic effect at cell proliferation, viability, morphology, phenotype, migration and secretome biomolecules, while ultimately aiming for angiogenesis enhancement, both in vitro and ex vivo.

Outline

Vascular diseases have emerged as a major global cause of death, emphasizing the demand to create a vascularized tissue. Here we present for the first time the use of external magnetic fields to stimulate Mesenchymal Stromal Cells (MSCs) to increase the production of the angiogenic molecule Vascular Endothelial Growth Factor-A (VEGF-A). Magnetic scaffolds of PVA and Gelatin, doped with iron oxide nanoparticles, were designed to optimize the stimulation on the cells. Although not impacting on MSCs proliferation, viability and multipotency profiles, static magnetic fields direct MSCs morphology and alignment, while enhancing the secretory activity of VEGF-A in 24h. This magnetic approach is able to drive Human Umbilical Vein Endothelial Cells (HUVECs) towards angiogenesis by increasing the number of vessels formed in the presence of MSCs conditioned media both *in vitro* and *in vivo*. The study shows the potential to manipulate cellular processes through short-term magnetic stimulation.

Keywords: magnetic fields, scaffolds, PVA, Gelatin, MNPs, MSCs, HUVECs, VEGF, angiogenesis

IV.1. Introduction

The concept of therapeutic angiogenesis followed evidence that angiogenic factors responsible for blood vessel formation could be delivered to ischemic tissues and restore blood flow[1]. Yet vascular diseases, especially cardiovascular, are still recognized as a major cause of mortality and morbidity, causing more than 30% of global deaths every year[2,3]. In the past years, and despite the primarily treatment with pharmacological agents, surgery or endovascular intervention, no better treatment has become available for the patients who have not achieved a complete revascularization or are not suitable for revascularization[1,4].

Novel strategies in tissue engineering requiring the ability to promote adequate vascularization for tissue substitutes are therefore a critical and yet unmet need these days. A main challenge in this field is related with mass transfer limitations, which in turn limits the size of any tissue constructs grown *in vitro* and the subsequent integration of these constructs *in vivo*[5]. Additional strategies for enhancing vascularization and ensuring the survival of large tissue-engineered grafts include scaffold design, the inclusion of angiogenic factors and both *in vivo* and *in vitro* prevascularization[6,7].

The growth of new blood vessels (neovascularization) is an important component in reproduction and embryonic development while also participating in the stimulation of tissue survival after ischemic events[7]. A combined cooperation of endothelial cells, pericytes and junctional molecules, such as VEGF and ANG-1, play a remarkable role in the regulation of the whole process of vessel branching during angiogenesis[7,8]. Consequently, therapeutic strategies based on vascular stem cells are under research for the treatment of several clinical conditions. Mesenchymal stromal cells (MSCs) have also become scientifically interesting given the variety of molecules they release when properly stimulated[9,10,11,12]. VEGF, a potent angiogenic factor and often released as a cell-survival signal, is one of the paracrine factors involved in the regulation of the interactions between MSCs and endothelial cells where the formation of microvessel-like structures has been demonstrated[9,4,13]. This molecule has been exhaustively studied as a target molecule to stimulate or inhibit angiogenic phenomena[4,7,13,9].

Some papers have reported how the induced mobilization of VEGF from bone marrow-derived endothelial progenitor cells is able to potentiate cells differentiation *in vitro* as well as trigger neovascularization *in vivo*[4,14]. Other studies demonstrated how

MSCs are capable to inhibit endothelial proliferation and angiogenesis through cell-cell contact and modulation of the VE-cadherin/ß-Catenin signaling pathways[15]. Still a powerful challenge in this emerging field involves the development of a controlled system to stimulate the secretome of MSCs into releasing cell-survival signals to promote the formation of microvessel-like structures.

Notably, our previous work describes the ability to reversibly and non-invasively regulate protein-sorption release mechanisms using magnetic hydrogels when exposed to an external magnetic field[16]. Although inconsistent toxic effects of static magnetic fields on different cell types have been reported over the years, some recent works confirmed a potential benefit in using magnetic stimulation over cell fate regulation shifting towards mechanical stimulation and induction of mechanotransduction phenomena in the process. Most of these works highlight the effect of the magnetic forces on promoting cell differentiation on *in vitro* models or even to enhance bone repair *in vivo*[17,18,19]. An interesting neuronal model of ischemia/reperfusion (I/ R) injury confirmed the neurobiological mechanisms of frequency-dependent repetitive magnetic stimulation in I/R injury-treated neuronal cells while magnetically-responsive hydrogels have been used to modulate chondrogenic differentiation in adipose-derived stem cells[20,21]. Additionally, static magnetic fields have also been reported to significantly decrease the proliferation rates of MSCs, suggesting differentiation inducing effects[22].

The current study aims to investigate whether non-invasive magnetic stimulation can address the unmet challenge to promote vascularization, overcoming tissue dimension limitations. Hence, the effects of applying a remote static magnetic field (alone or in combination with magnetic responsive scaffolds) to stimulate VEGF secretion by bone marrow-derived MSCs, and subsequent formation of microvessel-like structures from human umbilical vein endothelial cells (HUVECs), are discussed in this chapter. The study includes: (1) the development and characterization of a novel hydrogel of gelatin, doped with iron oxide nanoparticles (MNPs), for MSCs support and adhesion, and the use of a magnetic scaffold of polyvinylalcohol (PVA), previously developed for reversibly regulation of protein-sorption release upon non-invasively action of an magnetic field[25];(2) the evaluation of the impact of the magnetic forces on the proliferation, viability, distribution and phenotypic identity of the MSCs cultivated in 2D or 3D, first on standard tissue culture plates (TCP) and then on magnetic responsive scaffolds; (3) the analysis of expression and quantification of VEGF-A produced and secreted by MSCs, upon seeding on both PVA and Gelatin scaffolds, and under static

magnetic field exposure; (4) further investigation of the potential effect of the magnetic field on the formation of new microvessels, *in vitro* and *ex vivo,* as well as the impact on enhancing *in vitro* wound healing and MSC migration.

Ultimately, this work aims at highlighting the potential of these magnetic scaffolds as possible therapeutic approaches based on cell fate and behavior modulation through application of external magnetic stimulation.

IV.2. Experimental Section

Scaffold Fabrication. Magnetic nanoparticles (MNPs) were synthesized by chemical co-precipitation of iron salts $FeCl_3$ and $FeCl_2$ (Sigma-Aldrich) in alkaline media. The MNPs used with gelatin were synthetized according to the protocol previously published by Izquierdo et al.[23] An aqueous solution with 25% of ammonium hydroxide (NH_4OH) (Fluka) was added to a mixture of $FeCl_3$ and $FeCl_2$ at 80ºC, under permanent stirring at 1250 rpm in N_2 atmosphere. The MNPs used in combination with PVA were synthetized according to the protocol previously published by Olle et al.[24] In this case, potassium oleate and ammonium persulfate (Sigma-Aldrich) were added to the reaction to produce Fe_3O_4-coated particles to minimize aggregation and Hitenol-BC (Sigma-Aldrich) worked as a surfactant. Porcine skin gelatin (8% m/v, type A, G2500, Sigma-Aldrich) and PVA (10% m/v, Mowiol 10849, Sigma-Aldrich) were dissolved in milli-Q water (10% m/v) at 60ºC in two different preparations. In both situations, MNPs were dispersed by sonication (3h, 60ºC) in polymeric solutions. For PVA, 1% of glycerol (Sigma-Aldrich, > 99%), followed by 3% of Glutaraldehyde (cross-linking agent, 25% in H_2O, Sigma-Aldrich) and 3% of HCl (37%, Sigma-Aldrich) were added to the solution before casting onto glass plates. The gelatin matrices were cast onto glass plates and left overnight at 4ºC. The samples were removed from the glass plates and immersed in an aqueous solution containing 1% of glutaraldehyde (25% in H_2O) for 3h. The magnetic hydrogels were then washed by immersion in a demineralized water bath. The procedure was followed by UV-Vis spectroscopy overtime (252 nm). For sterilization, the samples were cut according with the shape and size of the 24-well cell culture plates (TCP, Corning®) and immersed in a PBS solution containing 1% of antibiotic-antimycotic (Gibco). For better conditioning of the cells on the scaffolds, the hydrogels were pre-conditioned in cell culture media for 3h before seeding the cells on top of the hydrogels.

MNPs and Magnetic Responsive Scaffold Characterization. The MNP size distribution was assessed by transmission electron microscopy (TEM) using a TEM Hitachi H8100 (LAB6 filament; acceleration tension of 200 kV). The MNP sizes were determined using ImageJ software and the average particle size was obtained by statistical analysis of a total of 320 counts (95% confidence). Dispersion quality of the MNPs was investigated by optical microscopy using a microscope (Olympus BH-2) set with a photo camera (Casio Exilim Pro, EX-F1). Before application, the scaffolds were washed in a demineralized water bath to remove unbound material. As the gelatin softness was not suitable for the tip of the equipment and, for comparison purposes, surface roughness values for both scaffolds were obtained by confocal microscopy using a confocal laser scanning microscope (LSM 700/ Carl Zeiss) for 3D imaging of the surfaces. Imaging was performed using hydrogels in their maximum swollen state, upon immersion of the membranes in water for 30 min. Afterwards, image analysis was performed using ZEN 2.1 software (Carl Zeiss). Surface contact angles of the scaffolds were determined using glycerol as the liquid phase in the absence and presence of a magnetic field with a maximum intensity of 0.08 T. The magnetic field was created by a neodymium magnet placed underneath the hydrogel membranes. The dynamic glycerol contact angles were determined by sessile drop technique using a drop shape analyzer system coupled to a video camera connected to a PC for data acquisition. The average contact angle values were obtained for at least three triplicates. Magnetization measurements were performed using Vibrating Sample Magnetometer (VSM) module of a Physical Property Measurements System from Quantum Design, Inc., at UNIZAR (Zaragoza, Spain). Major hysteresis loops and initial magnetization was recorded for the scaffold with MNPs at 300 K in applied magnetic field up to 5 T. The measurement was obtained with the magnetic field in a perpendicular position to the scaffold basal plane.

Cell culture. Human bone-marrow MSCs lines used in this chapter are part of the cell bank available at Stem Cell Engineering Research Group (SCERG), iBB-Institute for Bioengineering and Biosciences at Instituto Superior Técnico (IST). Bone marrow aspirates were obtained from Instituto Português de Oncologia Francisco Gentil, Lisboa-Portugal under collaboration with iBB-IST. All human samples were obtained from healthy donor after written informed consent, in accordance with the Directive 2004/23/EC of the European Parliament and of the Council of 31 March 2004 on setting standards of quality and safety for the donation, procurement, testing, processing,

preservation, storage, and distribution of human tissues and cells (Portuguese Law 22/2007, June 29), with the approval of the Ethics Committee of the respective clinical institutions[25]. Isolated cells were cryopreserved in liquid/vapor nitrogen tanks until further use. Isolated human bone marrow MSCs (BM MSCs) were cultured using low-glucose Dulbecco's Modified Eagle's Medium (DMEM, Gibco, Grand Island, NY) supplemented with 10% (v/v) fetal bovine serum (FBS MSC qualified, Gibco) and 1% antibiotic-antimycotic (Gibco) and kept at 37ºC, 5% CO_2 and 21% O_2 in a humidified atmosphere. Three independent donors, with ages ranging between 33 and 68 years old, were used on the experiments (n=3). HUVECs were purchased from Lonza (Basel, Switzerland) and maintained in commercial endothelial growth medium-2 (EGM-2, Lonza) and kept at 37ºC, 5% CO_2 in a humidified atmosphere. Medium renewal was performed every 3-4 days. All the experiments were performed using cells between passages 4 and 7.

MSCs were seeded on the scaffolds at a density of 75000 cell/ cm^3 using expansion medium (DMEM + 10% FBS) on cell culture plates with a covalently bound hydrogel layer to inhibit cellular attachment (Costar® 24 ultra-low attachment well plates). As a control, MSCs were seeded as a monolayer (2D cultures) on cell culture plates (TCP, Corning®) at a density of 75000 cell/cm^2. MSCs were allowed to adhere to the supporting material (TCP or scaffolds) for 24 h at 37ºC in humidified atmosphere, before magnetic exposure.

3D culture featuring MSCs spheroids was obtained by hanging drop technique. According to the technique, several drops 10 µL of cell culture media, containing 1,000 cells/µL, were placed on the top part of a petri dish (Fisher Scientific) and incubated for 24h to force cell aggregation at 37ºC in a humidified atmosphere. The method resulted in spheroids with 10,000 cells, which were carefully collected using the tip of a 20 µl micropipette and placed in culture using expansion medium in ultra-low attachment well plates (Costar® 24 ultra-low attachment well plates) for another 24h before magnetic stimulation.

Magnetic stimulation was performed by placing a circular neodymium magnetic on the second day of the cell culture, with a maximum intensity of 0.08 T beneath the cell culture plates containing MSCs, under 2D or 3D cultures or growing on scaffolds (PVA, Gelatin) for periods of 24 h or 5 days, and allowing a maximum intensity of 0.08 T at the cell culture. This step requires precision to ensure the entire area of the cell culture wells are covered by the magnet. Prior to the exposure, collected powder MNPs were used to

determine the vertical position of the magnetic forces towards the cells and a gaussmeter was used to determine the magnetic intensity sensed by MSCs (0.08 T).

Human Bone Marrow Mesenchymal Stromal Cells (BM MSC) metabolic activity and proliferation curves. The metabolic activity of MSCs was evaluated using AlamarBlue® cell viability reagent (Molecular proves, Eugene, OR). AlamarBlue® cell viability reagent was added to the cells and incubated at 37ºC for 2 h. Fluorescence was quantified at a wavelength range of 560-590 nm. Prior to analysis, a calibration curve for different MSCs densities (10000, 20000, 50000, 75000, 100000, 150000 cells/ mL) was obtained relating cell counting to the metabolic activity of the MSCs measured by AlamarBlue® cell viability reagent, following manufacturer instructions. The calibration curve was used to convert the obtained metabolic values into cell numbers and determine the proliferation curves associated with each condition. All conditions were tested in triplicates using three different donors (donors 1, 2 and 3).

Cell viability and morphology assay. MSCs viability and morphology (cultured in 2D- 3D cultures and in scaffolds of PVA and Gelatin) were assessed at experimental day 1 and day 5, after magnetic exposure. Cells were washed twice with PBS (Phosphate Buffer Saline, Dulbecco's Sigma-Aldrich), and stained using LIVE/DEAD^{TM} Viability/ Cytotoxicity Kit, for mammalian cells (ThermoFisher Scientific, L3224) according to the manufacturer protocol, for 20 min. MSCs were imaged in a fluorescence microscope (Leica DM IL LED with EC3 camera system), and afterwards washed again twice with PBS and fixed with 4% Paraformaldehyde (Sigma-Aldrich) for 20 min. Cells were permeabilized with 0.1% Triton X-100 for 10 min and incubated with Phalloidin-TRITC (Invitrogen, 1.5 µg/ml) or Alexa Fluor 488 (ThermoFisher, 4 µg/ mL) for 20 min and DAPI (ThermoFisher Scientific, 1.5 µg/ mL) for 5 min, then washed with PBS for fluorescence imaging.

Metabolite analysis. Glucose and lactate concentrations were determined in the conditioned media of the samples collected from MSCs overtime (Day 0, 1 and 5) using an automatic analyzer (YSI 7100MBS; Yellow Spring Instruments).

Immunophenotype characterization of magnetically stimulated MSCs. For immunophenotypic characterization, MSCs were tested by flow cytometry after 5 days, with and without magnetic exposure, for expression of cell surface markers indicative of MSCs using a panel of mouse anti-human monoclonal antibodies (PE-conjugated) against: $CD73^+$, $CD90^+$, $CD105^+$, $CD14^-$, and human leukocyte antigen $HLA\text{-}DR^-$ (all from Biolegend). The cells were incubated with the monoclonal antibodies for 15 min in the dark at room temperature. Then, cells were washed with PBS and fixed with 4% paraformaldehyde (Sigma-Aldrich). Appropriate isotype controls (IgGy1 and IgGy2b) were also prepared. A minimum of 7,000 events were collected for each sample, and Cell Quest (Becton Dickinson) and FlowJo® (LLC) software were used for acquisition and analysis, respectively.

Cytotoxicity Assay. The biocompatibility of the scaffolds (PVA and Gelatin) was demonstrated through a cytotoxicity assay using fibroblasts cell line. Fibroblasts (L929 mouse line) were seeded at 80,000 cells/ cm^2 in a 24 well plate and incubated for 48h with low-glucose Dulbecco's Modified Eagle Medium (DMEM, Gibco, Grand Island, NY) supplemented with 10% fetal bovine serum (Gibco) and 1% antibiotic-antimycotic (Gibco) and kept at 37ºC, 5% CO_2 and 21% O_2 in a humidified atmosphere. Indirect assay was performed using latex material as the positive control and fibroblasts culture media as the negative control. The lixiviates of the scaffolds incubated for 48h to allow release of eventual toxic substances to the media were used as a replacement for the fibroblasts culture media and incubated for another 24h. MTT solution (1 mg/ mL) was prepared and replaced the lixiviates in the fibroblasts culture, in a 2 h incubation period. MTT solvent (HCl and IPA – 1:100, Sigma-aldrich) is added to MTT solution in the cell culture and stirred for 5 min. Absorbance is quantified at 570 nm to determine total cell viability. Sterile scaffolds were placed on top of fibroblasts monolayer for 24h and then observed on the optical microscope for quantification of the halo formed in the area between the scaffold and the monolayer.

Quantitative reverse transcription-polymerase chain reaction analysis (RT-PCR). The expression levels of key angiogenesis growth factors genes (human VEGF-A, bFGF and hGF) was quantified from the extraction of the RNA of MSCs for all the experimental groups (2D-3D cultures, cultures on scaffolds of PVA and gelatin). MSCs were detached (either from scaffolds or cell culture plates) and lysed, after 24 h or

5 days of magnetic exposure, using consistent up and down pipetting movements for 10 min and a lysis buffer (RLT), which is part of the RNeasy Mini Kit (Qiagen, Hilden, Germany) for RNA extraction. The detachment process was aided by placing the culture plates in a stirring plate (300 rpm) for 10 minutes. Cell lysates were stored at -80ºC. Subsequent procedures for total RNA extraction were performed following the manufacturer's instructions on the RNeasy Mini Kit. Complementary DNA was synthesized from 20 ng of total RNA using iScript Reverse Transcription Supermix (Bio-Rad, Hercules, CA). Reaction mixture (20 μL) was incubated in a 96-well thermal cycler (Applied Biosystems, Foster City, CA) for 5 minutes at 25ºC, 30 minutes at 42ºC and 5 minutes at 85ºC and then maintained at 4ºC. Gene expression levels of VEGF, basic Fibroblast Growth Factor (bFGF) and Hepatocyte Growth Factor (HGF) were assessed. The sequences of the specific primer sets are given in Table IV. S1. The quantitative reverse transcription-polymerase chain reaction (qRT-PCR) was performed using SYBR Green PCR Master Mix (Applied Biosystems). All reactions were carried out at 95ºC for 10 minutes, followed by 40 cycles of 95ºC for 15 seconds and 60ºC for 1 minute, according to manufacturer's instructions. Glyceraldehyde 3-phosphate dehydrogenase (GAPDH) was used as internal control to normalize differences in total RNA levels in each sample. A threshold cycle (C*t*) was observed in the exponential phase of amplification, and quantification of relative expression levels was performed using standard curves for target genes and endogenous control. Geometric means were used to calculate the $\Delta\Delta Ct$ values and are expressed as $2^{-\Delta\Delta Ct}$. The mean values from triplicate analysis were compared. All conditions were tested in triplicates using three different donors (donors 1, 2 and 3).

Quantification of VEGF secretion by enzyme-linked immunosorbent assay (ELISA). For quantification of the total amount of exogenous angiogenic VEGF-A protein present in MSCs conditioned media in all groups of analysis, an ELISA experiment was performed. To quantify ELISA, culture supernatant was collected at each time point (24 h, 5 days) for MSCs in 2D-3D cultures or cultivated on scaffolds (PVA and Gelatin) and exposed or not to the magnetic field (0 T and 0.08 T). The conditioned media was kept at -80ºC until further analysis. Human VEGF-A kit (RayBiotech) was performed following the manufacturer's instructions. All conditions were tested in triplicates using three different donors (donors 1, 2 and 3).

***In vitro* endothelial cell tube formation assay.** A functional assay to assess the capacity of HUVECs to form microvessels upon culture in Matrigel substrate (Corning®, NY) was used to evaluate the angiogenic potential of the magnetic system. The effect of the exogenous VEGF-A present in the conditioned media of the conditions of analysis was evaluated in a 3D capillary-like tube formation assay. Briefly, HUVECs ($2x10^4$ cells/ cm^2) were cultured on Matrigel (50 µL/ well) in a 96-well plate (Corning® 96-well microplates) and supplemented with the conditioned media from MSCs in 2D cultures or cultivated on scaffolds of PVA and Gelatin. The conditioned media was collected after 24 h and 5 days of exposure to the magnetic field (0.08 T) or without magnetic exposure (0 T). After incubation for 6h at 37ºC, photomicrographs of the center of the well were taken using a light microscope (Leica DM IL LED with EC3 camera system) and the number of tubular-like structures and branch points formed were counted using ImageJ (NIH) software. For this experiment, independent experiments of magnetic stimulation were performed where MSCs were incubated with Endothelial Cell Basal Medium (EBM-2, Lonza) throughout the experiment. All conditions were tested in triplicates using three different donors (donors 1, 2 and 3).

Wound healing and MSCs migration assay. A functional assay to assess wound healing was developed using silicone inserts featuring two chambers with a maximum volume capacity of 70 µL and a compartment-gap width of 500 µm (Culture-insert 2-well 35 mm, IBIDI®). After inserting the constructs on 24-well plates (TCP, Corning®), HUVECs ($2x10^2$ cells) were then cultured on each chamber until reaching confluency. The construct was then carefully removed leaving a gap between the cells from each chamber. HUVECs were treated with conditioned media from MSCs exposed to magnetic field for 24h (0.08 T) and a control for MSCs not exposed to magnetic forces (0 T). The gap area was measured overtime through microscopic images of the same region. A second independent experiment was carried out to evidence the direct impact of the magnetic field in the ability of the MSCs to migrate and close the wound. MSCs were cultured on 24-well plates (TCP, Corning®) and allowed to reach confluency. A micropipette (20 µL tip) was then used to scratch the monolayer of confluent MSCs and create a gap on the MSCs monolayer. From this moment onwards, a magnet (0.08 T) was placed underneath the wells and microscopic images were taken overtime to monitor the closing of the gap. A control group with no magnetic exposure (0 T) was also assessed

overtime to compare the performance of both groups. All conditions were tested in triplicates using two different donors (donor 2 and 3).

Chick Chorioallantoic Membrane (CAM) assay and neo-vessel quantification. The angiogenic potential of the secretome of MSCs exposed to a magnetic field for 24 h was evaluated using the CAM assay under the following analysis conditions: MSCs cultured on gelatin scaffold (0.08 T and 0 T); 2D cultures of MSCs (0.08 T and 0 T), as controls. Briefly, fertilized chick (*Gallus gallus*) eggs were horizontally incubated at 37 °C in a humidified atmosphere. Three days after the embryonic day, 1.5-2 mL of albumin was removed to allow the detachment of the developing CAM and a square incision was made on the eggshell under sterile conditions. The window was sealed with sterile transparent adhesive tape and the eggs returned to the incubator. At day 10-post fertilization, a 3 mm silicon ring was placed on top of the CAM and 10 µL of the conditioned media to test were added on the CAM of the chicken embryo (n = 6-10 per experimental group, using two different donors: 2 and 3). To avoid additional variability, one pair of conditions (the secretome under magnetic exposure: 0.08 T, and the respective control: 0T), were combined in the same egg and individually placed on different sections of the chicken embryo. Sterile parafilm tape was used to seal back the window and the eggs were further incubated for 3 days, being hydrated every day. Gestational process was terminated with the embryos being euthanized with fixative (2 mL) on top of the CAM and the ring was removed for the CAM to be excised. The inoculation area was then observed under a stereoscope, at 20x magnification (Olympus, SZX16, coupled with a DP71 camera)[26,27]. The number of new vessels, lower than 20 µm diameter, growing radial towards the ring area were registered. All animal procedures were carried out in accordance with the guidelines of the European Directive 2010/63/EU and the national Decreto-Lei nº 113/2013.

Statistical analysis. All measurements were made at least three times, in independent conditions. All results are shown as the mean $\pm$ standard deviation (SD). Two-way ANOVA following Sidak's multiple comparisons test was used to compare the mean of three values obtained from three independent conditions for each donor in a total of 3 donors (n=3). This statistical analysis was applied in RT-PCR, ELISA and *in vitro* Sprouting experiments, using GraphPad Prism version 7 (GraphPad Software, La Jolla,

CA). The parametric student's *t* test, two-sided, was performed to determine statistically significant differences on *in vitro* Wound Healing and *ex-vivo* CAM assay experiments; *$p < 0.05$ indicates a significant result; **$p < 0.01$ a very significant result, ***$p < 0.001$ a highly significant result, and ****$p < 0.0001$ an extremely significant result.

IV.3. Results

3.1. Scaffolds magneto-responsiveness are modulated by MNPs load and magnetic exposure.

In Chapter III, it was reported the effect of coupling a neodymium magnet to hybrid 2D material-based scaffolds of PVA doped with magnetic nanoparticles on protein sorption[16]. Based on this concept, here we proposed to regulate cell-matrix interactions and investigate whether this type of interactions could potentiate enhanced vascularization for tissue regeneration. Two magnetic responsive scaffolds were employed: the previously developed magnetic PVA hydrogel, made of a synthetic polymer, and a newly developed magnetic scaffold based on biodegradable denatured collagen (gelatin), a natural polymer suitable to promote cell adhesion on tissue culture[28].

Nanoparticles integrated on the PVA scaffold were prepared with chemical functionalization, avoiding aggregation and granting an average diameter of 8.73 ± 0.15 nm (Figure IV. 1a). Non-functionalized nanoparticles aggregates, reaching an average diameter of 12.8 ± 0.38 nm (Figure IV. 1a), were incorporated on gelatin-based scaffolds, to investigate the possibility of achieving enhanced magnetic response.

The hydrogels obtained were characterized in terms of MNPs dispersion by optical microscopy, with evident nanoparticle aggregation observed in the gelatin matrix and a more uniform MNPs dispersion of nanoparticles on the PVA hydrogel (Figure IV. 1b). PVA magnetic gel stability in water was previously confirmed[16] and gelatin scaffold stability was here established through UV spectroscopy analysis, with no detection of release of MNPs to the media that could compromise the cellular experiments (Figure IV. S1a). Structurally, gelatin evidenced a higher swelling degree than PVA (Figure IV. S1b). PVA hydrogel average surface roughness increased, up to nearly 10 μm in roughness, with the increase of MNPs concentration (0%, 0.25% and 1%). While similar low average roughness was obtained for low MNP load (0% and 0.25%), gelatin scaffold roughness

steeply increased to the higher MNPs load (1%) used, reaching an average roughness of 18 µm (Figure IV. 1c).

As previously reported for the magnetic PVA hydrogels[16], an increase on the hydrophilic surface properties is also observed for the magnetic gelatin hydrogels as a response to magnetic exposure, corresponding to 20º surface contact angle decrease for gelatin hydrogels prepared with the highest MNPs loads (Figure IV. 2a).

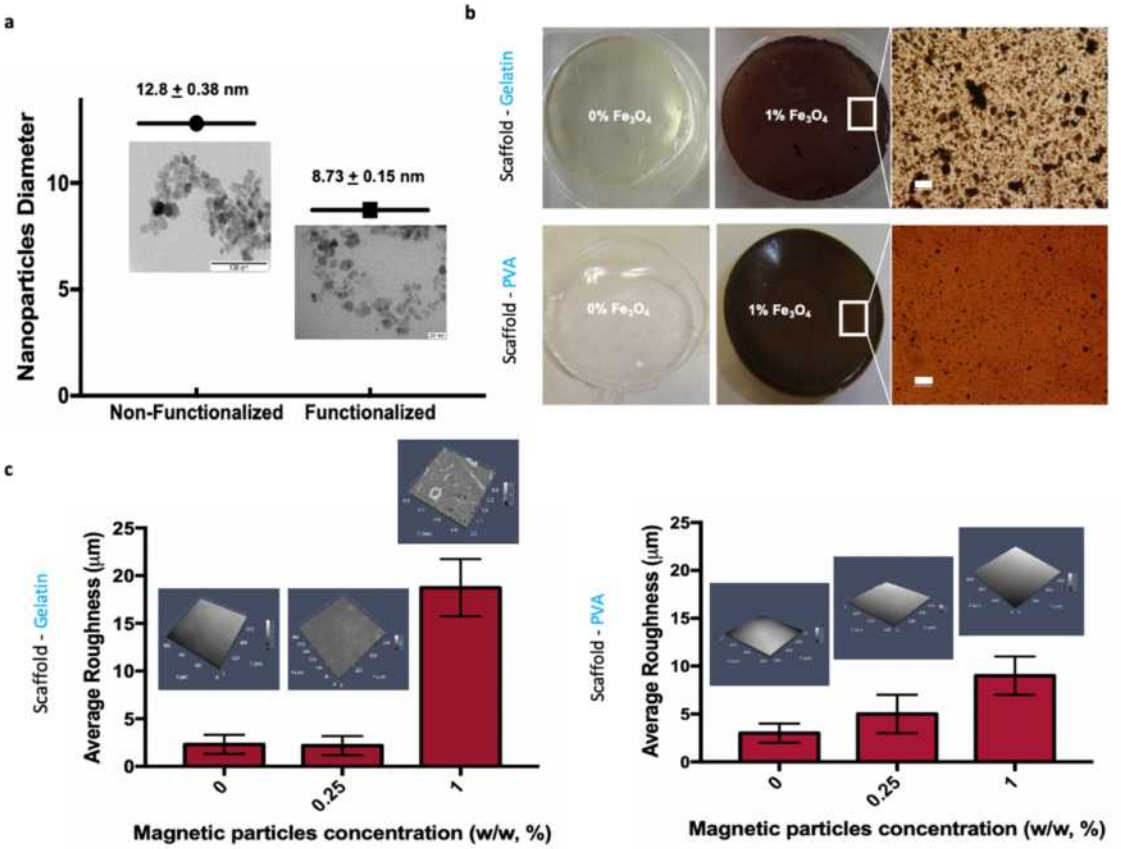


Figure IV. 1. Gelatin and Polyvinylalcohol (PVA) roughness is magnetic load-dependent. **a)** To develop an effective method for vascular tissue regeneration, scaffolds integrating MNPs were fabricated through the chemical functionalization of the PVA batch while purposely allowing the gelatin batch to form clusters. A representative TEM (Transmission Electron Microscopy) image of the used MNPs allowed for the representation of the average diameter of the particles. **b)** Macroscopic and microscopic images of the hydrogels without addition of MNPs and with MNPs incorpated in their composition. Scale bar = 100 µm. **c)** The average roughness of the scaffolds with different magnetic loads was determined and compared though 3D confocal imaging of the hydrogels surface showing a roughness increase with the magnetic concentration. Data are presented as means ± SD.

The ferromagnetic properties of the scaffolds were also characterized by Vibrating-Sample Magnetometer (VSM) technique (Figure IV. 2b), highlighting the increased magnetization potential of the PVA, with maximum saturation magnetization

at 0.19 ± 1.1 x 10^{-2} emu/g for 1% MNPs, in comparison with the gelatin, which showed a maximum stabilization threshold at 0.09 ± 1.6 x 10^{-4} emu/g.

Overall, the magnetic responsiveness of the hydrogels was better for the highest magnetic particles load assessed. Therefore, cellular experiments were performed with 1% of MNPs to ensure enhanced magnetic impact on the cells.

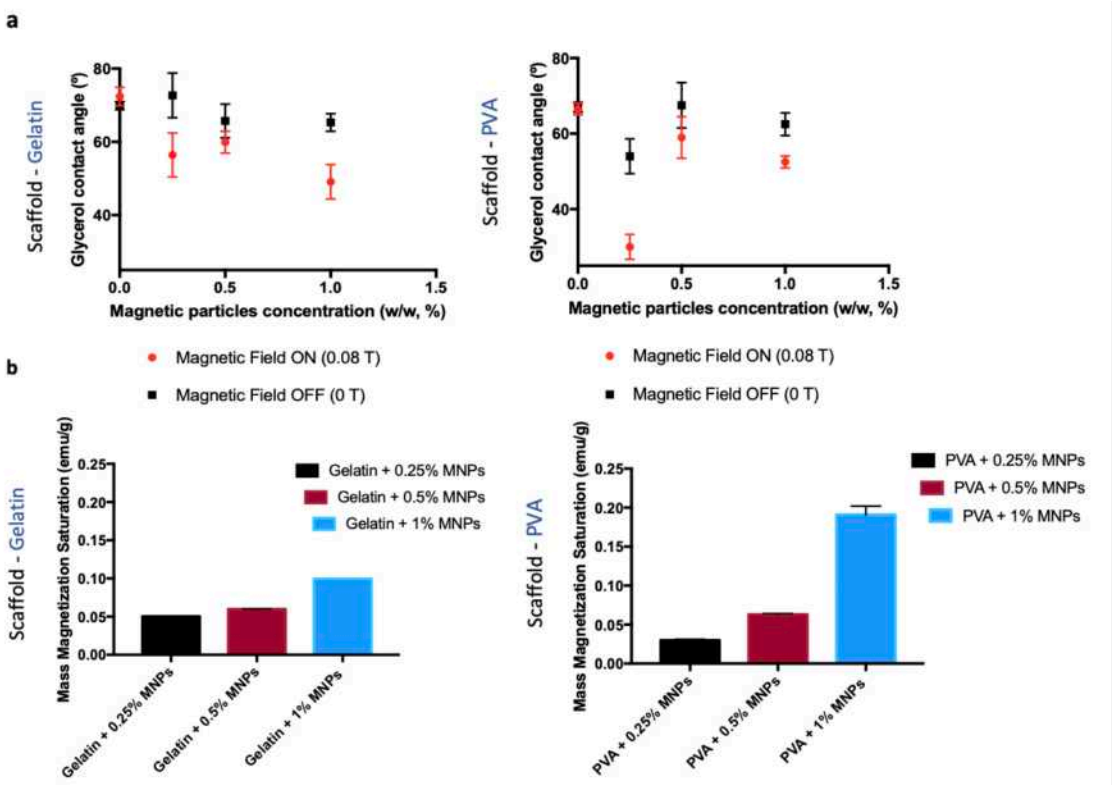


Figure IV. 2. Magnetic field impacts on the surface properties of the scaffolds increasing the hydrophilicity of the hydrogels. **a)** Determination of the contact angle observed in PVA and Gelatin scaffolds according with the magnetic load and the presence of a magnetic field of low intensity (0.08T). The results showed a significant decrease (~20º) in the hydrophilicity of the surfaces containing magnetic load. **b)** The magnetic properties of Gelatin and PVA with incorporated MNPs were characterized by VSM (Vibrating-Sample Magnetometer) technique, showing the ferromagnetic properties of both scaffolds and the higher magnetization of the PVA scaffold (0.2 emu/g) in comparison with the gelatin (0.1 emu/g). Data are presented as means ± SD.

3.2. Magnetic forces impact on 2D and 3D cultures of MSCs.

Cell culture on monolayer (2D) were performed on standard polystyrene cell culture plates (TCP), in the absence and in the presence of the magnetic field. This study allows to investigate the impact of the magnetic field on the MSCs without effects driven from the interactions between cell and scaffolds. MSCs proliferation and immunophenotype profile were characterized. The number of MSCs increased steeply on

the first days, reaching confluency after 48h, with a total amount of 50000 cells/ mL. Cells number started then to slowly decrease until the end of the experiment (120 h). Notably the magnetic field does not seem to impact on the proliferation curves, which show the same behavior overtime in the presence and absence of the magnetic field at a value of 0.08 T (Figure IV. 3a). Accordingly, some works reported similar results for MSCs in co-cultures while others enhanced the magnetic effect on the decrease of MSCs proliferation[22,29].

Metabolites analysis (glucose and lactate) confirmed that glucose and lactate concentrations remain, respectively, above the critical value of 1 mM and below toxic threshold of 10 mM indicating a healthy glucose/ lactate balance in the culture, without carbon source limitations (Table IV. S2).

Cells identity phenotype was assessed before and after 5 days of continuous exposure to the magnet. No statistical significance was obtained for these results, suggesting that the exposure to 0.08T magnetic fields do not affect MSC phenotype (Figure IV. 3b).

Previous works have reported changes in the phenotype of immune cells (macrophages) through magnetic exposure[30] and others stated the promotion of malignant phenotypes in neuroblastoma cells via electromagnetic interference[31]. Such changes were attributed to mechanotransduction phenomena, in which external stimuli resulted in remodeling of the cytoskeleton inducing internal cell stress and ultimately affecting certain cellular components (e.g. focal adhesions, actin-filament polymerization)[30].

MSCs were also cultivated in 3D as cellular aggregates (spheroids), in the presence and absence of magnetic field, as a 3D cell model, and cells morphology and viability were compared with MSCs cultured on monolayer. 2D and 3D cultures were observed by confocal microscopy imaging (Figure IV. 3c) showing, as expected, the characteristic stretched cell shape for 2D monolayer and the cell clustering morphology for 3D cultures. Despite the high number of living cells in both the control and the magnetic exposed conditions, the Life/Dead assay images (Figure IV. 3d-f) suggested some cell death on 2D cultures during the magnetic-induced cell alignment, possibly affected by the intensity of the magnetic orientation lines in that region.

For a better understanding of the complexity of the neodymium magnet, orientation lines were drawn by powder MNPs, showing higher magnetic intensity closer to the borders of the neodymium bar (Figure IV. 3e).

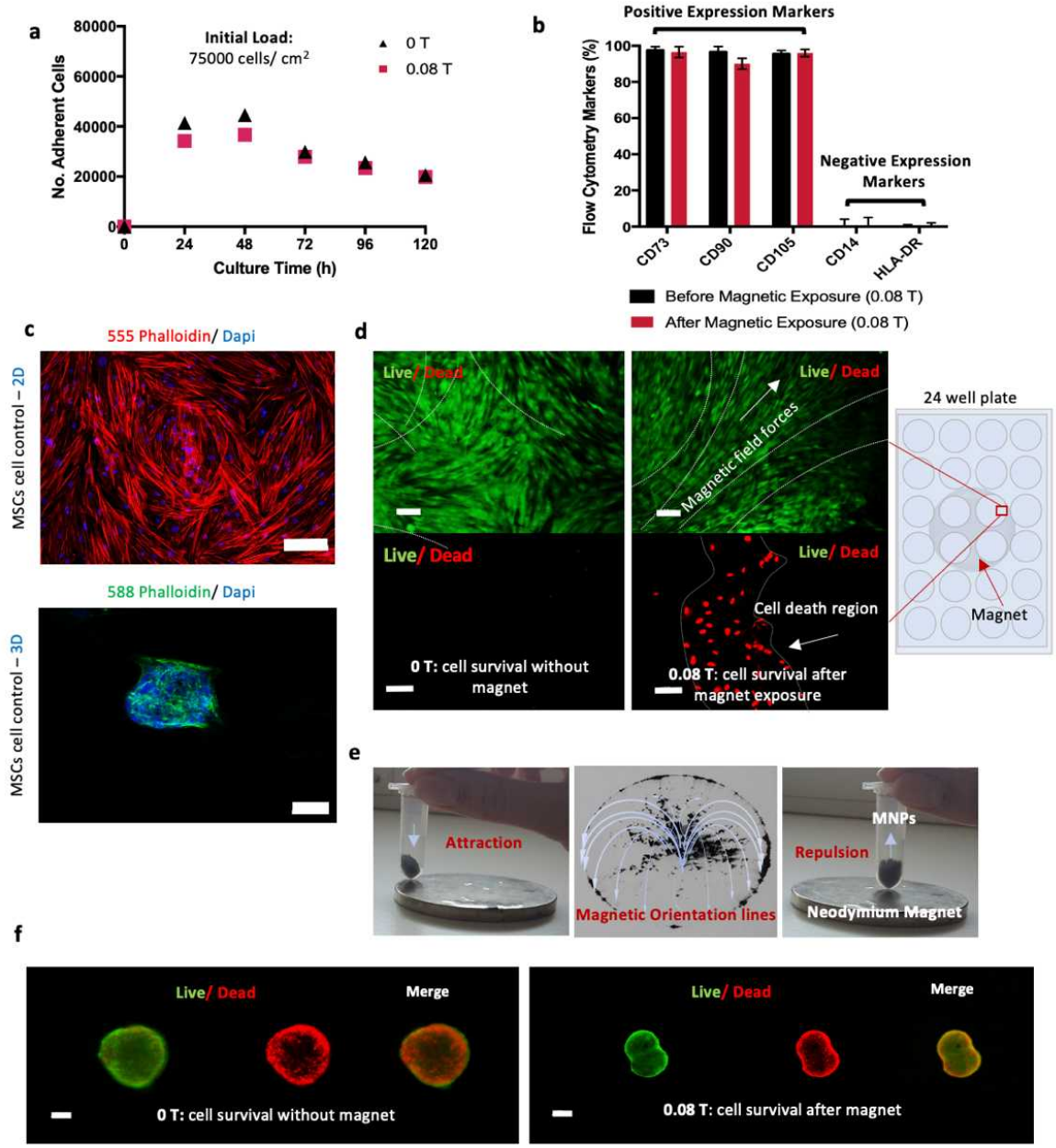


Figure IV. 3. Magnetic effect in a 2D culture of MSCs reflects on cell alignment while 3D cultures does not show magnetic impact. **a)** Proliferation rates of the MSCs under magnetic field against control conditions show that the magnetic field does not impact on cell growth. The metabolic activity of the cells was obtained using Alamar Blue staining proliferation assay. **b)** Representation of the expression of specific MSCs positive and negative markers by flow cytometry suggests the magnetic field does not modify the phenotype of the MSCsc after 5 days of continuous exposure. **c)** Confocal images of the morphology of MSCs monolayer stained with 555 phalloidin (red) and dapi (blue) and MSCs in 3D stained with 588 phalloidn (green) and dapi (blue). Scale bar: 100 µm. **d)** Live (Green)/ Dead (Red) microscopic images of the MSCs showing how the magnetic field leads to the orientation of the cells in the monolayer toward the stronger intensity of the field, also resulting in cell death in the region. Scale bar: 100 µm. **e)** Powder MNPs were used to characterize the magnetic field lines and determine the vertical direction of the magnetic forces on different regions of the neodymium magnet. **f)** MSCs in 3D form do not show magnetic field impact. Scale bar: 100 µm. Data are presented as means ± SD.

Cells displayed a random orientation when the culture was not exposed to magnetic field. However, the MSCs in monolayer showed the ability to move and orientate in the direction of the maximum magnetic intensity (Figure IV. 3d). Regarding the 3D cell culture, no relevant differences were observed by the exposure to the magnetic field, possibly due to the capacity of these structures to move within the media diminishing the prolonged impact of the static magnetic field over these spheroids (Figure IV. 3f). However, a necrotic core was observed overtime in the MSCs spheroids (200-400 μm), with or without magnetic stimulation, which can be associated with oxygen and nutrients depletion and accumulation of waste products in their core. This effect has been described before, limiting cell spheroids diameter to 200 μm[32,33].

3.3. MSCs geometry and alignment in scaffolds are magnetic field-dependent.

The interactions of cells, scaffolds and magnetic field is here studied. The potential cytotoxicity of MNPs, placed within the scaffold, was assessed through ISO 10993 using fibroblasts. Indirect contact measurement using MTT assay confirmed the biocompatibility by revealing a cell viability over 90% for scaffolds doped with MNPs (Figure IV. S2b), which is consistent with our results where no released MNPs were detected. The contact assay showed no formation of inhibition halo in the contact area between the scaffolds and the fibroblasts layer, suggesting the biocompatibility of these magnetic scaffolds for MSCs culture (Figure IV. S2a). MSCs cultures showed initial cell adhesions of 37 - 50% and 51% - 67% after 24h, respectively, for cells cultivated on magnetic PVA and gelatin-based scaffolds (Figure IV. 4a-b). Similar MSC proliferation behavior between magnetically stimulated cultures and controls was observed.

The concentrations of glucose and lactate in the media, were, for all conditions, higher than 1 mM and lower than 10 mM, indicating a healthy balance without carbon source limitations and no accumulation of lactate to toxic levels (Table IV. S2). The morphology of MSCs on magnetic gelatin was investigated in the presence of magnetic field of 0.08 T (Figure IV. 4b-c), emphasizing the stretched and oriented behavior of the cells towards the field lines with maximum magnetic intensity. Cell elongation (was statistically significantly higher in the presence of the magnetic field (120.2 $\pm$ 32 μm) than for the control condition (45.6 $\pm$ 24 μm) (Figure IV. 4c). This observation can be associated to the rearrangement of the cytoskeleton as previously reported[30,31].

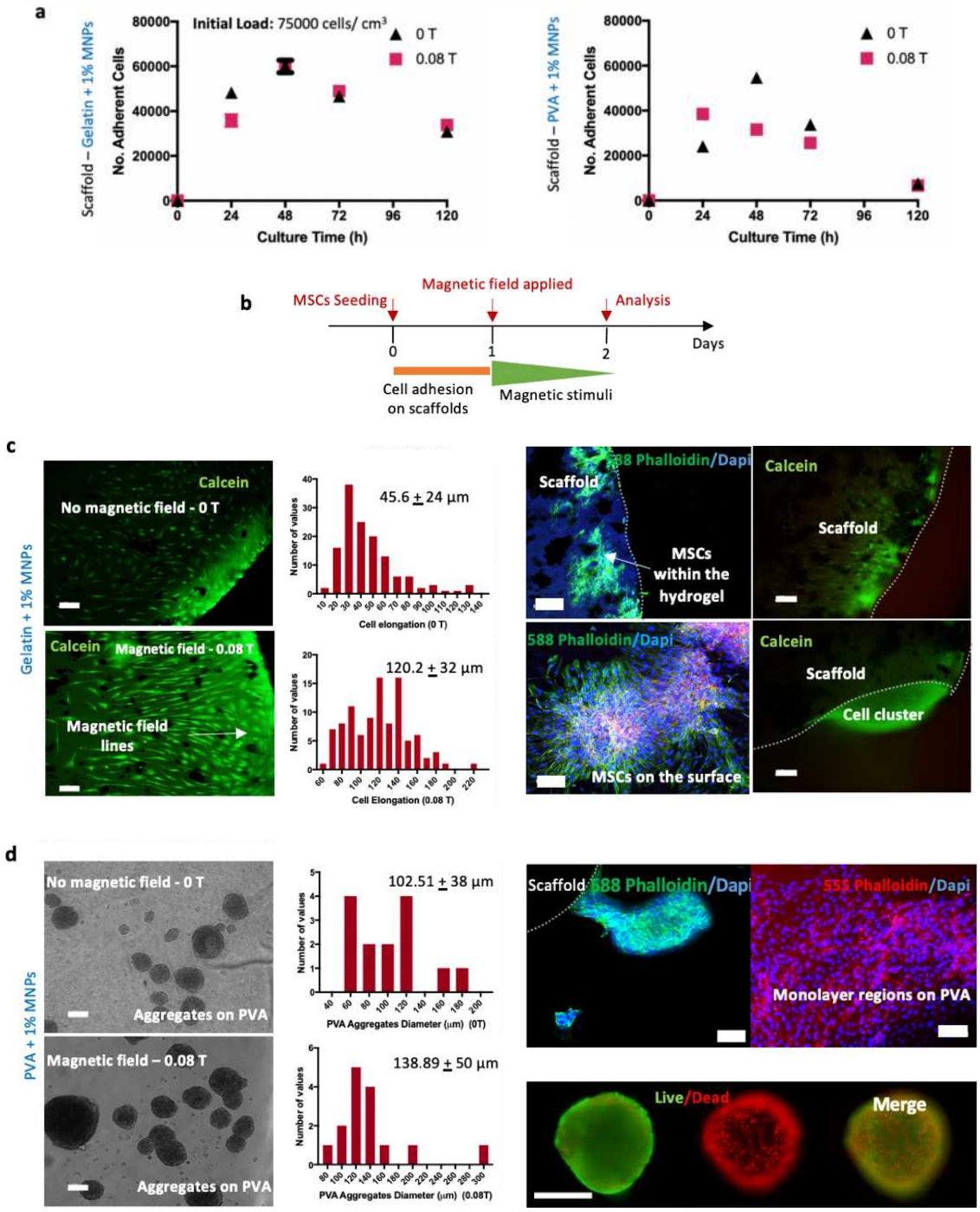


Figure IV. 4. MSCs interaction with magnetic scaffolds revealed differences depending on the nature of the scaffold and the magnetic exposure. **a)** Proliferation rates of the MSCs was used to investigate the adhesion of the cells to the scaffold (adhesion efficiency: 47-67% for the Gelatin and 33%-50% for the PVA). The magnetic field indicated a slight increase in proliferation in the PVA but no differences were observed for the Gelatin. Cell survival decreases in the PVA but stabilizes for the Gelatin. The long-term survival of the cells seemed to be independent of the magnetic exposure. **b)** Schematic of the magnetic application conditions and sample collection times and analysis. **c)** The external magnet impacts on the MSCs morphology cultured on the gelatin, leading to cell stretching and alignment towards the maximum magnetic intensity. In some regions MSCs populate the surface of the scaffold while most spontaneously migrated inside the material forming a 3D biostructure. Scale bar: 100 µm. **d)** Heterogeneous regions were observed in the PVA scaffold, with the formation of necrotic aggregates attached to the hydrogel surface and some monolayer regions. The exposure to the magnetic field does not induce differences on the PVA. Scale bar: 100 µm. Data are presented as means ± SD.

Confocal imaging revealed that, in addition to the formation of a monolayer of MSCs on the surface of the gelatin, a high number of MSCs migrated inside the scaffold, where they were still be capable to align and stretch fowling the magnetic field lines. A z-stack confocal microscopy scanning of the gelatin scaffold (up to 50% of total gel thickness) corroborated the migration effect by showing MSCs in different depth levels of the hydrogel (Figure IV. S3). These findings are aligned with MSCs association with perivascular cells (pericytes), multi-functional mural cells embedded within the walls of capillaries[34,35]. The concentration of encapsulated MSCs concentrated near the border of the gelatin also suggests the ability of the cells to migrate to areas following stronger magnetic attraction forces (Figure IV. 4b). Other possible interpretation is related with encapsulated MSCs migration towards gradients of oxygen and nutrients outside the scaffold. Confocal imaging shows heterogeneous regions on the PVA surface, alternating between monolayer areas and aggregates loosely attached to the polymeric surface. The spontaneous formation of MSC aggregates on the surface of the PVA matrix (Figure IV. 4c), resulted on similar diameter distribution of these 3D structures ($p < 0.05$) regardless of the application of the magnetic field. This suggested that the formation of these aggregates is probably due to the poor affinity of the cells to the matrix of the scaffold and not related with magnetic stimulation effects.

Live/Dead assay on the PVA loosed 3D MSC aggregates, and on MSC spheroids prepared by hanging drop technique (control), evidenced the presence of a necrotic core surrounded by a thin layer of living cells similarly to that observed for MSC aggregates formed at the PVA scaffolds. Likewise, this observation suggests the difficulty to cells in the 3D structures core to get proper access to nutrients or avoid accumulation of metabolites (Figure IV. S4).

3.4. Magnetic exposure enhances VEGF-A production in MSCs cultured on magnetic scaffolds.

Vascular Endothelial Growth Factor is a potent angiogenic factor secreted by MSCs via paracrine mechanisms. The influence of magnetic stimulation on the expression and secretion of this factor is crucial to understand and predict the effect of MSCs conditioned media on the sprouting of endothelial cells.

VEGF-A mRNA expression was assessed via RT-PCR for monolayer 2D culture of MSCs (control for the magnetic gelatin culture), 3D aggregates (control for the PVA culture), MSCs cultures on gelatin scaffolds and MSCs on PVA (Figure IV. 5a-b).

Statistically significant increases in VEGF-A expression due to magnetic stimulation (0.08 T) were observed for the control 2D MSCs monolayer, when compared to non-stimulated cultures. Moreover, the use of a magnetic scaffold further enhanced VEGF-A expression of MSCs cultivated on magnetic gelatin scaffolds, both in comparison with MSCs cultured on the same scaffolds without magnetic field (0 T) or when cultivated on 2D monolayer conditions (0 T and 0.08 T). Interestingly, a different behavior was obtained with the PVA culture, where the exposure to the magnet (0.08 T) revealed a significant decrease on the expression of VEGF-A. Possibly due to the mobility freedom of the control spheroids within the media, the effect of the magnetic field is not homogenous, leading to inconclusive results for those conditions. Similar VEGF-A expression profiles were observed for both the control 2D and 3D cell cultures without magnetic exposure.

The translation of VEGF-A mRNA expression into VEGF-A protein release in the cell culture media was assessed by ELISA measurements (Figure IV. 5c). The results obtained for the gelatin culture as well as the control 2D monolayer were aligned with the RT-PCR results as the same pattern was observed with an increase verified for the condition exposed to magnetic field. Once more, RT-PCR and ELISA results are in agreement for MSC cultures on PVA scaffolds, with inhibition of the VEGF-A expression when the scaffold is stimulated by the magnet. However, for one of the donors (donor 2), VEGF expression on the RT-PCR result did not match the VEGF-A protein quantification in 3D control culture. The magnetic effect on 3D cultures remained inconclusive in these analyses and, consequently, 2D cultures were used as the only control for the further experiments.

Overall the results showed robustness and consistency throughout the experiments, pointing out for the interesting contrast between magnetic induction of VEGF-A release by MSCs cultures on PVA and gelatin, with potentially different future applications.
To complement the study and investigate whether longer magnetic exposure could lead to improved results, the experiment was extended up to 5 days.

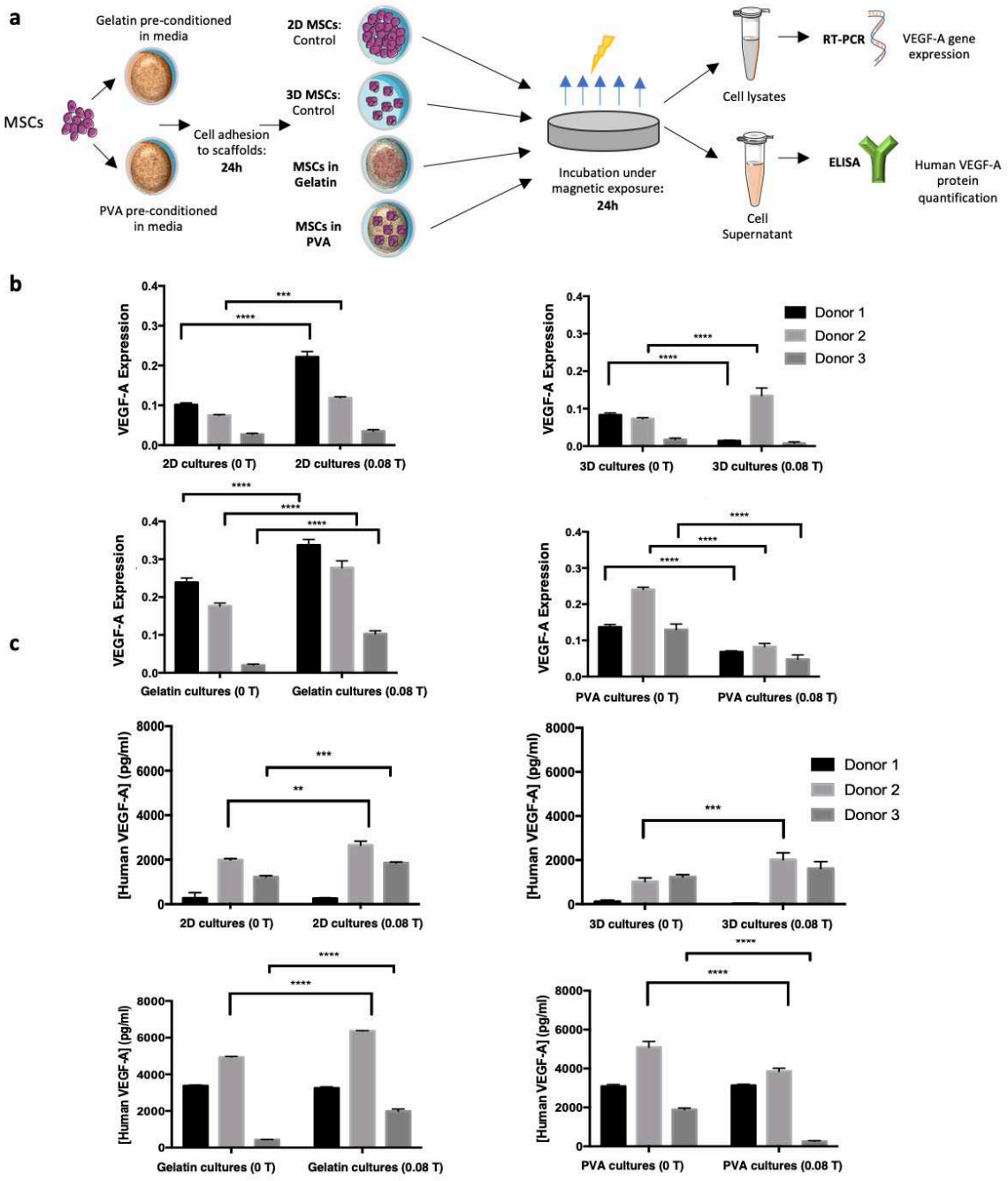


Figure IV. 5. Magnetic gelatin elicits enhanced angiogenic potential whereas magnetic PVA reveals potential for angiogenesis inhibition. **a)** Schematic of the procedure involved in the measurement of the VEGF-A expression and its quantification in the MSCs secretome**. b)** RT-PCR technique was used to assess the expression of human vascular marker VEGF-A gene. Regardless of the variability associated with MSCs donors, the same pattern was observed in the results. MSCs monolayer control indicated increased VEGF-A expression from 24h of magnetic exposure. These values are increased upon using a scaffold of Gelatin. Non conclusive results were observed for the 3D culture of MSCs aggregates. Interestingly, inhibition of VEGF-A expression was determined when using a PVA scaffold. **c)** ELISA specific assay for human VEGF-A was performed to validate the mRNA expression values obtained for VEGF-A. Despite donor 1 VEGF-A expression not translating into VEGF-A protein values as expected, the other results confirm and complement the mRNA conclusions. Statistical significance was determined using two-Way ANOVA. Data are presented as means ± SD.

However, the obtained results with the gelatin scaffold seemed to annul the increased expression of VEGF-A observed after 24h of magnetic exposure (Figure IV. S5). The result implied a potentially reversible and time-dependent effect, suggesting a probable adaptation of the cells to the magnetic stimulation after 5 days. The 5-day results obtained for PVA were controversial and therefore inconclusive. Other genes involved in the angiogenesis process, such as Hepatocyte Growth Factor (hFGF) and basic Fibroblast Growth Factor (bFGF), were analyzed but revealed no changes upon magnetic exposure (Figure IV. S6). Consequently, further functional assays focused on VEGF-A as the molecule of interest. Therefore, the following up studies were focused on the use of MSC conditioned media to perform angiogenic functional assays.

3.5. Improved HUVECs *in vitro* sprouting induced by MSCs exposure to magnetic stimulation.

The complex network of the vascular system is composed by tubular structures responsible for distributing nutrients, oxygen and cells to the organs. The previous determination of higher levels of VEGF-A in the media of MSCs cultivated under magnetic exposure (MSCs cultured on 2D TCP and on gelatin-based scaffolds) suggested a positive effect of the magnetic field using MSCs to promote angiogenesis. Hence the impact of these findings in the angiogenesis process was explored through an *in vitro* study on the capacity of these VEGF-A molecules to induce the formation of tube networks in the presence of HUVECs (Figure IV. 6b).

The sprouting quality was quantified in terms of tube number, branch points and tube length induced by the use of conditioned media from MSCs, cultured on the scaffolds (PVA and gelatin), and as 2D cell monolayer on TCP (control) (Figure IV. 6b).

The results showed significant effect of the magnetic field for the control 2D cell monolayer and gelatin, with higher tube numbers and branch points being formed using the conditioned media from MSCs exposed to 0.08 T. Oppositely, PVA scaffolds coupled with the magnetic field induced a reduction of number of tubes and branch points, for most of the donors studied. Additionally, the scaffolds matrix itself hints at being an important tool to promote angiogenesis as a higher tube numbers and branch points were formed on cultures using the conditioned media coming from MSCs cultured on scaffolds, rather than on MSCs cultured on TCP.

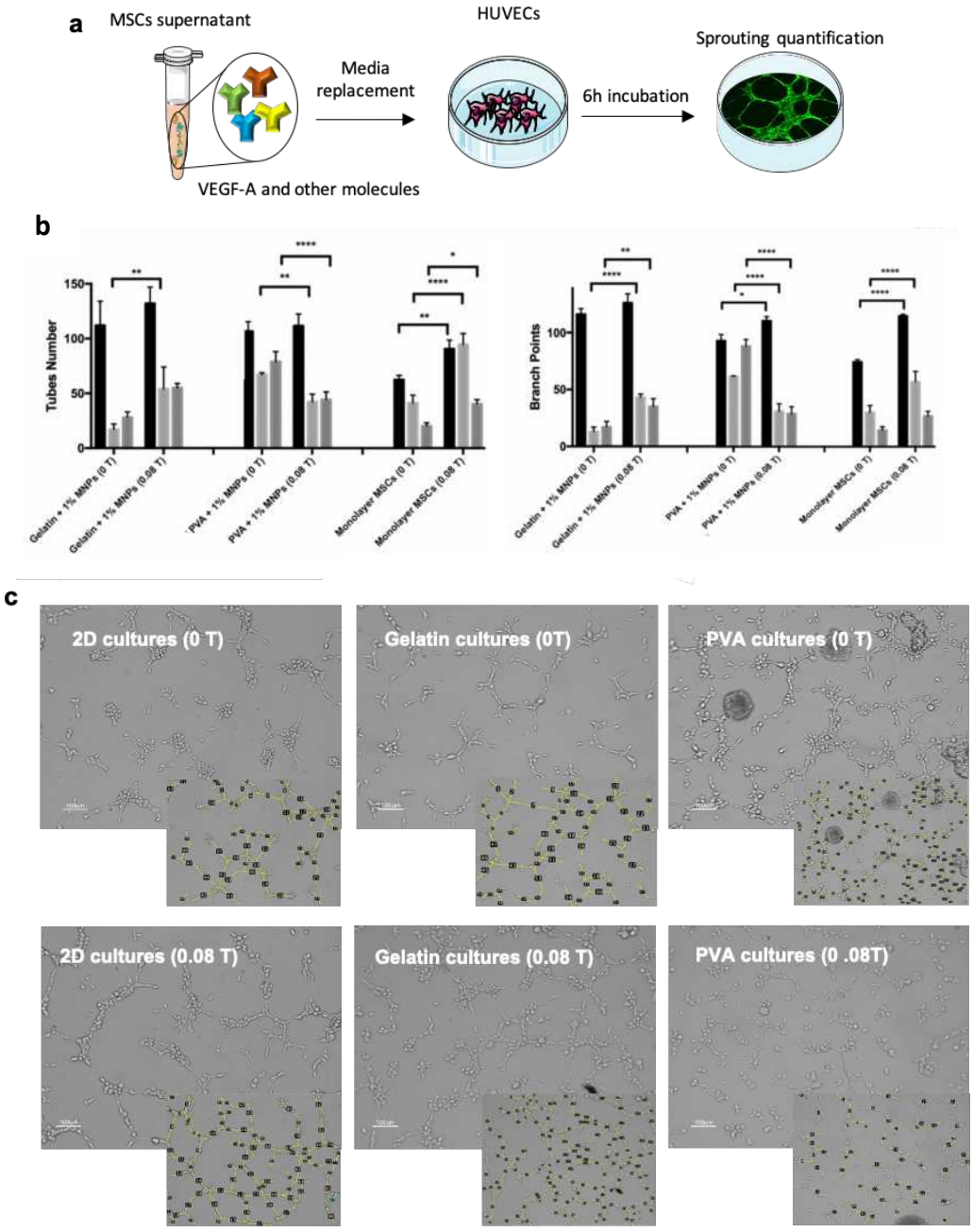


Figure IV. 6. *In vitro* angiogenic sprouting of human endothelial cells (HUVECs) enhanced though indirect magnetic stimulation. **a)** Schematic of the procedures followed for sprouting quantification. **b)** The quality of the sprouting was evaluated in terms of the average number of tubes formed after 6h of incubating HUVECs with MSCs conditioned media for each condition (24h of magnetic exposure). The number of branch points and the length of the tubes was also assessed. While tube length parameter did not provide conclusive information (Figure IV. S7), the number of tubes and branch points showed statistical improvement derived from magnetic stimulated conditions for both the monolayer and the gelatin scaffold. PVA scaffold provided opposite results, inducing sprouting inhibition under magnetic exposure. Gelatin scaffold also revealed better angiogenic potential in comparison with the MSCs control monolayer. **c)** Representative microscopic images of the sprouting effect observed for each condition. A higher number of ramifications is observed due to magnetic stimuli in MSCs monolayer and gelatin scaffold conditions and angiogenic inhibition is associated with the magnetic impact on PVA scaffold. Scale bar: 100 µm. Statistical significance was determined using two-Way ANOVA. Data are presented as means $\pm$ SD. Three independent donors were tested for each condition and tube formation were performed in triplicates.

Qualitatively, this impact can also be observed on the representative images of the branching resulting from the treatment with conditioned media (Figure IV. 6c).

Tube length did not provide conclusive data from any tested group possibly due to the high heterogeneity of tubes analyzed (Figure IV. S8).

Analysis obtained for the prolonged exposure to the magnetic field (5 days) did not result into quantifiable vessel branching. This is probably due to the lower expression, and secretion, of growth factors such as VEGF-A, with the exception of the results obtained with the PVA scaffold non-exposed to magnetic stimulation (Figure IV. S6b). Overall this information can be correlated with data obtained from mRNA expression and protein quantification.

3.6. Induced faster response on HUVECs wound healing and MSCs migration are related with magnetic field incidence.

Wound healing mechanisms involve several cellular processes, including cell adhesion and migration, and is mediated by several extrinsic and intrinsic cues associated with inflammatory process. The role of MSCs and HUVECs in *in vitro* wound healing was here investigated as complementary functional assays. This assay aimed to investigate the effect of the magnetic field on the MSCs alone, without the contribution from the effects driven from the scaffolds. Therefore, the conditioned media obtained from MSCs cultured in 2D monolayer with and without magnetic stimulation were considered (Figure IV. 7a).

Spatial gaps were created on HUVECs confluent culture and the time periods necessary to close these gaps and for MSCs migration, on MSCs confluent cultures, were quantified.

The results (Figure IV. 7b, Figure IV. S8) revealed a significant enhancement on would healing performance, with the conditioned media from MSCs cultures exposed to magnetic field (CM - 0.08 T for 4h) inducing a faster repair of the wound. The closing of the gap created on a HUVEC confluent layer was completed after 22h, while the controls (CM – 0 T) took 30h to achieve the same effect. This result is in agreement with the fact that higher concentration of VEGF-A is present on the conditioned media driven from magnetic stimulated cultures. The other aspect explored in this study focused on the possibility of mobilizing MSCs to migrate into injured tissues during healing and accelerate the process (Figure IV. 7c, Figure IV. S9).

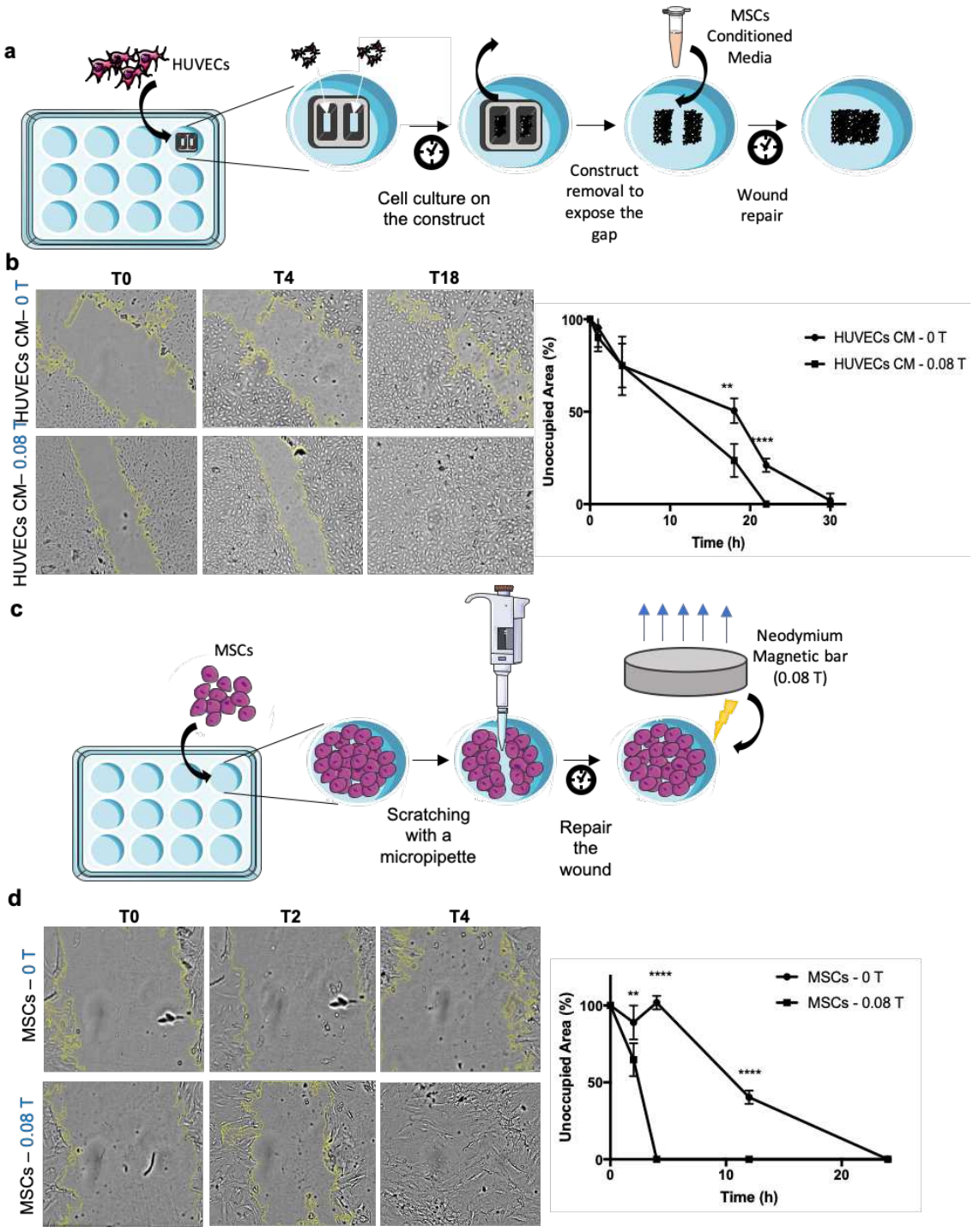


Figure IV. 7. Magnetic fields can be used to increase the velocity of wound healing by treating HUVECs with conditioned media resulting from the MSCs exposure to the magnetic source. Improvement of MSCs migration through their capability to elongate and migrate according with the intensity of the magnetic field. **a)** and **c)** Schematic of the two methodologies used in the migration assay. **b)** HUVECs were incubated for 30h with the conditioned media (CM) from MSCs treated with magnetic field and HUVECs migration was evaluated in comparison with HUVECs treated with CM of MSCs not exposed to magnetic field. A faster repair in the scratch region was obtained for the magnetic exposure condition after 22h. **d)** A total repair of the scratch was observed after 4h in the condition where MSCs were directly exposed to the magnetic source whereas the control condition took 24h to reach the same effect. Statistical significance was determined using multiple t-tests. Data are presented as means ± SD.

Usually this trafficking process is regulated by mechanical and chemical factors hence a similar effect obtained through magnetic stimulation would be a remarkable discover.

In this study the magnet was applied directly underneath the culture of MSCs after the formation of the gap on a confluent layer of MSCs 2D monolayer. The results (Figure IV. 7d) exhibited a very significant difference with a complete closure of the wounded area after 4h for magnetic stimulated (0.08 T) MSC cultures, while no signs of wound repair were observed for the control (0 T) over the same time period. In fact, 22 h were needed to completely repair on the absence of magnetic stimulation.

As noted previously, MSCs under magnetic forces tend to orientate towards the magnetic force lines which proved to be an important feature for this experiment as MSCs ability to migrate under magnetic exposure might have contributed to the faster closure of the wound. These outcomes, both using HUVECs conditioned with MSCs media after magnetic exposure or the results using MSCs under magnetic stimulation, indicated a noteworthy potential of the use of magnetic fields combined with therapy MSCs for blood vessel repair.

3.7. MSCs magnetic effect prompts increased *ex vivo* vessel formation.

Considering the promising *in vitro* results and the more stringent magnetic effects observed on the production of VEGF-A in MSCs cultured on gelatin-based scaffolds, such culture system was selected for *ex vivo* assays. Moreover, to investigate the effect of the magnetic field on the MSCs alone, without the contribution from the effects driven from the scaffolds, the conditioned media driven from MSCs cultured in 2D monolayer (with and without magnetic stimulation) was also considered.

CAM assays (Chick Chorioallantoic Membrane) were performed using fertilized chicken embryos inoculated with the conditioned media coming from MSCs cultured on gelatin scaffolds or as 2D cell monolayers (Figure IV. 8a, Table IV. S3).

After three days of inoculation, the incision area was microscopically observed detecting a difference between the controls (0 T) and the conditions treated with magnetic stimulation (0.08 T), which induced the formation of more vessels (Figure IV. 8b).

A comparison between the conditions revealed that, for one donor, it was observed an enhancement of the number of vessels for the conditioned media driven from MSCs 2D monolayer and gelatin scaffold cultures exposed to the magnetic field (Figure IV. 8c).

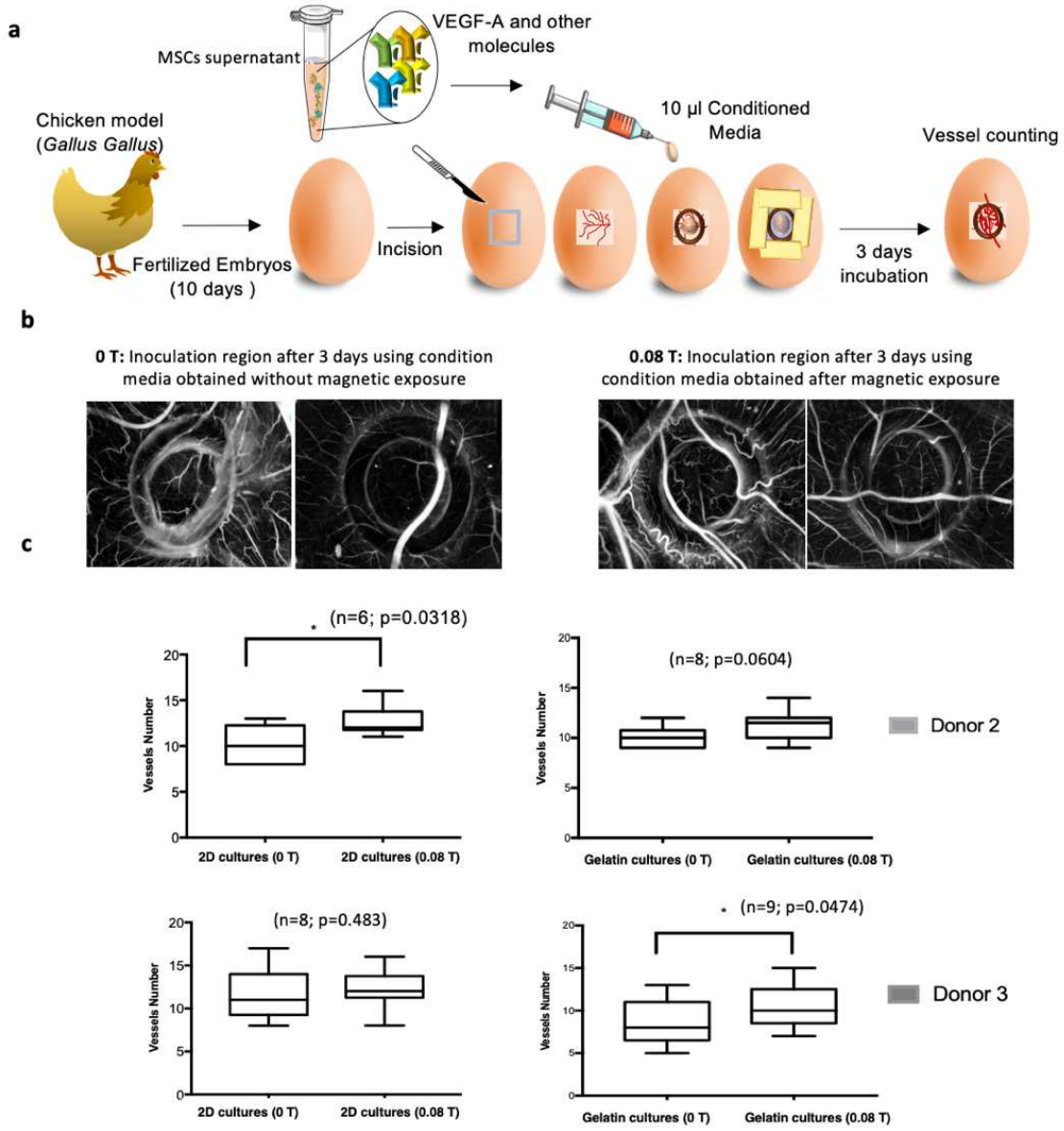


Figure IV. 8. Magnetic stimulation improves *ex vivo* angiogenesis. The conditions that provided better results *in vitro* were selected to implement CAM (Chick Choriollantoic Membrane) assay. **a)** Schematic of the simplified procedure involving the development of the CAM assay to assess angiogenesis phenomena allowing for an *ex-vivo* validation platform of the studied conditions. **b)** Microscopic images of the region of incision after 3 days of incubation with the conditioned media from MSCs exposed to magnetic stimulation (0.08 T) and the respective control condition (0 T). The determination of the number of new vessels (< 20 µm) growing towards the inoculation site during incubation period (3 days). **c)** The magnetic effect on the *ex-vivo* platform is shown through statistically significant results of the MSCs control in monolayer from donor 2 where an increased number of vessels were formed due to magnetic exposure. The impact observed for the conditioned media associated with the magnetic gelatin also shows a tendency for increased angiogenic response when exposed to magnetic field however no statistical significance was observed in these results. Statistical significance was determined using paired t-tests.

While the other conditions have not reported significant results, the same pattern was obtained on the scaffold condition for the other donor, revealing values close to statistical significance (p=0.0604). Although major conclusions are difficult to report due to the variability associated with living embryos, collectively our findings uncovered the opportunity to explore magnetic fields as an important tool for angiogenesis improvement.

IV.4. Discussion

Several studies have emphasized the importance of therapeutic angiogenesis as a valuable tool in the pathogenesis and treatment of cardiovascular diseases by stimulating the growth of new blood vessels from pre-existing vessels[36,37]. The ultimate efficacy resides in the controlled delivery of the therapeutic proteins to targeted tissues to actively sustain their long-term bioactivity [38]. Yet, as tissue regeneration implicates months to heal and requires persistent stimulation of growth factors, these systems are still far from representing an ideal condition. Thus, a therapeutic intervention in which the cells are continuously and non-invasively stimulated to secrete growth factors to a targeted tissue is an interesting approach that remains to be developed. To overcome the aforementioned challenges, a strategy was devised in this work to remotely enhance the secretion of growth factors by MSCs using magnetic scaffolds loaded with MNPs to drive the magnetic effect to the targeted material. We successfully demonstrated that low intensity static magnetic fields can efficiently induce the release of growth factors, specifically VEGF-A, from MSCs and prompt angiogenesis *in vitro*. However, the underlying mechanism remains unclear.

Previous reports have highlighted that cells are able to communicate by transmission of electromagnetic cues and that endogenous electrical potentials appear in wounded tissues and disappear during the regeneration process, demonstrating the importance of applying the external stimuli in a specific stage of healing instead of continuously throughout the entire process[39,40,41]. In our experiments, magnetic stimulation was applied for a maximum of 24h to minimize adverse effects to the cells such as oxidative stress and genotoxic effects[42]. In fact, when the study was extended for a longer period of continuous exposure (5 days, Figure IV. S5-6), the impact on the cells decreased and did not prompt angiogenesis anymore. The potentially toxic effect observed after longer magnetic exposure might be attributed to the situation where the

spin of electrons in free radicals becomes affected leading to changes in chemical reaction kinetics and possibly altering cellular functions[43]. As a consequence, for this angiogenic strategy to be translated to an *in vivo* environment in the future, the magnetic stimulation should be applied for shorter periods of time, potentially involving cycles of stimulation to maintain cell stress and the secretion of VEGF-A.

In our study we were able to identify some effects of the static magnetic field on the MSCs. Accordingly, the proliferation rate and the plasticity of the MSCs, determined by their capability to differentiate into different cell types, does not seem influenced by the moderate intensity[41] magnetic exposure. However, we reported a magnetic impact on MSCs shape, alignment and migration, as well as in the paracrine effect associated with the secretion of molecules. Other works have explained how static magnetic fields stimulate the movement of cellular ions, increasing the consumption of oxygen by the cells and activating integrins, thus modulating cellular metabolism, clonogenic potential and cell cycle[44,45,46]. Consequently, beneficial effects have been observed on nerve regeneration, inflammation, united fractures and pain management[44,45,46]. As described, magnetic exposure modifies the shape of MSCs and promotes cell orientation according with the polarization forces. This can be justified since the magnetic field interferes in the cell key ion distributions and has been described to activate Na^+/K^+ channels and regulate Ca^{2+} transport, consequently affecting cell shape, size, membrane surface and distribution of cellular organelles by modulating Ca^{2+} concentration and triggering changes in the actin microdomain[47,48,49].

The effect of magnetic field on MSCs migration was observed in the scratch assay, leading to a faster repair of wounds created within the monolayer. Partially, this effect can be explained by the trophic and immunomodulatory properties of MSCs, which play an important role in tissue regeneration[50]. These properties identify MSCs as sensors of the inflammatory microenvironment through cell-to-cell contact and regulatory molecule secretion, including growth factors, chemokines, cytokines and extracellular vesicles[51]. Still, we observed a significantly faster response to wound healing when using magnetic stimulation. In adipose-derived stem cells, the magnetic effect also results in restoring cell polarity, interfering with different types of mechanoreceptors such as integrins. The overexpression of such molecules has been shown to mediate shear-stress and induce cell migration[48,52,53]. It was also reported that static magnetic fields enhanced the secretion of anti-inflammatory cytokines (IL-10), while controlling the secretion of pro-inflammatory cytokines (IL-6, IL-8 or TNF-alpha) to exert its anti-inflammatory properties[54].

In the present work, despite donors heterogeneity, we demonstrated a clear influence of the magnetic field on the secretion of VEGF-A molecule. The role of MSCs on the differentiation of endothelial progenitor cells through paracrine mechanisms involving the secretion of the cytokines (e.g. VEGF) has also been reported, with a potentially high contribution in endothelial repair and angiogenesis following ischemia, which is the focus of our work[4]. A particular study has described effective endothelial sprouting angiogenesis event using VEGF-A as a single angiogenic factor dependent on the Notch signaling in a microvessel-on-a-chip[55]. Here we also demonstrate differences on the sprouting quality of HUVECs based on the amount of VEGF-A present in the conditioned media of MSCs exposed to different scaffolds and magnetic exposure conditions. Naturally, other molecules might also be involved in the observed sprouting effect however other growth factor molecules investigated (bFGF and hGF) did not show any variation upon magnetic application.

Interestingly, our scaffolds of PVA and gelatin induced different cell behavior. PVA was associated with the inhibition of the VEGF-A production from MSCs when magnetic field was applied, consequently preventing HUVECs maturation and sprouting. This denoted a probable inhibition of the VEGF pathway as demonstrated in reports targeting the inhibition of tumor cell proliferation and tumor angiogenesis[56]. Contrarily, gelatin scaffold increased VEGF-A signaling prompting angiogenesis phenomena. These differences are possibly related with the nature of the matrix and cells interaction with these surfaces. In comparison with synthetic polymer PVA, gelatin possesses an excellent bio-affinity and mimics the components of the ECM, providing better environment for cell attachment and growth[57]. The high porosity of low concentration gelatin coupled with MSCs ability to migrate might also explain the encapsulation of the MSCs in the gelatin. In 3D scaffolds oxygen supply is more complex than in monolayer cultures, influenced by the chemistry and dimensions of the scaffold, cell type, density and diffusion mechanisms, with oxygen concentration decreasing from the periphery toward the center of the scaffold, creating a more hypoxic environment inside[58].

In the bone marrow niche, MSCs are also under an hypoxic condition, justifying the tendency of these bone marrow-derived cells to seek similar oxygen gradient[58]. Consequently, hypoxia conditions are known to increase VEGF-a expression, and actively affecting angiogenesis[59,60], suggesting that the higher amount of VEGF secreted in gelatin scaffolds might be related with the MSCs encapsulation within the gelatin. In our previous report the effect of the magnetic field on the scaffold was ascribed to

mechanical structural changes and MNPs particle-particle and particle-field attraction[16]. Assuming these structural modifications impact on the encapsulated MSCs, this effect, combined with the magnetic stress induced on the cells, might be enough to elucidate the increased VEGF-A expression and secretion upon magnetic stimulation. Contrarily, MSCs poor adhesion to synthetic PVA and the heterogeneous impact of the magnetic field over both aggregates and monolayer regions might explain the decreased secretion of VEGF-A observed.

The specific pathways activated through magnetic exposure are however still unclear. Some studies explored the enhancement in the proliferation of stem cells in response to magnetic stimulation by activating the p38 mitogen-activated protein kinase (MAPK) pathway[61]. Another pathway potentially associated with the magnetic stimulation is the phosphoinositide 3-kinase/Akt (PI3K/Akt) pathway which plays a crucial role in cell proliferation, survival and metabolism[62]. Yet in our study MSCs proliferation was not affected by magnetic exposure. Instead the overexpression of VEGF-A in MSCs monolayer and gelatin conditions seems to indicate that angiogenesis-related pathways were activated. Lately researchers have demonstrated that angiogenesis mechanisms are highly complex and likely to involve multiple pathways, with VEGF receptors being only expressed by endothelial cells and VEGF considered to act exclusively via paracrine pathway[63,64]. While the prosurvival effects of VEGF are known to be mediated by the PI3 kinase/Akt pathway, the endothelial cell proliferation induced by VEGF is related with the protein kinase C-Raf-Mek-Erk pathway[65,66]. Our study suggests both pathways to be indirectly activated by magnetic influence when using gelatin-based scaffold.

Little information is found in the literature concerning the application of magnetic fields to stimulate VEGF-A secretion in MSCs, which represents the novelty of this study.

Aligned with the results here found, a promising study investigated the therapeutic approach of using magnetically iron-labeled adipose-derived stem cells to promote heart function recovery after myocardial infarction using externally applied magnetic fields[67]. Another work revealed the use of magnetic fields in clinical applications to increase the secretion of stem cell-derived microvesicles, known for transporting several trophic/ signalling molecules including VEGF in equine adipose-derived stem cells[68,69]. Still, technical challenges limit large-scale microvesicles production and their therapeutic potential[68,69,70].

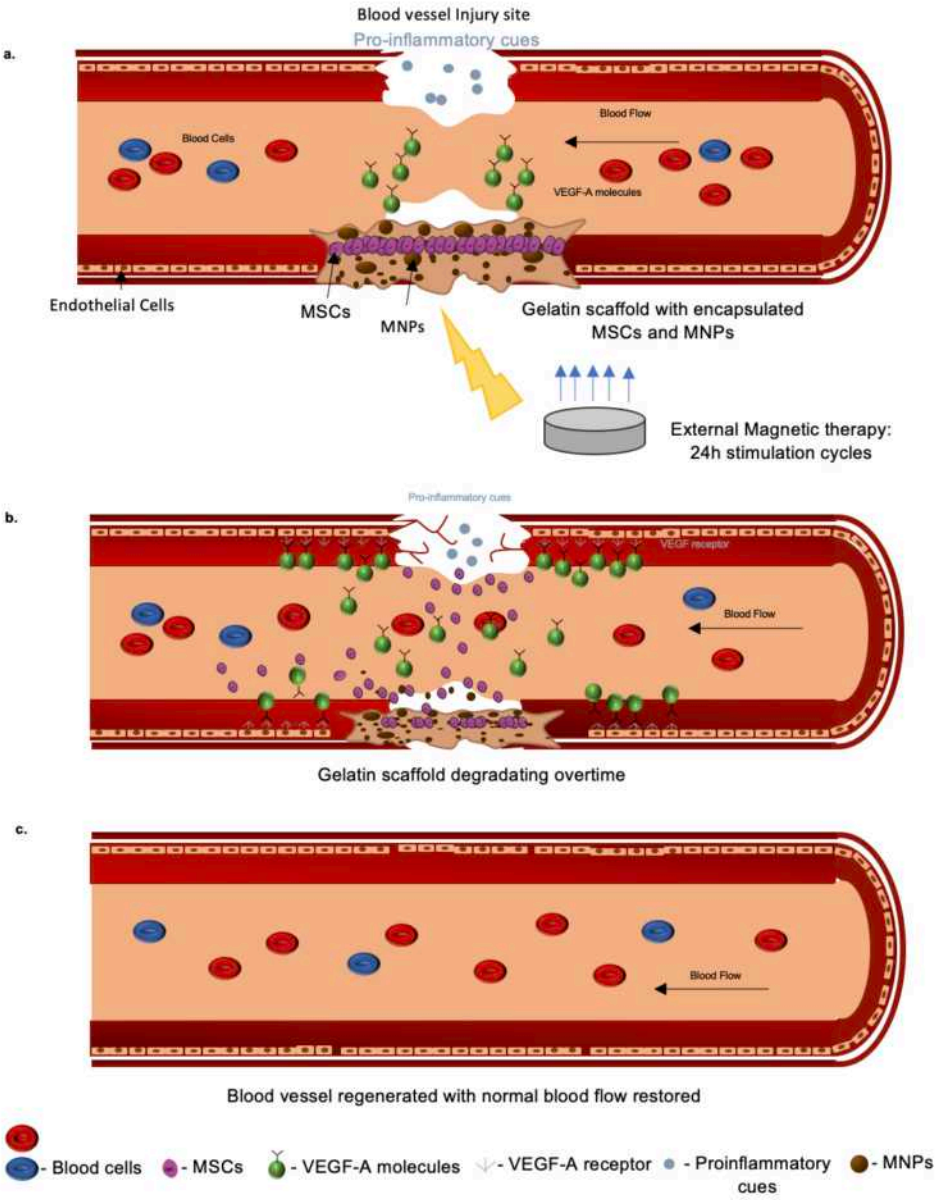


Figure IV. 9. Schematic of the hypothetical process involved in blood vessel regeneration using a magnetic gelatin scaffold. **a)** Cell therapy using magnetic gelatin as a vessel for encapsulated MSCs is activated by an external magnetic source with 24h stimulation cycles. The magnetic stimulation prompts MSCs to secrete VEGF-A molecules to the circulation. **b)** VEGF-A binds to its receptor (VEGFR-2) on the membrane of blood vascular endothelial cells, leading to its dimerization and initiating the signaling cascade responsible for endothelial proliferation. The activation of the angiogenesis system prompts the formation of sprouts and its progress towards hypoxic tissues. At the same time, gelatin scaffold starts to degrade due to shear stress, releasing the MNPs and MSCs which are reabsorbed in the circulation. The homing effect and immunomodulatory potential of MSCs might also accelerate the regeneration. **c)** Vascularization of the injured tissues promotes the repair of the blood vessel, restoring blood circulation.

Although positive effects of intravenous administration of angiogenic factors on tissue regeneration have been reported, the short half-life of VEGF-A *in vivo* (~30 minutes) and its off-target site toxicity represent drawbacks[71]. Our results also highlight the magnetic field impact is stronger when directly applied on the MSCs, losing some impact as conditioned media, as observed in sprouting and wound healing assays. *Ex vivo* CAM assay might have also improved with a continuous release of growth factor to increase branching formation.

A potential clinical approach of our system would involve magnetic gelatin as a cell support for controlled delivery of angiogenic cytokines, such as VEGF-A, externally mediated by the magnetic field to the injured blood vessel repair while promoting adequate vascularization (Figure IV. 9). In summary, and while the mechanism requires further evaluation and *in vivo* experiments, PVA scaffold coupled with magnetic exposure shows potential in cancer therapeutics by inhibiting vascularization during tumor growth while magnetic gelatin, able to maximize vascularization, is a promising treatment strategy for ischemic diseases. Taken together, we believe that our findings in this area represent a valuable therapeutic tool in vascular engineering.

IV.5. Conclusions

This study explores the effect of static magnetic fields of low intensity (0.08 T) on MSCs behavior and angiogenic secretory activity, aiming at the possibility to enhance angiogenesis with the formation of tube-like structures. The work compared the performance of magnetic stimulation on MSCs cultured on magnetic scaffolds (PVA and Gelatin) and directly on TCP, in 2D or 3D cultures. Although the magnetic stimulation reported no effects on MSCs proliferation, phenotypic identification or viability, it was observed a strong impact on the secretion of angiogenic growth factor, VEGF-A, by MSCs under magnetic exposure. The magnetic effect revealed a significant increase in the VEGF-A secretion by MSCs cultured on gelatin scaffolds on in 2D cultures and a reduction in MSCs cultured on PVA scaffolds. An important highlight of this work refers to the magnetic responsiveness of MSCs cultured on TCP in 2D, which was demonstrated through cell alignment, migration and increased secretion of VEGF-A.

The secretome of MSCs cultured on 2D or in the gelatin, enriched in VEGF-A molecules, proved to be able to induce the formation of new microvessels by endothelial cells, both *in vitro* and *ex vivo*. On the other hand, MSCs cultured on PVA showed potential for angiogenesis inhibition on HUVECs.

Overall, this unique discovery of the magnetic impact on angiogenesis phenomena highlights the potential to contribute for novel treatments associated with cardiovascular diseases.

IV.6. References

1. Zhang, H., Van Olden, C., Sweeney, D. & Martin-Rendon, E. Blood vessel repair and regeneration in the ischaemic heart. *Open Hear.* **1**, 1–14 (2014).
2. Biglu, M.-H., Ghavami, M. & Biglu, S. Cardiovascular diseases in the mirror of science. *J. Cardiovasc. Thorac. Res.* **8**, 158–163 (2017).
3. Hinton, W. *et al.* Incidence and prevalence of cardiovascular disease in English primary care: A cross-sectional and follow-up study of the Royal College of General Practitioners (RCGP) Research and Surveillance Centre (RSC). *BMJ Open* **8**, 1–9 (2018).
4. Ge, Q. *et al.* VEGF secreted by Mesenchymal stem cells mediates the differentiation of endothelial progenitor cells into endothelial cells via paracrine mechanisms. *Mol. Med. Rep.* **17**, 1667–1675 (2018).
5. Lovett, M., Lee, K., Edwards, A. & Kaplan, D. L. Vascularization Strategies for Tissue Engineering. *Tissue Eng. Part B Rev.* **15**, 353–370 (2009).
6. Rouwkema, J., Rivron, N. C. & van Blitterswijk, C. A. Vascularization in tissue engineering. *Trends Biotechnol.* **26**, 434–441 (2008).
7. Johnson, K. E. & Wilgus, T. A. Vascular Endothelial Growth Factor and Angiogenesis in the Regulation of Cutaneous Wound Repair. *Adv. Wound Care* **3**, 647–661 (2014).
8. Carmeliet, P. & Jain, R. K. Molecular mechanisms and clinical applications of angiogenesis. *Nature* **473**, 298 (2011).
9. Berendsen, A. D. & Olsen, B. R. How Vascular Endothelial Growth Factor-A (VEGF) Regulates Differentiation of Mesenchymal Stem Cells. *J. Histochem. Cytochem.* **62**, 103–108 (2014).
10. Cunningham, C. J., Redondo-Castro, E. & Allan, S. M. The therapeutic potential of the mesenchymal stem cell secretome in ischaemic stroke. *J. Cereb. Blood Flow Metab.* **38**, 1276–1292 (2018).
11. Ferreira, J. R. *et al.* Mesenchymal Stromal Cell Secretome: Influencing Therapeutic Potential by Cellular Pre-conditioning. *Front. Immunol.* **9**, 2837 (2018).
12. Vizoso, F. J., Eiro, N., Cid, S., Schneider, J. & Perez-Fernandez, R. Mesenchymal stem cell secretome: Toward cell-free therapeutic strategies in regenerative medicine. *Int. J. Mol. Sci.* **18**, (2017).

13. Schubert, M. *et al.* VEGF expression by mesenchymal stem cells contributes to angiogenesis in pancreatic carcinoma. *Br. J. Cancer* **99**, 622–631 (2008).
14. Asahara, T. *et al.* VEGF contributes to postnatal neovascularization by mobilizing bone marrow-derived endothelial progenitor cells. *EMBO J.* **18**, 3964–3972 (1999).
15. Reitz, M. S. *et al.* Human Mesenchymal Stem Cells Inhibit Endothelial Proliferation and Angiogenesis via Cell–Cell Contact Through Modulation of the VE-Cadherin/β-Catenin Signaling Pathway. *Stem Cells Dev.* **22**, 148–157 (2012).
16. Manjua, A. C., Alves, V. D., Crespo, J. G. & Portugal, C. A. M. Magnetic Responsive PVA Hydrogels for Remote Modulation of Protein Sorption. *ACS Appl. Mater. Interfaces* acsami.9b03146 (2019). doi:10.1021/acsami.9b03146
17. Wu, C. *et al.* Recent Advances in Magnetic-Nanomaterial-Based Mechanotransduction for Cell Fate Regulation. *Adv. Mater.* **30**, 1–8 (2018).
18. Meng, J. *et al.* Super-paramagnetic responsive nanofibrous scaffolds under static magnetic field enhance osteogenesis for bone repair in vivo. *Sci. Rep.* **3**, 1–7 (2013).
19. Du, V. *et al.* A 3D magnetic tissue stretcher for remote mechanical control of embryonic stem cell differentiation. *Nat. Commun.* **8**, (2017).
20. Pyo, S. *et al.* The Differential Effects of Repetitive Magnetic Stimulation in an In Vitro Neuronal Model of Ischemia/Reperfusion Injury. *Front. Neurol.* **9**, 1–11 (2018).
21. Popa, E. G., Santo, V. E., Rodrigues, M. T. & Gomes, M. E. Magnetically-responsive hydrogels for modulation of chondrogenic commitment of human adipose-derived stem cells. *Polymers (Basel).* **8**, (2016).
22. Sadri, M., Abdolmaleki, P., Abrun, S., Beiki, B. & Samani, F. S. Static Magnetic Field Effect on Cell Alignment, Growth, and Differentiation in Human Cord-Derived Mesenchymal Stem Cells. *Cell. Mol. Bioeng.* **10**, 249–262 (2017).
23. Cruz-Izquierdo, Á., Picó, E. A., López, C., Serra, J. L. & Llama, M. J. Magnetic Cross-Linked Enzyme Aggregates (mCLEAs) of Candida antarctica lipase: An efficient and stable biocatalyst for biodiesel synthesis. *PLoS One* **9**, 1–22 (2014).
24. Olle, B. *et al.* Enhancement of oxygen mass transfer using functionalized magnetic nanoparticles. *Ind. Eng. Chem. Res.* **45**, 4355–4363 (2006).
25. Dos Santos, F. *et al.* Ex vivo expansion of human mesenchymal stem cells: A more effective cell proliferation kinetics and metabolism under hypoxia. *J. Cell. Physiol.* **223**, 27–35 (2010).
26. Janser, F. A., Ney, P., Pinto, M. T., Langer, R. & Tschan, M. P. The Chick

Chorioallantoic Membrane (CAM) Assay as a Three-dimensional Model to Study Autophagy in Cancer Cells. *Bio-protocol* **9**, e3290 (2019).

27. Marques, F. G. *et al.* Low Doses of Ionizing Radiation Enhance the Angiogenic Potential of Adipocyte Conditioned Medium. *Radiat. Res.* **192**, 517–526 (2019).
28. Nur Hanani, Z. A., Roos, Y. H. & Kerry, J. P. Use and application of gelatin as potential biodegradable packaging materials for food products. *Int. J. Biol. Macromol.* **71**, 94–102 (2014).
29. Mueller, C. E. *et al.* Influence of static magnetic fields on human myoblast/mesenchymal stem cell co-cultures. *Mol. Med. Rep.* **17**, 3813–3820 (2018).
30. Wosik, J. *et al.* Magnetic Field Changes Macrophage Phenotype. *Biophys. J.* **114**, 2001–2013 (2018).
31. Falone, S. *et al.* Power frequency magnetic field promotes a more malignant phenotype in neuroblastoma cells via redox-related mechanisms. *Sci. Rep.* **7**, 11470 (2017).
32. Groebe, K. & Mueller-Klieser, W. On the relation between size of necrosis and diameter of tumor spheroids. *Int. J. Radiat. Oncol.* **34**, 395–401 (1996).
33. Egger, D., Tripisciano, C., Weber, V., Dominici, M. & Kasper, C. Dynamic Cultivation of Mesenchymal Stem Cell Aggregates. *Bioeng. (Basel, Switzerland)* **5**, 48 (2018).
34. Fu, Y. *et al.* Trophic Effects of Mesenchymal Stem Cells in Tissue Regeneration. *Tissue Eng. Part B Rev.* **23**, 515–528 (2017).
35. Caplan, A. I. New MSC: MSCs as pericytes are Sentinels and gatekeepers. *J. Orthop. Res.* **35**, 1151–1159 (2017).
36. Liao, Y. Y. *et al.* New progress in angiogenesis therapy of cardiovascular disease by ultrasound targeted microbubble destruction. *Biomed Res. Int.* **2014**, (2014).
37. Deveza, L., Choi, J. & Yang, F. Therapeutic angiogenesis for treating cardiovascular diseases. *Theranostics* **2**, 801–814 (2012).
38. Chu, H. & Wang, Y. Therapeutic angiogenesis: Controlled delivery of angiogenic factors. *Ther. Deliv.* **3**, 693–714 (2012).
39. RAHNAMA, M. *et al.* EMISSION OF MITOCHONDRIAL BIOPHOTONS AND THEIR EFFECT ON ELECTRICAL ACTIVITY OF MEMBRANE VIA MICROTUBULES. *J. Integr. Neurosci.* **10**, 65–88 (2011).
40. Levin, M. Bioelectromagnetics in morphogenesis. *Bioelectromagnetics* **24**, 295–

315 (2003).

41. Marycz, K., Kornicka, K. & Röcken, M. Static Magnetic Field (SMF) as a Regulator of Stem Cell Fate - New Perspectives in Regenerative Medicine Arising from an Underestimated Tool. *Stem cell Rev. reports* **14**, 785–792 (2018).
42. Ghodbane, S., Lahbib, A., Sakly, M. & Abdelmelek, H. Bioeffects of static magnetic fields: Oxidative stress, genotoxic effects, and cancer studies. *Biomed Res. Int.* **2013**, (2013).
43. BROCKLEHURST, B. & McLAUCHLAN, K. A. Free radical mechanism for the effects of environmental electromagnetic fields on biological systems. *Int. J. Radiat. Biol.* **69**, 3–24 (1996).
44. Gmitrov, J., Ohkubo, C. & Okano, H. Effect of 0.25 T static magnetic field on microcirculation in rabbits. *Bioelectromagnetics* **23**, 224–229 (2002).
45. Rumbaut, R. E. & Mirkovic, D. Magnetic therapy for edema in inflammation: a physiological assessment. *Am. J. Physiol. Circ. Physiol.* **294**, H19–H20 (2008).
46. Xu, S., Okano, H. & Ohkubo, C. Acute effects of whole-body exposure to static magnetic fields and 50-Hz electromagnetic fields on muscle microcirculation in anesthetized mice. *Bioelectrochemistry* **53**, 127–135 (2001).
47. Bauréus Koch, C. L. M., Sommarin, M., Persson, B. R. R., Salford, L. G. & Eberhardt, J. L. Interaction between weak low frequency magnetic fields and cell membranes. *Bioelectromagnetics* **24**, 395–402 (2003).
48. Teodori, L. *et al.* Static magnetic fields affect cell size, shape, orientation, and membrane surface of human glioblastoma cells, as demonstrated by electron, optic, and atomic force microscopy. *Cytom. Part A* **69A**, 75–85 (2006).
49. Yan, J., Dong, L., Zhang, B. & Qi, N. Effects of Extremely Low-Frequency Magnetic Field on Growth and Differentiation of Human Mesenchymal Stem Cells. *Electromagn. Biol. Med.* **29**, 165–176 (2010).
50. Pers, Y.-M., Ruiz, M., Noël, D. & Jorgensen, C. Mesenchymal stem cells for the management of inflammation in osteoarthritis: state of the art and perspectives. *Osteoarthr. Cartil.* **23**, 2027–2035 (2015).
51. Guerrouahen, B. S., Sidahmed, H., Al Sulaiti, A., Al Khulaifi, M. & Cugno, C. Enhancing Mesenchymal Stromal Cell Immunomodulation for Treating Conditions Influenced by the Immune System. *Stem Cells Int.* **2019**, 7219297 (2019).
52. Marędziak, M., Śmieszek, A., Tomaszewski, K. A., Lewandowski, D. & Marycz,

K. The effect of low static magnetic field on osteogenic and adipogenic differentiation potential of human adipose stromal/stem cells. *J. Magn. Magn. Mater.* **398**, 235–245 (2016).

53. Marędziak, M., Tomaszewski, K., Polinceusz, P., Lewandowski, D. & Marycz, K. Static magnetic field enhances the viability and proliferation rate of adipose tissue-derived mesenchymal stem cells potentially through activation of the phosphoinositide 3-kinase/Akt (PI3K/Akt) pathway. *Electromagn. Biol. Med.* **36**, 45–54 (2017).
54. Vergallo, C. *et al.* In Vitro Analysis of the Anti-Inflammatory Effect of Inhomogeneous Static Magnetic Field-Exposure on Human Macrophages and Lymphocytes. *PLoS One* **8**, e72374 (2013).
55. Pauty, J. *et al.* A Vascular Endothelial Growth Factor-Dependent Sprouting Angiogenesis Assay Based on an In Vitro Human Blood Vessel Model for the Study of Anti-Angiogenic Drugs. *EBioMedicine* **27**, 225–236 (2018).
56. Wilhelm, S. M. *et al.* BAY 43-9006 Exhibits Broad Spectrum Oral Antitumor Activity and Targets the RAF/MEK/ERK Pathway and Receptor Tyrosine Kinases Involved in Tumor Progression and Angiogenesis. *Cancer Res.* **64**, 7099 LP – 7109 (2004).
57. Hoque, M., Nuge, T., Yeow, T., Nordin, N. & Prasad, R. Gelatin Based Scaffolds for Tissue Engineering-a Review. *Polym. Res. J.* **9**, 15 (2015).
58. Sahai, S. *et al.* Tracking hypoxic signaling in encapsulated stem cells. *Tissue Eng. Part C. Methods* **18**, 557–565 (2012).
59. Ejtehadifar, M. *et al.* The Effect of Hypoxia on Mesenchymal Stem Cell Biology. *Adv. Pharm. Bull.* **5**, 141–149 (2015).
60. Kim, S. H. *et al.* Hypoxia-inducible Vascular Endothelial Growth Factor-engineered Mesenchymal Stem Cells Prevent Myocardial Ischemic Injury. *Mol. Ther.* **19**, 741–750 (2011).
61. Lew, W.-Z. *et al.* Static magnetic fields enhance dental pulp stem cell proliferation by activating the p38 mitogen-activated protein kinase pathway as its putative mechanism. *J. Tissue Eng. Regen. Med.* **12**, 19–29 (2018).
62. Yu, J. S. L. & Cui, W. Proliferation, survival and metabolism: The role of PI3K/AKT/ mTOR signalling in pluripotency and cell fate determination. *Dev.* **143**, 3050–3060 (2016).
63. Namiki, A. *et al.* Hypoxia induces vascular endothelial growth factor in cultured

human endothelial cells. *J. Biol. Chem.* **270**, 31189–31195 (1995).

64. Frumovitz, M. & Sood, A. K. Vascular endothelial growth factor (VEGF) pathway as a therapeutic target in gynecologic malignancies. *Gynecol. Oncol.* **104**, 768–778 (2007).
65. Gerber, H.-P. *et al.* VEGF regulates haematopoietic stem cell survival by an internal autocrine loop mechanism. *Nature* **417**, 954–958 (2002).
66. Takahashi, T., Ueno, H. & Shibuya, M. VEGF activates protein kinase C-dependent, but Ras-independent Raf-MEK-MAP kinase pathway for DNA synthesis in primary endothelial cells. *Oncogene* **18**, 2221–2230 (1999).
67. Wang, J. *et al.* Externally Applied Static Magnetic Field Enhances Cardiac Retention and Functional Benefit of Magnetically Iron-Labeled Adipose-Derived Stem Cells in Infarcted Hearts. *Stem Cells Transl. Med.* **5**, 1380–1393 (2016).
68. Collino, F. *et al.* Exosome and Microvesicle-Enriched Fractions Isolated from Mesenchymal Stem Cells by Gradient Separation Showed Different Molecular Signatures and Functions on Renal Tubular Epithelial Cells. *Stem Cell Rev. Reports* **13**, 226–243 (2017).
69. Marędziak, M., Marycz, K., Śmieszek, A., Lewandowski, D. & Toker, N. Y. The influence of static magnetic fields on canine and equine mesenchymal stem cells derived from adipose tissue. *Vitr. Cell. Dev. Biol. - Anim.* **50**, 562–571 (2014).
70. Marędziak, M., Marycz, K., Lewandowski, D., Siudzińska, A. & Śmieszek, A. Static magnetic field enhances synthesis and secretion of membrane-derived microvesicles (MVs) rich in VEGF and BMP-2 in equine adipose-derived stromal cells (EqASCs)—a new approach in veterinary regenerative medicine. *Vitr. Cell. Dev. Biol. - Anim.* **51**, 230–240 (2015).
71. Simón-Yarza, T. *et al.* Vascular endothelial growth factor-delivery systems for cardiac repair: an overview. *Theranostics* **2**, 541–552 (2012).

Chapter IV. Supplementary Information

Table IV. S1. Supplementary sequences of the primers used for qRT-PCR analysis.

Genes	Sequences
hGAPDH	For: 5' GGT CAC CAG GGC TGC TTT TA 3' Rev: 5' CCT GGA AGA TGG TGA TGG GA
hVEGF-A	For: 5' GGA GGA GGG CAG AAT CAT CAC 3' Rev: 5' GGT CTC GAT TGG ATG GCA GT 3'
HGF	For: 5' TCC ACG GAA GAG GAG ATG AGA 3' Rev: 5' GGC CAT ATA CCA GCT GGG AAA 3'
bFGF	For: 5' GCC CAG GTC CTG TTT TGG AT 3' Rev: 5' GGT CAC CAG GGC TGC TTT TA 3'

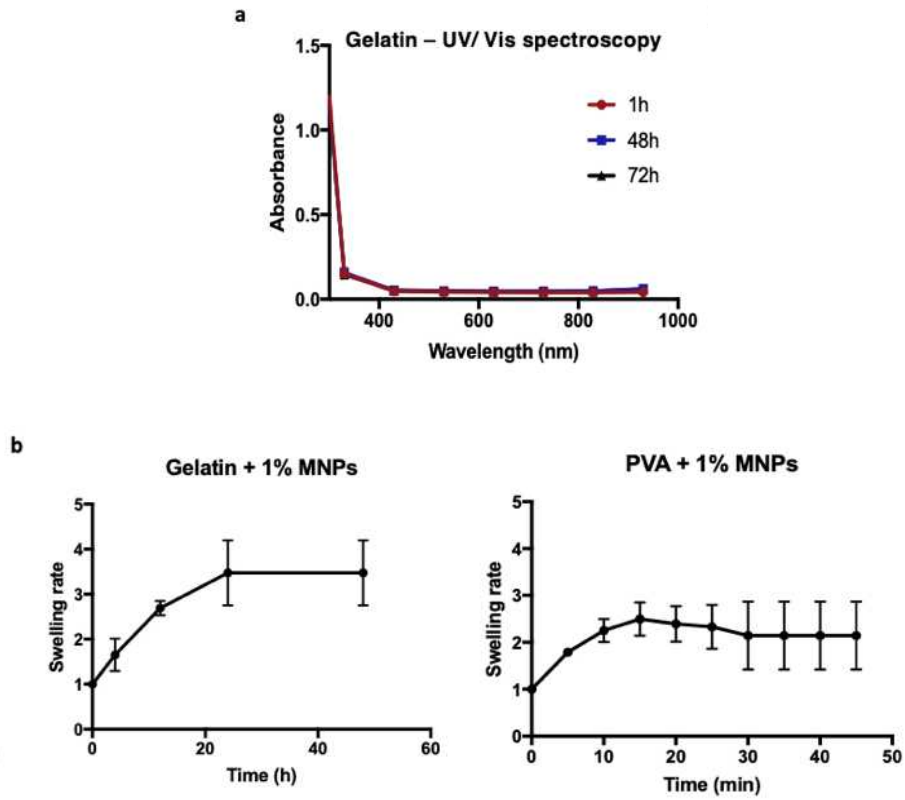
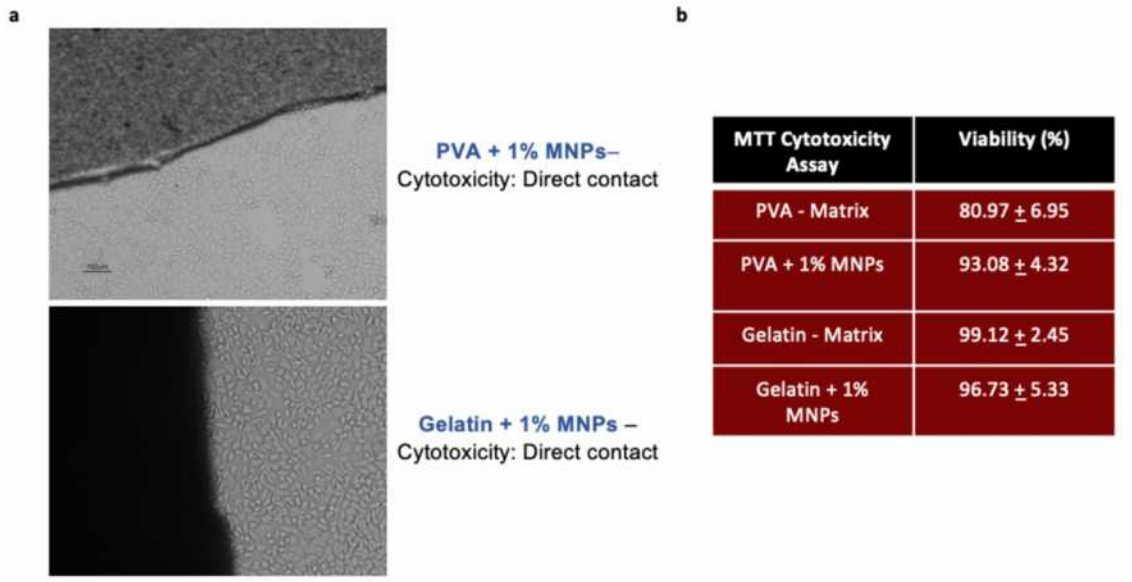


Figure IV. S1. Structural characterization of Gelatin to complement the characterization included in the main report. a UV spectroscopy analysis of gelatin scaffold with 1% of MNPs overtime points to no release of unloaded material, in particular MNPs, which absorbance peak is known to be around 400-450 nm. The eventual release of this material to the cell culture media could bring toxicity to the cells and compromise the experiments. Wash spectrum for the PVA are reported in our previous Chapter. b Gelatin swelling, determined by mass measurement overtime, reveals maximum swelling reached after 24h of immersion in water. Maximum swelling of PVA is reached after 30 min of immersion.

Table IV. S2. Validation of the results through the quantification of metabolites released from the MSCs throughout the experiments (day 1 to 5). This table allows to conclude that the results obtained regarding the angiogenic expression and protein release of VEGF-A were not related to the stressful condition of the cells for depletion of glucose and nutrients. The MSCs values of lactate even after 5 days were still above 1 mM and the levels of lactate were satisfactory.

N=3	Day	Glucose (mM)	Lactate (mM)
Cell Culture Medium	0	5.6 ± 0.5	1.8 ± 0.2
Gelatin + 1% MNPs (0 T/ 0.08 T)	1	3.3 ± 2.3	6.8 ± 1.2
Gelatin + 1% MNPs (0 T/ 0.08 T)	5	4.0 ± 1.9	5.0 ± 0.9
PVA + 1% MNPs (0 T/ 0.08 T)	1	5.3 ± 2.3	2.7 ± 1.2
PVA + 1% MNPs (0 T/ 0.08 T)	5	4.3 ± 2.3	5.5 ± 1.2
MSCs Monolayer (0 T/ 0.08 T)	1	4.7 ± 1.1	3.7 ± 1.1
MSCs Monolayer (0 T/ 0.08 T)	5	1.3 ± 0.8	11 ± 3.2



MTT Cytotoxicity Assay	Viability (%)
PVA - Matrix	80.97 ± 6.95
PVA + 1% MNPs	93.08 ± 4.32
Gelatin - Matrix	99.12 ± 2.45
Gelatin + 1% MNPs	96.73 ± 5.33

Figure IV. S2. Magnetic scaffolds did not compromise fibroblasts viability in cytotoxicity assay. a Direct contact of the scaffolds with the fibroblasts monolayers did not result in inhibition halo showing cells populating the scaffold region. b MTT assay presented viabilities higher than 80%, revealing the potential biocompatibility of these materials for cellular experiments. Scale bar: 100 µm.

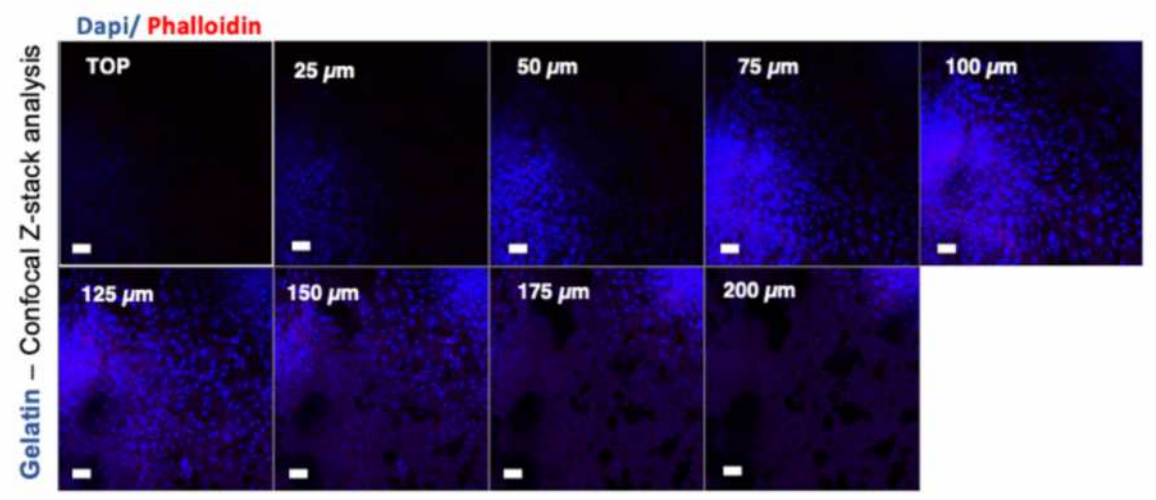


Figure IV. S3. Supplementary sequence of confocal microscopy images of the MSCs stained with DAPI (blue) and Phalloidin (red) embedded within the gelatin + 1% MNPs matrix (material total thickness = 400 μm). Z-stack images obtained from surface (top) to half the thickness of the gelatin (200 μm). Scale bar: 100 μm.

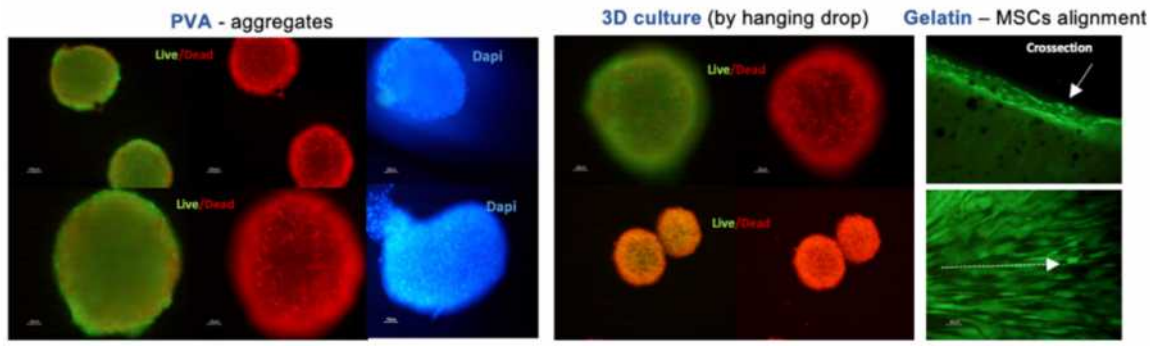
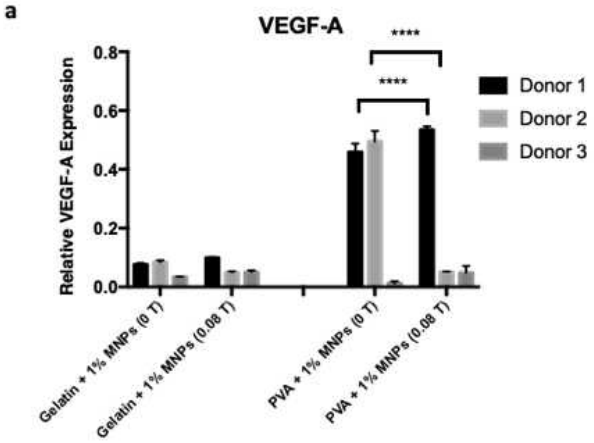


Figure IV. S4. Supplementary images of the aggregates spontaneously formed by the low adherence of the MSCs to the PVA matrix after 24h in comparison with the aggregates produced by hanging drop and the adherence and alignment in the gelatin. The necrotic center of the PVA aggregates is similar to those of the aggregates formed by hanging drop technique, showing that the technique adopted was suitable to form the 3D structures as a control for the MSCs on the PVA. Additionally, MSCs alignment and encapsulation on gelatin can be observed with further detail in these images.



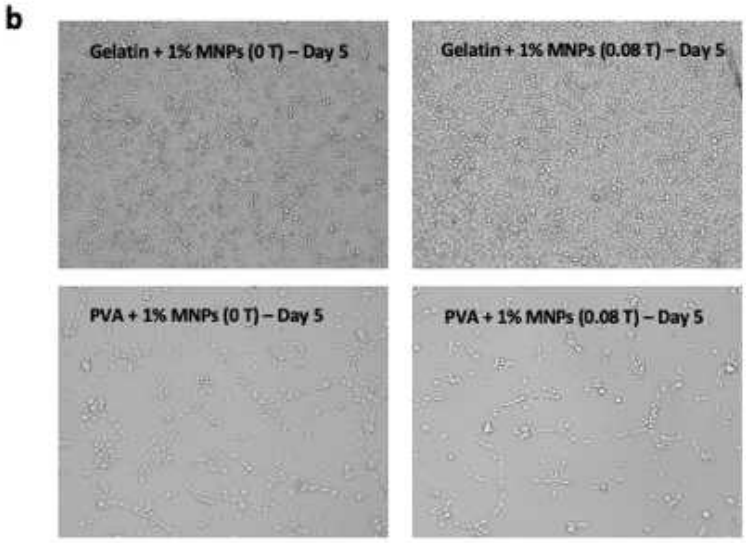


Figure IV. S5. Prolonged experiments of 5 days show a decrease in the angiogenic potential of the gelatin whereas PVA results are inconsistence between the donors. **a)** The data compares the values obtained for the scaffold of gelatin and PVA after 5 days of continuous exposure to magnetic field. Overall the VEGF-A expression decreases significantly after 5 days for the gelatin scaffold and there is no statistical significance between the conditions regarding the absence of magnetic field and its exposure. On PVA some donors express higher values of VEGF-A after 5 days of magnetic perturbation in comparison with 24h, however consistency between the conditions is not observed. **b)** HUVECs sprouting was not observed for any of the conditions tested after 5 days of magnetic exposure, with the exception of the condition where is not exposed to magnetic field, which is in concordance with mRNA relative VEGF-A expression for the PVA.

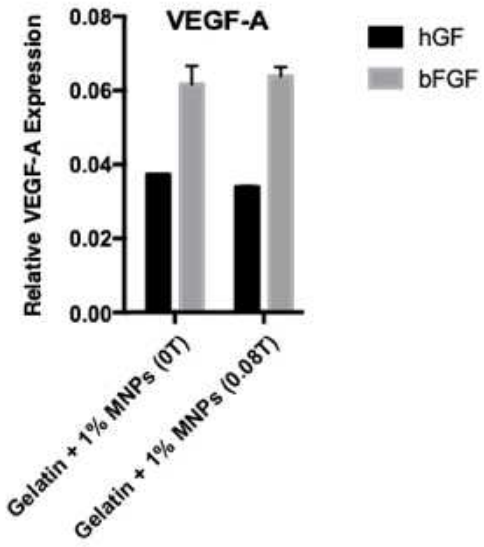


Figure IV. S6. Magnetic exposure does not induce overexpression of other angiogenic genes (bFGF, hGF). Focusing on the gelatin scaffold, some other genes associated with angiogenesis phenomena were studied. Contrary to the values obtained for VEGF-A, hGF and bFGF expression was very low for all the tested conditions, therefore these genes were not considered in the main report.

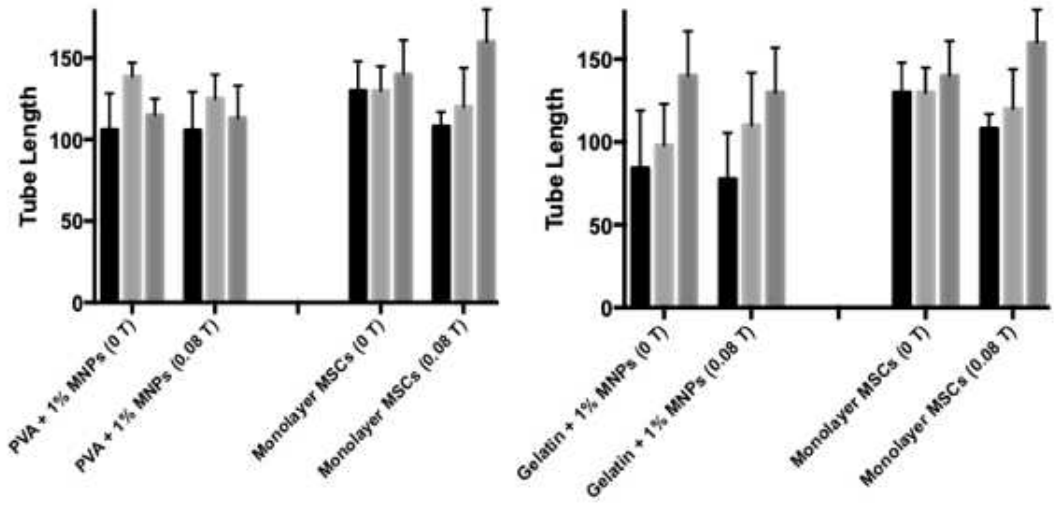


Figure IV. S7. Tube length is not significantly affected by magnetic influence in sprouting assessment. Contrary to the number of branch points and tubes, the tube length did not conduct major conclusions hence it was not included in the major report.

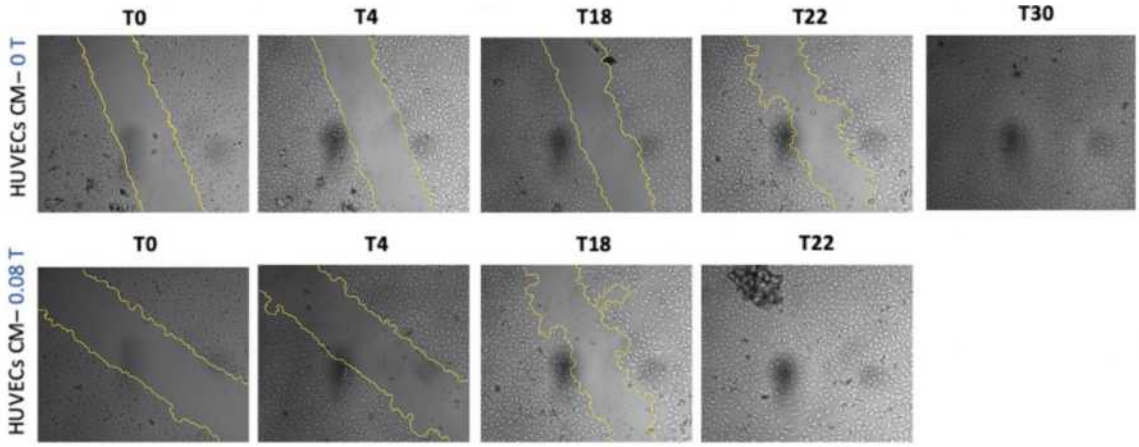


Figure IV. S8. Supplementary images of the entire process of HUVECs monolayer repair improved by the conditioned media (CM) of MSCs magnetically stimulated in comparison with the control where magnetic was not applied. Only some timepoints of representative images were included in the main report.

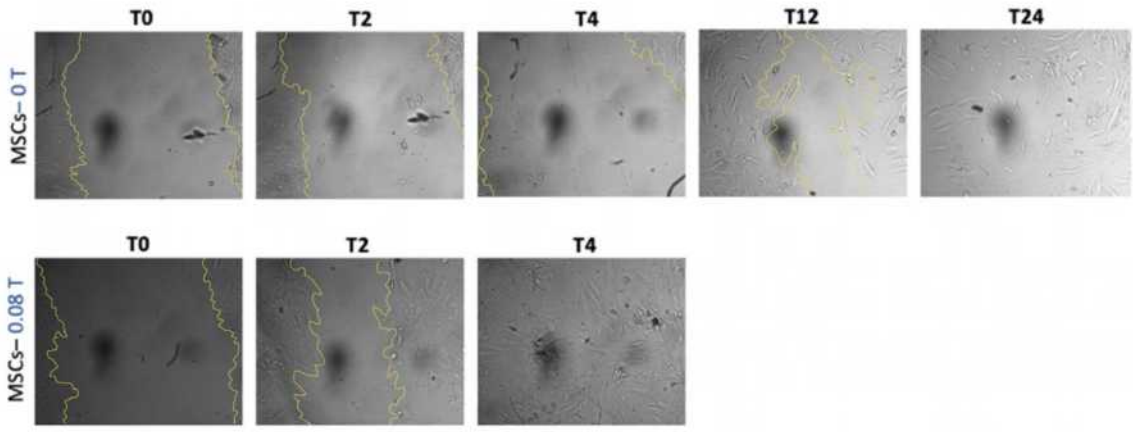


Figure IV. S9. Supplementary images of the entire process of MSCs monolayer repair directly induced by magnetic field exposure in comparison with the control condition where the MSCs were left to naturally repair the monolayer. Only some timepoints of representative images were included in the main report.

Table IV. S3. Supplementary details from the inoculation process of CAM assay. The table features information regarding the number of inoculated eggs, the number of eggs that survived the process, the total number of embryos used for analysis and the total number of pairs.

	Monolayer: Donor 2		Gelatin + 1% MNPs: Donor 2		Monolayer: Donor 3		Gelatin + 1% MNPs: Donor 3	
	0 T	0.08 T	0 T	0.08 T	0 T	0.08 T	0 T	0.08 T
Inoculated	9		14		9		10	
Alive	6		12		9		10	
Used for analysis	6	6	9	9	8	9	9	9
Nr of pairs	6		8		8		9	

Chapter V



Magnetic Field Configurations For Improved Control Of The Angiogenic Potential Of Mesenchymal Stromal Cells

CHAPTER V – Magnetic field configurations for improved control of the angiogenic potential of mesenchymal stromal cells

This chapter offers an insight on the potential to regulate angiogenesis phenomena by manipulating the configuration of the magnetic field in terms of the intensity and variation regime (static or dynamic under different frequencies).

Outline

This work compares for the first time the application of static and dynamic magnetic fields in an angiogenesis *in vitro* model to stimulate mesenchymal stromal cells (MSCs) into producing angiogenic molecule, VEGF-A, while exploring the effect of different magnetic intensities and intensity variation regimes. Tissue scaffolds of gelatin doped with randomly dispersed iron oxide nanoparticles (MNPs) were used as a platform for MSCs proliferation. Analyses on the effect of magnetic field intensity on cell behavior showed that higher magnetic field intensity was associated with increased cell death and poor angiogenic effect. To properly characterize MSCs stimulation, the magnetic field was applied for a maximum of 24 h in different magnetic field variation regimes: static and dynamic (low and high intensity variation frequency). It was observed that static and dynamic magnetic stimulation with higher frequencies led to an improved angiogenic performance on endothelial cells in comparison with lower frequency regime. This work showed the possibility to control VEGF-A secretion by MSCs through suitable modulation of the magnetic field. The study offers promising perspectives of the use of magnetic field as a non-invasive short-term therapeutic option for several diseases, i.e. by increasing the vascularization in damaged tissues as required in vascular ischemia or by inhibiting metastasis formation as a necessary measurement to hamper cancer progression.

Keywords: magnetic field, tissue scaffold, mesenchymal stromal cells, endothelial cells, VEGF, angiogenesis

V.1. Introduction

The formation of new blood vessels from existing ones (angiogenesis) is a relatively rare phenomena in adults and occurs mostly in post-injury regeneration areas or during tumor growth[1]. Although these two types of angiogenesis are promoted by similar angiogenic signals, the application outcomes are very different. While regenerative angiogenesis repairs functional and interconnected vessels, tumor angiogenesis is characterized by a high number of immature and disorganized vessels[2,3].

Provascularization strategies have been explored to treat a number of diseases related to reduced vascular perfusion such as peripheral vascular disease, ischemic heart disease, wound healing, cell and tissue transplantation[4]. Contrarily, anti-angiogenic procedures are also being exhaustively investigated mainly to reduce tumor growth in cancer patients[5,6].

Understanding the mechanisms regulating healthy and pathological angiogenesis is crucial to provide valuable information for the fabrication of tissue engineered constructs embedded with robust and mature vasculature.

Despite experimental induced-ischemia in animals having shown promising results, human trials using therapeutic vascularization have reported poor success rates[7]. Most proangiogenic strategies have mainly focused on the delivery of various isoforms of growth factors VEGF (vascular endothelial growth factor) or even FGF (Fibroblast Growth Factor) in clinical trials[8,9,10,11,12]. However, the intravenous administration of these growth factors is limited by reduced half-life *in vivo* of these factors (~ 30 minutes)[13].

On the other hand, cell transplantation therapy has shown promising results in clinical applications to treat myocardial and peripheral ischemia by attenuating secondary symptoms of the disease although still failed to provide a significant improvement in the patients quality of life[14]. One of the most promising approaches to provide continuous growth factor delivery to the injured tissues has been explored through scaffold functionalization[15]. So far, collagen coated with PDGF (platelet derived growth factor) has shown promise by enhancing capillary formation in a dermal wound healing model[16,17] while loading alginate scaffolds with VEGF has shown to promote vascularizarion[18]. Increased vascularization has also been obtained by mixing VEGF with synthetic scaffolds such as PLGA (polylatic-co-glycolic acid)[19,20].

However, the fast degradation of these polymers and the release of the embedded molecules overtime exposes the limitation of these approaches and brings to light the need to establish an external source of stimulation able to maintain a continuous release of growth factors to the *in vivo* environment injury site through a steady stimulation of the cells growing on the scaffold.

To date, static magnetic fields have emerged with a strong potential in tissue engineering not only as a system to control the release of drugs, growth factors and miRNA, but also by enhancing stimulatory responses able to influence cell behavior, mobility and growth[21,22,23]. Moderate intensity magnetic fields (1mT to 1T) have been associated with new bone formation, increase of mineral bone density and enhanced metabolic activity in the repair of cartilage while stronger magnetic fields (up to 8T) have also induced bone formation by promoting matrix formation and osteoblast differentiation *in vitro* and *in vivo*[24,25,26,27].

Distinct magnetic-induced biological effects, under dynamic regime, have been described in literature. Dynamic magnetic fields revealed capacity to promote morphological and intracellular changes driving cell differentiation into osteoclast-like cells [28,29]. However, dynamic magnetic field inhibitory effects on embryonic development[30] and angiogenesis processes[31] have also been reported.

Low-frequency magnetic field of 2 mT was found to inhibit angiogenesis processes by significantly reducing the VEGF signal transduction pathway on Human Umbilical Vein Endothelial Cells (HUVECs)[31]. Also, the direct exposure of Chick Embryo Chorioallantoic Membrane (CAM) to a static magnetic field of 0.7 T and electromagnetic field of 0.04T resulted in angiogenic inhibition[32,33]. Other works described similar inhibitory effects of stronger intensity static magnetic fields (0.4-0.6 T) on vascularization and tumor growth in *in vivo* mice models and *ex vivo* experiments[34,35].

Mesenchymal stromal cells (MSCs) are known to improve angiogenesis behavior through the secretion of angiogenic growth factors such as VEGF-A[36]. Although the impact of magnetic fields on the secretory activity of MSCs has not been reported yet, the sensitivity of MSCs to static and dynamic magnetic field have already been proved through the magnetic field capacity to enhance cellular differentiation and increase intracellular free calcium concentration[37,38].

As described, the ability of magnetic fields to influence cellular processes and, in particular, angiogenesis is clear but the way magnetic field conditions impact on these

processes is not totally understood, bringing to light the need to further investigate and properly compare these effects.

Hence, this study aimed at providing a better understanding about the capacity of magnetic fields to modulate angiogenesis of endothelial cells by proper stimulation of the production of VEGF from MSCs. This study compares for the first time the impact of static and dynamic magnetic fields, applied at different intensities and variation regimes, on the secretion of VEGF-A (key molecule in angiogenesis development) by MSCs cultured on magnetic gelatin scaffolds (Figure V. 1).

Ultimately, this work aims at defining the magnetic modulation strategies which allow for a more efficient control of VEGF-A secretion by MSCs, envisaging their use in co-cultures as regulators/ stimulators of vessel sprouting in HUVECs. This approach thus highlights the therapeutic potential of the combination of MSCs and magnetic fields for the treatment of several vascular-related diseases and also as an inhibitor of tumor metastasis during cancer progress.

V.2. Experimental Section

Scaffold Fabrication. Magnetic nanoparticles (MNPs) were synthesized by chemical co-precipitation of iron salts $FeCl_3$ and $FeCl_2$ (Sigma-Aldrich) in alkaline media, according to the protocol published by Izquierdo et al.[39] Briefly, an aqueous solution with 25% of ammonium hydroxide (NH_4OH) (Fluka) was added to a mixture of $FeCl_3$ and $FeCl_2$ at 80ºC, under permanent stirring at 1250 rpm by purging N_2. Porcine skin gelatin (8% m/v, type A, G2500, Sigma-Aldrich) was dissolved in milli-Q water (10% m/v) at 60ºC. MNPs were dispersed by sonication in the polymeric aqueous solution. The gelatin matrices were cast onto glass plates and left overnight at 4ºC. Finally, the samples were removed from the glass plates and immersed in an aqueous solution containing 1% of GA for 3h. Prior to use, the magnetic hydrogel membranes were washed by immersion in a demineralized water bath. For sterilization, the samples were immersed in a PBS solution containing 1% of antibiotic-antimycotic (Gibco). For better conditioning of the cells, the samples were immersed in cell culture media for 3h before seeding the cells on top of the hydrogels.

Magnetic profiles characterization and experimental setup. Two neodymium magnets with different magnetic intensities (circular magnet bar with a maximum intensity of 0.08T and square magnet with maximum intensity of 0.45T – Figure V. 1) were used for cell stimulation. For static continuous magnetic application, magnets were applied beneath cell culture plate for 24 h, with the magnetic lines oriented perpendicularly to the scaffold surface/cell plate for the desired stimulation. For dynamic setup, a motorized lab jack (MOZ-80-50, optics-focus) combined with a motion controller (For NEMA17, optics-focus) was programmed to transport the magnets to the cell culture plate using different configuration modes. The motorized lab jack, with the magnet on top, was placed inside the cell incubator and positioned at a proper distance to allow for the magnet to reach the cell culture plate at the elevator maximal amplitude. As shown in Figure V. 1, motion controller was connected to a computer and programmed for a motion velocity of 0.005 m/s for 24 h under the following conditions (Running Time=1; Max Speed=255; Delay=0; Displacement=$\pm$999999). For a lower frequency (LF) of $2.8x10^{-4}$ Hz, the magnet was kept 1h at maximum displacement, followed by 1h at minimum displacement from the cell plate in continuous cycles for 24 h. For a higher frequency (HF) of $1.7x10^{-2}$ Hz, the magnet alternated between maximum and minimum displacement in cycles of 60 s, reaching cell culture plate after 30s, for a total exposure of 24 h (Figure V. 2). The minimum distance to induce magnetic sensitivity on the cells was 3 cm for the circular magnet and 8.5 cm for the stronger square magnet, with intensities of 0.005T and 0.001T, respectively (Figure V. 2). A gaussmeter was used to measure the intensity of the magnets in each point and build the magnetic profile of each condition mode. Each experiment was conducted for 24 h indicating that cells were exposed to a total of 1440 ON/OFF magnetic field cycles in HF experiments and 12 ON/OF magnetic field cycles in LF experiments.

Cell culture. Human bone-marrow MSCs lines used in this chapter belong to the cell bank available at Stem Cell Engineering Research Group (SCERG), iBB-Institute for Bioengineering and Biosciences at Instituto Superior Técnico (IST). Bone marrow samples were retrieved from Instituto Português de Oncologia Francisco Gentil, Lisboa-Portugal under collaboration with iBB-IST. Human samples were obtained from healthy donors under informed consent, accordingly with the Directive 2004/23/EC of the European Parliament and of the Council of 31 March 2004 on setting standards of quality and safety for the donation, procurement, testing, processing, preservation, storage, and

distribution of human tissues and cells (Portuguese Law 22/2007, June 29), with the approval of the Ethics Committee of the respective clinical institutions [40]. Isolated cells were cryopreserved in liquid/vapor nitrogen tanks. Isolated human bone marrow MSCs (BM MSCs) were cultured on low-glucose Dulbecco's Modified Eagle Medium (DMEM, Gibco Grand Island NY) supplemented with 10% fetal bovine serum (FBS MSC qualified, Gibco) and 1% antibiotic-antimycotic (Gibco) and kept at 37ºC, 5% CO_2 and 21% O_2 in a humidified atmosphere. Three independent donors were used on the experiments (n=3, donor A, B, C). HUVECs used in this report were purchased from Lonza (Basel, Switzerland), cultured in commercial endothelial growth medium-2 (EGM-2, Lonza) and kept at 37ºC, 5% CO_2 in a humidified atmosphere. Medium renewal was performed every 3-4 days. All the cellular experiments were performed between passages 4 and 7.

Human MSC proliferation values. MSCs were seeded on the gelatin scaffolds at a density of 75000 cell/cm^3 using expansion medium (DMEM + 10% FBS). As a control BM MSCs were seeded as a monolayer on cell culture plates at a density of 75,000 cell/cm^2. The metabolic activity of MSCs was evaluated using AlamarBlue® cell viability reagent (Molecular proves, Eugene, OR). The experience was performed after 24 h of the beginning of the magnetic application using 3 independent donors (n=3). MSCs were treated with AlamarBlue® cell viability reagent and incubated at 37ºC in 5% CO_2 chamber for 2 hr. Fluorescence measurement was quantified at a range of 560-590 nm. A calibration curve specific for BM MSCs was used to convert the obtained metabolic values into cell numbers and determine the proliferation curves associated with each group of conditions. All conditions were tested in triplicates during this experiment.

Cell viability and morphology assay. To assess MSCs viability, cells were washed twice with PBS (Phosphate Buffer Saline, Dulbecco's Sigma-Aldrich) after 24 h of magnetic application and stained for 20 min using LIVE/DEAD™ Viability/ Cytotoxicity Kit for mammalian cells (ThermoFisher Scientific, L3224) according to the manufacturer protocol. After washing again with PBS cell imaging was obtained using a Fluorescence microscope (Leica DM IL LED with EC3 camera system). Living cells were stained with calcein probe and observed in a green coloring while dead cells were highlighted with a red nucleus by ethidium homodimer probe.

Quantitative reverse transcription-polymerase chain reaction analysis. MSCs RNA was extracted using a RNeasy Mini Kit (Qiagen, Hilden, Germany). Complementary DNA was synthesized from 20 ng of total RNA using iScript Reverse Transcription Supermix (Bio-Rad, Hercules, CA). Reaction mixture (20 µL) were incubated in a thermal cycler (Veriti 96-well thermal cycler: Applied Biosystems, Foster City, CA) for 5 minutes at 25ºC, 30 minutes at 42ºC and 5 minutes at 85ºC. Samples were then kept at 4ºC. Gene expression levels of VEGF were assessed. Quantitative reverse transcription-polymerase chain reaction (qRT-PCR) was performed using SYBR Green PCR Master Mix (Applied Biosystems). All reactions were carried out at 95ºC for 10 minutes, followed by 40 cycles of 95ºC for 15 seconds and 60ºC for 1 minute, according to manufacturer's instructions. All group of conditions were performed in triplicates in the experiment (n=3) using three different donors (donor A, B, C). Glyceraldehyde 3-phosphate dehydrogenase (GAPDH) was used as host gene control to normalize differences in total RNA levels for each condition. A threshold cycle (C*t*) was observed in the exponential phase of amplification, and quantification of relative expression levels was performed using standard curves for target genes and endogenous control. Geometric means were used to calculate the $\Delta\Delta Ct$ values and expressed as $2^{\Delta\Delta Ct}$ (Potency values). The mean values from triplicate analysis were compared.

Quantification of VEGF expression by enzyme-linked immunosorbent assay (ELISA). For ELISA, culture supernatant (conditioned media) was collected from MSCs cultures after 24 h of magnetic exposure (gelatin and monolayer). The conditioned media was kept at -80ºC until further analysis. Human VEGF-A kit (RayBiotech) was used, following the manufacturer's instructions. All conditions were tested in triplicates using three different donors (donors A, B, C).

***In vitro* endothelial cell tube formation assay.** To evaluate the effect of exogenous VEGF-A supplementation on angiogenic properties, a three-dimensional capillary-like tube formation assay was performed. For this experiment MSCs were incubated with Endothelial Cell Basal Medium (EBM-2, Lonza) during magnetic application. HUVECs ($2x10^4$ cells) were first cultured on Matrigel (50 µl/well) in a 96-well plate. Conditioned media (without FBS supplement) obtained from MSCs cultured on scaffolds or in monolayer were added to each well and compared with positive and negative controls for this experiment, respectively by using Endothelial Cell Growth

Media-2 (EGM-2), rich in growth factor supplements, and the conditioned media from MSCs growing in polystyrene without magnetic exposure. After incubation for 6h at 37ºC, photomicrographs of the center of the well were taken using a light microscope (Leica DM IL LED with EC3 camera system) and the number of tubular-like structures and branch points formed were counted using ImageJ (NIH) software. All conditions were tested in triplicates using three different donors (donors A, B, C).

Statistical analysis. All measurements were performed three times, under independent conditions. Results are shown as the mean $\pm$ standard deviation (SD). Two-way ANOVA Sidak's multiple comparisons test was used to compare the mean of three values obtained from three independent conditions, using GraphPad Prism version 7 (GraphPad Software, La Jolla, CA); *$p < 0.05$ indicates a significant result; **$p < 0.01$ a very significant result, ***$p < 0.001$ a highly significant result, and ****$p < 0.0001$ an extremely significant result.

V.3. Results

3.1. Effect of the magnetic field on MSCs proliferation and morphology

The toxicity of magnetic fields on MSCs, cultured on magnetic gelatin scaffolds and cell polystyrene plates (TCP), were assessed by analysis of the proliferation values of MSCs when exposed to a constant magnetic field at 0.08 T and 0.45 T (static mode) and to a cyclic variation of the magnetic field between 0 T and 0.08 T or 0.45 T (dynamic mode). The effect of magnetic field cyclic frequencies on MSCs behavior was also studied. In this regard, and as illustrated in Figure V. 1 and 2, MSCs were also exposed to cyclic variation of magnetic field at low frequency, LF (magnetic field was kept constant for subsequent periods of 30 min) and high frequency, HF (magnetic field was maintained for subsequent periods of 1 s).

As shown in Figure V. 3a, the increase of magnetic field intensity from 0.08 T to 0.45 T led to a decrease of the number of cells, observed either for MSCs cultured in gelatin scaffolds as well as for those cultured in the polystyrene cell plates (negative control). When comparing the effect of magnetic field applied under the different dynamic regimes, the LF operation mode resulted in lower number of cells than HF or

static mode, suggesting that LF operation mode might induce a higher disruption of the cells and irreversible oxidative stress leading to increased cell death, as a common effect of the magnetic forces on cells[41,42,43].

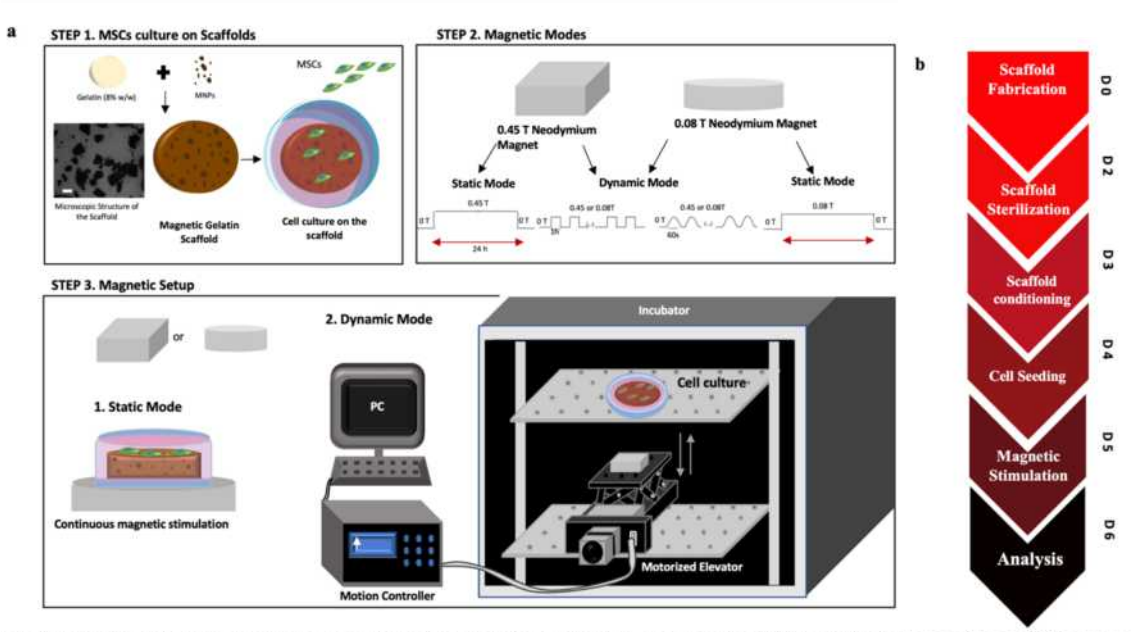


Figure V. 1. **a)** Setup for static and non-uniform magnetic field modes using neodymium magnets with different intensities. Step1 - Scheme of the scaffold components (gelatin 8% w/w and MNPs), microscopic image of the MNPs distribution on the scaffold (scale bar: 100 µm) and MSCs cell culture on top of the gelatin. Step 2 – Configurations of the cycles and frequencies used in each condition (dynamic and static mode). Step 3 – Setup of the position of the magnets on the bottom of the culture plate (1) and configuration of magnets on top of the lab jack elevator to stimulate the cell culture inside the incubator. **b)** Timeline for the stages of the experiment, from the scaffold fabrication to the analysis after the magnetic exposure.

Live/ Dead assays were performed to elicit about cell death and morphology induced by each magnetic field condition tested. Live/Death results (Figure V. 3b) did not show cell death for MSCs cultured on gelatin scaffolds in any magnetic field condition. Furthermore, it showed magnetic alignment of MSCs according to the magnetic field orientation vector independently of the magnetic intensity (0.08T and 0.45T) and without noticeable differences for MSCs exposed to different magnetic field dynamic regimes (static, LF and HF regime). For MSCs cultured on magnetic gelatin scaffolds, Live/ Dead assay showed a magnetic-induced alignment independent on the magnetic intensity (0.08T or 0.45T), without noticeable differences between the two intensity conditions. Between configurations (static, LF and HF) no differences were observed with the magnetic scaffold, resulting in the same pattern observed in the representative images shown in Figure V. 3b.

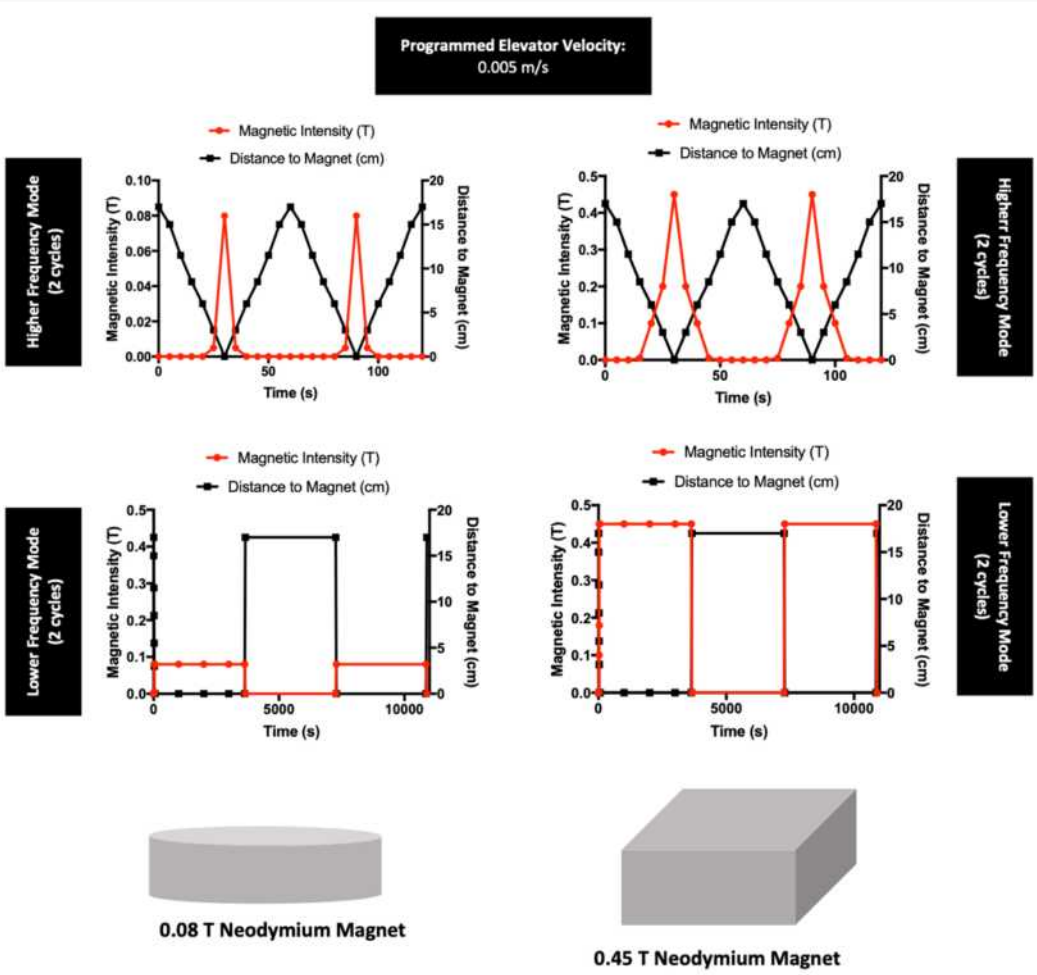


Figure V. 2. Magnetic profiles of each neodymium magnets (circular magnet of 0.08T and square magnet of 0.45T) used in MSCs experiments under dynamic mode, with a steady velocity of 0.005 m/s. Two cycles are displayed for each frequency according with the distance to the cell culture plate, in a total of 24h.

However, it was curious to observe that the response to magnetic field of MSCs cultured in TCP was substantially different. In this case, cell death was only detected in MSCs cultures exposed to a static 0.45 T magnetic field (Figure V. 3b). Furthermore, MSCs showed good cell alignment towards the magnetic field direction when exposed to static and HF dynamic magnetic field either at low and high magnetic field intensities (0.08 T and 0.045 T). However, poor cell orientation was observed for MSCs exposed to LF dynamic magnetic field at low magnetic field intensities (Figure V. 3b) whereas an irregular distribution of cells, evidenced by the observation of regions without cells (empty regions), was observed for MSCs exposed to an identical cyclic magnetic field regime but higher magnetic field intensity (0.45T).

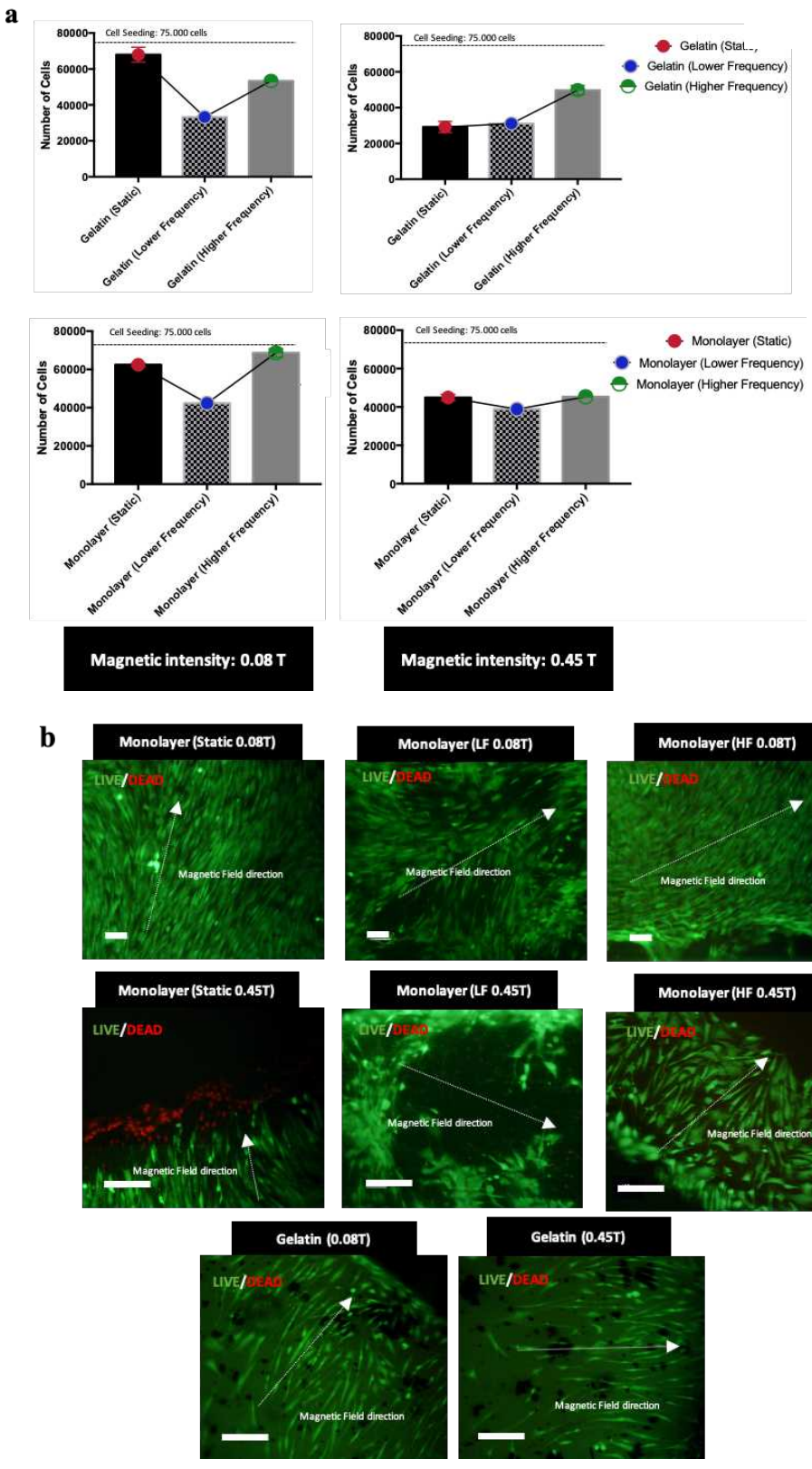


Figure V. 3. a) Proliferation curves for MSCs on gelatin scaffolds and MSCs monolayer exposed to static and non-uniform magnetic fields with 0.08T and 0.45T. **b)** Live (Green) and Dead (Red) cells images MSCs in monolayer for each condition, highlighting distinct cell orientation profiles and morphologies according with the intensity of the magnetic field. MSCs distribution on gelatin are also represented for the lower and higher maximum intensity (0.08T and 0.45T). Scale bar: 100µm.

3.2. Impact of the magnetic field on the expression of VEGF-A gene

The dependence of MSCs behavior on the magnetic intensity and dynamic conditions described in the previous results suggested the possibility to modulate cellular pathways in MSCs, in particular those concerning the VEGF-A expression, by adjustment of the magnetic field conditions. Hence, studies were performed to evaluate the effect of the different magnetic field dynamic regimes on the MSC capacity to express the angiogenic growth factor gene, VEGF-A.

The influence of the different magnetic field conditions on VEGF-A expression by MSCs cultured on gelatin scaffolds and in TCP (monolayer MSCs) was shown in Figure V. 4.

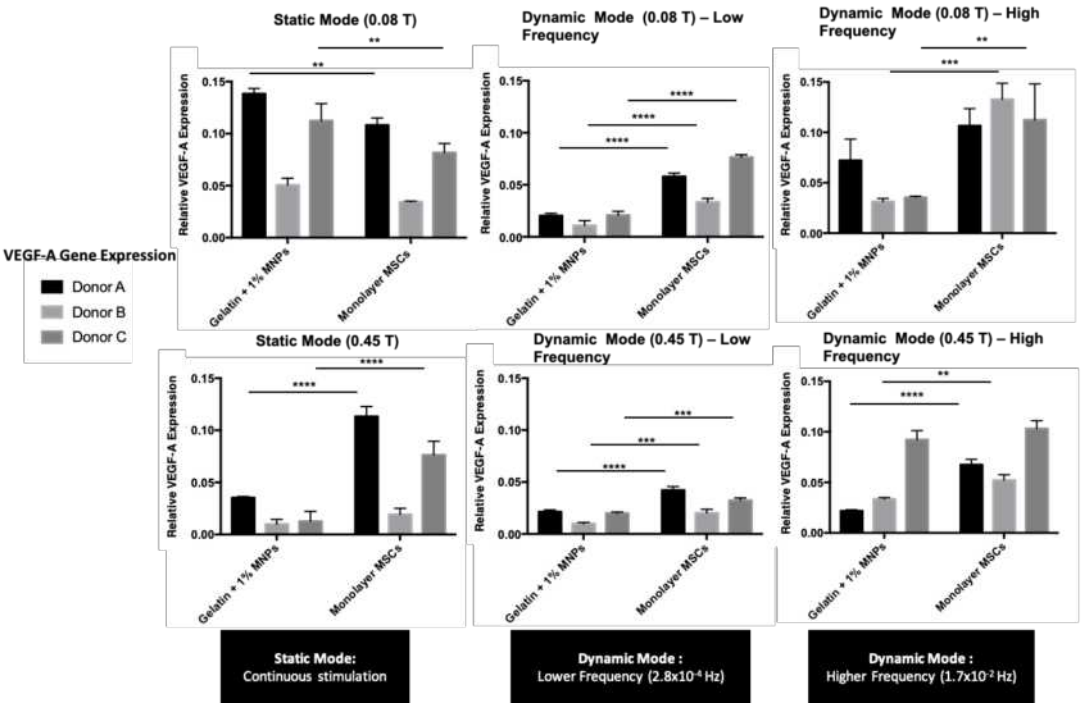


Figure V. 4. VEGF-A expression values using RT-PCR technique to compare static and dynamic modes (low and high frequencies) and magnetic intensities (0.08T and 0.45T). Relative expression of VEGF-A on gelatin scaffolds with 1% of MNPs is compared with monolayer MSCs as a control condition using three independent donors (A, B, C).

The results unveiled that VEGF-A expression by MSCs cultured in gelatin scaffolds was higher in the presence of static magnetic field and HF magnetic field cyclic conditions, whereas a reduced VEGF-A expression was observed for MSCs exposed to a LF magnetic field cyclic regime. Magnetic field intensity also seemed to have an effect on VEGF-A production. This effect was clear under static magnetic field conditions,

where the VEGF-A production was found to be higher at 0.08 T than at 0.45 T. Under cyclic variation of magnetic field conditions, the production of VEGF-A also seemed to be benefited by lower magnetic intensity (0.08 T), although the decreasing effect, triggered by the increase of the magnetic field intensity to 0.45 T, was not as impactful as in static conditions.

A comparative analysis between the performance of the MSCs cultured on the gelatin scaffold with the control condition (i.e. MSCs monolayers cultured in TCP), showed that, in most cases, the VEGF-A expression was higher for MSCs cultured in monolayer than for MSCs cultured in the gelatin scaffold. The exception was observed for cells exposed to 0.08 T static magnetic field conditions, where the VEGF-A production was higher for MSCs cultured in the gelatin scaffold. A comparative analysis of the effect of the different dynamic regimes showed lower VEGF-A expression under LF operation modes, suggesting a possible inhibition of the production of VEGF-A under these magnetic field conditions. However, and in contrast to that observed for MSCs cultured in gelatin scaffolds, it was interesting to note that the VEGF-A expression by MSCs monolayers under HF operation modes were enhanced in comparison to the VEGF-A expression obtained in static magnetic field conditions.

Overall, the analyses indicated that the VEGF-A expression by MSCs monolayers cultured in TCP (monolayer condition) was higher than for MSCs cultured in gelatin scaffolds.

3.3. Control of VEGF-A protein secretion under magnetic exposure

The expression of VEGF-A gene on MSCs was quantified in the previous section. However, this value reflected the capacity of MSCs to express VEGF-A, not necessarily corresponding to the amount of VEGF-A present in the external conditioned cell media, which is fundamental to induce angiogenic behavior on HUVECs. Therefore, the conditioned media of MSCs exposed to different configurations of magnetic field was assessed by analysis of the cell conditioned media by ELISA (Figure V. 5). The results obtained for the MSCs cultured on gelatin scaffolds depicted significant differences between the magnetic operation modes highlighting once more the influence of magnetic field dynamics on cell behavior and the need to determine the adequate magnetic field strategies that allow for an improved regulation of cell behavior, i.e. VEGF-A expression by MSCs. Once more, the results showed a significant reduction of VEGF-A secretion

by MSCs under stronger magnetic intensity (0.45 T) comparatively to VEGF-A expression achieved at lower magnetic field intensities (0.08 T). The result was coherent for all tested donors. As observed in Figure V. 4, comparable VEGF-A expression was obtained under static and HF dynamic regimes at 0.08T, while significantly lower values were observed for MSC cultures exposed to LF magnetic field cyclic condition. Similar conclusions were obtained in Figure V. 5 from the analysis of the VEGF-A secreted by the MSCs. Once again, the secretion of VEGF-A by MSCs monolayers was overall higher to that observed for MSCs cultured in gelatin scaffolds, with the exception of the condition for static and low intensity magnetic field.

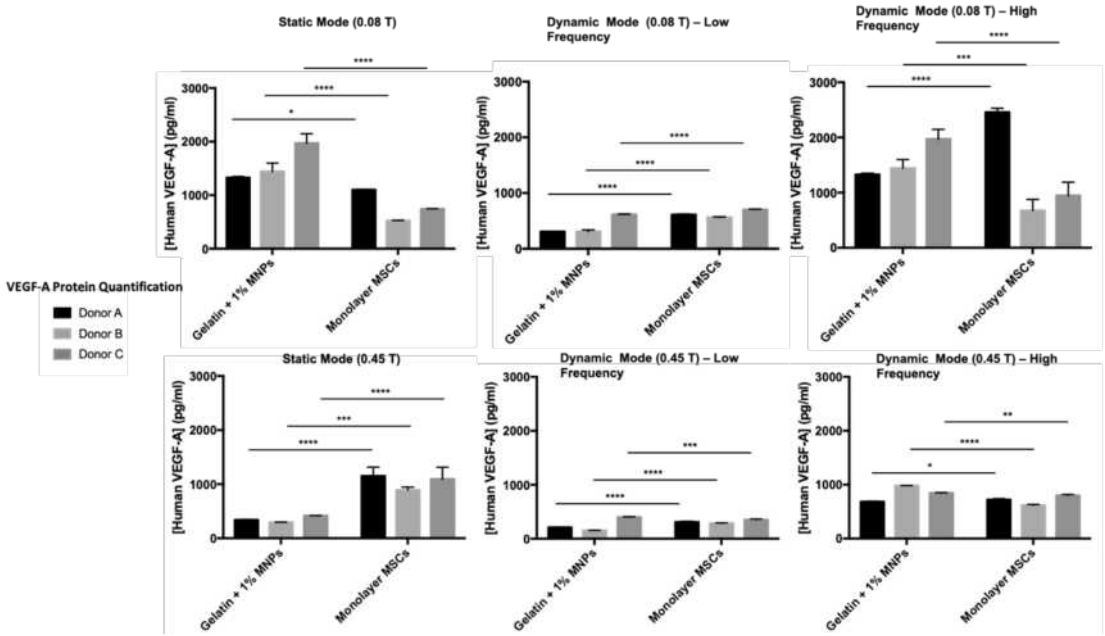


Figure V. 5. VEGF-A protein quantification for gelatin + 1% MNPs and control condition MSCs monolayer for each condition (static, lower and higher frequency) and corresponding donor (A, B, C), according with the magnetic intensity (0.08T and 0.45T).

3.4. Magnetic effect on the sprouting potential of HUVECs

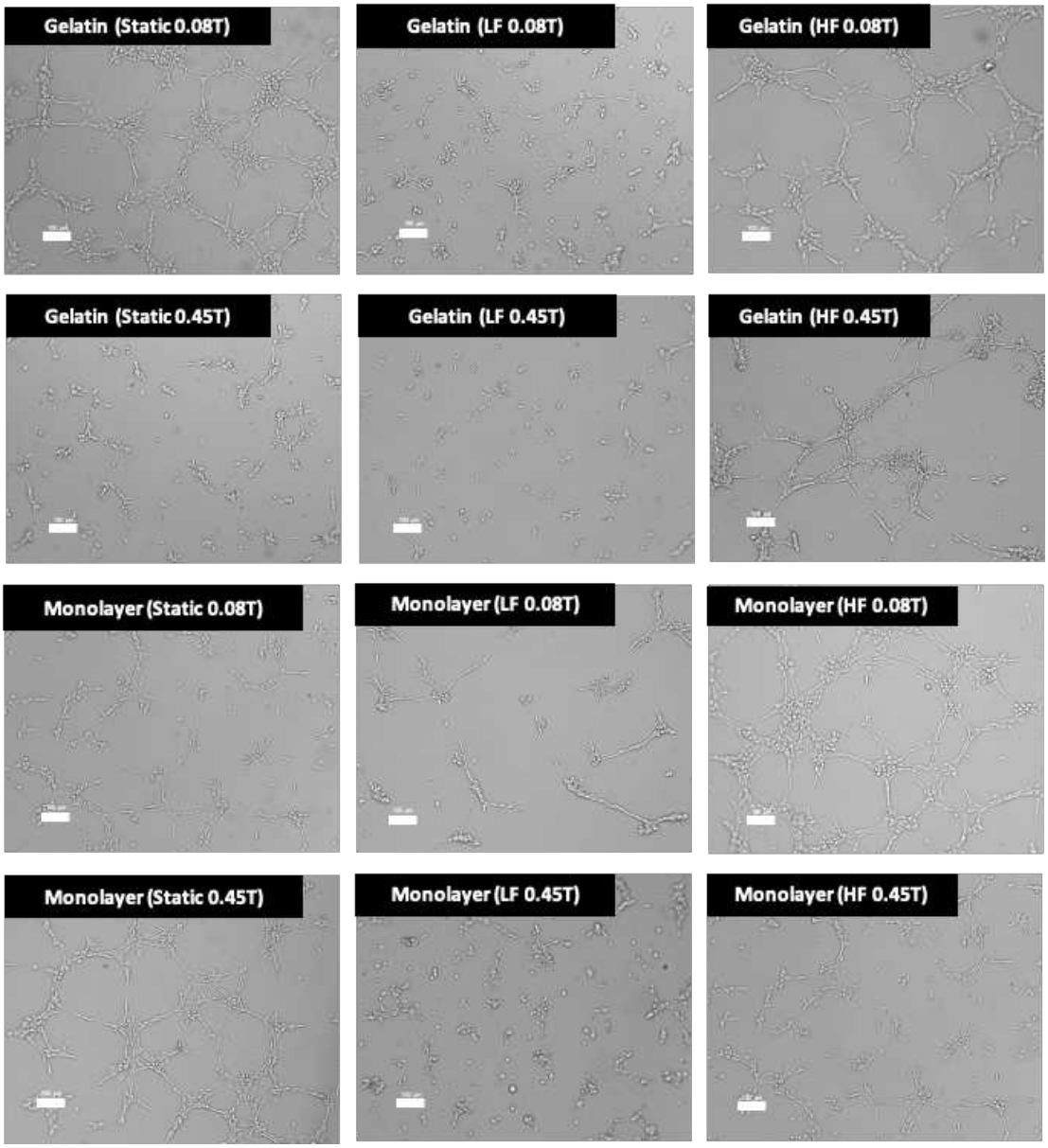
The conditioned media of MSCs was expected to induce angiogenesis on HUVECs through the formation of tube-like structures proportionally to the amount of growth factor (VEGF-A) in the media (Figure V. 6). The magnetic stimulation of VEGF-A expression by MSCs should then be followed by an improved HUVEC angiogenic potential.

The impact of magnetic field on the angiogenic potential was ultimately studied based on the ability to magnetically modulate the sprouting effect on endothelial cells (HUVECs) by using the MSCs conditioned media. Hence, functional assays were

performed to evaluate HUVEC sprouting by the formation of tube-like structures in the presence conditioned media from encapsulated MSCs on gelatin scaffolds and MSCs monolayers cultured on TCP, under different magnetic field conditions.

As shown in Figure V. 6a, functional assays carried out using the conditioned cell media obtained at higher magnetic field intensities (0.45 T) led to clear reduction of the number of tubes and branch points formed in these cases (Figure V. 6b) thus confirming the anti-angiogenic effect of such higher magnetic field intensity.

a



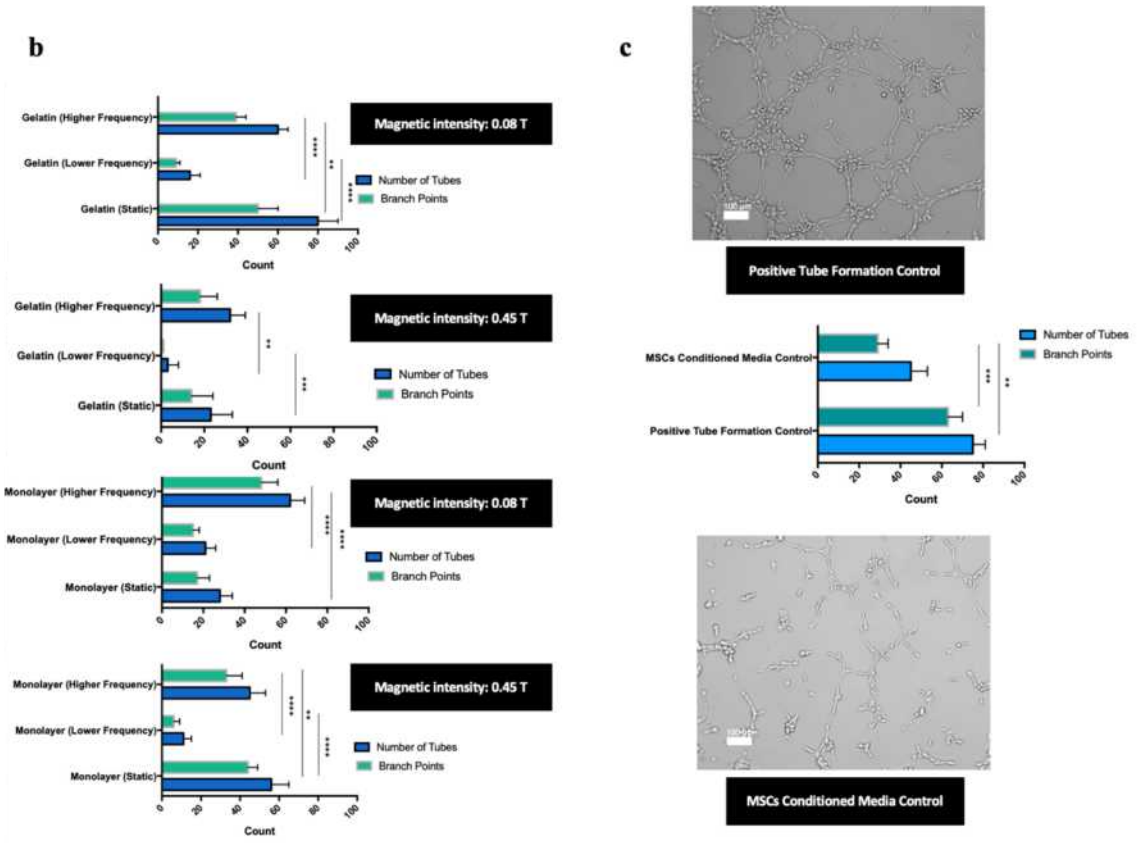


Figure V. 6. a) Representative images of endothelial cells tube-like structures obtained from MSCs conditioned media cultured in each condition (gelatin vs monolayer; 0.08T vs 0.45T; static vs lower frequency vs higher frequency). **b)** Number of tubes and number of branch points measured for each analysis condition of the tube formation assay. **c)** Representative images of the tube formation controls and respective measurement of tubes number and branch points. Positive tube formation control is obtained from endothelial cell media rich in growth factor supplements and MSCs conditioned media Control refers to the condition where MSCs were cultured in polystyrene without magnetic exposure.

Contrastingly, the conditioned media obtained from MSCs exposed to static magnetic field conditions at 0.08 T showed a more intense sprouting effect resulting in the formation of the highest number of tubes (82 tubes in average) and branch points (48 branch points), in agreement with the VEGF-A expression results. The negative effect of stronger magnetic field on tube formation was also perceived in experiments performed using the conditioned media from MSCs culture monolayers in TCP. However, the effect produced by the increase of magnetic field was not as clear as that observed when the conditioned media from MSCs in gelatin scaffolds was used. The number of tubes formed with the conditioned media obtained for MSC monolayers exposed to dynamic magnetic field regimes decreased with the increase of magnetic field to 0.45 T, but the opposite effect was observed for experiments conducted under static magnetic field.

These results also showed that the formation of microvessels with HUVECs was poorer in experiments using the conditioned media from MSCs exposed to dynamic magnetic field regimes in comparison with the results obtained with MSCs conditioned media under static magnetic field conditions. The lowest HUVEC sprouting effect (19 tubes and 8 branch points) was observed when conditioned media from MSCs exposed to LF magnetic field dynamic regimes were used. Similar results were obtained for functional assays using the conditioned media from MSC monolayers cultured in TCP.

To assess the possibility to achieve a controlled regulation of HUVECs sprouting, the tube formation observed for HUVECs under magnetic field regimes (static, LF, HF) was compared with a positive control condition using endothelial cell specific media, rich in growth factor supplements such as VEGF, and a negative condition using the conditioned media from MSCs cultured in polystyrene plates without magnetic stimulation (Figure V. 6c). HUVECs sprouting under positive control resulted in the formation of 75 tubes and 64 branch points (average count), being slightly surpassed by the condition from MSCs growing on gelatin under static magnetic field, 0.08 T (82 tubes and 48 branch points). On the other hand, the negative control (conditioned media from MSCs cultured on TCP without magnetic exposure) for HUVEC sprouting resulted in average 43 tubes and 28 branch points. These numbers were nonetheless higher than the results observed at 0.45 T (higher magnetic field intensity) for all magnetic field dynamic regimes tested and at LF magnetic field regimes independently of the magnetic field intensity (within the magnetic field range studied). This effect highlighted the possibility to effectively regulate angiogenesis, in a remote way, by selecting the magnetic field conditions responsible for triggering MSCs into secreting desirable levels of VEGF-A to prompt HUVEC maturation.

Hence, here we concluded that angiogenesis can be upregulated by exposing MSCs cultures to static or HF magnetic fields with low intensity whereas angiogenesis downregulation may be attained by simply increasing the magnetic field strength to values of 0.45 T (keeping the dynamic regime) or by imposing a LF magnetic field cycles while maintaining the magnetic field intensity. Combined, these results might contribute to the development of a controlled non-invasive magnetic responsive platform capable of enhancing vascularization in damaged tissues or to inhibit vascularization during tumor progression.

V.4. Discussion

The ability of MSCs to produce and secrete VEGF-A potentiates the indirect MSCs modulatory effect on the angiogenic behavior of HUVECs, leading to the formation of microvessel structures. The potential to regulate the angiogenic behavior on HUVECs can be associated with homeostatic feedback mechanisms and represents a key for controlling healthy (e.g. tissue regeneration) or pathological angiogenesis (e.g. tumor development) and provide a contribute for the treatment of several diseases.

Hence, understanding the possibility to establish a control over the secretion of VEGF-A by MSCs through the manipulation of external magnetic field stimulatory conditions might be the required answer to regulate angiogenesis in HUVECs. This possibility was explored during this study by analyzing the effect of different magnetic field conditions (static, LF, HF) and intensities (0.08 T and 0.45 T) on MSCs behavior, including proliferation, viability, morphology and secretion of VEGF-A. Ultimately, the impact of the secretome of MSCs, under these different stimulatory conditions, on HUVECs was evaluated based on the formation of microvessel structures.

Throughout this study it was observed that lower magnetic intensities (0.08 T) showed capacity to induce higher proangiogenic activity in comparison with 0.45 T intensity. The effect was confirmed through higher expression and secretion values of VEGF-A at lower magnetic field intensity and a better sprouting quality in HUVECs when fed with the conditioned media resultant from MSC cultures exposed to lower magnetic intensities.

The effect of low magnetic field intensity (0.02-0.12 T) has been described to have an effect on the growth and development of MSCs. Different works have been published reporting the influence of the magnetic field as promoters of the differentiation of MSCs, also altering the concentration of ions within the cytoplasm and impacting on cell morphology by modifying the polarization of cellular components[38,44,45].

The effect of a direct application of the magnetic field on endothelial cells has been mostly described to actively inhibit sprouting and angiogenic activity[46,32,34,35].

Cell proliferation and viability experiments provided some insights on the potentially different effect of high and low magnetic field intensities on cell toxicity and organization (Figure V. 3). Cell proliferation studies showed a decrease in the number of adherent cells exposed to 0.45 T, in comparison with the proliferation values obtained

with lower magnetic intensity of 0.08 T, but a decreased proliferation with LF condition was observed regardless of the magnetic intensity or the culture of MSCs, either in gelatin scaffold on in TCP (Figure V. 3a). This result suggested a potential effect of magnetic field on cell detachment or cell death[47] proportional to the magnetic field intensity. These conclusions were supported on results from Live/ Dead viability experiments which confirmed the presence of higher cell death and a more heterogeneous/irregular cell distribution at 0.45 T comparatively to that observed at 0.08 T (Figure V. 3b). The higher cell apoptosis at 0.45 T together with the eventual influence of magnetic field in VEGF-A expression regulatory cellular pathways may explain the reduced levels of VEGF-A expressed by MSCs exposed to 0.45 T (Figure V. 4).

On the other hand, it is known that VEGF-A secretion contributes to an anti-apoptotic effect on the cells[47,48]. Therefore, a balance is expectable between the apoptotic effect caused by the magnetic field and the anti-apoptotic influence triggered by VEGF-A expression, which may justify the existence of a significant number of viable and healthy MSCs in cell cultures exposed to the studied magnetic field conditions (Figure V. 3b).

Despite showing similar trends, it was observed that the magnetic response of MSCs monolayer on the expression of VEGF-A (Figure V. 4) was slightly superior to the gelatin scaffold condition (with the exception of the static low intensity condition). This could possibly be related to the higher adhesion of MSCs to protein-binding receptors present in gelatin[49] in contrast with the polystyrene plates, which do not contain cell binding receptors. The higher adhesion in the gelatin impairs cell mobility and the constant need of cell rearrangement. This idea is supported by the absence of changes in cell structural organization for MSC in gelatin scaffolds at the different magnetic field conditions, which contrasts with the clear capacity of MSCs monolayers cultured in cell plates to respond to the magnetic field, aligning according to the magnetic field direction

Furthermore, it is well known that ferrogels undergo volume contraction in the presence of magnetic field and contraction/distention switches when submitted to variable magnetic field conditions[50,51,52,53]. Therefore, the behavior of MSCs cultured in gelatin scaffolds may be also influenced by mechanical changes caused by hydrogel contraction/distention, thus affecting MSCs intrinsic cellular mechanisms, in particular those associated with the VEGF-A expression. It has also been reported that cells directly exposed to external stressors such as the magnetic field (e.g. the cells cultured in TCP) are prone to undergo cellular adaptation to stress, resulting in increased release of survival

growth factors (e.g. VEGF-A) during that period[54,55]. Based on this knowledge, it makes sense that MSCs in TCP might react faster, and also undergo faster adaptation, to the pulsed magnetic stimuli than MSCs in gelatin, who are more involved with indirect magnetic stimuli through the hydrogel. Consequently, the cells on the gelatin might not experience sufficient stress intensity to require the adaptation which is associated with increased secretion of survival molecules such as VEGF-A during dynamic stimulation regimes. However, when the magnetic field is applied continuously in static regime, the secretion of VEGF-A by MSCs cultured in gelatin exceeded the values obtained with MSCs in TCP. This seems to imply that, in contrast to pulsed stimulation, a static magnetic exposure may be able to increase the shear stress in the gelatin to levels that prompt the secretion by MSCs of higher levels of survival growth factors (e.g. VEGF-A).

The increased VEGF-A secretion was reflected in a higher tube formation and vessel ramification of HUVECs developed in the presence of conditioned media obtained along MSC exposure to static magnetic field. It is important to highlight that the proangiogenic effect of static magnetic field was able to surpass tube formation and ramification observed for HUVEC in positive controls. In contrast, LF dynamic modes led to the lowest VEGF-A production, leading in consequence to a weaker HUVEC maturation with reduced tube formation and branching. These results show that magnetic field may effectively regulate angiogenesis, once the magnetic induced pro-angiogenesis and anti-angiogenesis effect depends only on a proper selection of the magnetic field parameters, i.e. magnetic field intensity and/or magnetic field variation dynamics.

Partially, the differences in cell behavior could be, in a first stance, attributed to differences in the cell exposure period to the maximum magnetic field intensities. In static condition the cells are exposed to the maximum magnetic field intensity (0.08 T or 0.45 T) for the total experimental time (24 h). However, in dynamic conditions the period of exposure to maximum magnetic field intensity is reduced, not only because ON magnetic field stages are alternated with OFF magnetic field stages, but also because along the transition between ON and OFF states the cells are exposed to intermediary magnetic field intensities. Therefore, one may think that a reduced exposure time of MSCs to the magnetic field or the lower overall magnetic field intensity may explain the lower efficiency in MSC stimulatory effect observed under dynamic magnetic field conditions.

In fact, the average magnetic field intensity on the MSCs using HF mode was lower than static 0.08T intensity (0.0013 T and 0.0073 T), once more indicating that lower magnetic intensities are associated with better angiogenic performance. However, LF

mode carried out at 0.08 T also provides an average magnetic intensity of 0.045 T, closer to the static 0.08 T intensity. Yet the angiogenic results were significantly weaker under LF mode in comparison with static mode. Hence, the total period of exposure to magnetic field does not seem to be the most impactful parameter in regulating VEGF-A expression and angiogenesis.

A second theory is related with the possibility of the relaxation time of the magnetic field influencing cell behavior, which reports to the concept of cell adaptation to external stimuli. Cell adaptation has, however, been rarely discussed in the literature. Nonetheless, a particular study has reported how electrophysiological responses of olfactory cell receptors exhibited cell adaptation to step and multi-pulsed stimulation in a homeostatic feedback regulation[56]. This brings to light the fact that the cells might require an adaptation period after pulsed frequencies. That may not be the case for short-pulsed mode (HF) since the magnetic exposure may be too short (1s) to require cell adaptation, bringing the HF mode very similar to the static mode. The same is not valid for LF mode, where the cells remain exposed to the magnetic field for 1h and in the absence of magnetic field for an identical period. In this case, the relaxation period may be followed by cell magnetic relaxation effect or higher cell stress release due to a more efficient and long hydrogel volume distention period, resulting in a lower pro-angiogenic effect.

Nevertheless, more exhaustive investigation on the magnetic response of other cellular mechanisms involved in angiogenesis would be required for a clearer interpretation of these results.

Ultimately, this report highlights the capacity to remotely regulate angiogenic behavior through manipulation of magnetic configurations. The results evidenced the potential of using a LF magnetic configuration for anti-tumorogenic applications in cancer treatment. Likewise, the condition using a gelatin scaffold and a static low intensity magnetic field indicated enhancement of the angiogenic potential with possible applications for the improvement of vascularization on damaged tissues present in vascular diseases (e.g. vascular diseases, diabetes, atherosclerosis).

V.5. Conclusions

This study describes the impact of magnetic fields on the angiogenesis phenomena in MSCs while attempting to regulate the sprouting effect in HUVECs by remotely modulating MSCs angiogenic response through changes in intensity and application mode of the magnetic field. The lower intensity magnetic field (0.08T) was shown to induce an overall better performance in prompting increased production and secretion of growth factors, translated in a positive angiogenic effect in HUVECs with the formation of more tubes and branch points. This impact was consistent with the decreased proliferation rates for the higher intensity magnetic field, suggesting increased mortality of MSCs when exposed to high intensity fields.

The possibly toxic effect of the static 0.45 T on the MSCs proved however to be attenuated upon cyclic variation of the exposure frequency (LF and HF), revealing a potentially stronger impact on the cells by simply allowing cells to adapt and recover from the exposure before proceeding with further incidence (LF mode). While LF mode was associated with an anti-angiogenic performance, demonstrated by the lower number of tubes formed, HF and static regimes resulted in the enhancement of angiogenic behavior in HUVECs.

The magnetic effect was also improved with magnetic scaffolds under continuous exposure (static), however MSCs monolayer showed an overall satisfactory magnetic response without requiring a magnetic support to mediate the magnetic forces. Still, the process requires complementary studies of other frequencies and potentially longer exposure periods to properly characterize this effect. Nevertheless, this knowledge uncovers the unique remote stimulation properties of magnetic fields, offering the possibility to control angiogenesis mechanisms.

The magnetic stimulation was shown to be able to either function as a tool to reduce tumor growth in association with cancer treatments (using LF operation modes) or a possibility to promote the regeneration of diseased blood vessels (static and HF modes) in a contribution for vascular diseases treatments through cellular therapies.

V.6. References

1. Mastrullo, V., Cathery, W., Velliou, E., Madeddu, P. & Campagnolo, P. Angiogenesis in Tissue Engineering: As Nature Intended? . *Frontiers in Bioengineering and Biotechnology* **8**, 188 (2020).
2. Viallard, C. & Larrivée, B. Tumor angiogenesis and vascular normalization: alternative therapeutic targets. *Angiogenesis* **20**, 409–426 (2017).
3. Ziyad, S. & Iruela-Arispe, M. L. Molecular mechanisms of tumor angiogenesis. *Genes Cancer* **2**, 1085–1096 (2011).
4. Phelps, E. A. & Garcia, A. J. Update on therapeutic vascularization strategies. *Regen. Med.* **4**, 65–80 (2009).
5. Teleanu, R. I., Chircov, C., Grumezescu, A. M. & Teleanu, D. M. Tumor Angiogenesis and Anti-Angiogenic Strategies for Cancer Treatment. *J. Clin. Med.* **9**, 84 (2019).
6. Jászai, J. & Schmidt, M. H. H. Trends and Challenges in Tumor Anti-Angiogenic Therapies. *Cells* **8**, 1102 (2019).
7. Takeshita, S. *et al.* Therapeutic angiogenesis. A single intraarterial bolus of vascular endothelial growth factor augments revascularization in a rabbit ischemic hind limb model. *J. Clin. Invest.* **93**, 662–670 (1994).
8. van Weel, V., van Tongeren, R. B., van Hinsbergh, V. W. M., van Bockel, J. H. & Quax, P. H. A. Vascular Growth in Ischemic Limbs: A Review of Mechanisms and Possible Therapeutic Stimulation. *Ann. Vasc. Surg.* **22**, 582–597 (2008).
9. Simons, M. & Ware, J. A. Therapeutic angiogenesis in cardiovascular disease. *Nat. Rev. Drug Discov.* **2**, 863–872 (2003).
10. Renault, M.-A. & Losordo, D. W. Therapeutic myocardial angiogenesis. *Microvasc. Res.* **74**, 159–171 (2007).
11. Jacobs, J. Combating cardiovascular disease with angiogenic therapy. *Drug Discov. Today* **12**, 1040–1045 (2007).
12. Jörn, T., G., R. J. & W., L. D. Therapeutic Angiogenesis for Critical Limb Ischemia. *Circulation* **118**, 9–16 (2008).
13. Simón-Yarza, T. *et al.* Vascular endothelial growth factor-delivery systems for cardiac repair: an overview. *Theranostics* **2**, 541–552 (2012).
14. Lachmann & Nikol. Therapeutic angiogenesis for peripheral artery disease: Stem

cell therapy. *Vasa* **36**, 241–251 (2007).

15. Lovett, M., Lee, K., Edwards, A. & Kaplan, D. L. Vascularization strategies for tissue engineering. *Tissue Eng. Part B. Rev.* **15**, 353–370 (2009).
16. Royce, P. M., Kato, T., Ohsaki, K.-I. & Miura, A. The enhancement of cellular infiltration and vascularisation of a collagenous dermal implant in the rat by platelet-derived growth factor BB. *J. Dermatol. Sci.* **10**, 42–52 (1995).
17. Friess, W. Collagen – biomaterial for drug delivery1Dedicated to Professor Dr. Eberhard Nürnberg, Friedrich-Alexander-Universität Erlangen-Nürnberg, on the occasion of his 70th birthday.1. *Eur. J. Pharm. Biopharm.* **45**, 113–136 (1998).
18. Elçin, Y. M., Dixit, V. & Gitnick, G. Extensive In Vivo Angiogenesis Following Controlled Release of Human Vascular Endothelial Cell Growth Factor: Implications for Tissue Engineering and Wound Healing. *Artif. Organs* **25**, 558–565 (2001).
19. Huang, Y.-C., Kaigler, D., Rice, K. G., Krebsbach, P. H. & Mooney, D. J. Combined Angiogenic and Osteogenic Factor Delivery Enhances Bone Marrow Stromal Cell-Driven Bone Regeneration. *J. Bone Miner. Res.* **20**, 848–857 (2005).
20. Kaigler, D., Wang, Z., Horger, K., Mooney, D. J. & Krebsbach, P. H. VEGF Scaffolds Enhance Angiogenesis and Bone Regeneration in Irradiated Osseous Defects. *J. Bone Miner. Res.* **21**, 735–744 (2006).
21. Marędziak, M., Śmieszek, A., Chrząstek, K., Basinska, K. & Marycz, K. Physical Activity Increases the Total Number of Bone-Marrow-Derived Mesenchymal Stem Cells, Enhances Their Osteogenic Potential, and Inhibits Their Adipogenic Properties. *Stem Cells Int.* **2015**, 379093 (2015).
22. Marycz, K. *et al.* Endurance Exercise Mobilizes Developmentally Early Stem Cells into Peripheral Blood and Increases Their Number in Bone Marrow: Implications for Tissue Regeneration. *Stem Cells Int.* **2016**, 5756901 (2016).
23. Mierzejewska, K. *et al.* Hematopoietic stem/progenitor cells express several functional sex hormone receptors-novel evidence for a potential developmental link between hematopoiesis and primordial germ cells. *Stem Cells Dev.* **24**, 927–937 (2015).
24. Jaberi, F. M. *et al.* A Moderate-Intensity Static Magnetic Field Enhances Repair of Cartilage Damage in Rabbits. *Arch. Med. Res.* **42**, 268–273 (2011).
25. Xu, S., Tomita, N., Ikeuchi, K. & Ikada, Y. Recovery of small-sized blood vessels in ischemic bone under static magnetic field. *Evid. Based. Complement. Alternat.*

Med. **4**, 59–63 (2007).

26. Yamamoto, Y., Ohsaki, Y., Goto, T., Nakasima, A. & Iijima, T. Effects of Static Magnetic Fields on Bone Formation in Rat Osteoblast Cultures. *J. Dent. Res.* **82**, 962–966 (2004).
27. Kotani, H. *et al.* Strong Static Magnetic Field Stimulates Bone Formation to a Definite Orientation In Vitro and In Vivo. *J. Bone Miner. Res.* **17**, 1814–1821 (2002).
28. Qian, A.-R. *et al.* Large gradient high magnetic fields affect osteoblast ultrastructure and function by disrupting collagen I or fibronectin/αβ1 integrin. *PLoS One* **8**, e51036–e51036 (2013).
29. Di, S. *et al.* Large gradient high magnetic field affects FLG29.1 cells differentiation to form osteoclast-like cells. *Int. J. Radiat. Biol.* **88**, 806–813 (2012).
30. NEURATH, P. W. High Gradient Magnetic Field inhibits Embryonic Development of Frogs. *Nature* **219**, 1358–1359 (1968).
31. Delle Monache, S. *et al.* Inhibition of angiogenesis mediated by extremely low-frequency magnetic fields (ELF-MFs). *PLoS One* **8**, e79309–e79309 (2013).
32. Ruggiero, M. *et al.* 0.2 T magnetic field inhibits angiogenesis in chick embryo chorioallantoic membrane. *Bioelectromagnetics* **25**, 390–396 (2004).
33. Ai, Y. *et al.* Environmental Sciences. **6**, 271–275 (1819).
34. Strelczyk, D. *et al.* Static magnetic fields impair angiogenesis and growth of solid tumors in vivo. *Cancer Biol. Ther.* **8**, 1756–1762 (2009).
35. Wang, Z. *et al.* Inhibitory effects of a gradient static magnetic field on normal angiogenesis. *Bioelectromagnetics* **30**, 446–453 (2009).
36. Ge, Q. *et al.* VEGF secreted by Mesenchymal stem cells mediates the differentiation of endothelial progenitor cells into endothelial cells via paracrine mechanisms. *Mol. Med. Rep.* **17**, 1667–1675 (2018).
37. Zhao, W., Ma, W. & Wu, H. The effects of magnetic fields on the differentiation and intracellular free calcium of bone marrow mesenchymal stem cells. in *2008 World Automation Congress* 1–3 (2008).
38. Marycz, K., Kornicka, K. & Röcken, M. Static Magnetic Field (SMF) as a Regulator of Stem Cell Fate - New Perspectives in Regenerative Medicine Arising from an Underestimated Tool. *Stem cell Rev. reports* **14**, 785–792 (2018).
39. Cruz-Izquierdo, Á., Picó, E. A., López, C., Serra, J. L. & Llama, M. J. Magnetic Cross-Linked Enzyme Aggregates (mCLEAs) of Candida antarctica lipase: An

efficient and stable biocatalyst for biodiesel synthesis. *PLoS One* **9**, 1–22 (2014).

40. Dos Santos, F. *et al.* Ex vivo expansion of human mesenchymal stem cells: A more effective cell proliferation kinetics and metabolism under hypoxia. *J. Cell. Physiol.* **223**, 27–35 (2010).
41. Ghodbane, S., Lahbib, A., Sakly, M. & Abdelmelek, H. Bioeffects of Static Magnetic Fields: Oxidative Stress, Genotoxic Effects, and Cancer Studies. *Biomed Res. Int.* **2013**, 602987 (2013).
42. Wang, H. & Zhang, X. Magnetic Fields and Reactive Oxygen Species. *Int. J. Mol. Sci.* **18**, 2175 (2017).
43. Coballase-Urrutia, E. *et al.* Static Magnetic Fields Modulate the Response of Different Oxidative Stress Markers in a Restraint Stress Model Animal. *Biomed Res. Int.* **2018**, 3960408 (2018).
44. Yan, J., Dong, L., Zhang, B. & Qi, N. Effects of Extremely Low-Frequency Magnetic Field on Growth and Differentiation of Human Mesenchymal Stem Cells. *Electromagn. Biol. Med.* **29**, 165–176 (2010).
45. Marędziak, M., ¯mieszek, A., Tomaszewski, K. A., Lewandowski, D. & Marycz, K. The effect of low static magnetic field on osteogenic and adipogenic differentiation potential of human adipose stromal/stem cells. *J. Magn. Magn. Mater.* **398**, 235–245 (2016).
46. Okano, H., Onmori, R., Tomita, N. & Ikada, Y. Effects of a moderate-intensity static magnetic field on VEGF-A stimulated endothelial capillary tubule formation in vitro. *Bioelectromagnetics* **27**, 628–640 (2006).
47. Song, Y. S. *et al.* Bone marrow mesenchymal stem cell-derived vascular endothelial growth factor attenuates cardiac apoptosis via regulation of cardiac miRNA-23a and miRNA-92a in a rat model of myocardial infarction. *PLoS One* **12**, 1–18 (2017).
48. Pankajakshan, D. & Agrawal, D. K. Mesenchymal Stem Cell Paracrine Factors in Vascular Repair and Regeneration. *J. Biomed. Technol. Res.* **1**, 1–21 (2014).
49. Davidenko, N. *et al.* Evaluation of cell binding to collagen and gelatin: a study of the effect of 2D and 3D architecture and surface chemistry. *J. Mater. Sci. Mater. Med.* **27**, 148 (2016).
50. Filipcsei, G., Csetneki, I., Szilágyi, A. & Zrínyi, M. Magnetic field-responsive smart polymer composites. *Adv. Polym. Sci.* **206**, 137–189 (2007).
51. Szabó, D., Szeghy, G. & Zrínyi, M. Shape transition of magnetic field sensitive

polymer gels. *Macromolecules* **31**, 6541–6548 (1998).

52. Vikingsson, L. *et al.* Local deformation in a hydrogel induced by an external magnetic field. *J. Mater. Sci.* **51**, 9979–9990 (2016).
53. Zhou, G. Y. & Jiang, Z. Y. Deformation in magnetorheological elastomer and elastomer-ferromagnet composite driven by a magnetic field. *Smart Mater. Struct.* **13**, 309–316 (2004).
54. Poljšak, B. & Milisav, I. Clinical implications of cellular stress responses. *Bosn. J. basic Med. Sci.* **12**, 122–126 (2012).
55. Yuan, L., Sakamoto, N., Song, G. & Sato, M. High-level Shear Stress Stimulates Endothelial Differentiation and VEGF Secretion by Human Mesenchymal Stem Cells. *Cell. Mol. Bioeng.* **6**, (2013).
56. De Palo, G. *et al.* Common dynamical features of sensory adaptation in photoreceptors and olfactory sensory neurons. *Sci. Rep.* **3**, 1–8 (2013).

Chapter VI



Design Of Blood Vessel Devices For Vascularization Models Using Magnetic Scaffolds

CHAPTER VI – Design of blood vessel devices for vascularization models using magnetic scaffolds

This chapter follows previous knowledge and introduces fluidic dynamics with the fabrication of blood vessel models, in 2D and 3D, using magnetic stimulation to improve vascularization on chip and thus mimic the native vasculature microenvironment.

Outline

While traditional cell culture arrays are powerful tools to acquire biological information, key functional bottlenecks remain in miniaturized models capable to mimic the vascularized properties of the native microenvironment. Advances are needed to complement *in vitro* vascular disease modeling tools. Here, blood vessels, such as arteries and veins, were designed to facilitate cell proliferation, migration, and endothelial tissue formation using co-cultures of MSCs (mesenchymal stromal cells) and HUVECs (human umbilical vein endothelial cells), in both 2D and 3D. The microfluidic 2D platforms are comprised of microchannels made of magnetic polymers, where the different cell types are cultured, and PDMS microchannels, where continuous media flow is applied. The magnetic polymers were patterned using capillary line pinning technique to enable *in situ* co-culture of MSCs and HUVECs in confined compartments to simulate blood vessel walls. Magnetic fields were applied on chip to stimulate vascularization as a proof-of-concept study. Design parameters were informed by numerical simulation and empirical analyses of 3D diffusion of growth factor (VEGF) in the microfluidic chip. Unlike traditional cell culturing platforms, endothelium formation was successfully achieved thanks to the availability of microfluidic inlets where multiple seeding of HUVECs and applied magnetic stimulation were performed. A straightforward device for blood vessel modelling should advance the exploration of *in vitro* blood vessel strategies to regulate vascularization in disease modeling aiming to contribute for the development of more efficient therapeutics for cardiovascular diseases therapies.

Keywords: blood vessel, microfluidic technology, 3D molding design, MSCs, HUVECs, angiogenesis, sprouting, magnetic fields

VI.1. Introduction

Vascular diseases are ranked amongst the disorders with the highest morbidity worldwide, mostly due to the little knowledge of the disease and inadequate therapeutic approaches[1]. With current therapeutic programs relying on animal models to poorly predict the human pathophysiology and drug responses[2], the process of mimicking a patient's native tissue architecture remains as a challenge, hindering the development of novel treatment strategies.

Physiologically relevant blood vessel *in vitro* models highly depends on the study of blood vessel mechanics, responsible for mediating key functions of cellular and biochemical transport to perfuse tissues[3]. With complex geometries, the blood vessels diameter varies dramatically, ranging from a few millimeters to micrometers, thus hampering the biomimetic process[3,4].

Traditionally *in vitro* platforms relied on endothelial cells (ECs) growing on a coated 2D surface with adhesive proteins or monolayers of ECs within 3D hydrogel scaffolds encapsulated with specific growth factors (e.g. VEGF-A)[5]. Although these models offered insight into vessel assembly, they lack the capacity of simultaneous introduction of the required chemical and mechanical stimuli in adequate spatiotemporal conditions[6]. Alternatively, engineered tissue constructs (e.g. synthetic materials, biological scaffolds, porous hydrogels, fibrous meshes) with self-assembled cell aggregates have been developed to prompt cell adhesion, migration, and proliferation[7].

Ultimately, the development of microfluidic chips has brought uncountable advantages, namely (1) the ability to control the flow in physiological levels, (2) simulating a 3D microenvironment by using hydrogel scaffolds, (3) incorporating human cells and controlling the distribution of chemical molecules, (4) reducing the volume of required reagents in comparison with highly expensive animal models[8,9,10]. Microphysiological systems have already been demonstrated for the liver, lung, kidney, heart, and pancreas, achieving some promising results[11].

Regarding vascularization in microchips, recent reports have also demonstrated *in vitro* perfusable vessels with endothelialization of the hydrogel channels to mimic endothelial cell migration, vascular barrier function, and inflammatory response[12]. Unfortunately, they were limited to reconstitute features and responses of *in vivo* endothelial cells for lack of natural endothelial morphogenesis[9].

Overall, none of these methods allow for cell culture in confined compartments which can be critical for simulating physiological conditions including molecular transport and nutrient absorption[13]. Accordingly, a recent report describes the use of a temporary membrane to separate the parenchymal and the endothelial channels[14]. However, this strategy might induce channel occlusion if polymer residues are not properly removed from the chip.

On Chapter III we studied the combined effect of magnetic hydrogels and external magnetic fields for regulation of protein sorption/desorption processes[15] and cell behavior, highlighting the possibility to use external magnetic stimulation on the blood vessel chips as a novel contribution to this area. Gelatin biopolymer was used as an artificial replacement of the blood vessel elastic tissue and able to support the MSCs growth. A magnetic responsive scaffold was tailored by combining the gelatin with magnetic nanoparticles, i.e. iron oxide nanoparticles, to target the magnetic forces derived from an external neodymium magnet.

Here, we implemented this concept by taking the advantage of microfluidics. The capillary line pinning technique was introduced in a platform for controllable patterning of hydrogels in microchips[16,17,13]. Capillary barriers allow for precise control on precursor hydrogel trapping over large areas, offering high reliability and spatial resolution[17]. The success of this technique has been confirmed in a desalination microchip composed of alternated-patterned charged hydrogels compartments fabricated by capillary line pinning allowing for the study of ion transport[16]. This technique has also been applied to the long-term cell culture of intestinal bacteria (*E. coli*) and human intestinal epithelial cells (Caco-2) in well-controlled fluid flow confined compartments[13].

In this work, a platform was created to allow for comparative studies between molded 3D single channels and 2D chips. Capillary line pinning principle was implemented on 2D models to provide confined channels for HUVECs (in the lumen region of the 2D vessel) while MSCs remained encapsulated within the hydrogel channel made of hydrogel, aiming at establishing confined microenvironments by building microvascular constructs with selective barrier function similar to *in vivo*[18].

Different chip geometries were designed and evaluated taken into account the flow dynamic characteristics and its impact on cell culture behavior and angiogenesis development. The combination of MSCs and HUVECs in co-cultures have been described to induce an increased sprouting effect in previous studies, with MSCs playing

a key role in secreting growth factors (VEGF) to the media to induce HUVECs maturation[19,20,21,22].

Finally, and despite several 2D *in vitro* models being developed to investigate vascular network-related phenomena, only 3D *in vitro* models are capable to properly mimic physiological cell-cell and cell-matrix interactions within supporting matrices[23]. For this reason, the performance of 2D geometries using capillary barriers technique was compared with 3D macroscale models of single blood vessel constructs using crosslinked gelatin as the artificial tissue through 3D molding technologies.

Together, this study features novel *in vitro* models under an original technology involving the use of remote magnetic stimulation to prompt vascularization in artificial blood vessels to provide promising templates for cardiovascular diseases modeling, such as cardiac ischemia and drug screening.

VI.2. Experimental Section

2D Chips Fabrication. Different 2D chips were fabricated using polydimethylsiloxane polymer (PDMS, Dow Corning) following standard soft lithography techniques implemented in the MCS group of the University of Twente, The Netherlands. A PDMS layer was directly bonded to a glass layer (microscope slide) following traditional microfluidic procedures. The PDMS layer contained inlets and outlets directly connected to cell culture media to allow for fluid flow perfusion. Compartments for hydrogels patterning, cell culture reservoirs, media flow channels, and capillary barriers were included in the different chip types. Overall, chips with four different geometries were designed in Clewin software. However, only three geometries were used in this report due to similar performances found between two of the geometries (types I, II, III). Silica wafers containing the negative pattern of the chip designs were fabricated in the MESA+ cleanroom facility at the University of Twente. The silica wafers consisted of SU-8 master containing two SU-8 layers (Microchem), where the first layer contained microstructures for the channels and reservoirs while the second layer contained microstructures for the capillary barriers. The height of the first layer was 450 μm and the second layer (capillary barrier) was 150 μm. This average thickness of the SU-8 layers were measured using a Dektak surface profilometer (Bruker, Germany). The PDMS chip was fabricated by casting a prepolymer (10:1 w/w ratio of PDMS and curing

agent) on top of the SU-8 master of the silica wafers. After curing the prepolymer at 80 °C for 3 h, the PDMS layer was detached from the SU-8 master and cut in rectangular chips using a blade. The inlets and outlets were opened using hole punchers with 0.75 mm (media flow channels) and 3 mm (hydrogel channels) diameter in the PDMS layer. The patterned surface of the PDMS layer was treated with oxygen plasma at 300 mTorr for 60 seconds using a Harrick Plasma Cleaner (PDC-32G, USA) and immediately bonded with an oxygen plasma-treated glass layer. The hydrogel patterning on the chip was performed 2-3 days after oxygen plasma bonding and the microchips were kept at -4ºC. On type I, the total inner volume of each hydrogel compartment was 60 µL, for the media microchannels the inner volume was 10 µL, and for the endothelial cell reservoir, the volume was 40 µL. On type II, hydrogel compartments had a total volume of 40 µL, the media microchannels of 10 µL and the cell compartment of 20 µL. On type III, each media channel had a volume of 50 µL, and the hydrogel compartment an inner volume of 100 µL (Supplementary Figure VI. S3). The total dimensions of the chips were the same for all three types: 260 mm x 120 mm (width x breadth). In posterior experiments, a different strategy was used to maximize the volume of media within the channels. Two layers of PDMS of the same geometry were bonded together after the microscopic alignment of the compartments. Inlets and outlets were opened on the top layer and hydrogel patterning and cell seeding were performed 2-3 days after the assembly.

Magnetic Hydrogel Preparation. The magnetic hydrogel is composed of Porcine skin gelatin (8% m/v, type A, G2500, Sigma-Aldrich) doped with magnetic nanoparticles (MNPs) synthesized by chemical co-precipitation of iron salts $FeCl_3$ and $FeCl_2$ (Sigma-Aldrich) in alkaline media, according to the protocol published by Izquierdo et al.[46] For MNPs preparation, an aqueous solution containing 25% of ammonium hydroxide (NH_4OH) (Fluka) was added to a mixture of $FeCl_3$ and $FeCl_2$ at 80 ºC, under permanent stirring at 1250 rpm by purging N_2. MNPs were dried in ethanol solution at room temperature to form a magnetic powder. Porcine skin gelatin was dissolved in Milli-Q water (10% m/v) at 60 ºC. Powder MNPs were dispersed by sonication and mixed with gelatin polymeric aqueous solution to form a homogeneous solution. The solution was maintained at -20 ºC to prevent fungi contamination on the gelatin.

Magnetic Hydrogel Patterning. Prior to hydrogel patterning in the chips, the magnetic solution of gelatin and MNPs was heated at 70 ºC to ensure reduced viscosity

and avoid clogging issues. Immediately after heating, 1% of glutaraldehyde (v/v) (cross-linking agent, Sigma Aldrich) was added to the mixture for gelatin crosslinking and the patterning process occurred via capillary action (Figure VI. 1a and 2b). Excess hydrogel solution was removed with a Pasteur pipette to ensure that the hydrogel mixture remained between the endothelial cell reservoirs and the media microchannels due to the capillary pinning process. The chips were placed at -20 ºC before cell culture experiments to allow for hydrogel curing while avoiding the formation of air bubbles and hydrogel leakage to other compartments. Before seeding the cells, the magnetic coating was washed by perfusion of PBS solution (Phosphate Buffered Saline, Sigma Aldrich) three times to remove unbonded components. For sterilization, the samples were perfused by a PBS solution containing 1% of antibiotic-antimycotic (Gibco) for 3 h. As pre-conditioning for the cells, the samples were immersed in DMEM cell culture media (Dulbecco's Modified Eagle Medium, ThermoFisher Scientific) for 3 h before perfusing the cells through the media flow microchannels. The tubing and the microfluidic connectors used in the experiments were sterilized through rinsing with 70% (v/v) ethanol and afterward with PBS (phosphate buffered saline, Sigma Aldrich) solution.

3D Constructs Fabrication. 3D single-channel blood vessels aiming to mimic the dimensions of large arteries and veins were fabricated following molding techniques. Silicone tubings with different diameters were used as molds to fabricate models of an artery with 2.5 cm of lumen diameter and 2 mm of wall thickness and a vein with lumen diameters of 3 cm and a wall thickness of 1.5 mm. In the first stage, the tubing was coated with a solution of Gel Slick solution (Lonza) for surface treatment, to allow for an easier demolding, and air dried prior to use. The molding setup (Figure VI. 3a) consisted of a smaller tubing inserted within a larger one and glued to plastic support according to the desired artery and vein model dimensions. The space in between the tubing was then filled with the magnetic gelatin solution and placed at 4 ºC for gelation overnight. The outer tubing was then cut and removed while the sample was still frozen, and the inner tubing was gently demolded. The 3D molds were immersed in a solution containing 3% of Glutaraldehyde for crosslinking for 3 h. To remove unbound material, the molds were washed twice with PBS solution and sterilized using a PBS solution containing 1% of antibiotic-antimycotic for 3h. The molds were stored at -20 ºC and pre-conditioned with cell culture media (DMEM) prior to use.

Magnetic Gelatin Mechanical Characterization. Compression mechanical testing was performed to characterize the Young Modulus of the magnetic hydrogel of the 3D channels and the coating patterned on the chips. Magnetic hydrogel before and after the addition of the crosslinking agent were analyzed through mechanical compression. The samples were cut with a total area of 1 cm^2 and an average thickness of 1.5 mm, as the wall thickness of the 3D single channels. The samples were tested with a preload sample holder of 0.1 N with 0.1% strain with an Instron Tensile Compression equipment at Elastomer Technology and Engineering facilities at University of Twente. The tests were performed at room temperature using six samples for each condition of analysis up to the rupture of the sample, leading to the plot of stress-strain curves and the calculation of the Young Modulus for the magnetic gelatin before and after crosslinking.

Cell Culture. Human bone-marrow MSCs lines used in this report belong to the cell bank available at Stem Cell Engineering Research Group (SCERG), iBB-Institute for Bioengineering and Biosciences at Instituto Superior Técnico (IST). Bone marrow aspirates were obtained from Instituto Português de Oncologia Francisco Gentil, Lisboa-Portugal under collaboration with iBB-IST. All human samples were obtained from healthy donors after written informed consent, accordingly with the Directive 2004/23/EC of the European Parliament and of the Council of 31 March 2004 on setting standards of quality and safety for the donation, procurement, testing, processing, preservation, storage, and distribution of human tissues and cells (Portuguese Law 22/2007, June 29), with the approval of the Ethics Committee of the respective clinical institutions[25]. Isolated cells were cryopreserved in liquid/vapor nitrogen tanks until further use. Isolated human bone marrow MSCs (BM MSCs) were cultured using low-glucose Dulbecco's Modified Eagle Medium (DMEM, Gibco, Grand Island, NY) supplemented with 10% fetal bovine serum (FBS MSC qualified, Gibco) and 1% antibiotic-antimycotic (Gibco) and kept at 37 ºC, 5% CO_2 and 21% O_2 in a humidified atmosphere. HUVECs were purchased from Lonza (Basel, Switzerland) and maintained in commercial endothelial growth medium-2 (EGM-2, Lonza) at 37 ºC, 5% CO_2 in a humidified atmosphere. Medium renewal was performed every 3-4 days. All the experiments were performed using cells between passages 4 and 7.

Co-culture of MSCs and HUVECs and Magnetic Stimulation. MSCs (seeding density of $1.5x10^6$ cells/mL) were initially perfused onto the chips through the media channels and allowed to migrate and adhere to the magnetic hydrogel overnight. Some inlets were also punched on the PDMS layer above the hydrogel compartment, allowing for MSCs injection (1 µL) in those specific regions to boost cell proliferation (Figure VI. 1a). Matrigel solution (Corning, NY) was also perfused on the endothelial cell compartment to create a support for HUVECs while HUVECs (seeding density of $3x10^6$ cells/ mL) were seeded by perfusion on the compartment before allowing for matrigel gelation. A syringe pump (Harvard Apparatus, PHD2000) was connected to the media flow inlets of the chips and a volumetric flow of 300 µL/h was set to infuse cell culture media in the media flow microchannels. The outlets of the chips were connected to a recipient and the depleted stream was collected every day for further analysis (presence of growth factors, metabolites assessment). The syringes were replaced with fresh media every day, containing DMEM + 10% FBS and Endothelial Growth Medium-2 (EGM-2, Lonza) in a 1:1 proportion. The experiments in the chips were performed in incubators at 37 ºC in 5% CO_2 in a humidified atmosphere under normoxia conditions, for 5 days. For the magnetic stimulation proof of concept, a magnet with a maximum magnetic intensity of 0.08 T was placed beneath the chips for the last 24 h of the co-culture, on the final and optimized experiments. Exceptionally, type III chip was designed with only one compartment for both HUVECs and MSCs, which was therefore patterned with magnetic gelatin following the same procedures described for type I and II. Under these conditions, the cell compartment is not perfused with media or growth factor and instead the nutrients and growth factors from the cell culture media were diffused from the media channels to the gelatin where the co-culture was encapsulated.

Computational modeling of fluid flow and VEGF diffusion. Velocity profiles and VEGF (Human VEGF-A molecular mass: 40 kDa; density: 1.35 g/mL; relative diffusion coefficient: $1/\sqrt{d} = 0.74$[26]) diffusion from the media microchannels to the endothelial cell compartment in the 2D chips were simulated using COMSOL Multiphysics software. The simulations were carried out assuming the diffusion of the molecular species in diluted solutions parameter under steady laminar flow time-dependent regime. A shallow channel approximation was applied and an initial VEGF concentration of 2.5×10^{-5} mol/ m^3 was provided in the simulations.

The transport of diluted species was coupled with the calculated convection from either the laminar or the creeping flow module. The diffusion rate of VEGF in water was assumed to be $D_{cW} = 6.4x10^{-3}$ m^2/s[27], the diffusion rate of VEGF in the hydrogels channels was assumed to be similar to collagen, $D_{cH} = 1.4x10^{-10}$ m^2/s[28].

Flow velocity tracking measurement. Green polystyrene fluoSpheres with 15 μm (Invitrogen) were dissolved in PBS (1:1000 dilution) and perfused at a volumetric flow of 300 μL/ h in the media channels of 2D chips with a syringe pump. The fluorescent microbeads were used as tracers to better define the fluid flow patterns in the chips and thus determine the velocity of the circulating microbeads in different points of the media channels. The flow path of the fluorescent microbeads was recorded using a fluorescence microscope (Leica DM IL LED with EC3 camera system) with an exposure time of 500 ms. The velocity of these microbeads within the media microchannels was quantified using the tracking velocity analysis tool in ImageJ software.

VEGF and Endothelin-1 measurement using ELISA. ELISA experiments were performed, following the manufacturer's instructions, to quantify the total amount of exogenous angiogenic VEGF-A protein present in the depleted stream collected from the chips using the Human VEGF-A kit, RayBiotech. ELISA tests were also carried out using Endothelium-1 kit (RayBiotech) to quantify the total amount of vasoconstrictor peptide secreted by HUVECs, which was then correlated with the endothelium formation. All conditions were tested in triplicates using the same MSC donor to avoid further variability on the results.

Morphological analysis. Cell viability using calcein staining (Live & Dead kit, Invitrogen) was recorded throughout experiments using an EVOS FL imaging system equipped with GFP filter cube. For fluorescence staining, Dapi (Sigma Aldrich), Yo-Yo and Ethidium Bromide (ThermoFisher Scientific, USA) were used to stain the nuclei and the cytoplasm of HUVECs after fixation with 4% (v/v) of paraformaldehyde and permeabilization in 0.1% (v/v) Triton X-100 (Sigma Aldrich) for 10 min. After the staining process, the cells were scanned using a laser scanning confocal microscope (Zeiss LSM 510, Germany). Live and Dead images using a combination of Calcein and Ethidium Bromide staining (LIVE/DEAD™ Viability/ Cytotoxicity Kit, for mammalian

cells, ThermoFisher Scientific) were also obtained after 20 min of incubation with MSCs and HUVECs co-culture using a fluorescence microscope (Leica DM IL LED with EC3 camera system).

CD31 Immunostaining. HUVECs immunocharacterization was carried out using CD31 antibody after the co-culture (MSCs and HUVECs) fixation with 4% paraformaldehyde and blocking with 10% FBS (Fetal Bovine Serum, Gibco) in PBS solution. Primary antibody CD31 (1:50 dilution, mouse antibody, Dako) in block solution was perfused in the chips and incubated overnight. Secondary antibody Alexa 546 (1:500 dilution, goat anti-mouse, Abcam) was added to the chips and incubated for 30 min. Images were obtained using a fluorescence microscope (Leica DM IL LED with EC3 camera system) and a confocal laser scanning microscope (LSM 700/ Carl Zeiss).

Statistical analysis. All measurements were performed twice, under independent conditions. Two-way ANOVA Sidak's multiple comparisons test was used to compare the mean of three values obtained from three independent conditions in ELISA assay, using GraphPad Prism version 7 (GraphPad Software, La Jolla, CA); *$p < 0.05$ indicates a significant result; **$p < 0.01$ a very significant result, ***$p < 0.001$ a highly significant result, and ****$p < 0.0001$ an extremely significant result.

VI.3. Results

3.1. Design and Hydrogel Patterning of 2D chips for cell culture.

The 2D chips were fabricated to enable angiogenic development on cell culture compartments under controlled fluid flow (Figure VI. 1a). Three different geometries (type I, II, III) were fabricated and tested to improve the formation of microvessels in HUVECs (Figure VI. 1b). Types I and II have different geometry, thus enabling a comparison between the effect of angular (I) and linear (II) shaped channels on fluid flow and cell behavior, but similar transport and diffusion mechanisms for cells and molecules. The transport and diffusion of all molecules and cells coming in and out of the 2D chips, and the interactions between them, were represented in Figure VI. 1c.

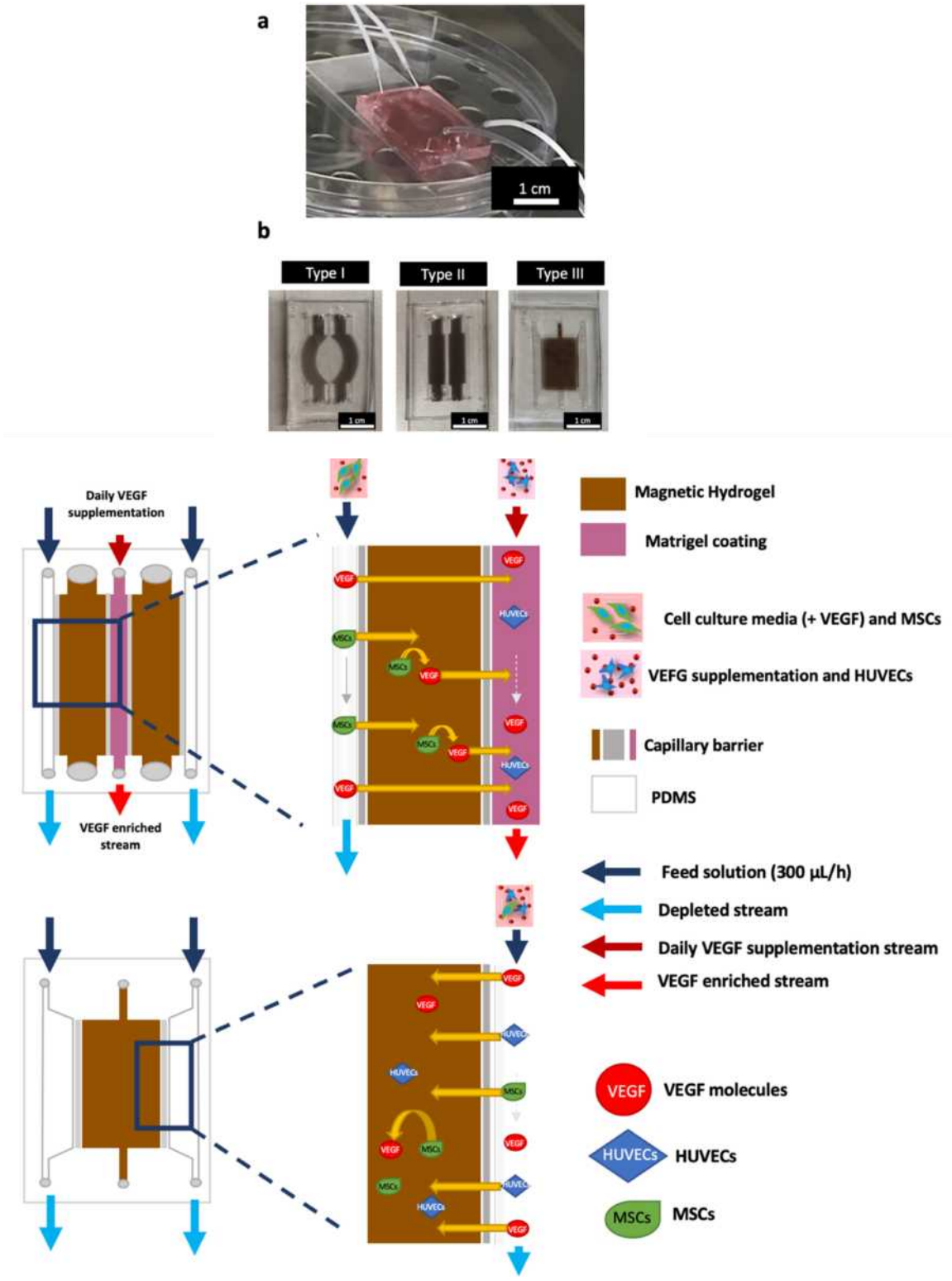


Figure VI. 1. a) Image of a representative assembled device during cellular experiments. **b)** Image of assembled 2D chips in all three geometries. **c)** Schematic representation of design II and III containing patterned hydrogels (Magnetic gelatin and Matrigel) and cell culture (MSCs and HUVECs). The scheme represents the mechanisms of cell seeding in the initial stage of the experiment and the process of VEGF transport into the HUVECs compartment. Type I has a similar mechanism to Type II.

For a better understanding of the timeframe of the experiments, the sequential steps of the processes including co-culture seeding, VEGF supplementation and magnetic stimulation of the final experimental model were schematically represented in Supplementary Figure VI. S1.

The processes involved in triggering angiogenesis are highly dependent on a continuous release of growth factor molecules, in particular VEGF, which plays a key role in driving a sprouting behavior on HUVECs. Therefore, three methods were used to increase and maintain a supply of VEGF in the chips: VEGF already contained in HUVECs cell culture media (1µg/ mL), VEGF daily supplemented to the cell culture (0.2 µg/mL) and a continuous release of VEGF by MSCs during the co-culture stage (Figure VI. 1c). Type I and II have two inlets for cell culture media, directly connected to corresponding outlets, and one inlet connected to HUVECs reservoir, destined for VEGF daily supplementation. This channel was connected to the outlet for the depleted stream of VEGF supplemented (Figure VI. 1c).

Type III contained a single reservoir for both HUVECs and MSCs and two inlets, for cell culture media and VEGF daily supplementation, connected to two outlets, where the depleted stream of the chip was collected. The different geometry and mass transport processes between Type I/II and III might impact on cell behavior and thus provide different responses to angiogenesis.

All the chips were fabricated in PMDS by soft lithography procedures (Figure VI. 2a) containing different channels and compartments with a height of 450 µm and separated by capillary line pinning barriers, made of PDMS with a height of 150 µm, to facilitate the success of magnetic gelatin patterning on specific channels and avoid hydrogel leakage to the media channels or other cell compartments (Figure VI. 2b). In the end, the gelatin channel was completely filled with the hydrogel, with an overall thickness of 450 µm, the total height of the channel. During co-culture stage, MSCs were expected to spread from the media channels, from where they were injected, to be encapsulated within the gelatin channel. Gelatin patterning was performed in all three Types I, II and III. On type III, both HUVECs and MSCs were encapsulated in the gelatin compartment.

Matrigel, a hydrogel suitable for endothelial cell culture and tube formation, was also patterned on the HUVECs compartment of Types I and II. In this case, only a thin layer was patterned for HUVECs support, with the excess material being carefully removed from the chip to allow for HUVECs culture on top of the matrigel. The hydrogels

patterning within the respective confined compartments was achieved with over 90% of success and the final result for Type I can be observed in Figure VI. 1a.

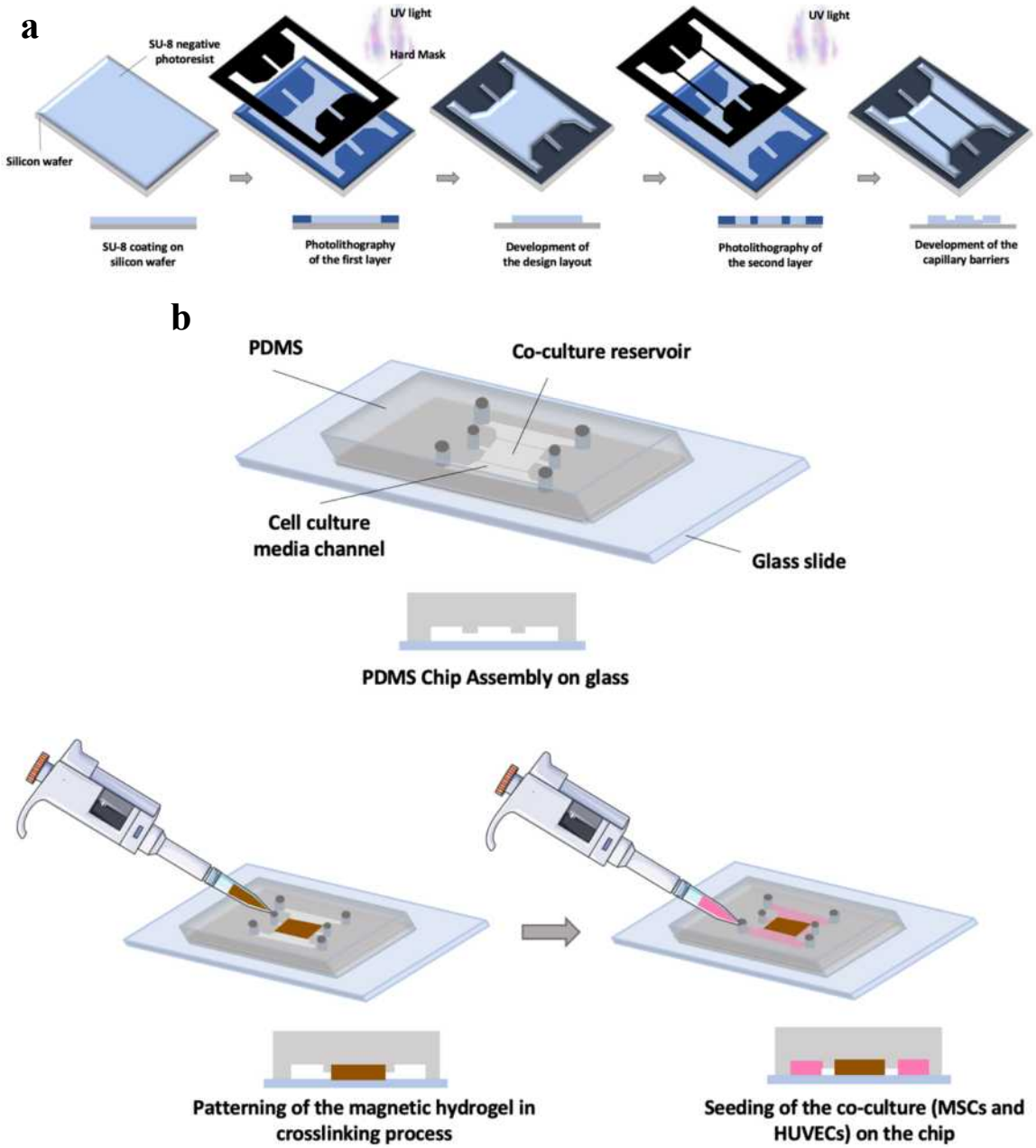


Figure VI. 2. Overview of the photolithography and soft lithography procedures, representing type III. **a)** Illustration of the photolithography process with a dashed line presenting the cross-sectional area. All other designs have identical fabrication procedures. **b)** Steps of PDMS assembly on the glass followed by patterning of the hydrogel and seeding of the co-culture of MSCs and HUVECs for type III. Type I and II have a more exhausting patterning mechanism as shown on Figure V. 1b).

3.2. Three-dimensional Single Channel Model fabrication and characterization.

The 2D microfluidic chip geometries were compared with a single-channel 3D construct fabricated through molding techniques to mimic the dimensions of larger arteries and veins (Figure VI. 3a).

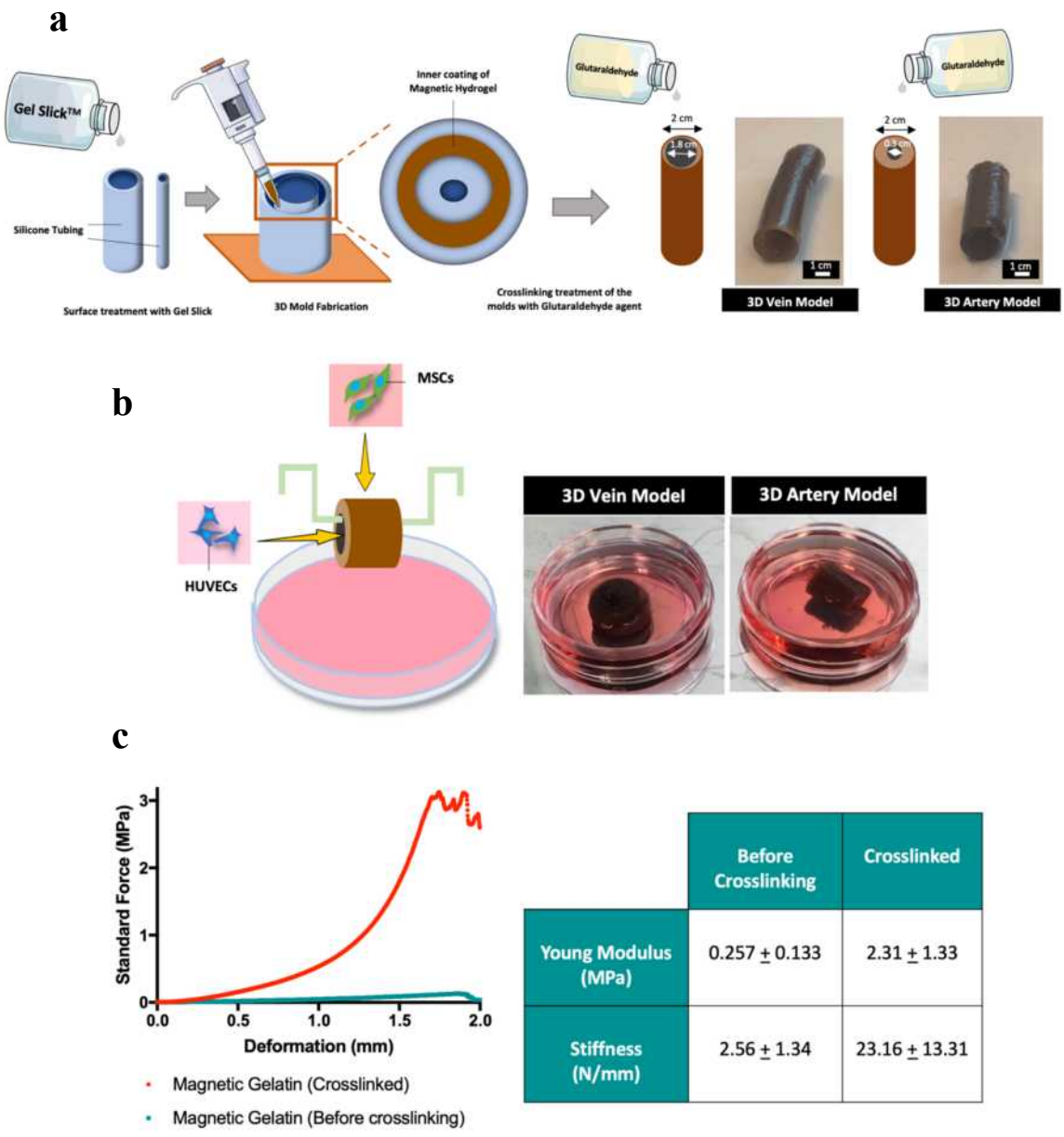
The Vein model comprised a larger inner diameter (1.8 cm) in comparison with the Artery model with 0.3 cm in the inner diameter. It was hypothesized that such changes might induce different cell responses in particular by facilitating cell migration and molecule diffusion through thinner gelatin walls on the vein model. Despite the inexistence of capillary barriers in these 3D models, MSCs were cultured on the outer wall and HUVECs were seeded on the lumen of the models to mimic biology (Figure VI. 3b). Mechanical testing of the magnetic gelatin was performed to compare the elasticity of the 3D model with the anatomic blood vessels, composed by elastin fibers (0.5 MPa[29]), smooth muscle (0.01 MPa[30]) and collagen fibers (500 MPa[29]), to ensure the suitability of the hydrogel as a blood vessel model (Figure 3c). Stress-strain curves plotting loading forces (MPa) with deformation (mm) were traced for each sample and the Young Modulus was calculated for the magnetic gelatin before crosslinking (0.257 $\pm$ 0.13 MPa) and after crosslinking procedure (2.21 $\pm$ 1.33 MPa).

Magnetic gelatin elasticity modulus obtained was higher than the elasticity modulus for elastin fibers and smooth muscle but lower than collagen fibers, suggesting the magnetic gelatin elasticity remained within the range of the native blood vessel components.

3.3. Cell Culture strategies on 2D and 3D models.

Cell culture conditions were optimized to prompt angiogenesis behavior on HUVECs and evaluated in terms of wall adherence and proliferation, migration within the channel lumen or walls, and the formation of an endothelial tissue with the development of tube-like forms (Table VI. 1). The optimization was performed using a culture of HUVECs to avoid MSCs-HUVECs interactions and eventual cell-cell inhibitions. The first optimization concerned the feeding mode: single daily renewal of the media, considered a static feeding condition, or perfusion using a syringe pump to infuse the media in the chips with a flow rate of 300 µl/h, allowing for constant renewal of the media.

Phase contrast images on 2D chips showed that, although both static and perfusion methods allowed for HUVECs adherence to the channel walls at day 2 (two days following HUVECs seeding,) a better performance was observed with the perfusion mode as it promoted a faster migration of HUVECs between compartments, starting at day 4 (Figure VI. 4a).



	Before Crosslinking	Crosslinked
Young Modulus (MPa)	0.257 ± 0.133	2.31 ± 1.33
Stiffness (N/mm)	2.56 ± 1.34	23.16 ± 13.31

Figure VI. 3. a) Molding fabrication procedures for the 3D single channel model of magnetic gelatin. **b)** Schematic representation of the cell culture on the 3D models. **c)** Representative stress-strain curves for the mechanical characterization by compression testing of the magnetic gelatin (arteries and vein models material) before and after crosslinking with glutaraldehyde. Corresponding Young Modulus values are indicated in the table.

Table VI. 1. Experimental strategies applied on 2D and 3D models to promote angiogenic behavior on HUVECs. Each model was assessed on stages of vasculogenesis based on the capacity of the HUVECs to adhere to the walls of the channels (A), the ability to migrate to the lumen region (M) and ultimately the capacity to form endothelial tissue (ET).

Experimental Strategy		3D Vein Model			3D Artery Model		
		A	M	ET	A	M	ET
Cell Concentration	MSCs ($5x10^4$ cells/ml) HUVECs ($1.5x10^5$ cells/ml)	-	-	-	-	-	-
	MSCs ($1.5x10^6$ cells/ml) HUVECs ($3x10^6$ cells/ml)	✓	-	-	✓	-	-
Feeding [HUVECs - $3x10^6$ cells/ml]	Static	✓	-	-	✓	-	-
	Perfusion	✓	-	-	✓	-	-
Experimental Time [Perfusion; HUVECs - $3x10^6$ cells/ml]	1 day	-	-	-	-	-	-
	4 days	✓	-	-	✓	-	-
	7 days	✓	-	-	✓	-	-
Stimulation of Endothelial Tissue [Perfusion; (HUVECs - $3x10^6$ cells/ml]	VEGF Supplementation	✓	-	-	✓	-	-
	Multiple HUVECs Seeding + VEGF Supplementation	✓	✓	-	✓	✓	-
Layer by Layer Structure (Additional 2D configuration) [Perfusion; HUVECs - $3x10^6$ cells/ml]		NA					

	2D Type I			2D Type II			2D Type III		
	A	M	ET	A	M	ET	A	M	ET
1	✓	✓	✓	✓	✓	✓	✓	✓	✓
2	✓	✓	✓	✓	✓	✓	✓	✓	✓
3	✓	✓	✓	✓	✓	✓	✓	✓	✓
4	✓	✓	✓	✓	✓	✓	✓	✓	✓
5	✓	✓	✓	✓	✓	✓	✓	✓	✓
6	✓	✓	✓	✓	✓	✓	✓	✓	✓
7	✓	✓	✓	✓	✓	✓	✓	✓	✓
8	✓	✓	NA	✓	✓	NA	✓	✓	NA
9	✓	✓	✓	✓	✓	✓	✓	✓	✓

This motile process of endothelial cell migration is known to be regulated by VEGF concentration gradients and is compatible with HUVECs behavior on a pre-angiogenesis stage, prior to their remodeling into tubular structures[31]. The movement of HUVECs towards the gelatin channel borderline can be explained by the increased concentration of VEGF being diffused from the cell culture media channels to the gelatin channel. HUVECs adhesion was registered on the 3D models, but no differences between static or perfusion modes (Table VI. 1).

The duration of the experiments was also analyzed (by microscopic imaging of day 1, day 4 and day 7) through viability microscopic images, using calcein staining for living cells (Figure VI. 4b). The results showed that, while in day 1 few HUVECs were attached to the magnetic gelatin walls on 3D models or 2D chips, 7 days were enough to establish a ramified monolayer of endothelial cells on 2D chip type II (Figure VI. 4b).

While type I showed the same performance, no formation of endothelial tissue was observed on type III (Table VI. 1).

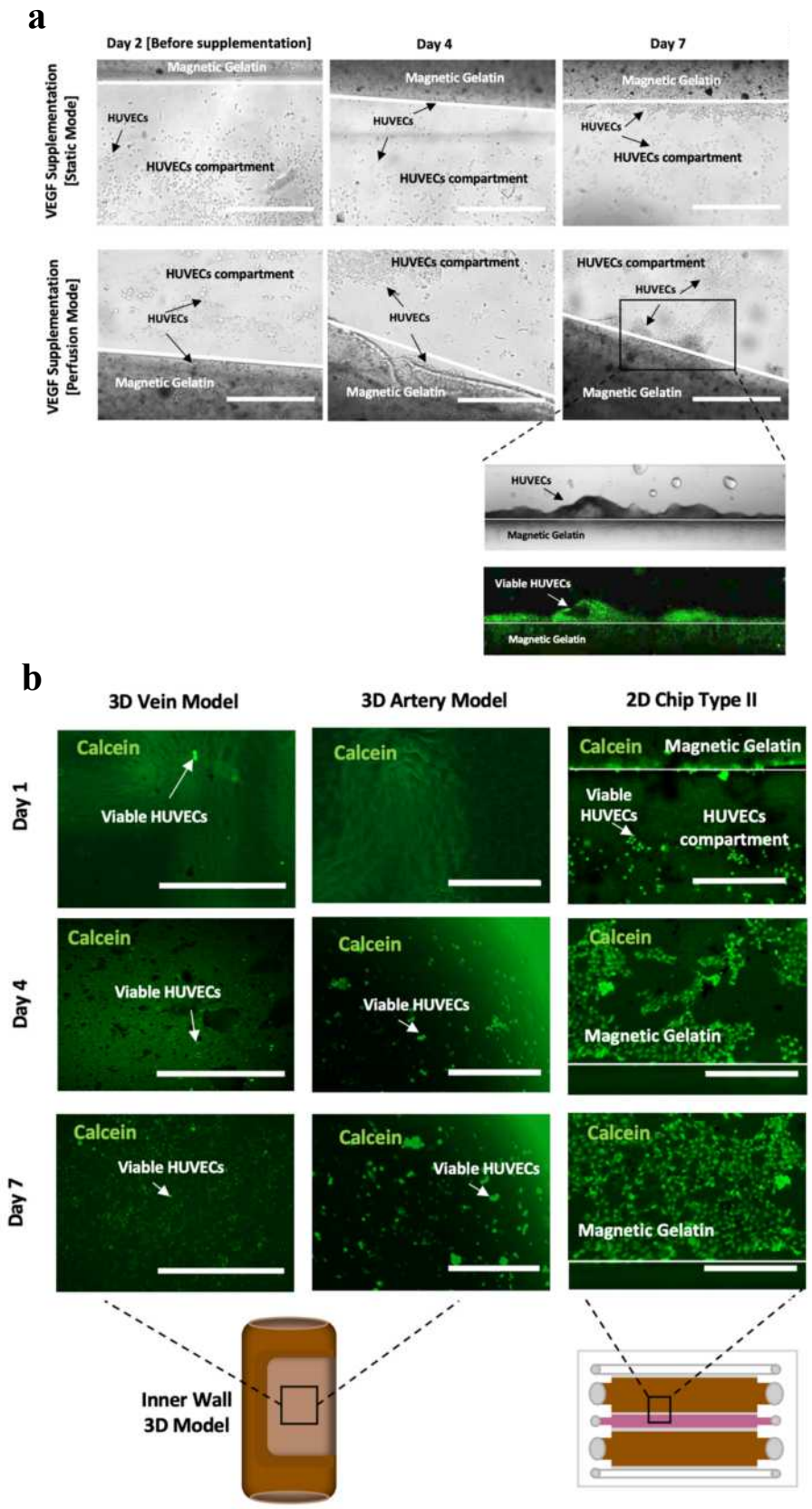


Figure VI. 4. a) Top view phase contrast images of HUVECs migration overtime before VEGF supplementation (day 2) and after supplementation (day 4 and 7) depending on the feeding mode (static or perfusion) on 2D chips. Scale bar: 1000 µm. **b)** Fluorescent imaging of viable HUVECs to assess adherence and proliferation (days 1, 4, 7) under perfusion mode for 2D and 3D models. Scale bar: 1000 µm.

Single-channel 3D models did not show further improvement after 4 days of experimental time, with the observation of some HUVECs adhered to the walls on days 4 and 7 but no signs of sprouting structures being formed (Figure VI. 4b). Possible migration into the gelatin construct was also not observed on these models (Table VI. 1). Interestingly, the 3D artery model showed poorer adhesion of HUVECs to the magnetic gelatin walls, displaying fewer cells on the inner surface in comparison with the 3D vein model (Figure VI. 4b). Regarding these outcomes, the artery model was not featured in the following experiments.

Optimization experiments concerning a co-culture MSCs and HUVECs concentration were performed during a preliminary co-culture trial. Initial lower concentration of MSCs ($5x10^4$ cells/mL) and HUVECs ($1.5x10^5$ cells/mL) resulted in a poor outcome in terms of adhesion, migration and sprouting whereas a significantly higher concentration of $1.5x10^6$ cells/mL for MSCs and $3x10^6$ cells/mL for HUVECs demonstrated overall better adhesion to the *in vitro* models (Table VI. 1).

Sequentially, some different strategies/approaches for vasculogenesis stimulation were tested and evaluated. First, the addition of VEGF daily supplementation (0.2 µg/mL) directly on the cell culture compartment on type I and II was tested to increase the gradient of this molecule on the compartment and stimulate the maturation of HUVECs into the formation of an endothelial tissue (Table VI. 1).

Contrarily to type I and II, type III did not prompt the formation of an endothelial monolayer using the strategy of VEGF supplementation (Table 1). This is possibly attributed to nutrient and VEGF transport limitations in type III, as the only source of nutrients requires the diffusion through the gelatin, where HUVECs are encapsulated. No improvement was observed on 3D models from VEGF supplementation (Table 1). Hence, this strategy alone was not efficient in triggering an angiogenic behavior on HUVECs, leading to the additional approach of seeding HUVECs every day, at a lower concentration ($3x10^4$ cells/mL), onto the HUVECs compartment in 2D chips and in the lumen of 3D models. To form endothelium the seeding process of HUVECs should be repeated often[32], therefore the strategy of VEGF supplementation was combined with multiple cell seeding to boost HUVECs performance. This combination ensured a microvascular monolayer on the channels of the chips I and II (Table VI. 1), indicating a successful proangiogenic effect with the formation of tube-like structures (Figure VI. 5a). The endothelization process was not observed using type III or the 3D models (Table VI.1). Another chip configuration featuring two layers of the same design properly

aligned and bonded together was developed to maximize the circulating volume of cell culture media within the chips and compared with traditionally fabricated chips (Type I, II, III).

The strategy of combining VEGF supplementation and HUVECs multiple seeding was evaluated using these two different configurations (Figure VI. 5b), concluding that the layer-by-layer structure promoted cell proliferation on the chip, migration behavior (cells migrated from their compartment to the gelatin channel), and progressive formation of microvascular monolayer after 7 days of the experiment.

The promising results were also observed on type III, which was not accomplished using the traditional configuration (Figure VI. 5b). This positive result was possibly derived from an easier access to nutrients and growth factor molecules to the cells since the cell culture media circulates freely on the top layer of the chip and above the cell culture layer.

The sprouting quantification was obtained, for both traditional chip and layer-by-layer structure, by analyzing three regions from independent experiments and measuring the number and length of tubes formed using ImageJ software (95% of confidence level). The analysis showed more promising results with the layered structures, with average 98 microtubes formed, in contrast with 59 average tubes quantified with traditional chips (Figure VI. 5b). Additional representative images of the results summarized in Table VI. 1 are presented in Supplementary Figure VI. 2.

3.4. VEGF diffusion and velocity profile simulations on 2D chips.

As a key molecule in the processes to trigger sprouting and promote vasculogenesis, the present work involves several strategies to increase the supply of the VEGF molecule (molecular weight: 40 kDa[26]) to the HUVECs and thus stimulate HUVECs maturation. Consequently, vessel permeability regarding the diffusion of VEGF through the channels of 2D models was predicted in computational models using COMSOL software (Figure VI. 6a).

The vessel permeability was computed assuming the diffusivity coefficients for VEGF in water, representing the cell culture media, and in the hydrogels (gelatin and matrigel), assuming a similar diffusivity to the collagen, which is reported in the literature.

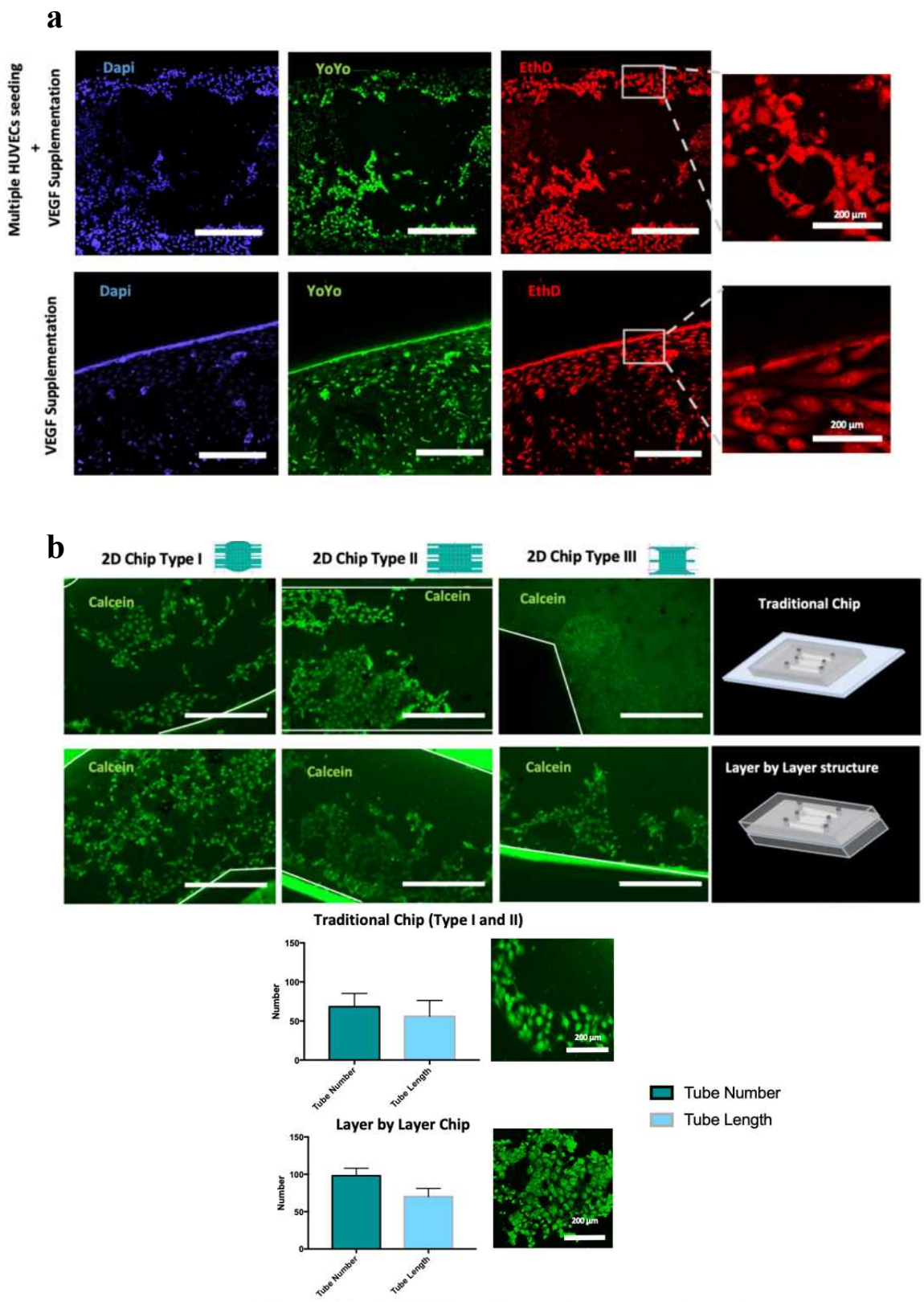


Figure VI. 5. a) Confocal imaging (Dapi, YoYo, EthD) of endothelial tissue and sprout ramifications for 2D chips Type II (7 days, perfusion mode) using VEGF supplementation strategy. Comparison with the strategy combining VEGF supplementation and multiple HUVECs seeding. Scale bar: 1000 µm. **b)** Characterization of viable HUVECs proliferation and tissue formation after 7 days using traditional one-layer configuration and layer-by-layer chip (for all three types) under perfusion, VEGF supplementation and HUVECs multiple seeding conditions. Scale bar: 1000 µm. Dashed line represents the quantification of tube number and tube length, for each configuration.

The simulation represented the initial stage of the process, assuming only the VEGF concentration in the media (1 μg/mL, 2.5 x 10^{-5} mol/m^3), and diffused from the media channels. Therefore, the VEGF supplemented directly in the HUVECs reservoir from experimental day 2 onwards was not assumed here. The residual VEGF released from MSCs at the co-culture stage is also not included in the simulated model. The simulation results for the transport of VEGF within the channels showed that, despite the hydrogel patterning, the VEGF molecule was able to diffuse into the HUVECs compartment in all the types, highlighting however a similar behavior with type I and II but a faster diffusion with type III.

Although VEGF posterior supplementation or secreted from MSCs during co-culture was not considered in the simulation, it was nonetheless quantified in the experimental validation of the computational models. The experimental validation was obtained by quantifying the total amount of VEGF present on the depleted streams of the chips after 7 days using Human VEGF-A ELISA (Enzyme-linked Immunosorbent Assay) (Figure VI. 6b). The VEGF quantification was accompanied by a scheme showing the differences in the obtainment of the depleted stream accordingly with the mechanism of each type (Figure VI. 6b). Interestingly, the quantification of VEGF showed a slight increase in type I, in comparison with type II. As the concentration of the daily supplementation was identical between types, the changes might be explained by the geometry of the types, suggesting an easier diffusion to the hydrogel channel due to the angular shape of the media channel on type I.

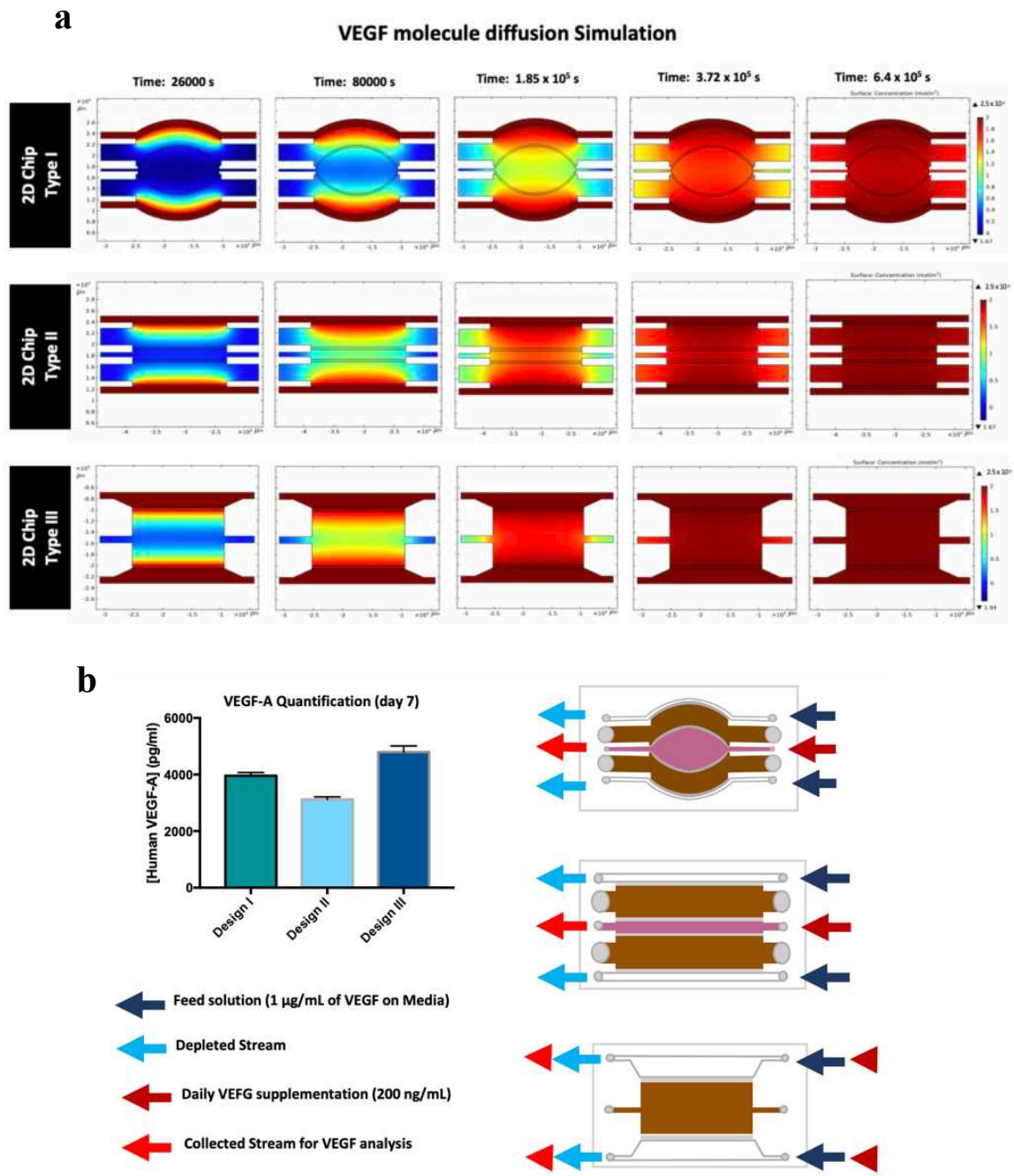
Even though the VEGF concentration values were not comparable, the experimental validation confirmed that VEGF was transported through the HUVECs reservoir to the depleted stream for types I and II. For type III, the depleted stream corresponds to the same media flow channel where the VEGF was infused, impairing the measurement of the actual concentration diffused to the HUVECs. This also explains the higher VEGF concentration measured on type III which did not translate into better angiogenic performance, as shown on images of Figure VI. 5b.

The linear velocity on the media channels was also simulated on COMSOL software, once more emphasizing the similarities in the performances of type I and II while indicating a lower velocity profile on type III (Figure VI. 6c).

To simplify the simulation, only the media channels were considered as it was assumed that no media was perfused inside the HUVECs compartment due to the

existence of Matrigel patterning in the compartment, even though experimentally the thickness of the hydrogel coating allows for perfusion though the compartment.

The experimental validation for the simulation of the linear velocity was achieved adding fluorescent microbeads (15 µm) to a buffer solution to the chips and perfusing the solution into the media flow channels of the chips to track the path of the microbeads using initial flow rate of 300 µL/h. The tracking of the microbeads in different regions of the media channels allowed for the calculation of the average velocity within the channels using manual tracking analysis on ImageJ.



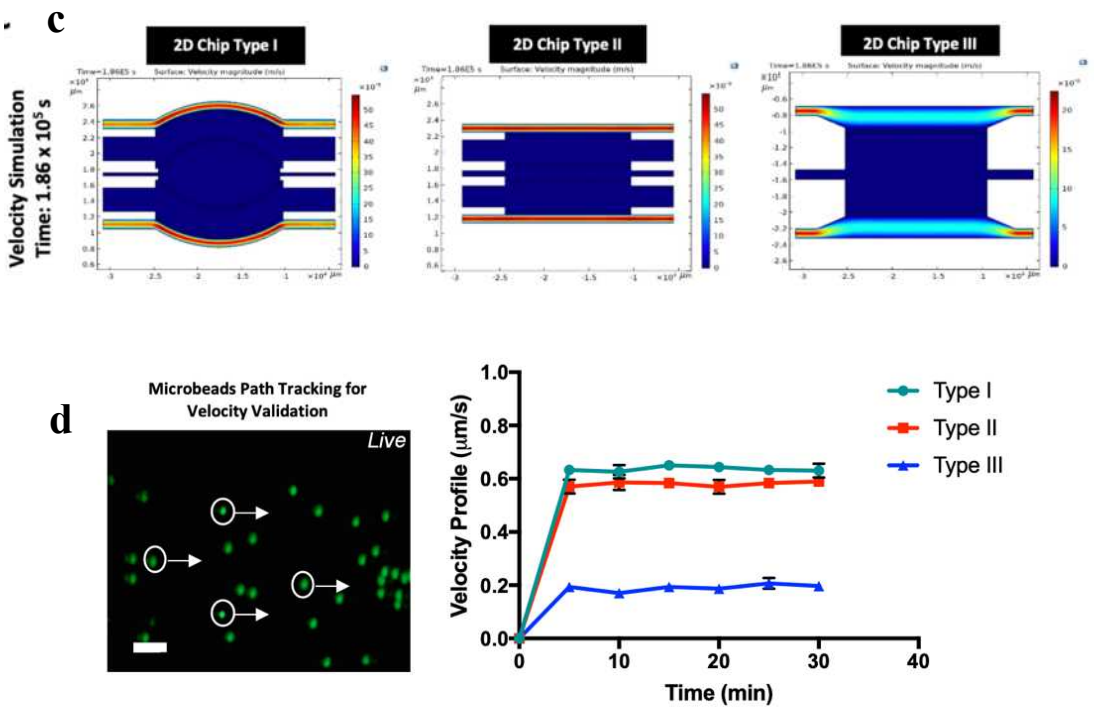


Figure VI. 6. a) Computational models of 2D chips for VEGF time-dependent diffusion from the media channels to the endothelial cell (HUVECs) culture compartment through the hydrogels. The sequential images of the VEGF diffusion are presented with a contour plot of the surface concentration of VEGF inside the chips. In the simulation, only VEGF contained on the cell culture media was considered while VEGF supplementation and VEGF secreted from MSCs culture were not included. **b)** Validation of the VEGF diffusion model with the quantification of the concentration of VEGF obtained on the collected stream for the analysis using ELISA quantification kit. The depleted stream for VEGF analysis was dependent on the geometries as shown on the schematic design representation. **c)** Computational fluid flow modeling to predict linear velocities distribution within the 2D media channels. **d)** Validation of the prediction model using green fluorescence microbeads (15 µm) was used to trace velocity profiles for the 2D chips. Microbeads tracking velocity was obtained using ImageJ software with experimental flow velocity of 300 µL/h. Tracking analysis was performed on three points of the channel for each design. Scale bar: 100 µm.

The results associated an average velocity of 0.67, 0.55 and 0.2 µm/s to type I, II and III, respectively, providing coherence with the computational simulation. Details of the computational simulations are presented in Supplementary Figure VI. S3.

3.5. Co-culture and magnetic stimulation.

As a proof of concept, a combination of the best conditions to promote endothelialization (7 days, perfusion, VEGF supplementation and multiple HUVECs seeding), types (I and II) and 3D models (Vein model) were selected for implementing

the MSCs and HUVECs co-culture while applying magnetic stimulation (0.08 T) over the last 24h of the experiment (day 6).

On 3D models, confocal imaging of the lumen, the cross-section and the outer wall showed the ability of the cells to populate the three regions of the 3D structure. However, the formation of an endothelial monolayer, representing the initial stages of an endothelial tissue, was only observed after the application of the magnetic field on the vein model whereas the artery model showed individualized cells throughout the observation areas (Figure VI. 7a).

On 2D chips, no significant differences were obtained on different types of chips, therefore only representative images were presented in Figure VI. 7b, c, d. Live (green Calcein) and dead (red EthD) markers revealed increased cell death on the chips not exposed to the magnetic stimulation in comparison with the magnetically stimulated cultures (Figure VI. 7b). Additionally, the cell death observed in the gelatin channel (Figure VI. 7b) might be attributed to MSCs-HUVECs inhibitions despite the initial seeding of the cells on different compartments. This contact between MSCs and HUVECs possibly originated from cell migration between channels, as observed on the images in Figure VI. 7b for the non-exposed condition.

Surprising results were obtained on magnetic stimulated chips with the observation of reduced cell death and viable cells populating the channels (Figure VI. 7b), added to the formation of an interconnected endothelial monolayer, which was not present on chips not exposed to the magnetic field (Figure VI. 7c).

Immunostaining using specific HUVECs antibody (CD31) and Dapi (marker for HUVECs and MSCs) was used to distinguish between the colonies of HUVECs and MSCs on 2D chips (Figure VI. 7d). The results allowed to observe that, while the HUVECs compartment was mostly populated by HUVECs, with cells simultaneously marked by Dapi and CD31, the gelatin channel presented some few HUVECs (marked by Dapi and Dapi) mixed with MSCs (marked only by Dapi). This observation confirmed the discussed motility of the HUVECs between the channels despite the efficiency of the capillary barriers to confine MSCs on the gelatin channel.

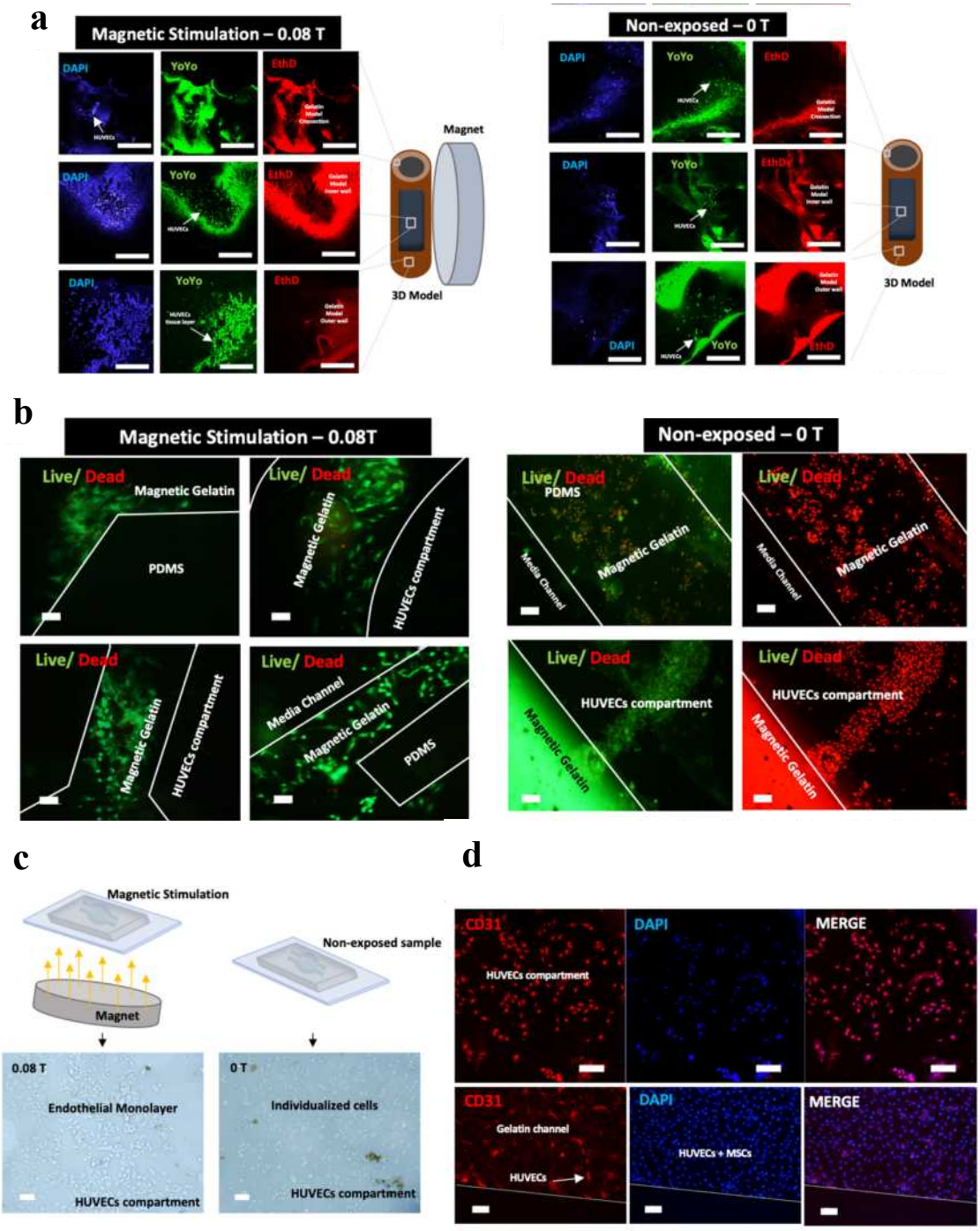


Figure VI. 7. a) Confocal imaging (Dapi, YoYo and EthD) of MSCs and HUVECs co-culture (day 7) on the 3D models. A magnetic field (0.08 T) was applied on day 6 for a total exposure of 24 h. and directly compared with non-exposed samples (control) Scale bar: 1000 µm. **b)** Live and dead (Calcein and EthD) representative images of 2D chips (Type I) in a co-culture of MSCs and HUVECs exposed to magnetic stimulation (0.08 T) on the last 24h of the experiment (7 days) and compared with non-exposed samples. Scale bar: 100 µm. **c)** Phase contrast images of the endothelialization on HUVECs compartment at day 7 after magnetic stimulation and comparison with the control condition. Scale bar: 100 µm. **d)** Immunofluorescence images (CD31 and Dapi) of the co-culture to distinguish between the population of HUVECs and MSCs. Scale bar: 100 µm.

3.6. Endothelin-1 secretion by HUVECs on 2D and 3D models.

Endothelin-1 is a vasoconstrictor secreted by endothelial cells and enhanced by physical factors (such as shear stress or growth factors) whose effects are regulated through inhibition or stimulation of endothelin-1 release directly from the endothelium[33]. As a main regulator of the vascular function, the presence of this molecule on the chips and 3D models was assessed and quantified using Endothelin-1 ELISA (Figure VI. 8) to confirm the endothelium formation.

The effect of static mode and perfusion on the secretion of Endothelin-1 on 2D chips and 3D models showed a significant increase in concentration of Endothelin-1 through perfusion mode on 2D chips while 3D models did not present significant changes (Figure VI. 8a). The ultimate effect of the strategies to increase the supply of growth factor VEGF to the chips were analyzed in terms of the presence of Endothelin-1 molecule in the media collected from each condition of analysis.

The results revealed a positive increase after HUVECs daily seeding, similarly to the VEGF supplementation strategy on traditional fabrication chips, which also resulted in a slight increase in Endothelin-1 secretion (Figure VI. 8b).

The most prominent result however was obtained with the layered fabrication technique, which resulted in a significant increase on the secretion of Endothelin-1 in comparison with all other conditions. Additionally, this increment was accentuated upon combination with VEGF supplementation, highly boosting the secreting of the vascular regulator molecule (Figure VI. 8b).

Finally, magnet stimulation (0.08 T) was applied on the models over the last 24h of the experiment (at day 6), a positive magnetic effect was demonstrated on both 2D and 3D models through the increase in the concentration of endothelin-1 molecule in the media, observed as a significant difference between day 6 and day 7 (Figure VI. 8c). The increased concentration of endothelin-1 upon magnetic stimulation thus reveals the importance of the low intensity static magnetic exposure to trigger angiogenic mechanisms and to the overall endothelization of tissues without further need to implement strategies for VEGF supplementation.

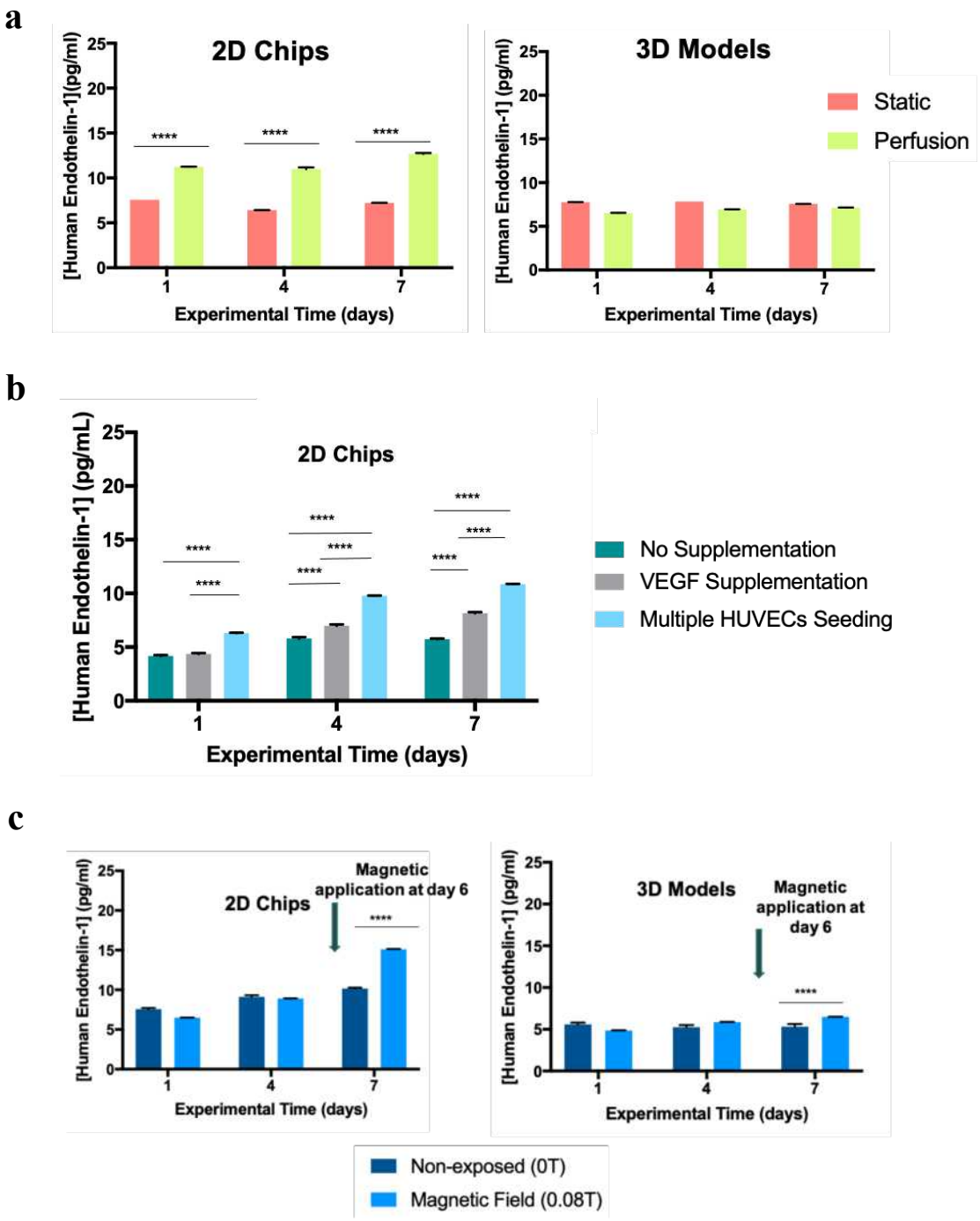


Figure VI. 8. a) Quantification of Endothelin-1 on 2D chips (Type I, II) and 3D models comparing the effects of static and perfusion mode on the stimulation of endothelium tissue formation. No magnetic field was applied in this comparison. **b)** Impact of the different tested strategies using perfusion mode to improve endothelial tissue formation on the 2D Chips (multiple HUVECs seeding to boost sprouting or VEGF daily supplementation) without magnetic stimulation, combined with the evaluation of the impact of different fabrication techniques (Layer by Layer structure and traditional one-layer fabrication) on the increase of Endothelin-1 concentration. No magnetic field was applied on these conditions. **c)** Representation of the concentration of Endothelin-1 molecule derived from magnetic stimulation applied on the last day of the experiment on 2D Chips (Type I and II) and 3D Models using perfusion mode. Non-exposed samples were used as a control (0 T). No strategies for VEGF supplementation (multiple HUVECs seeding and daily VEGF supplementation) were followed during these experiments with magnetic application.

VI.4. Discussion

This work focused on the development of blood vessel platforms to promote angiogenic behavior on HUVECs, through vasculogenesis in the formation of a microvessel monolayer, hoping to envision novel treatments to reverse tissue damage in cardiovascular conditions such as cardiac ischemia. A comparison between the angiogenic performance of 2D chips under three different geometries (I, II, III) and 3D models with different inner diameters to mimic larger arteries and veins was studied. Artery and vein 3D models were fabricated in magnetic gelatin, containing 1% of MNPs, and crosslinked to ensure the model survival throughout the experimental time under perfusion. However, the mechanical compression results showed a significantly higher elasticity modulus on the crosslinked magnetic gelatin (2.31 $\pm$ 1.33 MPa) in contrast with the young modulus of the components of blood vessels (collagen, elastin and smooth muscle), on the order of the few MPa (Figure VI. 3c). Non-crosslinked magnetic gelatin (Figure VI. 3c) presented a lower young modulus (0.257 $\pm$ 0.133 MPa) but still higher than the elasticity of native blood vessel walls, on the order of few MPa. Modifications in the mechanical properties of arteries have been associated with various diseases of aging, including coronary heart disease and atherosclerosis, where a higher thickness is associated with increased stiffness of carotid arteries[34,30].

Stolz *et al.*[35] have demonstrated that in diseased tissue, the decline in cartilage begins at the molecular level and results in structural and functional damage. Therefore, in using magnetic gelatin we were simulating a diseased blood vessel, which might have compromised HUVECs affinity and adhesion. This fact might have impaired the angiogenic stages of the vascularization process in the 3D models, resulting in the overall failure of those models. Furthermore, better results were obtained with the 3D vein model probably due to the reduced wall thickness, which might have contributed for better cell adhesion and to facilitate molecule diffusion between outer and inner walls while enabling cell migration (Figure VI. 6a).

Alternatively, 2D chips (in particular type I and II) performed successfully after some optimization on the experimental conditions. The angular geometry of type I seemed to have a slightly beneficial effect on the diffusion of VEGF to the HUVECs compartment and velocity profiles over type II (Figure VI. 6b) yet both types offered promising angiogenic results in comparison with type III (Figure VI. 5b). Type III revealed a poor performance in this report due to its configuration, which hampered the

access of cell culture media, and nutrients, to the single cell culture reservoir (Figure VI. 5c) while also forcing a direct contact on MSCs and HUVECs co-culture, and making it impossible to have a matrigel coating suitable for HUVECs adhesion, which has been exhaustively described as a beneficial hydrogel to promote angiogenesis[36].

Sprouting angiogenesis is conditioned by the migration of endothelial progenitor cells to the injury site and by the release of vascular endothelial growth factors (VEGF) to prompt endothelial progenitor cell proliferation and differentiation into capillary[37,38]. Here several strategies were used to prompt vasculogenesis on the chips while the capacity of the cells to adhere and proliferate on the chips, the migration activity, and ultimately the formation of a microvessel monolayer of human umbilical vein endothelial cells (HUVECs) were assessed as key factors in the vasculogenesis phenomena developmental stage. In particular, the observed HUVECs migration (Figure VI. 4a) and MSCs migration on the co-culture experiments non-exposed to magnetic influence (Figure VI. 7b) seemed to be dependent on the flow diffusion and VEGF gradient, confirming some reports on the biological effect of VEGF-guidance in angiogenic sprouting of HUVECs[39,40] and VEGF-induced migration of MSCs to injury sites and hypoxic tissues[41].

The importance of the free access to nutrients in the culture media was highlighted by the development of layer-by-layer structure (with flowing media circulating on the top layer of the construct), which showed better performance on vasculogenesis development (Figure VI. 5b) and on the secretion of molecule Endothelin-1, as a consequence of increased endothelium formation (Figure VI. 8b). This could possibly be attributed to a higher volume of cell culture media flowing through every compartment and changes in shear stress, which are described to be associated with HUVECs stimulation and angiogenic sprouting[42].

Mostly, the success of the concept after the co-culture with MSCs and HUVECs was based on their selective separation by trapping hydrogels mixtures (magnetic gelatin and matrigel) on different compartments via capillary line pinning technique (Figure VI. 7d). As described in previous studies, the direct contact of MSCs and HUVECs could result in angiogenesis inhibition through the miR-211/Prox1 pathway[43] or through cytotoxic effects of MSCs towards HUVECs[44]. In fact, major cell death was observed in the regions where MSCs and HUVECs were in colonies subsequent to MSCs migration from the magnetic hydrogel compartment to the HUVECs reservoir (Figure VI. 6b). Yet, MSCs are able to efficiently mediate angiogenesis behavior on HUVECs via paracrine

mechanisms through the release of growth factors such as VEGF-A[45,46]. This secretory activity has been reported several times in the literature[47,48,49], thus justifying MSCs choice for the co-culture on the blood vessel models. Our group has previously described the increased angiogenic potential of MSCs growing on magnetic gelatin by exposure to a low-intensity magnetic field. The effect was ascribed to the stimulation of the paracrine activity of MSCs represented by VEGF release upon mechanotransduction stress induced by magnetic forces. Here, we observed a positive influence of the magnetic forces on the formation of a microvessel structure on the channels by HUVECs both on 2D and 3D models (Figure VI. 8c), with increased release of endothelin-1 molecule. Accordingly, the advantages in culturing MSCs on the chips to offer additional secretion of growth factors into the flowing media towards the HUVECs compartment were mostly successfully implemented through the separation with capillary barriers as an ideal solution to minimize the contact between cell types.

Ultimately, with this study we were able to explore the effect of geometry, mechanical stiffness, molecule diffusion, magnetic stimulation, shear stress and fabrication techniques on the optimization and simulation of biological features to induce vasculogenesis in *in vitro* blood vessel platforms suitable for cardiovascular disease modeling.

VI.5. Conclusions

In this study, we investigated the performance of *in vitro* 2D chips and 3D models of arteries and veins, aiming to induce HUVECs maturation and stimulate angiogenesis for cardiovascular disease modeling. Experimental conditions were designed to sustain cell adhesion and a viable cell culture while providing an increased supply of growth factor VEGF to the HUVECs culture compartment. A platform of functional conditions was devised including feeding mode (perfusion, 300 µl/h), experimental time (7 days), cell concentration (MSCs: $1.5x10^6$ cells/mL; HUVECs: $3x10^6$ cells/mL), and VEGF supply strategy (VEGF daily supplementation combined with daily HUVECs seeding). While the performance of 3D models was possibly impaired by the structure's high mechanical stiffness, similar to a diseased tissue, 2D chips offered promising results on the stimulation of HUVECs angiogenic behavior triggered by the magnetic stimulation effect on a co-culture with MSCs. Magnetic gelatin was patterned on the 2D chips to provide biocompatible support for MSCs growth while targeting the magnetic forces to the cells

through magnetic compounds (ferromagnetic nanoparticles), alongside a coating of matrigel for HUVECs support. Regarding 2D chips efficiency, the geometry, VEGF supply mechanism, and fabrication procedures demonstrated differences in the cell behavior, allowing to define the best geometries for VEGF diffusion mechanisms (type I and II) and highlighting the potential of the layer-by-layer configuration instead of traditional fabrication methods to achieve the desired sprouting effect. Ultimately, our study revealed a promising platform for the simulation of cardiovascular conditions such as the development of cardiac ischemia disease modeling while applying the explored angiogenesis-inducing tools to potentially provide novel treatment options by reversing blood vessel tissue damage.

VI.6. References

1. Abhishek, S. As featured in : Lab on a Chip. (2019). doi:10.1039/c9lc00469f
2. Bracken, M. B. Why animal studies are often poor predictors of human reactions to exposure. *J. R. Soc. Med.* **102**, 120–122 (2009).
3. Matsumoto, T., Sugita, S. & Yaguchi, T. Biomechanics of Blood Vessels: Structure, Mechanics, and Adaptation. in 71–98 (2015). doi:10.1007/978-3-662-46836-4_4
4. Hasan, A., Paul, A., Memic, A. & Khademhosseini, A. A multilayered microfluidic blood vessel-like structure. *Biomed. Microdevices* **17**, 88 (2015).
5. Gagnon, E. *et al.* Human vascular endothelial cells with extended life spans: In vitro cell response, protein expression, and angiogenesis. *Angiogenesis* **5**, 21–33 (2002).
6. Smith, Q. & Gerecht, S. Microfluidic Platforms in Vascular Tissue Engineering. *Curr Opin Chem Eng* 42–50 (2015). doi:10.1016/j.coche.2013.11.001.Going
7. Miri, A. K. *et al.* Multiscale bioprinting of vascularized models. *Biomaterials* **198**, 204–216 (2018).
8. Kim, S., Kim, W., Lim, S. & Jeon, J. S. Vasculature-on-a-chip for in vitro disease models. *Bioengineering* **4**, (2017).
9. Zhang, W. *et al.* Elastomeric free-form blood vessels for interconnecting organs on chip systems. *Lab Chip* **16**, 1579–1586 (2016).
10. Chiu, D. T. *et al.* Small but Perfectly Formed? Successes, Challenges, and Opportunities for Microfluidics in the Chemical and Biological Sciences. *Chem* **2**, 201–223 (2017).
11. Yasotharan, S., Pinto, S., Sled, J. G., Bolz, S. S. & Günther, A. Artery-on-a-chip platform for automated, multimodal assessment of cerebral blood vessel structure and function. *Lab Chip* **15**, 2660–2669 (2015).
12. Kim, S., Lee, H., Chung, M. & Jeon, N. L. Engineering of functional, perfusable 3D microvascular networks on a chip. *Lab Chip* **13**, 1489–1500 (2013).
13. Gumuscu, B., Albers, H. J., Van Den Berg, A., Eijkel, J. C. T. & Van Der Meer, A. D. Compartmentalized 3D Tissue Culture Arrays under Controlled Microfluidic Delivery. *Sci. Rep.* **7**, 1–9 (2017).
14. Tibbe, M. P., Leferink, A. M., van den Berg, A., Eijkel, J. C. T. & Segerink, L. I.

Microfluidic Gel Patterning Method by Use of a Temporary Membrane for Organ-On-Chip Applications. *Adv. Mater. Technol.* **3**, 1–6 (2018).

15. Manjua, A. C., Alves, V. D., Crespo, J. G. & Portugal, C. A. M. Magnetic Responsive PVA Hydrogels for Remote Modulation of Protein Sorption. *ACS Appl. Mater. Interfaces* acsami.9b03146 (2019). doi:10.1021/acsami.9b03146
16. Gumuscu, B. *et al.* Desalination by Electrodialysis Using a Stack of Patterned Ion-Selective Hydrogels on a Microfluidic Device. *Adv. Funct. Mater.* **26**, 8685–8693 (2016).
17. Gumuscu, B., Bomer, J. G., Van Den Berg, A. & Eijkel, J. C. T. Large scale patterning of hydrogel microarrays using capillary pinning. *Lab Chip* **15**, 664–667 (2015).
18. Wang, X., Sun, Q. & Pei, J. Microfluidic-based 3D engineered microvascular networks and their applications in vascularized microtumor models. *Micromachines* **9**, 1–26 (2018).
19. Ferreira, J. R. *et al.* Mesenchymal Stromal Cell Secretome: Influencing Therapeutic Potential by Cellular Pre-conditioning. *Front. Immunol.* **9**, 2837 (2018).
20. Johnson, K. E. & Wilgus, T. A. Vascular Endothelial Growth Factor and Angiogenesis in the Regulation of Cutaneous Wound Repair. *Adv. Wound Care* **3**, 647–661 (2014).
21. Schubert, M. *et al.* VEGF expression by mesenchymal stem cells contributes to angiogenesis in pancreatic carcinoma. *Br. J. Cancer* **99**, 622–631 (2008).
22. Ge, Q. *et al.* VEGF secreted by Mesenchymal stem cells mediates the differentiation of endothelial progenitor cells into endothelial cells via paracrine mechanisms. *Mol. Med. Rep.* **17**, 1667–1675 (2018).
23. Jeon, J. S. *et al.* Generation of 3D functional microvascular networks with mural cell-differentiated human mesenchymal stem cells in microfluidic vasculogenesis systems. *Integr. Biol.* **100**, 130–134 (2012).
24. Cruz-Izquierdo, Á., Picó, E. A., López, C., Serra, J. L. & Llama, M. J. Magnetic Cross-Linked Enzyme Aggregates (mCLEAs) of Candida antarctica lipase: An efficient and stable biocatalyst for biodiesel synthesis. *PLoS One* **9**, 1–22 (2014).
25. Dos Santos, F. *et al.* Ex vivo expansion of human mesenchymal stem cells: A more effective cell proliferation kinetics and metabolism under hypoxia. *J. Cell. Physiol.* **223**, 27–35 (2010).

26. Holmes, D. I. R. & Zachary, I. The vascular endothelial growth factor (VEGF) family: angiogenic factors in health and disease. *Genome Biol.* **6**, 209 (2005).
27. Young, M. E., Carroad, P. A. & Bell, R. L. Estimation of diffusion coefficients of proteins. *Biotechnol. Bioeng.* **22**, 947–955 (1980).
28. Ramanujan, S. *et al.* Diffusion and convection in collagen gels: Implications for transport in the tumor interstitium. *Biophys. J.* **83**, 1650–1660 (2002).
29. Vosse, V. Der. Mechanics of the vessel wall. *Cardiovascular Fluid Mechanics* 51–61
30. Akhtar, R., Sherratt, M. J., Cruickshank, J. K. & Derby, B. Characterizing the elastic properties of tissues. *Mater. Today* **14**, 96–105 (2011).
31. Laurent, L., Fabrice, L. B. & Jacques, H. Endothelial Cell Migration During Angiogenesis. *Circ. Res.* **100**, 782–794 (2007).
32. Zhang, W. *et al.* Elastomeric free-form blood vessels for interconnecting organs on chip systems. *Lab Chip* **16**, 1579–1586 (2016).
33. Marasciulo, F. L. & Potenza, M. M. and M. A. Endothelin-1: The Yin and Yang on Vascular Function. *Current Medicinal Chemistry* **13**, 1655–1665 (2006).
34. Ebrahimi, A. P. Mechanical properties of normal and diseased cerebrovascular system. *J. Vasc. Interv. Neurol.* **2**, 155–162 (2009).
35. Stolz, M. *et al.* Early detection of aging cartilage and osteoarthritis in mice and patient samples using atomic force microscopy. *Nat. Nanotechnol.* **4**, 186–192 (2009).
36. Skovseth, D. K., Küchler, A. M. & Haraldsen, G. The HUVEC/Matrigel Assay BT - Target Discovery and Validation Reviews and Protocols: Volume 1, Emerging Strategies for Targets and Biomarker Discovery. in (ed. Sioud, M.) 253–268 (Humana Press, 2007). doi:10.1385/1-59745-165-7:253
37. Sarker, M. D., Naghieh, S., Sharma, N. K. & Chen, X. 3D biofabrication of vascular networks for tissue regeneration: A report on recent advances. *J. Pharm. Anal.* **8**, 277–296 (2018).
38. Pauty, J. *et al.* A Vascular Endothelial Growth Factor-Dependent Sprouting Angiogenesis Assay Based on an In Vitro Human Blood Vessel Model for the Study of Anti-Angiogenic Drugs. *EBioMedicine* **27**, 225–236 (2017).
39. Liu, L., Ratner, B. D., Sage, E. H. & Jiang, S. Endothelial Cell Migration on Surface-Density Gradients of Fibronectin, VEGF, or Both Proteins. *Langmuir* **23**, 11168–11173 (2007).

40. Gerhardt, H. VEGF and Endothelial Guidance in Angiogenic Sprouting BT - VEGF in Development. in (ed. Ruhrberg, C.) 68–78 (Springer New York, 2008). doi:10.1007/978-0-387-78632-2_6
41. Ke, C., Chen, J., Guo, Y., Chen, Z. W. & Cai, J. Migration mechanism of mesenchymal stem cells studied by QD/NSOM. *Biochim. Biophys. Acta - Biomembr.* **1848**, 859–868 (2015).
42. Galie, P. A. *et al.* Fluid shear stress threshold regulates angiogenic sprouting. *Proc. Natl. Acad. Sci. U. S. A.* **111**, 7968–7973 (2014).
43. Pan, J., Wang, X., Li, D., Li, J. & Jiang, Z. MSCs inhibits the angiogenesis of HUVECs through the miR-211/Prox1 pathway. *J. Biochem.* **166**, 107–113 (2019).
44. Otsu, K. *et al.* Concentration-dependent inhibition of angiogenesis by mesenchymal stem cells. *Blood* **113**, 4197–4205 (2009).
45. Brewster, L. *et al.* Expansion and angiogenic potential of mesenchymal stem cells from patients with critical limb ischemia. *J. Vasc. Surg.* **65**, 826-838.e1 (2017).
46. Javan, M. R., Khosrojerdi, A. & Moazzeni, S. M. New Insights Into Implementation of Mesenchymal Stem Cells in Cancer Therapy: Prospects for Anti-angiogenesis Treatment. *Front. Oncol.* **9**, 840 (2019).
47. Ge, Q. *et al.* VEGF secreted by mesenchymal stem cells mediates the differentiation of endothelial progenitor cells into endothelial cells via paracrine mechanisms. *Mol. Med. Rep.* **17**, 1667–1675 (2018).
48. Ahn, S. Y. *et al.* Vascular endothelial growth factor mediates the therapeutic efficacy of mesenchymal stem cell-derived extracellular vesicles against neonatal hyperoxic lung injury. *Exp. Mol. Med.* **50**, 26 (2018).
49. Tao, H., Han, Z., Han, Z. C. & Li, Z. Proangiogenic Features of Mesenchymal Stem Cells and Their Therapeutic Applications. *Stem Cells Int.* **2016**, 1314709 (2016).

Chapter IV. Supplementary Information

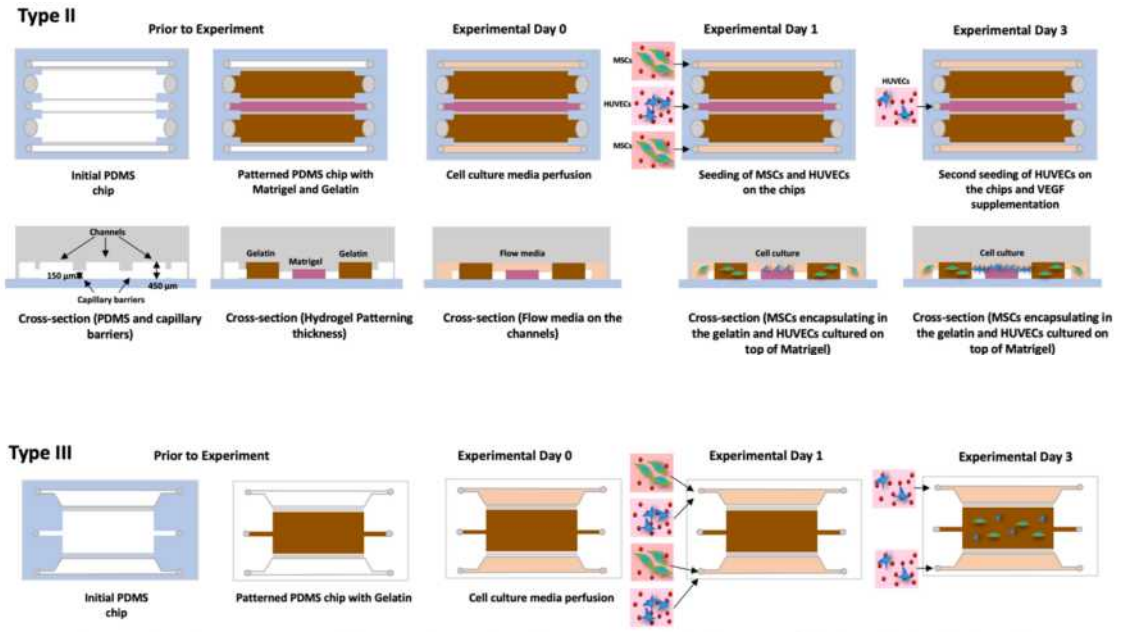


Figure VI. S1. Schematic representation of the sequential steps of the first days of experiment, including the patterning of the chips with hydrogels (gelatin and matrigel), the cell culture pre-conditioning and the cell seeding on the chips type II and III.

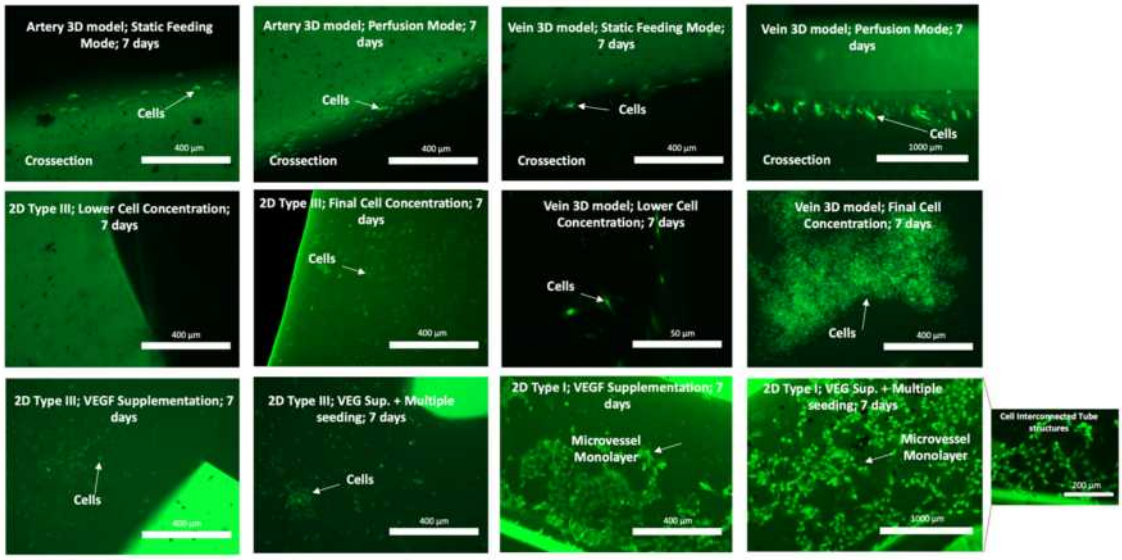


Figure VI. S2. Fluorescence Imaging (Calcein staining of viable cells) for the optimization procedures described in Table 1, featuring the representative images for the effects reported with the different strategies on 3D models and 2D chips.

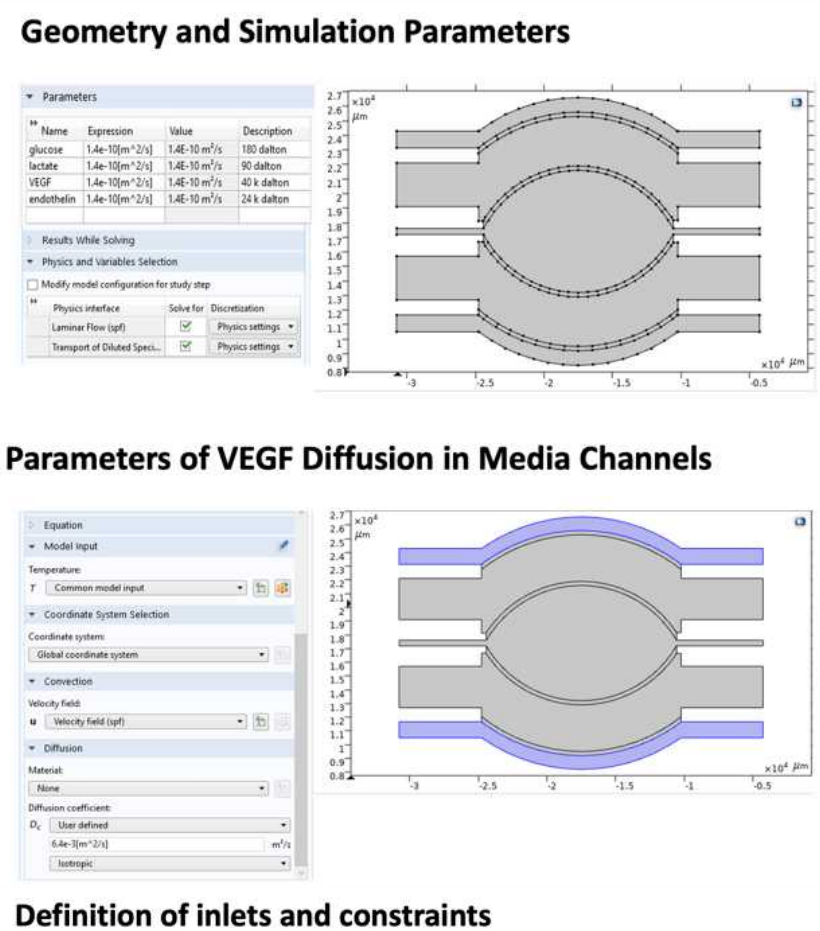


Figure VI. 3. Parameters and assumptions of the computational model for VEGF diffusion on 2D chips Type I. Identical parameters were applied for Type II and III.

Chapter VII



Cardiac Ischemia Disease modelling In Magnetic *In Vitro* Models Of Vascular Network

(Conceptual Chapter with Preliminary Results)

CHAPTER VII – Cardiac ischemia disease modeling in magnetic *in vitro* models of vascular network

The present chapter compares the performance of 2D blood vessels models with two novel models. The study aims to induce ischemia disease modeling on the chips followed by reoxygenation/ reperfusion under magnetic stimulation to revert the ischemic damage. Some parts of the experimental section are still conceptual.

Outline

Ischemic heart disease, or myocardial ischemia, is one of the main causes of sudden cardiac death, and the most common cardiovascular disease. Therefore, basic and translational research is required to better understand the underlying biological mechanisms of these conditions as well as its consequences for cardiac structure and function. Developing experimental models to study ischemic heart disease is necessary for a better understanding of the biological mechanisms required to improve the therapeutic approaches and restore tissue function following injury. The aim of this study is to develop an *in vitro* hypoxic/re-oxygenation model to simulate the ischemic condition while comparing the performance of three different models: a 2D chip blood vessel model and a 3D vascular network featuring the dimensions of arteries and arterioles, compared with a commercial disease modeling Transwell constructs as a control condition. The ischemia model is composed by a co-culture of endothelial cells (HUVECs) to demonstrate the potential of revascularization of the model and mesenchymal stromal cells (MSCs) to mediate the inflammatory response while stimulating the angiogenic behavior on HUVECs through the release of growth factors. Ultimately, the work pretends to propose an original proof of concept using remote magnetic stimulation in novel *in vitro* blood vessel models of ischemia to provide platforms to incorporate in potential cardiac ischemia treatments.

Keywords: ischemia, disease modeling, blood vessel, reperfusion, MSCs, HUVECs, magnetic fields, hypoxia, normoxia

VII.1. Introduction

Ischemic heart disease is a condition caused by the narrowing of large heart coronary arteries causing cardiomyocyte death and loss of tissue function, becoming one of the major causes of death worldwide[1,2]. These arteries supply blood to the heart muscle and, upon their clogging, the blood flow to the muscle is blocked, causing the death of the muscle cells and the beginning of a myocardial infarction[3,4].

Over the past decade, the evaluation of ischemic heart disease has evolved significantly, with several clinical trials reporting the benefits of revascularization in patients with acute ischemic syndrome[5]. However, the complex mechanisms of cardiac arrhythmias in acute ischemia and the rapidity of ischemia induced-changes have hampered the understanding of the disease[3]. For this reason, computation simulations have initially attempted to provide insight over ischemic abnormalities, with high spatiotemporal resolution, for a better diagnosis tool[3,6]. Yet, it became crucial to develop experimental models ranging from animal models designed to mimic the human clinical condition to miniaturized reliable *in vitro* models able to improve the therapeutic approaches and restore blood vessel function following injury, in cost-effective high-throughput screening assays[7].

So far, most ischemic *in vitro* models have been developed for ischemic stroke, both *in vitro* and *in vivo*, using rodent models while cardiac ischemia remains largely unexplored[8]. For cardiovascular science to continue advancing these *in vitro* miniaturized models should be robust and reproducible while simulating the *in vivo* conditions and blood vessel dimensions[9,10]. Additionally, accurate blood vessel *in vitro* models require the understanding of blood vessel mechanics and previous endothelization to properly simulate tissue perfusion and mimic endothelial cell migration, vascular barrier and inflammatory response[11]. Unfortunately, endothelialized perfusable *in vitro* vessels are limited to reconstitute features and responses of *in vivo* endothelial cells for lack of natural endothelial morphogenesis[12]. Also, the majority of these microfluidic devices are composed by rectangular channels, which do not mimic the shape of the native blood vessels, despite non-rectangular channels were described to enhance the performance[13,14].

Models of cardiac ischemia has been demonstrated in bioreactors using cardiomyocytes cultured in 3D aggregates to observe the loss of cardiomyocyte viability with disruption of cellular ultrastructure and evaluate the increased angiogenic potential

through the secretion of proangiogenic and proinflammatory cytokines[2]. Another model of cardiac ischemia/reperfusion was described using HUVECs to study the mechanism of the upregulation in autophagic myocardial injury, in the presence/ absence of antioxidants[15].

Important model cells for cardiac ischemia study are the MSCs, potent mediators of cardiac repair and, consequently, attractive for *in vitro* experiments, as well as in pre-clinical and clinical trials. Because of MSCs ability to secrete a large array of soluble factors, these cells have demonstrated effects on pathogenic cardiac remolding, fibrosis, immune activation, cardiac stem cell proliferation within the damaged heart and also angiogenic prompting[16]. The benefic paracrine activity of MSCs in cardiovascular medicine has also been reported using MSCs conditioned medium to reduce myocardial infarct size[17].

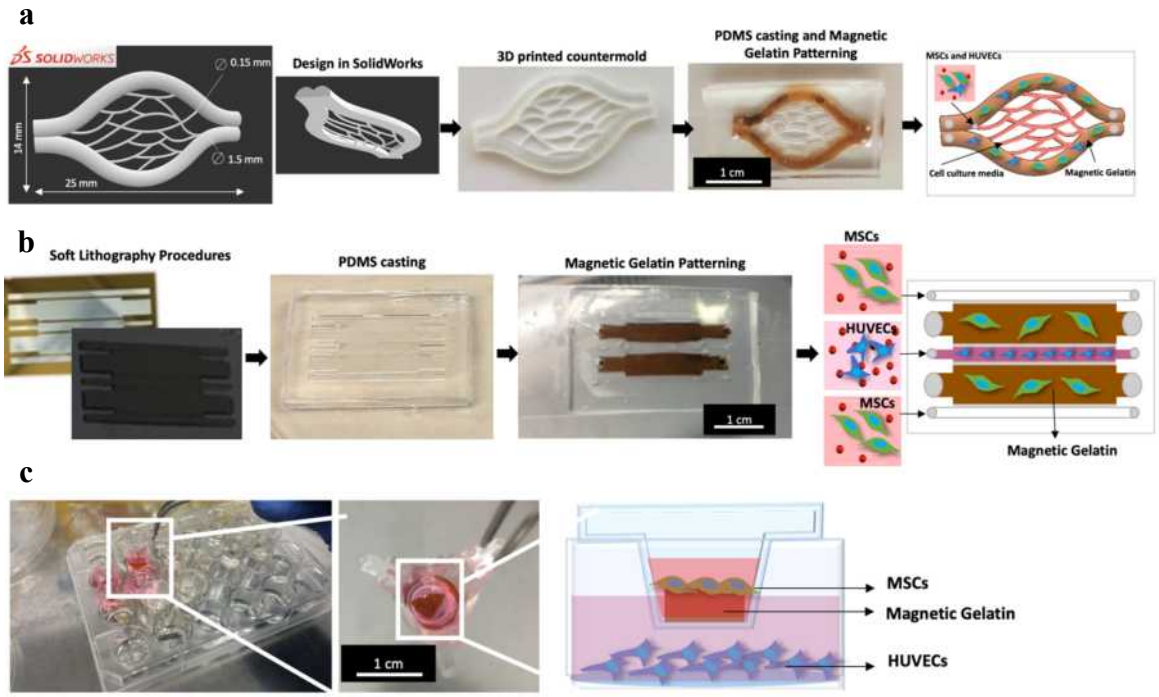


Figure VII. 1. Representation of the three models used for HUVECs and MSCs co-culture for ischemic disease modeling. **a)** Multi-branched mesoscale model designed in SolidWorks software and 3D printed in M3 Crystal material as a countermold for PDMS casting. The device was then patterned with magnetic gelatin on the larger channels. **b)** A linear shaped 2D chip was fabricated by soft lithography following microfluidic technology and using silicon wafers as counter molds for PDMS casting. Alike the mesoscale model, the 2D chip was patterned with magnetic gelatin and seeded with MSCs and HUVECs on different compartments. **c)** Commercial insert TRANSWELL was used to separate the co-cultures of HUVECs and MSCs using magnetic gelatin as a support for MSCs growing.

Here, we describe a method to study ischemia condition and reperfusion damage (hypoxic/re-oxygenation model of ischemia) on three different *in vitro* blood vessel models (3D vascular network, 2D blood vessel model and commercial transwell construct as a control model) using a co-culture of HUVECs and MSCs (Figure VII. 1 a, b, c). We aim to simulate ischemic disease by exposing the models to hypoxia condition, followed by attempts to reverse the tissue damage by readjusting the normal oxygen conditions and nutrient supplements to the cells and compare the repair of the induced injury site through magnetic exposure. This study thus provides innovative *in vitro* models involving the use of remote magnetic stimulation to prompt vascularization in artificial blood vessels to provide promising templates for novel cardiac ischemia therapies.

VI.2. Experimental Section

Fabrication of 2D chips. Briefly, the chips were fabricated using polydimethylsiloxane polymer (PDMS, Dow Corning) bonded to a glass layer, following standard soft lithography techniques on the University of Twente, The Netherlands. Silica wafers containing the two layers of SU-8 photoresist were fabricated in the MESA+ cleanroom facility at the University of Twente. The height of the first SU-8 layer was 450µm and the second layer (capillary barrier) was 150µm. The PDMS chip was fabricated by casting a prepolymer (10:1 w/w ratio of PDMS and curing agent) on top of the SU-8 master of the silica wafers. After curing the prepolymer at 80°C for 3 h, the PDMS layer and the glass layer were treated with oxygen plasma and immediately bonded together (Figure VII. 1). The magnetic hydrogel patterning on the chip was performed 2-3 days after oxygen plasma bonding, and the microchips were stored at -4ºC.

Design and Fabrication of the Vascular Hierarchical 3D Model. A ramified vascular network 3D model was designed to fill the gap in blood vessel mesoscale models, capable to mimic the size of arteries/veins (with biological dimensions of 0.5 – 2.5 mm[18]) with 1.5 mm of diameter connected to bifurcations simulating the dimensions of arterioles/venules (anatomically ranging from 40-250 µm[18]) with a diameter of 150 µm. The design was inspired in embryonic vascular plexus, where the vascular network is still a relatively simple structure with a hierarchical structure including primary and secondary branches[19]. A more complex system would include primary, secondary and tertiary

branches ending in vessels down to 6 mm in diameter, with diameters ranging from 150-230 mm[19]. The total dimensions of the construct were 25 x 14 mm. Initial square design was accomplished using 3Ds max modeling software and was later improved to a more biological round channel structure using SolidWorks software. Before printing, the design was sectioned in two halves for molding purposes. The model was then 3D printed using ProJet MJP 3600 (from 3D Systems) high resolution 3D printer using a combination of M3 Crystal for the structural part and Visijet S300 as a support material, both available from 3D Systems. Each part of the structure was used as a mold for PDMS, following similar fabrication and casting procedures as described for 2D chips fabrication (Figure VII. 1).

Magnetic Hydrogel Preparation. Magnetic hydrogel was composed of Porcine skin gelatin (8% m/v, type A, G2500, Sigma-Aldrich) doped with magnetic nanoparticles (MNPs). These nanoparticles were previously synthesized by chemical co-precipitation of iron salts $FeCl_3$ and $FeCl_2$ (Sigma-Aldrich) in alkaline media, according to the protocol published by Izquierdo et al.[20] Porcine skin gelatin was dissolved in milli-Q water (10% m/v) at 60ºC while powder MNPs were dispersed by sonication and mixed with gelatin polymeric aqueous solution to form a homogeneous solution. For a control condition in the ischemia experiments, commercially available cell culture inserts Transwell (VWR) were used (Figure VII. 1). In this situation, a piece of a previously crosslinked magnetic hydrogel was placed on top of the transwell membrane to allow for MSCs seeding on the hydrogel. Consequently, the magnetic gelatin solution was cast onto glass plates and left overnight at 4ºC. Finally, the samples were removed from the glass plates and immersed in an aqueous solution containing 1% of Glutaraldehyde (cross-linking agent, Sigma-Aldrich) for 3h. Prior to use, the magnetic hydrogel membranes were washed by immersion in a demineralized water bath and sterilized in a PBS solution containing 1% of antibiotic-antimycotic (Gibco).

Magnetic Hydrogel Patterning on 2D chips and vascular hierarchical model. Prior to the patterning in the chips, the magnetic solution of gelatin and MNPs was heated at 70ºC and mixed with 1% of glutaraldehyde (v/v) (cross-linking agent, Sigma Aldrich). The patterning process occurred via capillary action and, after jellification, was washed with PBS solution (Phosphate Buffered Saline, Sigma Aldrich)

by perfusion. The samples were also sterilized by perfusion a PBS solution containing 1% of antibiotic-antimycotic (Gibco). Finally, the samples were perfused with DMEM cell culture media (Dulbecco's Modified Eagle Medium, ThermoFisher Scientific) for pre-conditioning of the cells. Tubing and microfluidic connectors used in the experiments were sterilized through rinsing with 70% (v/v) ethanol and with PBS (phosphate buffered saline, Sigma Aldrich).

Cell culture. Human bone-marrow MSCs lines belong to the cell bank available at Stem Cell Engineering Research Group (SCERG), iBB-Institute for Bioengineering and Biosciences at Instituto Superior Técnico (IST). Bone marrow aspirates were obtained from Instituto Português de Oncologia Francisco Gentil, Lisboa-Portugal under collaboration with iBB-IST. All human samples were obtained from healthy donors after informed consent, accordingly with the Directive 2004/23/EC of the European Parliament and of the Council of 31 March 2004 on setting standards of quality and safety for the donation, procurement, testing, processing, preservation, storage, and distribution of human tissues and cells (Portuguese Law 22/2007, June 29), with the approval of the Ethics Committee of the respective clinical institutions[21]. Isolated human bone marrow MSCs (BM MSCs) were cultured using low-glucose Dulbecco's Modified Eagle Medium (DMEM, Gibco, Grand Island, NY) supplemented with 10% fetal bovine serum (FBS MSC qualified, Gibco) and 1% antibiotic-antimycotic (Gibco). The cells were cultured at 37ºC, 5% CO_2 and 21% O_2 in a humidified atmosphere. HUVECs were purchased from Lonza (Basel, Switzerland) and supplied with commercial endothelial growth medium-2 (EGM-2, Lonza) at 37ºC, 5% CO_2 in a humidified atmosphere. Medium renewal was performed every 3-4 days. The experiments were performed using cells between passages 4 and 7.

Co-culture on the models. MSCs (seeding density of $1.5x10^6$ cells/mL) were initially perfused onto the chips through the media channels and allowed to migrate and adhere to the magnetic hydrogel overnight. Microholes were also punched on the PDMS layer above the hydrogel compartment, allowing for MSCs injection in those specific regions to boost cell proliferation. Matrigel solution (Corning, NY) was also perfused on smaller channels/ compartments while HUVECs (seeding density of $4x10^6$ cells/mL) were seeded by perfusion on the compartment before allowing for matrigel gelation. Media renewal was performed every day. The cells in the models were incubated for three days under

these conditions. The depleted stream of the chips was collected every day for analysis. The syringes were replaced with fresh media every day, containing DMEM + 10% FBS and Endothelial Growth Medium-2 (EGM-2, Lonza) in a proportion 1:1.

Ischemia Disease Induction. For ischemia condition simulation, the co-culture was exposed to hypoxia by oxygen deprivation, reducing oxygen levels to <0.4%. Glucose, FBS and VEGF supplements were also removed from the media. The cells were kept for 2 h under hypoxia in serum and glucose free medium to induce ischemia in the models. After 2 h, one of each model was sacrificed to characterize the effects of ischemia modeling. Cell morphology and viability was observed using Live/Dead kit (ThermoFisher Scientific, L3224), according with the manufacturer protocol, by staining the cells in the co-culture with calcein to stain viable cells and ethidium bromide (EthD) to identify dead cells using a fluorescence microscope (Leica DM IL LED with EC3 camera system). Two models of each condition were sacrificed at this stage for microscopical observation.

Reperfusion and Magnetic therapy to reverse Ischemia condition.
Aiming to allow for a revascularization of the tissue at the onset of ischemia induction, it was important to restore the oxygen and nutrients balance by returning the models to normal oxygen conditions and replacing the ischemic culture buffer for cell culture media enriched in glucose (high glucose media). The recovery treatment associated with reperfusion involved the exposure of the ischemic models to a magnetic field of low intensity (0.08 T) to stimulate MSCs to secrete growth factors required for the revascularization process. The cells in the models were incubated under these conditions for 8h. The comparison between the models was analyzed by cell morphology using DAPI (blue cell nuclei staining) and Alexa 594 (red cell cytoskeleton staining) fluorescence markers. In the future, this experiment will be complemented with a control condition where the samples were exposed to reperfusion without magnetic exposure, also with the addition of another condition

Endothelin-1 measurement using ELISA (Conceptual experiment: On going).
The preservation and recovery of the endothelial monolayer are evaluated by ELISA experiments (Endothelin-1 kit, RayBiotech), following the manufacturer's instructions, to quantify the total amount of exogenous vasoconstrictor peptide secreted by HUVECs

(Endothelin-1), which can then be correlated with the endothelium/ cardiac tissue formation or destruction. All conditions were tested in triplicates using the same MSC donor to avoid further variability on the results.

Immunohystochemical analysis (Conceptual experiment). Immunohistochemistry (IHC) analysis is a method for demonstrating the presence and location of proteins in tissue sections and useful for assessing the progression and treatment of diseases. To carry out the histochemical and immunohistochemical investigation, µm-thick sections of paraffin blocks are cut. Each section would have been previously stained with Hematoxylin-Eosin. Immunostaining is performed with the following primary antibodies: antifibronectin (rabbit monoclonal antibody, ab32419, diluted 1:200; Abcam, Cambridge, UK), anti-Cx43 (Abcam; rabbit monoclonal antibody, ab11370, diluted 1:2000), anti-npCx43 (Invitrogen, mouse monoclonal antibody, CX-1B1, diluted 1:50), anti-ZO-1 (Invitrogen, Carlsbad, CA, USA; mouse monoclonal antibody, ZO1-1A12, diluted 1:50). Tissue sections are blocked by 3% hydrogen peroxide for 12 min, followed by heat induced antigen retrieval. Following overnight incubation with the primary antibody at 4°C, immunoreactions are then visualized using the avidin-biotin method, followed by color development with diaminobenzidine. This experimental part will be performed for a future publication with these results.

Immunofluorescence confocal laser microscopy (Conceptual experiment). Macrophage-derived chemokine **(**MDC) is a proposed marker for autophagic vacuoles to assess ischemic conditions on HUVECs. HUVECs are cultured on poly-L-lysine coated coverslips overnight. Then the media is switched to ischemic buffer for 30 min followed by replacement with normal media in the absence or presence of beta-Hydroxybutyric acid (BHA) (0.1 mM) and nascent polypeptide-associated complex (NAC) (5 mM) for 24 h, and then rinsed with PBS. The samples are then stained with 50 µM MDC at 37°C for 1 h. After incubation, the cells are fixed for 15 min with ice-cold 4% paraformaldehyde at 4°C and washed twice with PBS. This confocal experiment will be included in future publication with these results.

Electron microscopy (Conceptual experiment). Electron microscopic analysis was performed by fixing HUVECs for 30 min with ice-cold 3% glutaraldehyde in 0.1 M Cacodylate buffer, embedded in epon resin, and processed for transmission electron

microscopy using standard procedure. This observation will be assessed for a future complete publication with these results.

VII.3. Results and Discussion

3.1. *In vitro* Ischemia Characterization.

Initially the co-culture of MSCs and HUVECs were cultivated on three different models for disease modeling. Prior to ischemia induction, the culture was incubated for 3 days for the achievement of endothelialized blood vessel models. Some of the models were sacrificed to characterize the formation of a microvessel monolayer on the models using Live/Dead assay (Figure VII. 2).

On 2D chips, patterned with magnetic gelatin and Matrigel, it was observed the formation of a well-organized 3D endothelial network on the middle channel, although some tube-like structures were also observed on the magnetic gelatin. Additionally, it was observed endothelialized channels (Figure VII. 2a). The ischemia simulation in the 2D chips however revealed a major destruction of the organized endothelial network with the possible formation of increased endothelial extracellular matrix (Figure VII. 2b). This extracellular matrix is an attribute of mature endothelial cells[22], also known as perivascular matrix, is responsible for the organs specific vascular niche *in vivo*, and is associated with growth factor and angiocrine signaling required for tissue homeostasis and organ repair[23]. The effect observed with experimental ischemia might thus be associated with the activation of homeostatic mechanisms to prevent cell apoptosis under ischemic conditions.

The results observed with the novel multi-branched mesoscale device indicated the formation of a premature microvascular monolayer with some interconnections between the endothelial cells (Figure VII. 3a). It was also observed that the cells were unable to proliferate into the smaller channels, rather concentrating on the larger main channels where the magnetic gelatin was injected. This can possibly be ascribed to nutrients depletion in those internal regions due to issues on the circulation of cell culture media inside the device. This could be overcome by increasing the overall scale of the device while keeping the proportions to simulate the hydraulic pressure resulting from the macroscale channels converging into the microscale channels. The ischemia

condition induced a similar effect on the cells as previously described for the 2D chips (Figure VII. 2b and Figure VII. 3b) with the destruction of the cell arrangement into cell aggregation with cell-cell interactions, also resembling the formation of additional endothelial extracellular matrix (Figure VII. 3b). Interestingly, the ischemia seemed to have forced the cells to increase the population on the smaller inner channels of the device. The hypoxia microenvironment has been described to enhance the migration of the cells by stimulating the HIF(hypoxia-inducible factor)-1alpha signaling patways[24,25] which could justify the observed effect.

With the commercially available TRANSWELL model, three days of cell proliferation revealed the formation of a completely organized tube-like arrangement of HUVECs, envisioning tubes with large dimensions, while MSCs were dispersed on the magnetic gelatin scaffold (Figure VII. 4a). However, upon ischemia induction, major changes were observed on the HUVECs compartments, where the organization of tubes was almost completely disrupted. A few regions of microtubes monolayer were observed but the majority of the cells returned to the usual individualized morphology (Figure VII. 4b). MSCs also showed some disorganization and cell aggregation upon ischemia simulation.

Overall, in all three tested models, it was observed significant differences in cell behavior, mostly cell morphology and organization, upon ischemia simulation, which might be associated with generation of oxidative stress and cell survival mechanisms[15]. Furthermore, the presence of reactive oxygen species is known to induce changes in mitochondrial membrane permeability to trigger autophagy and result in HUVECs injury[26].

3.2. Reversible Ischemia condition.

After 2h under ischemic conditions, the models were returned to normoxia conditions under high glucose supplemented culture media and placed under magnetic stimulation (0.08 T) for 8h. The magnetic stimulation, while increasing cellular stress, was meant to trigger the increased secretion of growth factors, mainly VEGF-A, by MSCs and thus induce a faster response of HUVECs towards their angiogenic behavior. Future experiments will include more control conditions, such as treatment with reperfusion in the absence of magnetic stimulation and also drug treatment conditions.

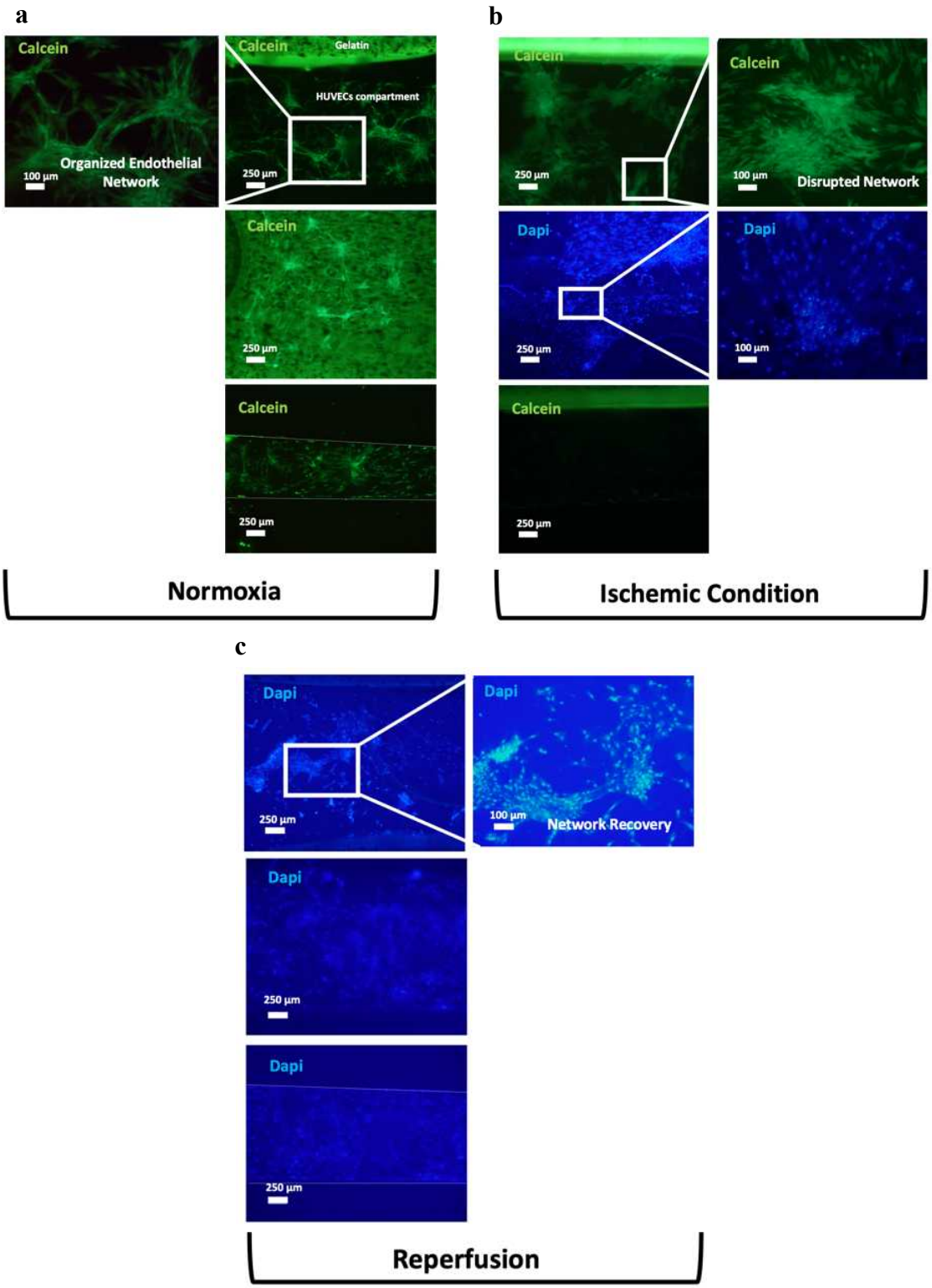


Figure VII. 2. Representation of the effect induced by hypoxic/ reperfusion condition on a co-culture of MSCs and HUVECs in 2D chips of PDMS. Viable cells were stained with calcein (green) while cell nuclei were stained with Dapi (blue). **a)** Representative microscopic images of the cells on different regions of the channels displayed an organized formation of tube-like structures after incubation for 3 days in normoxia conditions. **b)** Representative images of the same regions after 2h under hypoxic conditions showed the disruption of the organized network previously obtained with the formation of increased extracellular matrix involving the cells. **c)** Representative images after 8h of reperfusion under normal conditions evidenced signs of cell reorganization following the same microvessel structures obtained under initial conditions.

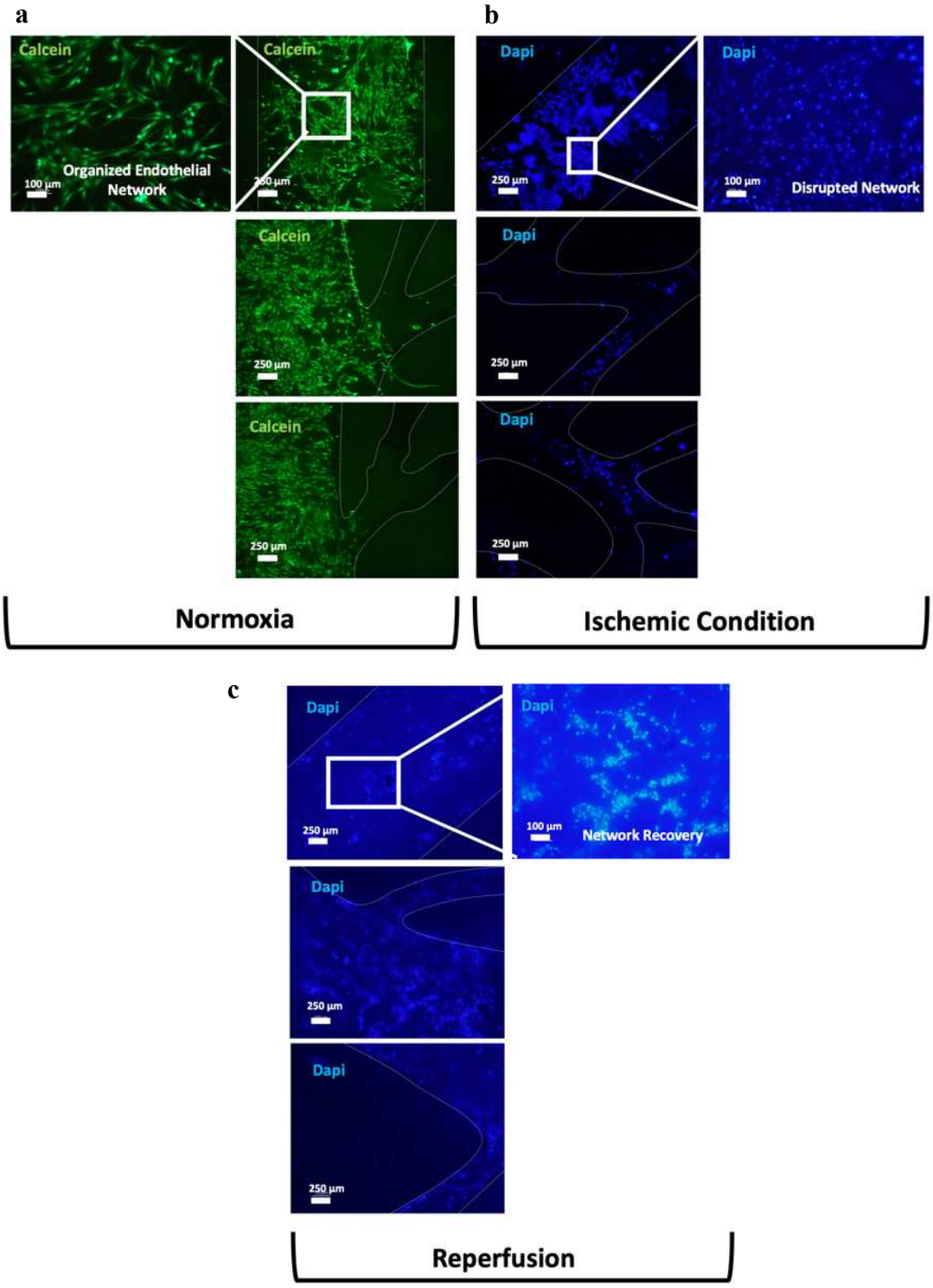


Figure VII. 3. Representation of the effect induced by hypoxic/ reperfusion condition on a co-culture of MSCs and HUVECs in a mesoscale device featuring the hierarchical organization of the native blood vessels. Viable cells were stained with calcein (green) while cell nuclei were stained with Dapi (blue). **a)** Representative microscopic images of the cells on different regions of the channels showed an organized distribution of the cells with indications of initial formation of microvessel structures after incubation for 3 days in normoxia conditions. **b)** Representative images of the cells after 2h under hypoxic conditions showed increased cell aggregation and a throwback on the evidences of a potential tube-like formation. **c)** Representative images after 8h of reperfusion under normal conditions revealed signs of cell reorganization under potential tube-like structures.

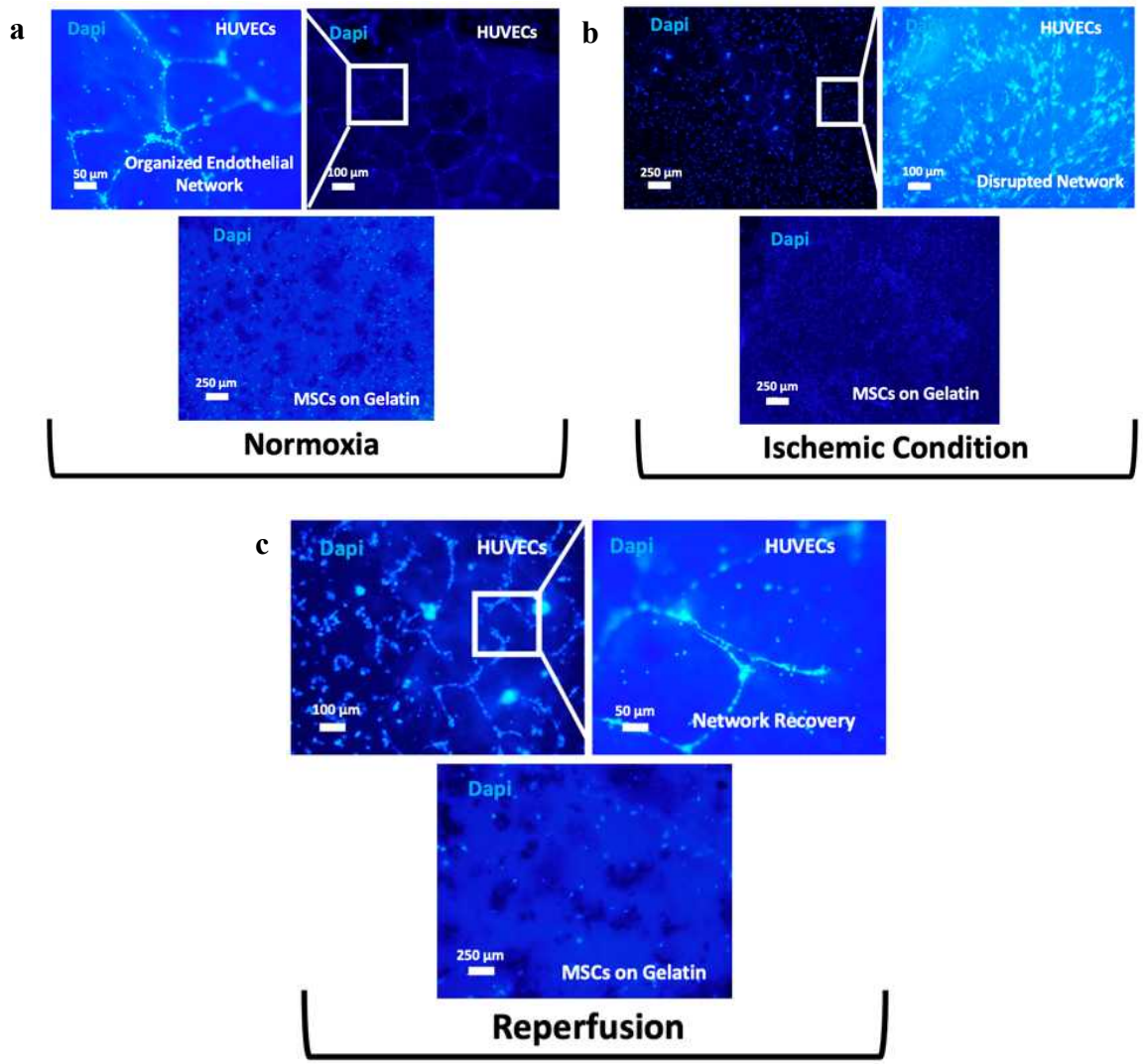


Figure VII. 4. Representation of the effect induced by hypoxic/ reperfusion condition on a co-culture of MSCs and HUVECs using a commercial TRANSWELL with a magnetic scaffold of gelatin to culture MSCs separately of the HUVECs, cultured in a standard polystyrene culture plate. Cell nuclei were stained with Dapi (blue). **a)** Representative microscopic images of the HUVECs forming tube-like structures and MSCs cultures on gelatin after 3 days of incubation under normoxia conditions. **b)** Representative images of the cells after 2h under hypoxic conditions showed partial destruction of the branch points in the tubes formed under normoxia. The images also highlight major concentration of MSCs on top of the gelatin. **c)** Representative images after 8h of reperfusion under normal conditions revealed reorganization of HUVECs into tube formation. A decreased concentration of MSCs was observed on top of the gelatin.

In these preliminary results, the effect of reperfusion on 2D chips revealed a tendency to return to the initial stage by rearranging the cells into an organized network (Figure VII. 2c). However, more time was probably required to completely revert the impact of ischemia on the vascularized channels. A similar behavior was observed with the multi-branched hierarchical model, where the cells also displayed a potential to reorganize into an interconnected endothelial tissue (Figure VII. 3c). A positive impact

was observed on the proliferation of the cells in the inner channels, which increased during ischemic conditions, and seemed to be maintained after reperfusion, thus highlighting the benefits of HUVECs motility during ischemia.

Finally, the most impactful reversibility in the reperfusion post-ischemia was obtained with the TRANSWELL models, in which an almost complete recovery of the initial state was observed with the formation of a ramified monolayer (Figure VII. 4c). Nonetheless, despite the formation the microvessel structures, it was possible to observe some regions with individualized HUVECs, suggesting the need to extend the reperfusion for periods longer than 8h. This is consistent with other publications in which the reperfusion time was usually maintained for 72h[26].

Other studies have provided insight on the potential effects of the ischemic/ reperfusion simulation at the molecular level by describing an increased lactate production, consistent with cell behavior under hypoxic microenvironment, and also membrane damage with morphologic alterations, mitochondrial damage with Ca^{2+} accumulation and consequent ATP (adenosine triphosphate) degradation through a decrease in cell pH associated with cell anaerobic metabolism during ischemia induction[27,28]. Although these effects of cell structural and metabolic changes were reported to be present after only 90 min of ischemia induction, a prolonged interval of 2h were responsible to enhance these abnormalities[29].

Interestingly, and in contrast with the results obtained in this study, it has been reported in the literature that the reperfusion strategy could lead to the exacerbation of tissue injury and necrosis, triggering several pathological events associated with inflammation and increased cell toxicity[30]. To further understand the underlying mechanisms involved in the processes of ischemia and reperfusion it would be necessary to properly characterize the effects observed during this study through immunohistochemical analysis of the injury created in the models, analysis of the supernatant of these conditions for metabolite and endothelium molecules quantification, as well as investigation of the molecular damage and the pathways involved in these processes. These experiments will be performed in the future to complete the study through glucose and lactate measurement (metabolites assessment), endothelin-1 quantification through ELISA (endothelium molecules), immunofluorescence detection of calcium channels and determination of the involved pathways through western blot analysis.

VI.4. Conclusions

In the present study, we explored the potential of using three different models (2D blood vessel chips, 3D hierarchical blood vessel and a commercial TRANSWELL construct as a control) in a co-culture of MSCs and HUVECs to efficiently simulate vascular ischemia condition.

The performance of the models was compared according with the behavior of the co-culture in the different stages of the experiments. Although differences were observed between the initial stage, the ischemic condition and the reperfusion effect under magnetic exposure for all the models, it was possible to conclude that, morphologically, the most impactful effect was obtained using the TRANSWELL model, followed by the 2D models. In these models, a disruption of the microvessel monolayer was observed upon ischemic simulation and the potential to revert the damage and restore vascularization in the models through the combination of reperfusion and magnetic stimulation. The hierarchical 3D model also evidenced signs of ischemia and recovery during reperfusion, however HUVECs were not initially rearranged in a matured microvessel monolayer, which contributed to the observation of more subtle differences under ischemia/ reperfusion.

Despite the need for further optimization and for more experimental analysis to complete the study and to be able to characterize the effect at the molecular level, as well as for the inclusion of placebo controls for magnetic stimulation, it was concluded the possibility to simulate vascular ischemia disease and revascularization using these models.

The results thus highlight the potential for cardiovascular disease modeling in these blood vessel models through the addition of cardiomyocytes for the development of a cardiac tissue, and the promise of a contribution for drug screening and assessment of novel treatments for cardiovascular diseases.

VI.5. References

1. P., Z. D. & J., W. H. J. Sudden Cardiac Death. *Circulation* **98**, 2334–2351 (1998).
2. Sebastião, M. J. *et al.* Bioreactor-based 3D human myocardial ischemia/reperfusion in vitro model: a novel tool to unveil key paracrine factors upon acute myocardial infarction. *Transl. Res.* **215**, 57–74 (2020).
3. Rodríguez, B., Trayanova, N. & Noble, D. Modeling cardiac ischemia. *Ann. N. Y. Acad. Sci.* **1080**, 395–414 (2006).
4. Harris, A. S., Bisteni, A., Russell, R. A., Brigham, J. C. & Firestone, J. E. Excitatory Factors in Ventricular Tachycardia Resulting from Myocardial Ischemia. Potassium a Major Excitant. *Science (80-.).* **119**, 200 LP – 203 (1954).
5. Institute of Medicine (US) Committee on Social Security Cardiovascular Disability Criteria. Cardiovascular Disability: Updating the Social Security Listings. Washington (DC): National Academies Press (US); 2010. 7, Ischemic Heart Disease. Available at: https://www.ncbi.nlm.nih.gov/books/NBK209964/%0A.
6. Loewe, A., Wülfers, E. M. & Seemann, G. Cardiac ischemia—insights from computational models. *Herzschrittmachertherapie + Elektrophysiologie* **29**, 48–56 (2018).
7. Hafez, P. *et al.* Development of an In Vitro Cardiac Ischemic Model Using Primary Human Cardiomyocytes. *Cardiovasc. Eng. Technol.* **9**, 529–538 (2018).
8. Holloway, P. M. & Gavins, F. N. E. Modeling Ischemic Stroke In Vitro: Status Quo and Future Perspectives. *Stroke* **47**, 561–569 (2016).
9. Lindsey, M. L. *et al.* Guidelines for experimental models of myocardial ischemia and infarction. *Am. J. Physiol. Heart Circ. Physiol.* **314**, H812–H838 (2018).
10. Ytrehus, K. Models of myocardial ischemia. *Drug Discov. Today Dis. Model.* **3**, 263–271 (2006).
11. Matsumoto, T., Sugita, S. & Yaguchi, T. Biomechanics of Blood Vessels: Structure, Mechanics, and Adaptation. in 71–98 (2015). doi:10.1007/978-3-662-46836-4_4
12. Zhang, W. *et al.* Elastomeric free-form blood vessels for interconnecting organs on chip systems. *Lab Chip* **16**, 1579–1586 (2016).
13. Chen, S. *et al.* A perforated microhole-based microfluidic device for improving sprouting angiogenesis in vitro. *Biomicrofluidics* **11**, 1–12 (2017).

14. Lee, J. *et al.* Microfluidics in structured multimaterial fibers. *Proc. Natl. Acad. Sci.* **115**, E10830–E10838 (2018).
15. Zeng, M. *et al.* Reactive oxygen species contribute to simulated ischemia/reperfusion-induced autophagic cell death in human umbilical vein endothelial cells. *Med. Sci. Monit.* **20**, 1017–1023 (2014).
16. White, I. A., Sanina, C., Balkan, W. & Hare, J. M. Mesenchymal Stem Cells in Cardiology. *Methods Mol. Biol.* **1416**, 55–87 (2016).
17. Timmers, L. *et al.* Reduction of myocardial infarct size by human mesenchymal stem cell conditioned medium. *Stem Cell Res.* **1**, 129–137 (2008).
18. Johnson, P. C. Introduction Overview of the Microcirculation.
19. Paulsen, S. J. & Miller, J. S. Tissue vascularization through 3D printing: Will technology bring us flow? *Dev. Dyn. an Off. Publ. Am. Assoc. Anat.* **244**, 629–640 (2015).
20. Cruz-Izquierdo, Á., Picó, E. A., López, C., Serra, J. L. & Llama, M. J. Magnetic Cross-Linked Enzyme Aggregates (mCLEAs) of Candida antarctica lipase: An efficient and stable biocatalyst for biodiesel synthesis. *PLoS One* **9**, 1–22 (2014).
21. Dos Santos, F. *et al.* Ex vivo expansion of human mesenchymal stem cells: A more effective cell proliferation kinetics and metabolism under hypoxia. *J. Cell. Physiol.* **223**, 27–35 (2010).
22. Kusuma, S., Zhao, S. & Gerecht, S. The extracellular matrix is a novel attribute of endothelial progenitors and of hypoxic mature endothelial cells. *FASEB J.* **26**, 4925–4936 (2012).
23. Witjas, F. M. R., van den Berg, B. M., van den Berg, C. W., Engelse, M. A. & Rabelink, T. J. Concise Review: The Endothelial Cell Extracellular Matrix Regulates Tissue Homeostasis and Repair. *Stem Cells Transl. Med.* **8**, 375–382 (2019).
24. Coutts, A. S. *et al.* Hypoxia-driven cell motility reflects the interplay between JMY and HIF-1α. *Oncogene* **30**, 4835–4842 (2011).
25. Barrak, N. H., Khajah, M. A. & Luqmani, Y. A. Hypoxic environment may enhance migration/penetration of endocrine resistant MCF7- derived breast cancer cells through monolayers of other non-invasive cancer cells in vitro. *Sci. Rep.* **10**, 1127 (2020).
26. Penna, C., Perrelli, M.-G. & Pagliaro, P. Mitochondrial pathways, permeability transition pore, and redox signaling in cardioprotection: therapeutic implications.

Antioxid. Redox Signal. **18**, 556–599 (2013).

27. Kalogeris, T., Baines, C. P., Krenz, M. & Korthuis, R. J. Cell biology of ischemia/reperfusion injury. *Int. Rev. Cell Mol. Biol.* **298**, 229–317 (2012).
28. Sanada, S., Komuro, I. & Kitakaze, M. Pathophysiology of myocardial reperfusion injury: preconditioning, postconditioning, and translational aspects of protective measures. *Am. J. Physiol. Heart Circ. Physiol.* **301**, H1723-41 (2011).
29. Tumiati, L. C., Mickle, D. A. G., Weisel, R. D., Williams, W. G. & Li, R.-K. An in vitro model to study myocardial ischemic injury. *J. tissue Cult. methods* **16**, 1–9 (1994).
30. O'Donnell, C. J. & Nabel, E. G. Genomics of cardiovascular disease. *N. Engl. J. Med.* **365**, 2098–2109 (2011).

Chapter VIII



Conclusions And Future Directions

CHAPTER VIII – Conclusions and Future Perspectives

This final chapter summarizes the major conclusions and outcomes of the research work developed during the thesis timeframe and finalizes with the identification of some limitations of the work as well as presenting possible future directions in this field.

VIII. 1. CONCLUSIONS

As a consequence of the growing sedentary lifestyles, the number of people suffering from cardiovascular diseases has been continuously increasing, currently representing 30% of global deaths worldwide (17 million deaths) and expected to rise to 23.6 million deaths globally in 2030. With these disappointing statistics, there is an urgent need for novel therapeutic approaches to restore proper blood flow in damaged blood vessels.

Despite major tissue engineering developments in the cardiovascular engineering area, mostly focus on delivery systems combined with stem cell therapies to supply growth factors release to the injured blood vessels. However, the short *in vivo* half-life of these molecules compromises the functionality of these methods, limiting their clinical translation. Hence, the fabrication of an implantable and pre-vascularized engineered tissue, supported by continuous release of growth factors for long-term functionality, would represent a major improvement in repairing the native structure of the vessels and reverting the disease.

In this thesis we explored the concept of *in vitro* angiogenesis to apply external magnetic stimulation on mesenchymal stromal cells (MSCs), cultured on tissue scaffolds with ferromagnetic properties, to enhance the secretion of VEGF growth factor, a key molecule to trigger angiogenesis on endothelial cells (HUVECs).

In later stages of the work, we attempted to replicate the microenvironment conditions and the mechanical and hierarchical properties of the blood vessels for disease modeling. On a clinical translation perspective, the external stimulation of cell behavior through magnetic forces towards the implanted magnetic graft (scaffold) could then

sustain the functionally of the native tissue by ensuring the continuous release of growth factors to the target site.

Fundamental understanding of the mechanisms associated with magnetic stimulation was however necessary to improve and optimize the quality of the resulting therapeutic strategy and tissue construct.

For this reason, we first studied the ability to remotely modulate protein sorption into magnetic PVA hydrogels by adjustment of the external magnetic field intensity (through ON/ OFF magnetic cycles), concluding on the unique properties of these magnetic-responsive hydrogels. In the presence of a low intensity magnetic field (0.08 T), PVA surface hydrophilicity decreased around 20º while protein sorption at the hydrogel surface was observed in the absence of the magnetic field (OFF) and desorption upon magnetic exposure (ON). The resulting magnetic-driven protein sorption/release was investigated and ultimately interpreted as due to the reversible switches of surface hydrophilicity and the peristaltic-like movements associated to magnetic induced hydrogel volume contraction/distention of the hydrogel when exposed to a cyclic variation of the magnetic field intensity (up to 1 T).

Following the confirmation of the magnetic responsiveness of the PVA hydrogel, we investigated the impact of static magnetic forces of 0.08 T on the secretory activity of MSCs cultured on: magnetic scaffolds of PVA or biocompatible gelatin, on standard polystyrene culture plates as monolayers (2D cultures) or as 3D aggregates. Within this study, we reported that, while the proliferation, viability and phenotypic identity of the MSCs were not affected by the magnetic fields, the cells showed a significant magnetic responsiveness by increasing the secretion of VEGF-A molecule, in comparison with non-magnetic stimulated controls, and by aligning towards the magnetic attraction lines. This effect was observed even on 2D cultures without the support of the scaffolds as magnetic actuators to drive the magnetic forces.

Finally, the presence of VEGF-A in the secretome of magnetically stimulated MSCs, in 2D cultures or cultivated on magnetic gelatin, was able to induce angiogenesis on HUVECs with the formation of new microvessels, both *in vitro* and *ex vivo.* Contrarily, MSCs cultured on magnetic PVA suggested a potential for angiogenesis inhibition, showing significant decrease in VEGF-A production and a decline in tube formation in HUVECs, derived from magnetic stimulation. The study thus highlighted the possibility to modulate cell fate and behavior, in particular towards angiogenesis, through magnetic stimulation.

The promising role of magnetic field over MSCs increased secretion of VEGF molecules triggered the interest to further explore the magnetic parameters able to optimize this effect. As a consequence, the modulation of MSCs angiogenic response, cultured on gelatin scaffolds or under 2D culture monolayers, was evaluated through changes in the intensity and in the application mode of the magnetic field. The effect of static (i.e. cells exposed to constant magnetic field of 0.08 T and 0.45 T) and dynamic magnetic field applied at high (HF) and low (LF) frequency cyclic regimes (cells exposed to ON/OFF magnetic field cycles, varying up to 0.08 T and 0.45 T) on VEGF-A expression by MSCs was studied . Lower magnetic intensity (0.08T) was shown to induce an overall better performance in prompting increased production and secretion of VEGF-A, which resulted in the formation of a higher number of microvessels by HUVECs (positive angiogenic effect). On the other hand, increased mortality of MSCs was associated with the higher intensity magnetic field (0.45 T) as well as a weaker angiogenic stimulation on MSCs.

The magnetic field application also showed to impact on VEGF-A secretion by MSCs. Higher frequency magnetic field cyclic regime was shown to stimulate the expression of VEGF-A by MSCs, tube formation and sprouting in HUVECs. However, lower frequency regimes revealed to actively inhibit VEGF-A secretion by MSCs and sprouting in HUVECs (downregulation of angiogenesis) independently of the maximum magnetic field intensity applied. *i.e.* 0.08 T or 0.45 T. The distinct effects with the cyclic variation regimes were ascribed to possible cell adaption to magnetic exposure depending on the relaxation times associated with each magnetic configuration. These results showed the ability for positive and negative regulation of angiogenesis, suggesting a potential to develop efficient pro- and anti-angiogenesis magnetic field-based therapies for treatment of cardiovascular related diseases or reduce tumor development.

On the final part of the research, we designed and investigated the performance of *in vitro* 2D chips (in three different configurations) and 3D models of arteries and veins, fabricated in magnetic gelatin, to mimic the *in vivo* microenvironment and dimensions of native blood vessels and stimulate angiogenesis. Despite cell adhesion to the engineered 3D tissue, it was concluded that the angiogenic efficiency of the 3D models was possibly impaired by HUVECs poor affinity to the thick magnetic gelatin construct, which possesses a mechanical stiffness similar to a diseased tissue. Contrarily, 2D chips, featuring independent cell compartments for MSCs (within channels filled with magnetic gelatin) and HUVECs (in compartments coated with matrigel), offered promising results

with the stimulation of angiogenic behavior in a co-culture of HUVECs and MSCs, triggered by magnetic stimulation. On 2D chips, the geometry, VEGF supply mechanism, and fabrication procedures demonstrated differences in cell behavior, allowing to determine the appropriate parameters to achieve the desired formation of an endothelial tissue monolayer on the chips. Hence, our 2D chips are promising models for cardiovascular disease modeling and drug screening.

Finally, a vascular ischemia disease modeling, featuring a co-culture of MSCs and HUVECs, was developed to compare the performance of 2D chips and a novel 3D model, designed to mimic the vascular hierarchical network (from arteries/ veins to arterioles/ venules dimensions), in efficiently reverting the tissue damage caused by ischemic conditions through magnetic exposure.

In summary, and even though our results could still require some improvement and further validation through complementary experiments, we believe that our findings in this area represent a valuable contribute towards the development of new therapeutic tools which may allow for future developments in the cardiovascular engineering.

VIII. 2. Limitations of the Work and Future Directions

During the timeframe of this PhD project, the combined identification of study limitations, research questions and potentially attractive alternatives were inspiring to devise promising strategies for future research lines. Here we summarize some limitations of the study and suggest interesting topics of investigation to complement and improve the work with future research.

On chapters III and IV we discussed the fabrication of novel magnetic hydrogels (of PVA and Gelatin), doped with iron oxide nanoparticles, for protein sorption and to trigger angiogenic cell behavior. The hydrogels were prepared with a random distribution of MNPs and over the chapters the properties of these materials were assessed in terms of surface roughness, hydrophilicity, swelling, mechanical resistance and overall magnetic properties. So far, most characterization techniques do not allow for measurement in the presence of the magnetic field which made it difficult to for us to

understand the structural response of the magnetic hydrogels to the magnetic field on chapter III. However, it is likely that a different surface pattern, with an ordered distribution of MNPs, featuring a patterned surface, would result in potentially different effects from both proteins and cells. In particular, the patterned surfaces might be responsible for a better cell organization and for facilitating cell communication and paracrine signaling phenomena. The organized topographical patterning has been reported to regulate cell-fate by influencing cell-microenvironment interactions through topographical cues able to affect the reconstruction of the cytoskeleton, to regulate the opening of Ca^{2+} ion channels, thus affecting the response of cell membrane receptors through a direct cell-scaffold mechanosensing[1]. For instance, micro-patterned scaffolds have shown to promote the elongation of the cells along the principal axis of the ridges whereas the formation of cell-bridges across the grooves was also observed and compared with the response of isotropic surfaces, where the effect was not visualized[2].

The possibility to impact on cell signaling, in particular by enhancing the response of VEGFR-2 transmembrane receptors for VEGF-A through surface micropatterning could possibly have advantages on further enhancing angiogenesis on HUVECs. Other studies have described that surface topography is more influential than surface chemistry in determining cell adhesion and alignment[3], which could be a promising alternative to solve the poor affinity of the MSCs to the PVA discussed on chapter IV. Moreover, the effect of micropatterned surfaces or even nanofibrous materials produced by electrospinning techniques on HUVECs has shown to enhance cell adhesion, proliferation, growth factors secretion and ultimately resulting in increased capillary-like tube networks[4]. In addition to the magnetic stimulation, the possibility to stimulate the cells with a micropatterned surface or through the seeding of cells in a nanofibrous microenvironment could be an interesting perspective with a wider focus on material engineering.

Throughout the thesis the goal to achieve a ramified microvessel monolayer, through stimulation of the angiogenic behavior on HUVECs, was accomplished by conditioning HUVECs culture with the supernatant from MSCs exposed to different magnetic field intensities and cyclic conditions. This way, we indirectly stimulated HUVECs using magnetic fields using a single dose of conditioned media containing growth factors (e.g. VEGF-A). However, this meant that the formed microvessels would not further develop into a matured tissue, as desired in future clinical translation approaches for tissue repair, due to lack of continuous supply of grow factor molecules

associated with its fast degradation. Supporting this statement are the non-significant results with *ex-vivo* CAM assays discussed on Chapter IV, which were possibly a consequence of the molecule degradation after the three-day incubation of the embryo sections with the supernatant of MSCs. In future experiments, those results could probably be improved with the inclusion of the magnetic scaffold, loaded with MSCs, in the CAM embryo section, to assess vascular reaction. This procedure with scaffold inclusion has already been described in the literature[5] and could be easily implemented to verify the effect of continuous supply of molecules in angiogenesis.

In our study, the issue with long-term sustainment of growth factors was addressed over the last chapters with the establishment of a co-culture of HUVECs and MSCs. It was demonstrated that the conjugation of these two cell types allows for the formation of the desired ramified endothelial network. However, a more exhaustive investigation is required in order to define improved strategies to avoid the observed apoptotic events associated with the low viability of HUVECs in the co-culture condition. Such apoptotic events may possibly be reduced by conducting the experiments under hypoxic environments, which has been reported to increase HUVECs survival in MSCs/HUVECs co-culture[6,], or through a combination with another cell type, such as smooth muscle cells, working as a mediator between HUVECs and MSCs, in attempt to better mimic the native composition of the vasculature[7,8].

In this thesis, our major focus was centered on using magnetic forces to stimulate angiogenesis through the secretion of growth factor molecules (i.e. VEGF-A) from MSCs. However, while this effect was successfully described during the chapters, the underlying mechanisms involved in the stimulation of the paracrine activity of MSCs upon magnetic induction were not fully explored. In particular, the identification of the signaling pathways associated with the detected overexpression of VEGF-A under magnetic stimulation would be an important investigation to complement this study and provide an answer to some speculation provided in the discussion sections. Further studies should include western blot analysis of the main signaling pathways associated with cellular responses to external stress (e.g. VEGF – involved in the regulation of vasculogenesis in embryonic development and angiogenesis, NF-kB, - plays a crucial role in inflammation and innate adaptation to stress, MAPK – associated with metabolic changes in response to extracellular stimuli and stress, p53 – coordinates cellular responses to DNA damage or hypoxia , TGF-beta – involved in the regulation of cell migration and

differentiation)[9,10] that might explain the effects observed on the cells such as magnetic induced alignment, migration and secretory behavior.

Moreover, due to the complex combination of molecules secreted by MSCs, it is probable that other molecules equally relevant to cell processes, besides angiogenesis, were also stimulated by magnetic exposure. It would then be interesting to proceed with proteomic and RNA sequencing tools[11] to provide a more complete characterization of the MSCs secretome when exposed to magnetic fields. Additionally, magnetic field has been described for driving differentiation in several cell types, including neuronal cells and MSCs[12,13,14,15]. In fact, preliminary studies were conducted during this thesis to discard the potential attribution of the observed magnetically-induced effects to MSCs early differentiation stage. Therefore, the investigation for detection of overexpressed early MSCs differentiation genes, such as SPP1 (secreted phosphoprotein-1, osteopontin precursor), FABP4 (fatty acid-binding protein, adipogenesis precursor), RGC32 (response gene to complement 32, associated with chondrogenic differentiation), in MSCs under static magnetic influence for 5 days evidenced a significant increase of SPP1 gene (data not shown). This was also the reason for shortening the magnetic exposure to 24h in subsequent experiments in order to avoid compromise the results due to potential cell differentiation, which was not within scope of the project. Nonetheless, it was identified a potential induction for osteogenesis differentiation due to magnetic stimulation, which could provide for interesting future study.

In Chapter IV, the culture of MSCs in magnetic PVA scaffolds under static magnetic exposure revealed a significant capacity to inhibit the formation of tube-like structures in HUVECs. In Chapter V, the application of dynamic magnetic fields under Low Frequency (LF) regime also evidenced a strong anti-angiogenic effect on either MSCs cultured on magnetic Gelatin or on tissue culture plates of polystyrene. It is important to note that these conditions (MSCs cultured on Gelatin and 2D MSCs cultures) had been previously identified as proangiogenic on Chapter IV, further highlighting the effect of the LF dynamic magnetic configuration. Based on these results, it would be of high clinical significance in the field of cancer research to open a new investigation line in a strategy to actively inhibit vascularization in cancer cell lines[16,17] by culturing the cells with the supernatant from MSCs, in a combination of cell culture in magnetic PVA scaffold and exposure to LF dynamic magnetic field regime, and characterize the effect on cancer cell lines. If successful, this study could be the bridge for a scaled-up approach

for implantation in cancer patients to reduce tumor growth and become an important contribute in clinical translational approaches.

Another future perspective could be to extend the study presented on Chapter V and further investigate the effect of cell adaption to external magnetic stimuli in a robust study focusing on the physics behind the magnetic exposure, the toxicity of prolonged exposure times, also adding more complexity to the investigation by studying an array of magnetic frequencies and potentially delving into the biological effects of the electromagnetic field in MSCs or neural cells, since many benefits have been associated with the influence of electric and electromagnetic fields on the regulation of neural stem cells[18] and neurodegenerative disease models[19,20].

Finally, on Chapter VI the project entered into microfabrication tools for the design of blood vessel models aiming at the development of disease modeling and drug screening high throughputs platforms. Unfortunately, the ambitious final part of the project with the disease modeling proof of concept was not completed due to time restrictions and, consequently, some research lines of study, although considered, were not yet executed. The study of ischemia modeling and treatment was initially designed to involve placebo controls during the treatment with oxygen/nutrient reperfusion (e.g. in the absence of magnetic exposure) and also drug screening controls to efficiently demonstrate the impact of magnetic stimulation on reverting the ischemic injury in contrast with commercially available treatment drugs.

Consequently, future work for this part of the work includes executing the open research lines and also finalize experiments described in Chapter VII as on-going "conceptual experiments" meant to close the study by properly characterizing the efficiency of the ischemic simulation and treatment, including quantification of the secreted molecules collected in the depleted streams using analyses of the metabolites and ELISA assays, immunohistochemical and SEM imaging of the injury sites. An additional experiment involves extending the reperfusion experimental time for a few days to assess the possibility of a fully repair of the microvessel structure.

Our initial goal focused on cardiovascular diseases. Therefore, for biomimetic purposes and an accurate representation of cardiac ischemia, HUVECs, smooth muscle cells and cardiomyocytes could be seeded on the models for assessment of the potential to magnetically stimulate the cells into cardiac tissue repair in a complex vascular network featuring organ-on-chip technology. Another promising future direction refers

to the possibility to widen the approach and utilize the developed models towards other diseases, such as neurodegenerative disease modeling.

Regarding the biofabrication of the models, there is also potential for improvement. Although the fabricated 2D chips were described to perform successfully in the formation of a microvessel endothelial monolayer on Chapters VI and VII, the multi-branch hierarchical model presented in Chapter VII, featuring the anatomical rounded design and the interconnections between arteries and arterioles, is the most promising device to mimic the blood vessel network in future research lines. Nonetheless, the drastic differences in the diameter of the channels for arteries and the channels to simulate arterioles, besides easily prone to collapse during fabrication (PDMS casting and demolding), creates an hydraulic pressure on the smaller channels that makes it difficult for the circulation of the culture media and, consequently, for cell distribution to those channels. An attractive future study would benefit from the sophisticated technology of a bioprinter to print (extrusor-based) the multi-branched model with encapsulated MSCs within a permeable 3D printing material (e.g. collagen or alginate)[21,22]. This method would allow for cell distribution within the model, with free access to nutrients and oxygen through the walls of the model, while maintaining the originality of the design and its biological dimensions.

VIII. 3. References

1. Zhang, K., Xiao, X., Wang, X., Fan, Y. & Li, X. Topographical patterning: characteristics of current processing techniques, controllable effects on material properties and co-cultured cell fate, updated applications in tissue engineering, and improvement strategies. *J. Mater. Chem. B* **7**, 7090–7109 (2019).
2. Sanzari, I., Humphrey, E. J., Dinelli, F., Terracciano, C. M. & Prodromakis, T. Effect of patterned polyacrylamide hydrogel on morphology and orientation of cultured NRVMs. *Sci. Rep.* **8**, 11991 (2018).
3. Hasirci, V. & Pepe-Mooney, B. Understanding the cell behavior on nano-/micro-patterned surfaces. *Nanomedicine (Lond).* **7**, 1375–1389 (2012).
4. Tan, A. W. *et al.* Enhanced in vitro angiogenic behaviour of human umbilical vein endothelial cells on thermally oxidized TiO2 nanofibrous surfaces. *Sci. Rep.* **6**, 21828 (2016).
5. Petrovova, E. *et al.* Preclinical alternative model for analysis of porous scaffold biocompatibility applicable in bone tissue engineering. *ALTEX* **36**, 121–130 (2019).
6. Zhang, B. *et al.* Co-culture of mesenchymal stem cells with umbilical vein endothelial cells under hypoxic condition. *J. Huazhong Univ. Sci. Technol. Med. Sci. = Hua zhong ke ji da xue xue bao. Yi xue Ying wen ban = Huazhong keji daxue xuebao. Yixue Yingdewen ban* **32**, 173–180 (2012).
7. Heydarkhan-Hagvall, S. *et al.* Co-culture of endothelial cells and smooth muscle cells affects gene expression of angiogenic factors. *J. Cell. Biochem.* **89**, 1250–1259 (2003).
8. Truskey, G. A. Endothelial Cell Vascular Smooth Muscle Cell Co-Culture Assay For High Throughput Screening Assays For Discovery of Anti-Angiogenesis Agents and Other Therapeutic Molecules. *Int. J. High Throughput Screen.* **2010**, 171–181 (2010).
9. Martin, G. S. Cell signaling and cancer. *Cancer Cell* **4**, 167–174 (2003).
10. Hotamisligil, G. S. & Davis, R. J. Cell Signaling and Stress Responses. *Cold Spring Harb. Perspect. Biol.* **8**, a006072 (2016).
11. Kehl, D. *et al.* Proteomic analysis of human mesenchymal stromal cell secretomes: a systematic comparison of the angiogenic potential. *npj Regen. Med.* **4**, 8 (2019).
12. Özgün, A., Marote, A., Behie, L. A., Salgado, A. & Garipcan, B. Extremely low

frequency magnetic field induces human neuronal differentiation through NMDA receptor activation. *J. Neural Transm.* **126**, 1281–1290 (2019).

13. Labusca, L. *et al.* The effect of magnetic field exposure on differentiation of magnetite nanoparticle-loaded adipose-derived stem cells. *Mater. Sci. Eng. C. Mater. Biol. Appl.* **109**, 110652 (2020).
14. Zhao, W., Ma, W. & Wu, H. The effects of magnetic fields on the differentiation and intracellular free calcium of bone marrow mesenchymal stem cells. in *2008 World Automation Congress* 1–3 (2008).
15. Marycz, K., Kornicka, K. & Röcken, M. Static Magnetic Field (SMF) as a Regulator of Stem Cell Fate - New Perspectives in Regenerative Medicine Arising from an Underestimated Tool. *Stem cell Rev. reports* **14**, 785–792 (2018).
16. Benouchan, M. & Colombo, B. M. Anti-angiogenic strategies for cancer therapy (Review). *Int. J. Oncol.* **27**, 563–571 (2005).
17. Teleanu, R. I., Chircov, C., Grumezescu, A. M. & Teleanu, D. M. Tumor Angiogenesis and Anti-Angiogenic Strategies for Cancer Treatment. *J. Clin. Med.* **9**, 84 (2019).
18. Cui, M. *et al.* Electromagnetic Fields for the Regulation of Neural Stem Cells. *Stem Cells Int.* **2017**, 9898439 (2017).
19. Wyszkowska, J., Jankowska, M. & Gas, P. Electromagnetic Fields and Neurodegenerative Diseases. *Prz. Elektrotechniczny* **95**, 129–133 (2019).
20. Chandos, B., Khan, A., Lai, H. & Lin, J. C. The Application of Electromagnetic Energy to The Treatment of Neurological and Psychiatric Diseases. *Biol. Eff. Magn. Electromagn. Fields* 161–169 (1996). doi:10.1007/978-0-585-31661-1_12
21. Sasmal, P., Datta, P., Wu, Y. & Ozbolat, I. T. 3D bioprinting for modelling vasculature. *Microphysiological Syst.* **2**, 9 (2018).
22. Tomasina, C., Bodet, T., Mota, C., Moroni, L. & Camarero-Espinosa, S. Bioprinting Vasculature: Materials, Cells and Emergent Techniques. *Mater. (Basel, Switzerland)* **12**, 2701 (2019).

LIST OF PUBLICATIONS

Oral Communications

11th International Congress on Membranes and Membrane Processes 2017, ICOM, San Francisco (USA), July 2017, **A.C. Manjua**, C.I. Daniel, C.A.M. Portugal, J.G. Crespo, Magnetic-responsive membranes for control of solute mass transport and protein-surface interactions.

4th International Congress on Biomaterials and Biosensors 2019, BIOMATSEN, Oludeniz (Turkey), 12-18 May 2019, **Ana C. Manjua**, J.G. Crespo, Joaquim M.S. Cabral, Carla A.M. Portugal, Frederico C. Ferreira, Promoting Angiogenesis Phenomena using Magnetic Scaffolds.

Tissue Engineering Therapies: From Concept to Clinical Translation & Commercialization, TERMIS EU 2019, Rhodes (Greece), 27-31 May 2019, **Ana C. Manjua**, J.G. Crespo, Joaquim M.S. Cabral, Carla A.M. Portugal, Frederico C. Ferreira, Magnetic Scaffolds to Promote Angiogenesis.

12th International Congress on Membranes & Membrane Processes 2020, ICOM, 2020, 6-11 December 2020, London, UK, **Ana C. Manjua**, J.G. Crespo, Joaquim M.S. Cabral, Frederico C. Ferreira, Carla A.M. Portugal, Magnetic hydrogel membranes for remote controlo of protein sorption and vascularization.

Poster Communications

Imagine Membrane Conference 2017, Faial, Azores, 24-29 September 2017, **Ana C. Manjua**, João G. Crespo, Carla A. M. Portugal, Magnetic-responsive hydrogels to control protein-surface interactions.

Ciência 2018, Lisbon, July 2018, **Ana C. Manjua**, J.G. Crespo, Joaquim M.S. Cabral, Carla A.M. Portugal, Frederico C. Ferreira, Promoting Vascularization in na Artificial

Blood Vessel using Magnetic Fields.

12th European Society of Biochemical Engineering, ESBES 2018, Lisboa, September 2018, **Ana C. Manjua**, J.G. Crespo, Joaquim M.S. Cabral, Carla A.M. Portugal, Frederico C. Ferreira, Control of the Angiogenesis Process Using Magnetic Scaffolds.

Articles in Peer-Reviewed International Scientific Journals

Ana C. Manjua, Vitor Alves, João G. Crespo, C.A.M. Portugal, Magnetic-responsive PVA hydrogels for remote modulation of protein sorption, ACS Applied Materials & Interfaces, ACS Appl Mater Interfaces 11(23):21239-21249 (2019).

Ana C. Manjua, Joaquim M.S. Cabral, Carla A.M. Portugal, Frederico Castelo Ferreira, Magnetic stimulation combined with magnetic-responsive scaffolds to enhance the angiogenic potential of MSCs in vascular tissue engineering (Under submission).

Ana C. Manjua, Joaquim M.S. Cabral, Frederico Castelo Ferreira, Carla A.M. Portugal, Magnetic field configurations for improved control of mesenchymal stromal cells angiogenic potential (Under submission).

Ana C. Manjua, Burcu Gumuscu, Joaquim M.S. Cabral, Frederico Castelo Ferreira, Carla A.M. Portugal, Design of Blood Vessel devices for vascularization models using magnetic scaffolds (In preparation for submission).

Shabnam Majidi, **Ana C. Manjua**, Benny Belviso, C.A.M. Portugal, Isabel Coelhoso, Valentina Mirabelli, Enrica Fontananova, Rocco Caliandro, João G. Crespo, Efrem Curcio, Gianluco Di Profio, Hydrogel Composite Membranes Incorporationg Iron Oxide Nanoparticles as Topographical Designers for Controlled Heteronucleation of Proteins, Crystal Growth & Design 18 (2018) 3317-3327.